



University  
of Glasgow

Adam, Martin Scott (2009) *An investigation of hydrogen bonded molecular systems using X-ray and neutron diffraction*. PhD thesis.

<http://theses.gla.ac.uk/556/>

Copyright and moral rights for this thesis are retained by the author

A copy can be downloaded for personal non-commercial research or study, without prior permission or charge

This thesis cannot be reproduced or quoted extensively from without first obtaining permission in writing from the Author

The content must not be changed in any way or sold commercially in any format or medium without the formal permission of the Author

When referring to this work, full bibliographic details including the author, title, awarding institution and date of the thesis must be given

# An investigation of hydrogen bonded molecular systems using X-ray and neutron diffraction.

**Martin Scott Adam**

Doctor of Philosophy Degree in Chemistry

Department of Chemistry  
University of Glasgow



September 2008

Supervisor: Prof Chick C. Wilson

## **Declaration**

The thesis has been written in accordance with the University regulations and all work presented is original and performed by the author unless otherwise stated and referenced in the text.

©Martin Scott Adam, September 2008

Martin Scott Adam  
September 2008

## Abstract

The main focuses of this project have been investigations of a variety of hydrogen bonding systems for unusual behaviour such as disordered or migrating hydrogens/protons with both single crystal X-ray and neutron diffraction, crystallisation of a large number of molecular complexes of the chloranilic acid molecule, and examining the bifurcated hydrogen bond motif found in many of the chloranilic acid co-crystals discovered.

The neutron single crystal diffraction instruments SXD and VIVALDI have been used to provide conclusive results in cases of suspected unusual hydrogen bond behaviour in molecular materials. 2,4-dihydroxybenzoic acid and its isomer 2,5-dihydroxybenzoic acid have been examined using X-ray and neutron diffraction to investigate possible disordered cooperative hydrogen bond systems. The energy difference of the three possible tautomers of 2,4-dihydroxybenzoic acid in different environments have been calculated in theoretical computations which concur with the neutron results. Single crystal neutron diffraction experiments were also carried out on isonicotinamidium formate, 2-iodoanilinium picrate, chloranilic acid 2,4-lutidine and malonic acid, where unusual behaviour in the hydrogen systems was also suspected.

The molecular complexes of chloranilic acid with various pyridine-based molecules have been the main focus of the X-ray diffraction work of this thesis. Multiple crystallisations over a range of different conditions were set up for chloranilic acid with various series of molecules including lutidines (dimethylpyridines) and picolines (methylpyridines). This resulted in a large number of new crystal structures, determined by X-ray diffraction and all found to contain a bifurcated hydrogen bond motif producing two robust hydrogen-bonded supramolecular synthons. The investigation examines the bifurcated hydrogen bond interactions and the suitability of chloranilic acid complexes for crystal engineering. The two related supramolecular synthon units are discussed and difference Fourier maps and Hirshfeld surfaces used to examine the hydrogen bond architecture. Bromanilic acid co-crystals are also studied to examine the effect of the halogen in the crystal structures.

## Acknowledgements

I would like to begin by thanking my supervisor Chick for his help, guidance and encouragement throughout the course of the project. He unique and enthusiastic style produces a enjoyable atmosphere to work in, and a group that I'm glad to be associated with even when we are being made to dig holes in the Wilson garden. :)

I also wish to thank Andy Parkin for all the support he has provided and all the good memories; he will be sorely missed.

Thanks to Derek for all his work on the computational side of the project, even if there were a lot of straight-line graphs, Matthias and Garry for helping with the neutron experiments.

For all the fun and entertaining times I would like to sprinkle pink sparkles on Susie, shout a Roooaar at Marc, pour a cup of tea for Lynne, and dance like a banana for Gen Ken. A special thanks goes to Lynne who I'm now indebted to for all her help, especially for reading and correcting endless pages of thesis.

Cheers to the Chicklets and other deadbeats associated with the group with whom I have shared for several nights talking "science" over a pint.

Sausages & ketchups, chloranilic acid and Iceland tea bags are worth a mention.

Finally, thanks go to my parents for their support and patience throughout this project, and everything else...

## Table of contents

Declaration.....	II
Abstract.....	III
Acknowledgements.....	IV
Table of contents.....	V
1. Introduction and Methods.....	1
1.1 Preamble.....	1
1.2 Hydrogen bonds.....	1
1.2.1 Categorizing hydrogen bonds-focusing on Strong/Medium.....	3
1.2.2 Bifurcated hydrogen bonds.....	5
1.2.3 Potential energy wells, proton disorder and migration.....	8
1.3 Crystal engineering – designing and tuning intermolecular interactions.....	14
1.3.1 Molecular complexes and supramolecular synthons.....	15
1.3.2 Co-crystallisation.....	15
1.4 General approach.....	17
2. Theory.....	19
2.1 Crystallography.....	19
2.2 Theory of diffraction.....	20
2.2.1 The lattice.....	20
2.2.2 Diffraction.....	22
2.2.3 Bragg’s law.....	22
2.2.4 The Ewald sphere.....	23
2.2.5 X-ray Data collection.....	25
2.2.6 Fourier synthesis.....	25
2.2.7 Structure solution.....	27
2.2.8 Structure refinement.....	28
2.2.9 Difference Fourier maps (Finding hydrogen).....	30
2.3 Neutron diffraction (and reasons for its use in this work).....	31
2.4 Powder diffraction.....	35
2.5 Differential scanning calorimetry (DSC).....	37
2.6 Computational chemistry.....	39
2.6.1 Hartree-Fock methods.....	40
2.6.2 Density functional Theory (DFT).....	41
3. Techniques and apparatus.....	43
3.1 Sample preparation.....	43
3.1.1 Crystallisation methods.....	44
3.2 Characterisation and screening.....	45
3.2.1 Powder diffraction, DSC, sample identification and purity.....	46
3.2.2 Powder pattern analysis technique.....	47
3.3 Single crystal X-ray diffraction.....	47
3.3.1 Unit cell determination and indexing.....	47
3.3.2 Data collection.....	48
3.3.3 Variable temperature methods.....	48
3.4 Neutron sources.....	49
3.4.1 ISIS spallation neutron source.....	49
3.4.2 SXD, time-of-flight single crystal neutron diffractometer.....	51
3.4.3 Data collection method.....	52
3.4.4 ILL steady state reactor source.....	53
3.4.5 D9 and VIVALDI single crystal diffractometers.....	54

3.5	Examination and imaging of experimental results.....	55
3.6	Computational methods .....	56
3.6.1	CASTEP, Gaussian03, CRYSTAL06.....	56
3.6.2	Hybrid functionals – mixing Hartree-Fock and DFT .....	57
3.6.3	Calculations on hydrogen peroxide, H <sub>2</sub> O <sub>2</sub> .....	57
4.	SXD2001 data reduction software .....	64
4.1	SXD98, software for two position-sensitive detectors .....	64
4.2	SXD2001, software for array of eleven position-sensitive detectors .....	65
4.2.1	Flow Diagram .....	67
4.3	Peak searching and indexing.....	68
4.4	Unit cell refinement .....	70
4.5	Peak integration .....	71
4.6	Data correction, normalisation, absorption, extinction and refinement.....	72
5.	Hydrogen bonding in dihydroxybenzoic acids .....	74
5.1	Carboxylic acid dimer motifs in benzoic acids.....	75
2,4- and 2,5-dihydroxybenzoic acid, cooperative hydrogen bonding.....		76
5.2	2,4-dihydroxybenzoic acid.....	78
5.2.1	Experimental .....	78
5.2.2	Comprehensive variable temperature X-ray studies .....	78
5.2.3	SXD variable temperature neutron studies .....	82
5.2.4	Conclusions on 2,4-dihydroxybenzoic acid.....	87
5.3	2,5-Dihydroxybenzoic acid.....	87
5.3.1	Variable temperature X-ray diffraction .....	88
5.3.2	SXD multiple temperature neutron studies.....	92
5.3.3	Conclusions on 2,5-dihydroxybenzoic acid.....	95
5.4	Computational studies of dihydroxybenzoic acids .....	95
5.5.1	Computational Conclusions .....	98
6.	Neutron Structures Determined on SXD .....	99
6.1	Isonicotinamidium Formate .....	99
6.2	2-Iodoanilinium Picrate .....	111
6.3	Malonic acid.....	118
6.3.1	Background on Malonic Acid.....	118
6.3.2	SXD Neutron Experiment for Malonic Acid.....	120
6.3.3	VIVALDI measurements on malonic acid .....	124
7.	Complexes of Chloranilic Acid with Lutidines .....	126
7.1	Introduction to chloranilic acid.....	126
7.2	Historical and recent uses of chloranilic acid .....	130
7.3	Hydrogen bonding motifs, and pK <sub>a</sub> matching for proton transfer .....	131
7.4	Structure determinations of chloranilic acid-lutidine complexes .....	134
7.4.1	2,3-lutidine chloranilic acid 2:1 co-crystals.....	137
7.4.2	2:1 2,4-lutidine chloranilic acid polymorphs .....	139
7.4.3	2:1 2,5-lutidine chloranilic acid .....	141
7.4.4	2:1 2,6-lutidine chloranilic acid .....	142
7.4.5	2:1 3,4-lutidine chloranilic acid dihydrate .....	144
7.4.6	2:1 3,5-lutidine chloranilic acid hydrate trihydrate (100K).....	145
7.5	Powder patterns for chloranilic acid lutidine co-crystal crystallisations ...	147
7.6	Hydrogen-bonded supramolecular synthon; comparison of hydrogen bonding schemes .....	155
7.7	ILL neutron experiment on 2:1 2,4-lutidine chloranilic acid form 1.....	159
Neutron	.....	160

7.8	Conclusions.....	161
8.	Complexes of Chloranilic Acid with Picolines.....	163
8.1	Hydrogen bonding motifs, proton transfer and $pK_a$ matching.....	163
8.2	Structure determinations of CA-picoline complexes.....	164
8.2.1	Picoline chloranilic acid 1:1 structures.....	164
8.2.1.1	2-picoline chloranilic acid complex.....	164
8.2.1.2	3-picoline chloranilic acid.....	166
8.2.1.3	4-picoline chloranilic acid complex.....	167
8.2.2	Picoline chloranilic acid 2:1 structures.....	168
8.2.2.1	2-picoline chloranilic acid.....	168
8.2.2.2	3-picoline chloranilic acid complex, forms 1 and 2.....	169
8.2.2.3	4-picoline chloranilic acid complex.....	171
8.2.3	Picoline chloranilic acid solvates.....	172
8.2.3.1	2:1 3-picoline chloranilic acid dihydrate.....	173
8.2.3.2	3-picoline chloranilic acid hydrate 4:3:2 complex.....	174
8.2.3.3	2:1 4-picoline chloranilic acid tetra-hydrate.....	175
8.3	Hydrogen-bonded supramolecular synthon.....	176
8.3.1	Comparison of hydrogen bonding schemes.....	177
8.3.2	Fourier maps and Hirshfeld surfaces.....	177
8.3.3	Bifurcated hydrogen bond lengths and angles.....	185
8.4	Powder patterns.....	187
8.5	Gas phase calculations on the bifurcated hydrogen-bonded 2:1 CA-picoline structures.....	192
8.6	Additional chloranilic acid co-crystal structures.....	194
8.6.1	Caffeine co-crystals grown from common commercial tea.....	196
8.6.2	Chloranilic acid with sulfathiazole.....	198
8.7	Complexes of bromanilic acid with Picolines.....	200
8.7.1	2-picoline 2:1 bromanilic acid.....	200
8.7.2	3-picoline 2:1 bromanilic acid.....	202
8.7.3	4-picoline 2:1 bromanilic acid.....	203
8.7.4	Conclusions on bromanilic acid complexes.....	204
8.8	Conclusions.....	204
9.	Conclusions and Forward Look.....	209
9.1	Investigation of possible cooperative hydrogen bond disorder in 2,4-dihydroxybenzoic acid.....	209
9.1.1	2,4-dihydroxybenzoic acid calculations.....	209
9.2	Investigation of possible cooperative hydrogen bond disorder in 2,5-dihydroxybenzoic acid.....	210
9.3	Proton migration in isonicotinamidium formate.....	211
9.4	Neutron diffraction studies of 2-iodoanilinium picrate.....	211
9.5	Neutron diffraction studies of malonic acid.....	212
9.6	Molecular complexes of Chloranilic acid.....	212
9.6.1	<i>d</i> SNAP and the geometry of molecular complexes, a forward look..	216
9.6.2	VIVALDI data on 2:1 2,4-lutidine chloranilic acid form I.....	218
9.7	Molecular complexes of bromanilic acid.....	218
9.8	Additional Future work.....	218
	References.....	229

<b>Figure 1.1</b> Some examples of systems that have been referred to as bifurcated hydrogen bonds <b>a)</b> Two hydrogens between the donor atoms; <b>b)</b> one donor and two acceptor atoms (also called three-centred in literature, type referred to in this thesis); <b>c)</b> one donor possessing two hydrogen but only one acceptor; <b>d)</b> two hydrogen bonds share acceptor. (bifurcated acceptor bond) .....	5
<b>Figure 1.2</b> The sum of the angles $\alpha_1+\alpha_2+\alpha_3$ for the bifurcated hydrogen bond gives an indication of the planarity of the interaction.....	6
<b>Figure 1.3</b> Representation of <b>a)</b> highly BHB (symmetrical), <b>b)</b> weakly BHB (asymmetrical) with major and minor components. ....	7
<b>Figure 1.4</b> Two bifurcated hydrogen bonds forming a parallelogram shape in the crystal structure of 2,3,4,5-tetrafluoro-N-(4-fluorophenyl)-6-hydroxybenzamide. <sup>16</sup> .....	8
<b>Figure 1.5 Left:</b> 2,4-dihydroxybenzoic acid, X-ray difference Fourier map in the plane of the molecule showing small secondary density peaks that could be indicative of potential disordered hydrogen secondary sites, <b>Right:</b> Neutron difference Fourier map proves that there is no disorder in the proton position in this case; the apparent weak features in the X-ray map are attributable to noise or polarisation of the electron density towards the acceptor atom, a consequence of the relative difficulty in accurately locating hydrogen from X-ray data. ....	9
<b>Figure 1.6</b> The potential energy profile for an atom bonded to another located at the origin of the plot.....	10
<b>Figure 1.7</b> Different types of hydrogen bond potential: <b>a)</b> asymmetrical double minimum, <b>b)</b> symmetrical double well, <b>c)</b> flat bottomed single well.....	10
<b>Figure 1.8</b> Difference Fourier maps for urea-phosphoric acid showing migration of the proton toward the centre of the bond. <b>Left:</b> neutron <b>Right:</b> X-ray <sup>22</sup> .....	12
<b>Figure 1.9</b> Schematic diagram of chloranilic acid. ....	16
<b>Figure 2.1</b> Bragg's construct showing the additional path distance undertaken by the lower beam. ....	23
<b>Figure 2.2</b> Ewald circle with parallel planes representing Bragg's law. A reciprocal lattice point can only be observed if it occurs on the circumference of the circle and at the scattering vector from the origin. In 3 dimensions a sphere is formed. Adapted from Wilson 2000 <sup>45</sup> .....	24
<b>Figure 2.3</b> Ewald diagram for a (time-of-flight) Laue diffraction experiment with only one detector. The observed reciprocal lattice points (marked in blue) are limited by the wavelengths used, (area between Ewald circles) and the detector coverage (for each wavelength arc marked in green and over all enclosed by dotted lines). Adapted from Wilson 2000 <sup>45</sup> .....	24
<b>Figure 2.4 (Top)</b> The X-ray scattering factors (shown with dotted line) compared with neutron scattering factors. <b>(Bottom)</b> An expanded view of the neutron scattering length versus Z (for the principal isotopes). <sup>45</sup> .....	32
<b>Figure 2.5 Left:</b> Image of powder ring on an area detector <b>Right:</b> Powder pattern formed integrating round the powder ring, (before <b>(blue)</b> , and after <b>(orange)</b> background removed and pattern smoothed). Powder patterns can be used as a fingerprint for crystalline materials as each has a unique pattern.....	36
<b>Figure 2.6</b> DSC curve showing the three main types of event that can occur. A glass transition where the base level drops and remains there till another event, a crystallisation that forms an upward peak and a melting trough. A downward	

move shows extra energy is required, an upward move shows energy is given out. ....	38
<b>Figure 3.1</b> Photo of <b>a)</b> samples in a temperature controlled hot plate, <b>b)</b> typical sample vial and equipment, <b>c)</b> H-tube crystallisation of chloranilic acid and 3,5-dimethyl pyrazole at different stages. ....	45
<b>Figure 3.2</b> Layout of ISIS, with the synchrotron on the left and the target with the instruments surrounding it on the right <sup>65</sup> . ....	50
<b>Figure 3.3 a)</b> Diagram representing the layout of the 11 detectors on SXD <b>b)</b> Photograph of SXD from the top with the inlet of the neutron beam at the bottom of the picture and 6 equatorial detectors visible <sup>67</sup> . ....	52
<b>Figure 3.4 a)</b> Structure of H <sub>2</sub> O <sub>2</sub> showing the two positions of the H atom; the normal position is shown in white (E <sub>1</sub> ), and the centred position in green (E <sub>2</sub> ). <b>b)</b> The potential energy well with the barrier height and energies E <sub>1</sub> and E <sub>2</sub> for the normal and the centred hydrogen positions. ....	58
<b>Figure 3.5</b> Results of H <sub>2</sub> O <sub>2</sub> calculations showing variation in the energy barrier vs. HB lengths with different basis sets with pure DFT. ....	60
<b>Figure 3.6</b> Results of H <sub>2</sub> O <sub>2</sub> calculations showing variation in the energy barrier vs. HB lengths with different basis sets with 50 % mixture of HF and DFT. ....	60
<b>Figure 3.7</b> Results of from H <sub>2</sub> O <sub>2</sub> calculations showing variation in the energy barrier vs. HB lengths with different basis sets with pure HF. ....	61
<b>Figure 3.8</b> Results of H <sub>2</sub> O <sub>2</sub> calculations showing variation in the energy barrier vs. % HF with different unit cell volumes for the DZP basis set. ....	61
<b>Figure 3.9</b> Results of H <sub>2</sub> O <sub>2</sub> calculations showing variation in the energy barrier vs. % HF with different unit cell volumes for the 6-31G* basis set. ....	62
<b>Figure 3.10</b> Results of H <sub>2</sub> O <sub>2</sub> calculations showing variation in the energy barrier vs. % HF with different unit cell volumes for the 6-311G** basis set. ....	62
<b>Figure 3.11</b> Results of H <sub>2</sub> O <sub>2</sub> calculations showing the variation in the energy barrier vs. % HF with different basis sets and no compression of the cell. ....	63
<b>Figure 4.1</b> SXD before the upgrade, <b>left:</b> instrument box and some of the controls <b>right:</b> the sample environment with the two detectors (shielding removed).....	64
<b>Figure 4.2</b> Main display of SXD2001. From here it is possible to run all the different routines needed to process the neutron data. ....	65
<b>Figure 4.3</b> Eleven detector display showing the diffraction pattern. Below the display a plot of the counts vs. wavelength from a selected point is shown. ....	66
<b>Figure 4.4</b> Flow chart for processing data on SXD2001 from SXD. ....	67
<b>Figure 4.5</b> SXD2001 with raw data loaded and displayed in the viewer. ....	69
<b>Figure 4.6 a)</b> UB matrix refinement screen with added pop up screen of activated and indexed peaks. <b>b)</b> Indexed peak list from a single detector. ....	70
<b>Figure 4.7</b> Integration window allowing a varied array of customised integration. ...	72
<b>Figure 5.1</b> The two possible tautomers for benzoic acid carboxylic acid dimer. ....	75
<b>Figure 5.2</b> The dimerised structure of 2,4-dihydroxybenzoic acid with the classical representation of an unsymmetrical double well minimum indicating the possibility for proton disorder by thermal population of the slightly higher energy configuration. The dotted line indicates the alternative locations for the disordered protons. ....	76
<b>Figure 5.3</b> Scheme showing three possible tautomers of 2,4-dihydroxybenzoic acid. ....	77
<b>Figure 5.4</b> Structure of 2,4-dihydroxybenzoic acid showing a layer (viewed along the a-axis) that is held together by three hydrogen-bonding motifs: (A)	

intermolecular dimer; <b>(B)</b> intramolecular; <b>(C)</b> intermolecular. The view on the right shows the staggered $\pi$ - $\pi$ stacking. ....	79
<b>Figure 5.5</b> Structure 2,4-dihydroxybenzoic acid determined from X-ray data at <b>(left)</b> 90 K and <b>(right)</b> 150K with hydrogens allowed to refined isotropically. ....	80
<b>Figure 5.6</b> Difference Fourier maps of 2,4-dihydroxybenzoic acid at 90 K, 100 K, 110 K, and 150 K in the plane of C7, O8, and O9. RMS = 0.09 e/Å <sup>3</sup> , 0.09 e/Å <sup>3</sup> , 0.09 e/Å <sup>3</sup> , 0.09 e/Å <sup>3</sup> .....	81
<b>Figure 5.7</b> The structure of 2,4-dihydroxybenzoic acid refined from neutron data at <b>(a)</b> 20 K, <b>(b)</b> 90 K, and <b>(c)</b> 150 K .....	84
<b>Figure 5.8</b> Difference Fourier maps for 2,4-Dihydroxybenzoic acid at <b>(a)</b> 20 K, <b>(b)</b> 90 K, and <b>(c)</b> 150 K produced from neutron data collected on SXD, in the plane of C7, O8, and O9. The well-defined H atom density is apparent at all temperatures. The scale is in fm and the respective RMS on these values are <b>(a)</b> 0.07 fm/Å <sup>3</sup> , <b>(b)</b> 0.05 fm/Å <sup>3</sup> , and <b>(c)</b> 0.04 fm/Å <sup>3</sup> .....	85
<b>Figure 5.9</b> Molecule of 2,5-dihydroxybenzoic acid showing atom labels .....	88
<b>Figure 5.10</b> Structure of 2,5-dihydroxybenzoic acid in the plane of one of the flat ribbons also showing the perpendicular ribbons it is bonded to. The three hydrogen-bonding motifs are labelled: <b>(A)</b> intermolecular carboxylic acid dimer, <b>(B)</b> intramolecular, <b>(C)</b> intermolecular chain involving O5 and H5.....	89
<b>Figure 5.11</b> Structure models of 2,5-dihydroxybenzoic acid from the multiple temperature X-ray experiment. ....	89
<b>Figure 5.12</b> Difference Fourier maps of 2,5-dihydroxybenzoic acid at 100 K, 150 K, 200 K, 350 K in the plane of C7, O8, and O9. RMS = 0.08 e/Å <sup>3</sup> , 0.09 e/Å <sup>3</sup> , 0.08 e/Å <sup>3</sup> , 0.08 e/Å <sup>3</sup> .....	91
<b>Figure 5.13</b> The structure of 2,5-dihydroxybenzoic acid determined from neutron diffraction data at <b>(a)</b> 20 K, <b>(b)</b> 100 K, and <b>(c)</b> 200 K.....	92
<b>Figure 5.14</b> Bond lengths and angles for the hydrogen bonds in 2,5-dihydroxybenzoic acid from the neutron refinements. ....	93
<b>Figure 5.15</b> Difference Fourier maps of 2,5-dihydroxybenzoic acid shown at <b>(a)</b> 20 K, <b>(b)</b> 100 K, and <b>(c)</b> 200 K, produced from neutron data collected on SXD, in the plane of C7, O8, and O9. The well-defined H atom density is apparent at all temperatures. The scale is in fm and the respective RMS on these values are <b>(a)</b> 0.09 fm/Å <sup>3</sup> , <b>(b)</b> 0.06 fm/Å <sup>3</sup> , and <b>(c)</b> 0.04 fm/Å <sup>3</sup> .....	94
<b>Figure 5.16 a)</b> The deformation electron density $\rho_{\text{def}}(\mathbf{r}) = \rho_{\text{molecule}}(\mathbf{r}) - \sum \rho_{\text{atoms}}(\mathbf{r})$ of the isolated form I monomer of 2,4-dihydroxybenzoic acid. Solid, dashed and dot-dashed lines indicate positive-, negative- and zero-valued contours respectively <sup>92</sup> , <b>b)</b> The atomic numbering and hydrogen bond labelling for 2,4-dihydroxybenzoic acid. ....	98
<b>Figure 6.1 (a)</b> The X-ray structure of isonicotinamidium formate showing the ribbon structure with one dimer unit highlighted in green and the hydrogen bonds shown. <b>(b)</b> The ribbons stack in a staggered fashion as shown. ....	99
<b>Figure 6.2</b> Multiple temperature difference Fourier maps of isonicotinamidium formate showing the pyridyl formate hydrogen bond where the H has been removed from the model. RMS respectively = 0.10 e/Å <sup>3</sup> , 0.09 e/Å <sup>3</sup> , 0.09 e/Å <sup>3</sup> , 0.08 e/Å <sup>3</sup> and 0.07 e/Å <sup>3</sup> .....	101
<b>Figure 6.3</b> Multiple temperature difference Fourier maps of isonicotinamidium formate showing the dimer and amide formate hydrogen bonds where the hydrogen has been removed from the model. RMS respectively = 0.10 e/Å <sup>3</sup> , 0.09 e/Å <sup>3</sup> , 0.09 e/Å <sup>3</sup> , 0.08 e/Å <sup>3</sup> and 0.07 e/Å <sup>3</sup> .....	102

<b>Figure 6.4</b> Structure of isonicotinamidium formate as refined from the 40 K neutron diffraction data. ....	104
<b>Figure 6.5</b> Difference Fourier map of isonicotinamidium formate with H1 removed in the plane of O1,C1,N1 and C6, for neutron data collected at 40 K on SXD. RMS = 1.33 fm/Å <sup>3</sup> .....	106
<b>Figure 6.6</b> Difference Fourier map of isonicotinamidium formate with H7 and H6 removed in the plane of O41, C41, and N41, for neutron data collected at 40 K on SXD. RMS = 1.33 fm/Å <sup>3</sup> .....	107
<b>Figure 6.7</b> Refined neutron structures of isonicotinamidium formate at 100 K, 150 K, & 200 K.....	108
<b>Figure 6.8</b> 100K difference Fourier maps of isonicotinamidium formate, showing the HB hydrogen atom density. RMS = 0.80 fm/Å <sup>3</sup> .....	109
<b>Figure 6.9</b> 150K difference Fourier maps of isonicotinamidium formate, showing the HB hydrogen atom density. RMS = 0.72 fm/Å <sup>3</sup> .....	109
<b>Figure 6.10</b> 200K difference Fourier maps of isonicotinamidium formate, showing the HB hydrogen atom density. RMS = 0.40 fm/Å <sup>3</sup> .....	109
<b>Figure 6.11</b> Thermochromism, in 2-iodoanilinium picrate and associated proton transfer, salt to molecular. (For the 2 <sup>nd</sup> polymorph this happens between 330-360 K.) .....	112
<b>Figure 6.12</b> Refined neutron structure of 2-iodoanilinium picrate at 300K.....	115
<b>Figure 6.13</b> Refined neutron structure of 2-iodoanilinium picrate at 320 K.....	116
<b>Figure 6.14</b> Difference Fourier map in the plane of the complex, containing the hydrogen bond calculated from the <b>a)</b> 300 K, <b>b)</b> 310 K and <b>c)</b> 320 K neutron data of 2-iodoanilinium picrate. RMS = 0.30 fm/Å <sup>3</sup> , 0.27 fm/Å <sup>3</sup> , 0.58 fm/Å <sup>3</sup> .....	117
<b>Figure 6.15</b> Alternating positions of the hydrogen atoms in carboxylic acid dimers such as in malonic acid. ....	119
<b>Figure 6.16 a)</b> Chain of malonic acid molecules, <b>b)</b> representation of how the chains form into layers held together by O-O close contacts.....	120
<b>Figure 6.17</b> The structure of malonic acid at 75 K, 140 K, and 200 K.....	121
<b>Figure 6.18</b> 3D image of the difference Fourier map for O1/O2 hydrogen-bonded dimer of malonic acid at 75 K.....	122
<b>Figure 6.19</b> 3D image of the difference Fourier map for O1/O2 hydrogen-bonded dimer of malonic acid at 140 K.....	123
<b>Figure 6.20</b> 3D image of the difference Fourier map for O3/O4 hydrogen-bonded dimer of malonic acid at 75 K.....	123
<b>Figure 6.21</b> 3D image of the difference Fourier map for O3/O4 hydrogen-bonded dimer of malonic acid at 140 K.....	124
<b>Figure 7.1 a)</b> The general structure for the anilic acid family of molecules, where R represents a range of elements or chemical groups (Cl, Br, NO <sub>2</sub> , O, H...). <b>b)</b> Chloranilic acid has a inversion centre because of the symmetry of the molecule - it is therefore common for only half to be present in the asymmetric unit cell.	126
<b>Figure 7.2</b> The three charged forms of chloranilic acid, its neutral state H <sub>2</sub> CA, partially deprotonated HCA <sup>-</sup> (monoanion) and fully deprotonated, CA <sup>2-</sup> (dianion <sub>38</sub> .....	127
<b>Figure 7.3 a)</b> The netting structure of the hydrogen bonded layer within the chloranilic acid structure (with one of the hydrogen bonded four molecule loops highlighted in blue), and <b>b)</b> an illustration of the layers with the Cl·Cl close contact of 3.335 Å indicated <sup>111</sup> .....	129

<b>Figure 7.4 a)</b> 3-dimensional hydrogen bonded structure of chloranilic acid dihydrate.	
<b>b)</b> Hydrogen bonded unit of chloranilic acid with water molecules on either side and acceptor-donor lengths shown <sup>112</sup> .....	129
<b>Figure 7.5</b> Classification of 1:1 chloranilic acid-amine systems, showing the three types of hydrogen bond patterns <sup>37</sup> .....	132
<b>Figure 7.6</b> Representation of the <b>a)</b> 1:1 and <b>b)</b> 1:2 chloranilic acid lutidine hydrogen bonded supramolecular synthon units.....	135
<b>Figure 7.7 a)</b> 2:1 hydrogen bonded unit of 2,3-lutidine-chloranilic acid. <b>b)</b> Planes of the rings are near perpendicular but the lutidine is rotated so the N-H is directed towards one of the oxygens.....	137
<b>Figure 7.8 a)</b> Hydrogen bonded units in the 2:1 2,3-lutidine chloranilic acid complex stack with overlapping lutidines, <b>b)</b> Chloranilic acid surrounded by lutidines. ....	138
<b>Figure 7.9</b> Fourier maps of 2,3-lutidine chloranilic acid co-crystal at 100 K, 200 K and 300K taken in the plane of the N and two O involved in the bond. RMS= 0.06 e/A <sup>3</sup> , 0.06 e/A <sup>3</sup> and 0.05 e/A <sup>3</sup> .....	139
<b>Figure 7.10</b> Form I of 2,4-lutidine-chloranilic acid showing the 2:1 hydrogen bonded unit. ....	139
<b>Figure 7.11 a)</b> A parallel hydrogen bonded unit of the form I 2,4-lutidine chloranilic acid with the three molecules in the plane. <b>b)</b> zig-zag structure and $\pi$ - $\pi$ interactions form between the rings .....	140
<b>Figure 7.12 a)</b> 2,4-lutidine-chloranilic acid Form II with two separate 2:1 hydrogen bonded units. <b>b)</b> Packing of the structure. ....	140
<b>Figure 7.13 a)</b> Difference Fourier map for the Form I 2,4-lutidine chloranilic acid at 100 K. RMS= 0.08 e/A <sup>3</sup> <b>b,c)</b> Difference Fourier maps for the two independent BHBs in Form II of 2,4-lutidine chloranilic acid at 100 K, <b>b)</b> H1 <b>c)</b> H2. RMS= 0.06 e/A <sup>3</sup> .....	141
<b>Figure 7.14</b> The 2:1 HB unit of the 2:1 2,5-lutidine chloranilic acid co-crystal.....	141
<b>Figure 7.15 a)</b> Difference Fourier map of 2:1 2,5-lutidine chloranilic acid at 100 K, RMS= 0.08 e/A <sup>3</sup> <b>b)</b> view down the a-axis showing the packing of the zig-zag shaped synthon units. ....	142
<b>Figure 7.16</b> 2:1 hydrogen bonded unit of 2:1 2,6-lutidine chloranilic acid. ....	142
<b>Figure 7.17 a)</b> view down the a-axis of the lattice of chloranilic acid (red) forming a layer via Cl-O close contact in the structure of 2:1 2,6-lutidine chloranilic acid, <b>b)</b> view down the c-axis of the layer.....	143
<b>Figure 7.18 a)</b> Difference Fourier map of 2:1 2,6-lutidine chloranilic acid at 100 K, RMS= 0.08 e/A <sup>3</sup> <b>b)</b> Difference Fourier map of 2:1 3,4-lutidine chloranilic acid dihydrate at 100 K. RMS = 0.07 e/A <sup>3</sup> .....	143
<b>Figure 7.19</b> The 2:1 hydrogen bonded unit of 3,4-lutidine chloranilic acid dihydrate. ....	144
<b>Figure 7.20</b> The structure of 2:1 3,4-lutidine chloranilic acid dihydrate viewed along the <b>a)</b> c-axis (showing HB layer in purple) and the <b>b)</b> a-axis, shows a zig-zag layered HB structure with the water molecules connecting the 2:1 units via HB to the oxygens of the chloranilic acid. ....	145
<b>Figure 7.21</b> 2:1 hydrogen bonded unit of 3,5-lutidine chloranilic acid, and three water molecules. ....	145
<b>Figure 7.22 a)</b> The 2:1 HB units stack on top of each other displaced by half a unit, <b>b)</b> and are held together by a network of water molecules (shown in purple), <b>c)</b> Formation of water molecule network. ....	146
<b>Figure 7.23</b> Difference Fourier maps for 2:1 3,5-lutidine chloranilic acid trihydrate, <b>a)</b> hydrogen 1, <b>b)</b> hydrogen 2. RMS = 0.07 e/A <sup>3</sup> .....	146

<b>Figure 7.24</b> Powder pattern for the crystallisations of 2,3-lutidine and chloranilic acid, Green-1:1, and Red-2:1.....	147
<b>Figure 7.25</b> Powder pattern for the crystallisations of 2,4-lutidine and chloranilic acid, Green-1:1, Red-2:1 and Blue-water.....	148
<b>Figure 7.26</b> Powder pattern for the crystallisations of 2,5-lutidine and chloranilic acid, Green-1:1 and, Red-2:1.....	149
<b>Figure 7.27</b> Powder pattern for the crystallisations of 2,6-lutidine and chloranilic acid, Green -1:1, Red-2:1 and Blue-water.....	150
<b>Figure 7.28</b> Powder pattern for the crystallisations of 3,4-lutidine and chloranilic acid, Green -1:1, Red-2:1 and Blue-water.....	151
<b>Figure 7.29</b> Powder pattern for the crystallisations of 3,5-lutidine and chloranilic acid, Green-1:1, Red-2:1 and Blue-water.....	152
<b>Figure 7.30</b> Structure of the nitrogen, hydrogen and chloranilic acid fragments of the lutidine chloranilic acid co-crystals complexes studied, roughly overlaying the chloranilic acid to line up the structures. The nitrogen and hydrogen of the bifurcated hydrogen bond have been coloured for each co-crystal, 2,3-lutidine (yellow), 2,4-lutidine form I (blue), 2,4-lutidine form II H1 (orange), 2,4-lutidine form II H1 (red), 2,5-lutidine (green), 2,6-lutidine (purple), 3,4-lutidine (white), 3,5-lutidine H1 (brown), 3,5-lutidine H2 (grey). .....	155
<b>Figure 7.31</b> The 2:1 HB synthon unit from the neutron refinement of 2:1 2,4-lutidine chloranilic acid form I at 40 K.....	159
<b>Figure 7.32</b> Difference Fourier map of 2:1 2,4-lutidine chloranilic acid form I at 40 K. RMS = 0.04 fm/Å <sup>3</sup> .....	161
<b>Figure 8.1</b> The 1:1 hydrogen bonded unit from the 2-picoline chloranilic acid structure.....	165
<b>Figure 8.2 a)</b> Stacked HB units showing $\pi$ - $\pi$ interactions (purple) and adjacent rotated picolines (orange), <b>b)</b> stacked HB units end on.....	165
<b>Figure 8.3</b> The 1:1 structure of 3-picoline chloranilic acid, <b>a)</b> showing the 2:1 HB units connected via single O-H...O bonds and oxygen-chloride close contacts, <b>b)</b> the connector chloranilic acid (red) joining 4 separately coloured 2:1 HB units. ....	166
<b>Figure 8.4</b> Hydrogen bonded unit from the 1:1 4-picoline chloranilic acid. ....	167
<b>Figure 8.5 a)</b> HB units form chains in the structure of 1:1 4-picoline chloranilic acid, <b>b)</b> the packing together of these, here viewed down the b-axis.....	167
<b>Figure 8.6 a)</b> Hydrogen bonded unit of the 2:1 2-picoline chloranilic acid co-crystal at 100 K, the ellipsoids on the picoline show large values indicative of disorder, <b>b)</b> The two molecules shown at 200 K and, <b>c)</b> 300 K.....	168
<b>Figure 8.7</b> View of the 2:1 2-picoline chloranilic acid structure along the b-c plane showing the stacking of the hydrogen bonded units allowing space for the methyl groups.....	169
<b>Figure 8.8</b> The hydrogen bonded units from the structures of the two polymorphic forms of the 2:1 3-picoline chloranilic acid co-crystal complex <b>a)</b> Form 1 <b>b)</b> Form 2.....	169
<b>Figure 8.9</b> View showing different angles between the chloranilic acid (red) and 3-picoline (blue) for <b>a)</b> form 2, and <b>b)</b> form 1 of the 2:1 3-picoline chloranilic acid complex, <b>c)</b> the stacking present in form 1 viewed down the a-axis. ....	170
<b>Figure 8.10</b> The stacking viewed along the b-axis in 2:1 3-picoline chloranilic acid form 2.....	171
<b>Figure 8.11</b> 4-picoline chloranilic acid 2:1 co-crystal hydrogen bonded unit. ....	171
<b>Figure 8.12</b> The stack viewed along the b-axis in 2:1 4-picoline chloranilic acid. ..	172

<b>Figure 8.13</b> Flat hydrogen bonded unit within the 2:1 3-picoline chloranilic acid dihydrate. ....	173
<b>Figure 8.14</b> Interlocking hydrogen bonded saw-tooth layers within the 3-picoline chloranilic acid dihydrate.....	173
<b>Figure 8.15</b> The HB units contained in the structure of <b>a)</b> the 2:1 unit, <b>b)</b> the offshoot unit, in the 4:3:2 complex. ....	174
<b>Figure 8.16 a)</b> 2:1 HB units in the complex hydrate of 3-picoline with chloranilic acid are formed into hydrogen bonded chains through links made by water molecules, and additional chloranilic picoline groups stick out from this, forming BHB to the water <b>b)</b> colour coded version highlighting the chain of stacked 2:1 3-picoline chloranilic acid HB units ( <b>red</b> ), the HB unit bifurcated to the water molecules ( <b>blue</b> ), and the waters connecting the structure ( <b>green</b> ).....	174
<b>Figure 8.17</b> Hydrogen bonded unit with water molecules from the 2:1 4-picoline chloranilic acid tetrahydrate structure.....	175
<b>Figure 8.18</b> Interlocking HB layers of 4-picoline chloranilic acid tetrahydrate viewed down the b-axis. ....	176
<b>Figure 8.19</b> Difference Fourier maps for the 2:1 2-picoline chloranilic acid at 100 K, 200 K and 300K. RMS = 0.07 e/Å <sup>3</sup> , 0.06 e/Å <sup>3</sup> , 0.05 e/Å <sup>3</sup> .....	178
<b>Figure 8.20</b> Difference Fourier maps for the 100 K refinements of <b>a)</b> 1:1 2-picoline chloranilic acid, RMS = 0.06 e/Å <sup>3</sup> <b>b)</b> 2:1 3-picoline chloranilic acid form 2, RMS = 0.09 e/Å <sup>3</sup> <b>c)</b> 2:1 3-picoline chloranilic acid dihydrate. RMS = 0.06 e/Å <sup>3</sup> .....	178
<b>Figure 8.21</b> Difference Fourier maps for the 1:1 3-picoline chloranilic acid at 100 K, 200 K, and 300K. RMS = 0.09 e/Å <sup>3</sup> , 0.08 e/Å <sup>3</sup> , 0.07 e/Å <sup>3</sup> .....	179
<b>Figure 8.22</b> Difference Fourier maps for the 2:1 3-picoline chloranilic acid form 1 at 100 K, 200 K, and 300K. RMS = 0.10 e/Å <sup>3</sup> , 0.08 e/Å <sup>3</sup> , 0.07 e/Å <sup>3</sup> .....	180
<b>Figure 8.23</b> Difference Fourier maps for the stacked chain HB units of the 3-picoline chloranilic acid new hydrate. RMS = 0.13 e/Å <sup>3</sup> , 0.06 e/Å <sup>3</sup> , 0.06 e/Å <sup>3</sup> .....	180
<b>Figure 8.24</b> Difference Fourier maps for the offshoot HB units of the 3-picoline chloranilic acid new hydrate. RMS = 0.13 e/Å <sup>3</sup> , 0.06 e/Å <sup>3</sup> , 0.06 e/Å <sup>3</sup> .....	180
<b>Figure 8.25</b> Difference Fourier maps for the 2:1 4-picoline chloranilic acid at 100 K, 200 K, and 300K. RMS = 0.10 e/Å <sup>3</sup> , 0.06 e/Å <sup>3</sup> , 0.05 e/Å <sup>3</sup> .....	181
<b>Figure 8.26</b> Difference Fourier maps for the 100 K refinements of <b>a)</b> 1:1 4-picoline chloranilic acid RMS = 0.11 e/Å <sup>3</sup> <b>b)</b> 2:1 4-picoline chloranilic acid dihydrate. RMS = 0.12 e/Å <sup>3</sup> .....	181
<b>Figure 8.27</b> The Hirshfeld surface of the chloranilic acid in the 2:1 co-crystals complexes with <b>a)</b> 2-picoline <b>b)</b> 3-picoline form 1 <b>c)</b> 3-picoline form 2 <b>d)</b> 4-picoline. A sphere of atoms is also included to show the packing round the molecule. ....	182
<b>Figure 8.28</b> The Hirshfeld surface of the chloranilic acid in the 1:1 co-crystals complexes with <b>a)</b> 2-picoline, <b>b)</b> 3-picoline, <b>c)</b> 4-picoline. A sphere of atoms is also included to show the packing round the molecule. ....	183
<b>Figure 8.29</b> Powder pattern for the crystallisations of 2-picoline and chloranilic acid, Black-1:1, Red-2:1 and Blue-water .....	189
<b>Figure 8.30</b> Powder pattern for the crystallisations of 3-picoline and chloranilic acid, Black-1:1, Red-2:1 and Blue-water. ....	190
<b>Figure 8.31</b> Powder pattern for the crystallisations of 4-picoline and chloranilic acid, Black-1:1, Red-2:1 and Blue-water. ....	191

<b>Figure 8.32</b> The geometry optimised structures arising from the high level Gaussian03 calculations into the 2:1 HB supramolecular synthons for 2:1 <b>a)</b> 2-picoline, <b>b)</b> 3-picoline and <b>c)</b> 4-picoline, chloranilic acid structures. ....	193
<b>Figure 8.33 a)</b> A hydrogen bonded chain from the structure of 1:1 chloranilic acid caffeine molecular complex grown from tealeaves. <b>b)</b> The chains stack flat against each other in a regular pattern. ....	197
<b>Figure 8.34 a)</b> Structure of 2:1 sulfathiazole-chloranilic acid co-crystal complex showing the tubular construction and one of the disordered chains of acetonitrile that passes through the molecular netting frame. <b>b)</b> An isolated chain of disordered acetonitrile showing the repeating nature and the approximated molecules. ....	198
<b>Figure 8.35 a)</b> Stacked hydrogen bonded zig-zag layers in the chloranilic acid sulfathiazole complex, <b>b)</b> coloured sulfathiazole molecules forming double rings held together by chloranilic acid (red). ....	199
<b>Figure 8.36</b> Bond lengths of HB's and distances of Cl-O close contacts between chloranilic acid and sulfathiazole in the CA:sulfathiazole complex. ....	199
<b>Figure 8.37</b> 2-picoline bromanilic acid 2:1 hydrogen bonded unit showing the broken symmetry with the two different angles of the picoline molecule to bromanilic acid. ....	200
<b>Figure 8.38</b> HB units in the 2:1 2-picoline bromanilic acid complex form chains via close contacts between the O and Br. These stack in a complex interlocking style shown here with some of the chains coloured. ....	201
<b>Figure 8.39</b> HB unit of 3-picoline bromanilic acid 2:1 co-crystal complex. ....	202
<b>Figure 8.40</b> Stacking present in 2:1 3-picoline bromanilic acid co-crystal complex. ....	202
<b>Figure 8.41</b> HB unit of 2:1 4-picoline bromanilic acid co-crystal complex. ....	203
<b>Figure 8.42 a)</b> Stacking within the structure of the 2:1 4-picoline bromanilic acid complex, <b>b)</b> the diagonal stacking of the HB units viewed along the a-axis, showing some $\pi$ - $\pi$ interactions. ....	203
<b>Figure 9.1</b> Typical dendrogram from dSNAP showing level of similarity between different fragments. Each block at the bottom represents a different fragment coloured to represent the clustering. The lower a fragments is joined to another fragment by a tie-bar the more similar it is. The fragments are separated into the clusters by a cut level which can be moved up and down changing the level of similarity. Further tools are available in dSNAP that allow the geometries in each cluster to be analysed effectively; these will soon be fully available for user-input structures such as those determined in this work. ....	217
<b>Table 1.1</b> An example of some of the different types of hydrogen bond in the different categories <sup>5</sup> . ....	4
<b>Table 2.1</b> Unit cell types with length and angle associations indicated and possible Bravais lattices. ....	21
<b>Table 5.1</b> Crystallographic data for 2,4-dihydroxybenzoic acid at 90 K. ....	80
<b>Table 5.2</b> Bond lengths and angles for the hydrogen bonds in 2,4-dihydroxybenzoic acid from the neutron refinements. ....	86
<b>Table 5.3</b> The crystallographic data for 2,5-dihydroxybenzoic acid. At 100 K all H positions were fully refined. ....	90

<b>Table 5.4</b> Results from calculations on forms I and III of 2,4-dihydroxybenzoic acid in various environments as well as the energy of the dimer HB ( <b>A</b> ) and the stabilisation energy <b>A</b> gains from the crystalline environment. All energies in $\text{kJmol}^{-1}$ .....	97
<b>Table 6.1</b> The hydrogen distances and angles for the three crystallographically unique hydrogen bonds in the 40 K structure of isonicotinamidium.....	104
<b>Table 6.2</b> Hydrogen bond geometry in isonicotinamidium formate as a function of temperature. (The values showing the migrating proton are highlighted in grey, and show the proton to migrate by up to 0.06 Å in this short, strong HB).....	110
<b>Table 6.3</b> Unit cell dimensions for the co-crystal of 2-iodoanilinium picrate for both the published X-ray structure and the neutron structure for the three temperatures.....	115
<b>Table 7.1</b> Distances and angles for the bifurcated hydrogen bond in the lutidine chloranilic acid complexes studied, and angles between planes of the rings of the two molecules. ....	158
<b>Table 7.2</b> The HB lengths of 2:1 2,4-lutidine chloranilic acid form I for the 100 K X-ray and the 40 K neutron refinements.....	160
<b>Table 8.1</b> Bond lengths and angles for the BHB in the picoline ( <b>P</b> ) chloranilic acid ( <b>CA</b> ) complexes and angles between planes of their rings.....	185
<b>Table 8.2</b> Chloranilic acid complexes determined in this work (with previously determined structures from CSD that fit in series shown in grey), with unit cell dimensions and space group. ....	195
<b>Table 9.1</b> X-ray refinement data of chloranilic acid ( <b>CA</b> ) complexes with picoline ( <b>P</b> ). ....	219
<b>Table 9.2</b> X-ray refinement data of chloranilic acid ( <b>CA</b> ) complexes with picoline ( <b>P</b> ). ....	220
<b>Table 9.3</b> X-ray refinement data of chloranilic acid ( <b>CA</b> ) and bromanilic acid ( <b>BA</b> ) complexes with picoline ( <b>P</b> ). ....	221
<b>Table 9.4</b> X-ray refinement data of chloranilic acid ( <b>CA</b> ) complexes with lutidine ( <b>L</b> ). ....	222
<b>Table 9.5</b> X-ray refinement data of chloranilic acid ( <b>CA</b> ) complexes with lutidine ( <b>L</b> ) and other pyridine related molecules. ....	223
<b>Table 9.6</b> X-ray refinement data chloranilic acid ( <b>CA</b> ) complexes with pyridine related molecules. ....	224
<b>Table 9.7</b> X-ray refinement data 2,4- and 2,5- dihydroxybenzoic acid. ....	225
<b>Table 9.8</b> X-ray refinement data isonicotinamidium formate and neutron refinement data for 2,4-lutidine chloranilic acid from VIVALDI, ILL. ....	226
<b>Table 9.9</b> Neutron refinement data for 2,4- and 2,5- dihydroxybenzoic acid and Isonicotinamidium formate.....	227
<b>Table 9.10</b> Neutron refinement data for Isonicotinamidium formate, 2-Iodoanilinium Picrate and Malonic acid.....	228

# 1. Introduction and Methods

## 1.1 Preamble

Hydrogen bonding and techniques of X-ray and neutron diffraction are key to this project. Although generally well known, the basic concepts of crystallography with an added focus on neutron diffraction will be described here as well as an in depth introduction to hydrogen bonding, especially those hydrogen bonds that are bifurcated and disordered in character.

## 1.2 Hydrogen bonds

The term hydrogen bond started appearing in the 1930s, with probably the first use by Pauling in 1931 in a paper on the nature of the chemical bond<sup>1</sup>. The concept itself had been around long before with scientists like Latimer and Rodebush (1920)<sup>2</sup> and Huggins (1922)<sup>3</sup> describing weak bonds that we now classify as hydrogen bonds. Indeed intermolecular interactions that we would now know as hydrogen bonds were observed and referred to many years before this, but could not be explained. The importance of this type of interaction is seen in molecular association where its associated energy allows formation or dissociation of many hydrogen bonds at ambient temperatures, notably in biological reactions with the abundance of hydrogen, oxygen, and nitrogen in biologically important materials making it commonplace. The definition of the term hydrogen bond has evolved over the years, but even today there is some dispute over the less typical varieties and the boundaries of what should be included within the class of interaction.<sup>4,5</sup>

Although hydrogen bonds are much weaker than the conventional chemical bonds such as metallic, ionic and covalent, they are extremely important and significant in a wide range of materials. Affecting many physical and chemical properties of solids, liquids and gases, their importance can be seen in an enormous number of situations: melting and boiling points, solubility, the layout of crystal structures, viscosity, molar volume, reactivity, and colour, to name but a few.

The hydrogen bond plays a significant role in biological systems: for example, it is present in DNA and proteins and accounts for many of their important properties. Therefore it is not surprising that they are also important to synthetic chemists both organic and inorganic, where they determine structure and reactivity. Their applications range from biological and chemical fields to physics, where charge transfer and other physical properties can be important.

Infrared (IR) spectroscopy allows the vibrational modes of the hydrogen bond to be investigated. IR spectra showing the shifts in the peaks of OH groups give a measure of the effects of the interaction and this was the first technique able to prove the existence of hydrogen bonds<sup>4,6</sup>. Since then, many techniques have been and are still used to look at hydrogen bonds, but importantly, with the advent of X-ray crystallography, a direct visual representation could be produced. A diffraction experiment provides the average motion of the atoms about their equilibrium position, with the data typically being collected over several hours. More recently, neutron diffraction has provided an increasingly used tool to locate the proton in hydrogen bonds more accurately, and computational studies have opened many new routes to examine other aspects of the interaction, including the energies involved and the associated potential surfaces. Another major technique employed in the study of hydrogen bonds is (solid state) NMR; hydrogen bonding shifts the resonance signal of a proton to lower field. NMR can be used to look at the kinetics of hydrogen or deuterium transfer in the bonds by observing the chemical shifts of for example the OH group protons. There are many other techniques that are used to study the effects of hydrogen bonds.

While a typical covalent bond energy is around 420 kJ/mol (100 kcal/mol), the energy associated with hydrogen bonds ranges from around 168 kJ/mol to < 4.2 kJ/mol.<sup>4</sup> This wide range arises from the varying nature of hydrogen bonds.

A hydrogen bond can be viewed as a type of polar interaction with the electropositive hydrogen atom located between two electronegative atoms, often N or O. Hydrogen bonding occurs where the donor atom is an electronegative atom drawing the electrons away from the hydrogen atom forming a proton donor group<sup>7</sup> ( $D^{\delta-}-H^{\delta+}$  dipole). A lone pair of an acceptor (A) is attracted to the positive charge of the

partially shielded proton. Thus the hydrogen forms a proton bridge between two electronegative atoms. The hydrogen bond is a directional intermolecular interaction although a reasonable variation in angle ( $\angle \text{D-H}\cdots\text{A}$ ) can occur.

It is also possible to have multifaceted hydrogen bonds in which the donor forms hydrogen bonds with more than one acceptor simultaneously, or the reverse situation of one acceptor with multiple donors. For this to occur, several acceptor groups are required to be present in the same area. Bifurcated hydrogen bonds are the most common multifaceted hydrogen bond but trifurcated ones are also observed. Normally in such cases one acceptor forms the strongest component of the hydrogen bond with the others playing a weaker part in the bond<sup>7</sup>. Another possibility is a hydrogen bond being formed with the  $\pi$ -electrons of an aromatic group as the acceptor group, a situation that can be very important in biological systems.

### 1.2.1 Categorizing hydrogen bonds-focusing on Strong/Medium

The hydrogen bond can occur in a very wide range of motifs, covering a large span of energies. In the gas phase, or even liquid, hydrogen bonding is often the dominant force, whereas in crystals and other solid materials, packing forces and steric constraints, for instance the requirement for molecules to stack together, have a large influence on the structure, generating more variation in hydrogen bonding motifs<sup>4</sup>. Hydrogen bonds with a single donor-hydrogen-acceptor configuration are generally split into three types: these are strong, moderate and weak with bond energies in the ranges of  $\sim 168\text{-}62.8$  kJ/mol,  $\sim 62.8\text{-}16.7$  kJ/mol and  $\sim 16.7\text{-}4.2$  kJ/mol respectively. This classification is only made for practical reasons with no natural borderlines truly existing between these categories. Other characteristics can be used to differentiate between the categories, such as the geometry (directionality) of the hydrogen bond. The interaction is generally shorter and more linear ( $\text{D-H}\cdots\text{A}$  angle near to  $180^\circ$ ) for stronger hydrogen bonds. There is also a relationship between atom types of the donor and acceptor atoms and the strength of the hydrogen bond (*Table 1.1*).

Strong hydrogen bonds with energies in the range  $\sim 168\text{-}62.8$  kJ/mol are highly covalent in nature (sharing of electrons), and normally arise because of an increased attraction resulting from either a deficiency of electron density on the donor group or

a surplus of electron density on the acceptor group. With a deficiency of electrons on the donor group, some of the electron shielding of the hydrogen is removed increasing the positive charge on the atom. This increased charge will strengthen the bond. The same will happen if there is a surplus of electron density on the acceptor. The strong hydrogen bond tends to be linear ( $D-H\cdots A$  angle close to  $180^\circ$ ) with a short distance between the acceptor and donor atom of around 2.2 to 2.5 Å.

1	Weak donor, strong acceptor $C-H\cdots O=C$ $C-H\cdots N$ $C-H\cdots Cl^-$ $P-H\cdots O$ $Mo-H\cdots O=C$ $Ir-H\cdots Cl-Ir$
2	Strong donor, weak acceptor $N-H\cdots Ph$ $Cl-H\cdots CC$ $O-H\cdots CC$ $O-H\cdots F-C$ $O-H\cdots Se$ $N-H\cdots Co$
3	Weak donor, weak acceptor $CC-H\cdots CC$ $CC-H\cdots Ph$ $C-H\cdots F-C$ $C-H\cdots Pt$ $C-H\cdots Cl-C$ $C-H\cdots H-Re$
4	Other varieties Agostic $N-H\cdots H-B$ Formyl hydrogen bonds
5	Conventional but weak $O-H\cdots O-H$

**Table 1.1** An example of some of the different types of hydrogen bond in the different categories<sup>5</sup>.

Moderate hydrogen bonds have energies in the region of 62.8-16.7 kJ/mol and are also rather longer than strong hydrogen bonds, with typical distances of around 2.5 to 3.2 Å between the donor and acceptor atoms. The directionality of the bond is also generally less constrained, with  $D-H\cdots A$  bond angles typically in the range of  $130^\circ$  and above. The moderate hydrogen bond is mostly electrostatic in nature. The moderate hydrogen bond is a far more commonly observed interaction than the strong hydrogen bond and is found in acids, alcohols and hydrates as well as almost all biological molecules and in many other types of material. The donor and acceptor atoms are normally neutral for moderate hydrogen bonds.

Weak hydrogen bonds have even longer  $D\cdots A$  lengths (typically  $>3.2$  Å), bond angles in a still wider range (around  $90^\circ$  & above) and associated energies below  $\sim 16.7$  kcal/mol. The nature of the weak hydrogen bond is more in line with Van der

Waal force (weak electrostatic). Even so they can be important in such fields as crystal engineering where it is thought they can be used to tailor intermolecular interactions in arranging molecules to produce crystals with the desired architecture and hence properties.

### 1.2.2 Bifurcated hydrogen bonds

As previously discussed the conventional view of a hydrogen bond is that of a single hydrogen atom between an acceptor and a donor atom, but in reality the range of conformations, with both intra- and inter-molecular arrangements, that arise in the solid state is far more varied<sup>7-11</sup>. The hydrogen bond is a long-range interaction potentially allowing a donor hydrogen group (D-H) to interact with more than one acceptor (A). Where two acceptors or donor are involved it is called a bifurcated hydrogen bond or sometimes referred to in the literature as a three-centred hydrogen bond due to that fact the hydrogen is bonded to three atoms. Bifurcated hydrogen bonds exist in a range of situations from the simplest of molecules such as water<sup>12</sup>, to the more complex like DNA<sup>13</sup>. Hydrogen bonds with three or more acceptor groups are also possible but very rare and tend to be very geometrically constrained. In some cases the word bifurcated has been used to describe chelated or similar hydrogen bonds (*Figure 1.1*) or situations with two hydrogen donors and one acceptor, referred to as a bifurcated donor hydrogen bond<sup>14</sup>. In this text it will only be used to describe those as shown in *Figure 1.1 (b)*.

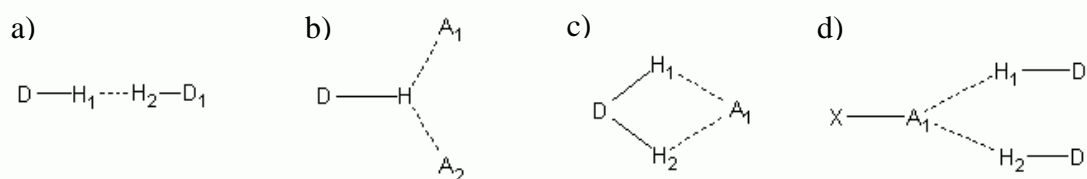


**Figure 1.1** Some examples of systems that have been referred to as bifurcated hydrogen bonds **a)** Two hydrogens between the donor atoms; **b)** one donor and two acceptor atoms (also called three-centred in literature, type referred to in this thesis); **c)** one donor possessing two hydrogen but only one acceptor; **d)** two hydrogen bonds share acceptor. (bifurcated acceptor bond)

Like the classical single hydrogen bond, the bifurcated hydrogen bond (BHB) has geometric constraints. The three individual bonds/interactions that make up the BHB are all attractive forces and cause the hydrogen of a BHB to lie close to the plane made by the donor and two acceptor atoms. An indication of this is that the sum of the angles  $\alpha_1 + \alpha_2 + \alpha_3$  add up to  $360^\circ$  when totally flat; the angle reduces the greater the system deviates from planarity (*Figure 1.2*)<sup>4</sup>.

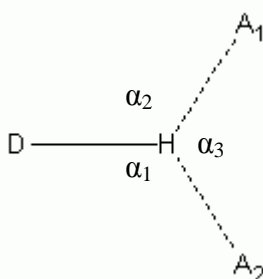


*Figure 1.2* The sum of the angles  $\alpha_1 + \alpha_2 + \alpha_3$  for the bifurcated hydrogen bond gives an indication of the planarity of the interaction.

When referring to bifurcated hydrogen bonds on occasions the nomenclature D-H $\cdots$ A<sub>1</sub>(A<sub>2</sub>) will appear, showing the second acceptor atom in brackets. Bifurcated hydrogen bonds are normally asymmetrical as it is uncommon that the two acceptor to hydrogen distances are the same. The dominant acceptor to hydrogen interaction, referred to as major component, has the shorter H $\cdots$ A distance and generally a larger D-H $\cdots$ A angle (i.e. closer to  $180^\circ$ ). The other A $\cdots$ H bond can be referred to as the minor component, generally with a longer bond length and smaller angle. In comparison to the classical hydrogen bond the bifurcated hydrogen bond generally has a major component that is equivalent in strength to a moderate hydrogen bond, and a minor part that is either moderate or weak in nature. This appears to be influenced by the fact that a majority of BHB are formed in acceptor-rich complexes where the second acceptor weakens the dominant interaction. For ease of comparison we will introduce the phrase “level of bifurcation” which is a rough classification of the ratios between the major and minor parts of the BHB. A highly (symmetrical) BHB would have almost equal major and minor parts and a weakly (asymmetrical)

bifurcated bond would represent the case where the BHB is made up of a very strong major component and a weak minor component.

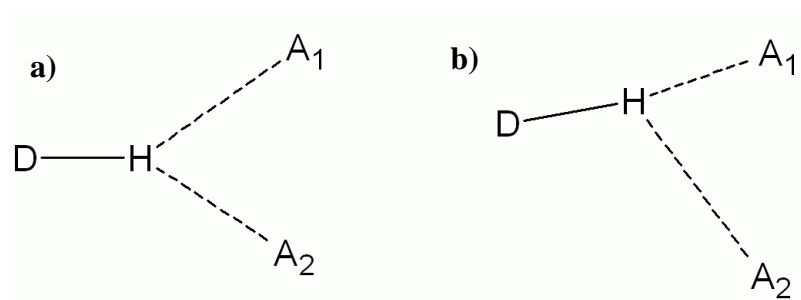


**Figure 1.3** Representation of **a)** highly BHB (symmetrical), **b)** weakly BHB (asymmetrical) with major and minor components.

This latter case could be better described as a classical HB having a very weak interaction with an additional acceptor, i.e. it is on the margin of what would be described as a BHB. The BHBs associated with one of the hydrogen-bond rich molecules studied in this work, involving chloranilic acid (**Chapter 8 and 9**), are in general highly bifurcated with some containing BHBs that have dominant and minor parts and some that are nearly equal. Bifurcated bonds can be a mixture of intra- and intermolecular bonds and evidence of this was seen from IR spectroscopy as long ago as 1969<sup>15</sup> in naphthoquinone. Another typical situation in which combined intra- and intermolecular BHB is often present is in a parallelogram shaped formation, where two BHBs are involved. This situation is relatively common especially with compounds that have the acceptor and donor atoms close together on the same molecule; the two bifurcated hydrogen bonds can share the same hydrogen acceptor atoms although the major and minor components are reversed thus forming the parallelogram shape<sup>16,17</sup>. This is shown in **Figure 1.4** in the structure of 2,3,4,5-tetrafluoro-N-(4-fluorophenyl)-6-hydroxybenzamide.

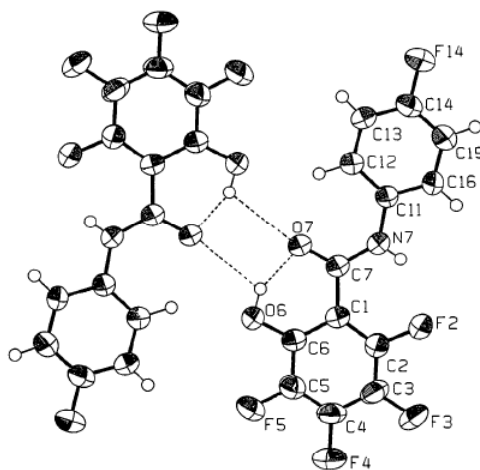


**Figure 1.4** Two bifurcated hydrogen bonds forming a parallelogram shape in the crystal structure of 2,3,4,5-tetrafluoro-*N*-(4-fluorophenyl)-6-hydroxybenzamide.<sup>16</sup>

The overall description of a BHB can be very varied, it can involve many atom types; intramolecular or intermolecular components; varying bond lengths and angles of both the major and minor parts; planarity; and any proton disorder that may be present.

### 1.2.3 Potential energy wells, proton disorder and migration

Since we are frequently looking for disorder or other “anomalous” behaviour in the hydrogen-bonded systems of interest in the type of work presented here, extensive use is made of difference Fourier maps generated in the plane of the hydrogen bond. Fourier maps are a schematic representation of the density (electron density in the case of X-rays diffraction) produced using the observed structure factors ( $|F_o|$ ) and the calculated phases for the current model. Difference Fourier maps are a schematic representation of the electron density not accounted for by the model, using the difference in structure factors ( $|F_o| - |F_c|$ ) and the phases from the model. Any disorder present in hydrogen bonds can be visualised using a difference Fourier map where the hydrogen under investigation has been removed from the model prior to calculating the map. In the first instance, these difference maps are calculated from X-ray diffraction data, as an initial diagnostic. If there is any hydrogen disorder or other anomalous effects present it will show up in distinct ways depending on the nature of potential energy surface governing the hydrogen bond, e.g. elongation of the

electron density associated with the H atom, or the presence of secondary sites. As an illustration **Figure 1.5 left** shows the X-ray difference Fourier map of 2,4-dihydroxybenzoic acid<sup>18</sup>. The hydrogen atoms show up as peaks while the two H atoms involved in the dimeric hydrogen bond show some indications of small secondary positive density peaks, often used as an indication of possible disorder and encouraging further diffraction investigation. The neutron difference Fourier map of the same material in fact reveals regularly shaped circular minima for the hydrogen atoms (hydrogen has a negative neutron scattering factor), ruling out the possibility of disorder.

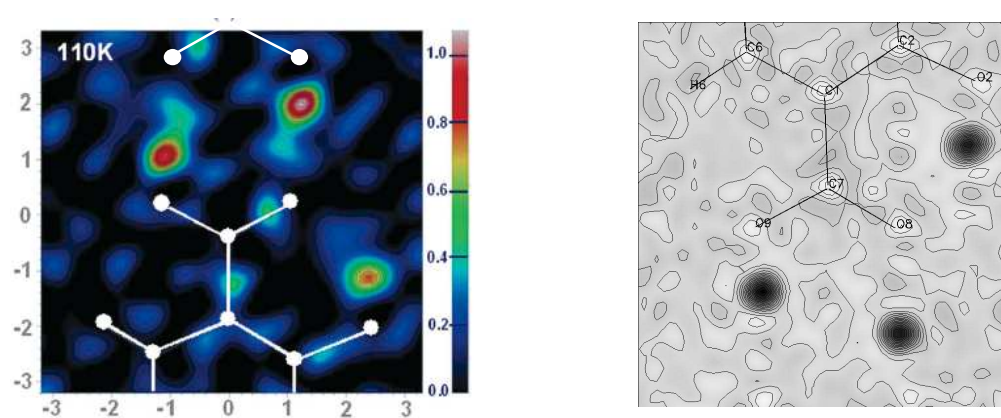


**Figure 1.5 Left:** 2,4-dihydroxybenzoic acid, X-ray difference Fourier map in the plane of the molecule showing small secondary density peaks that could be indicative of potential disordered hydrogen secondary sites, **Right:** Neutron difference Fourier map proves that there is no disorder in the proton position in this case; the apparent weak features in the X-ray map are attributable to noise or polarisation of the electron density towards the acceptor atom, a consequence of the relative difficulty in accurately locating hydrogen from X-ray data.

Potential energy surfaces bear resemblance to a geographical landscape, with maxima, minima, and saddle points dictated by the electrostatic nature of the atoms. A one-dimensional representation can be used to show the energy minimum in a covalently bonded atom-pair with the parent atom at the origin (**Figure 1.6**). Very close to the parent atom to which the subject atom is bonded, there is a large repulsive force, hence a large potential. Near the ideal bond length between the pair of atoms is the minimum and as the subject atom is moved further away the potential converges on the value for the two atoms being dissociated. Potential energy wells can be used to

represent the probability density of hydrogen in a hydrogen bond<sup>19</sup>. The minimum in the potential energy well corresponds to the equilibrium position of the hydrogen, with additional vibrational modes able to occupy more extended regions of the potential caused by increased temperature, etc.

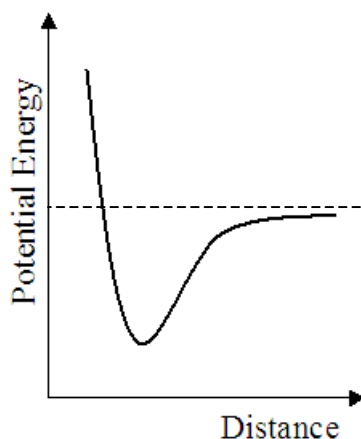


**Figure 1.6** The potential energy profile for an atom bonded to another located at the origin of the plot.

The potential energy surface describing a hydrogen atom in a hydrogen bond is different from this because it is interacting with two atoms. In **Figure 1.7** three possible hydrogen bond potential wells are shown; an asymmetrical double minimum, a symmetrical double well, a flat-bottomed single well.

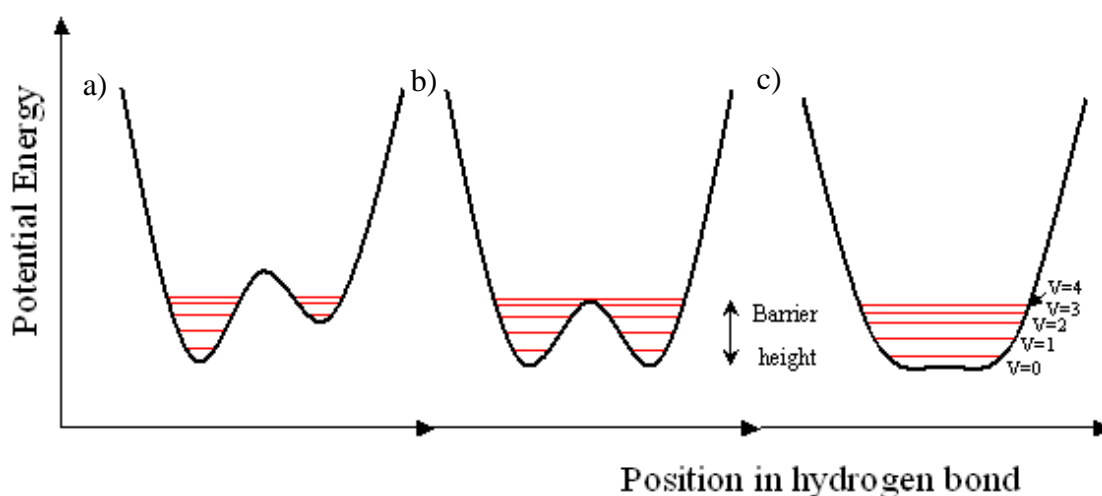


**Figure 1.7** Different types of hydrogen bond potential: a) asymmetrical double minimum, b) symmetrical double well, c) flat bottomed single well.

The unsymmetrical double minimum is the standard type for hydrogen bonds, where a second high energy minima is present due to the acceptor atom, although this is normally not occupied by the hydrogen atom. The symmetrical double well is essentially a special case of the double minimum, where the two minima have equal energy. Where the potential energy curve of the hydrogen bond has a double well potential, the proton can occupy both minima, but generally only one is populated. In some cases, particularly where the local environment is fairly symmetric, these two positions can be so close in energy that both are partly occupied with populations that change with varying temperature. As the vibrational modes increase in energy the second minimum can become accessible and the equilibrium level of occupancy of the higher energy minimum is governed by Boltzman statistics. Disordered hydrogen bonds with a second occupied hydrogen site are possible in both the symmetrical and unsymmetrical double potential wells.

A flat-bottomed single well arises when the two wells of the double well potential merge and the barrier height becomes very low (low barrier hydrogen bonds - LBHBs). Such energy profiles make it possible for the hydrogen to travel between the donor and acceptor atoms with only a small increase in energy. This type of potential also facilitates proton migration, as the equilibrium position for the hydrogen can move towards the middle of the potential well with the energy gained from increased temperature<sup>20,21</sup>.

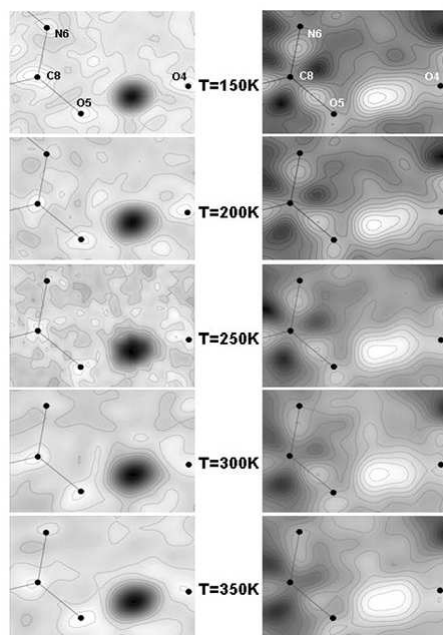


**Figure 1.8** Difference Fourier maps for urea-phosphoric acid showing migration of the proton toward the centre of the bond. **Left:** neutron **Right:** X-ray<sup>22</sup>.

Both X-ray<sup>23</sup> and neutron diffraction can be used to probe proton migration but the resulting images can be very different as the two techniques probe different aspects of the atoms involved. The structure of urea-phosphoric acid<sup>24</sup> shows migration within the hydrogen bond but the effect on the nuclear density, although definitely present, is less pronounced than that for the electron density. In **Figure 1.8 (Right)** the X-ray difference Fourier maps show that at 150 K the density associated with the hydrogen bonded hydrogen atom is positioned near O5 with a slight elongation of the density peak. As the temperature is increased the electron density peak is clearly moved towards the acceptor oxygen O4 and the shape becomes elongated; this represents the evolution of the electron density as the nature of the hydrogen bond changes slightly. On the **Figure 1.8 Left** the neutron data shows the same signs of the migration but the movement of the hydrogen nucleus probed by the neutron experiment is far less pronounced<sup>22</sup>.

The straightforward explanation for many of the observed examples of anomalous hydrogen atom behaviour can be related to the increasing ability of the H atom to explore different parts of the hydrogen bond potential as the temperature increases. However, because the hydrogen bond potential energy surface is also dependent on all

the atoms in the structure, and thus on lattice expansion as the temperature is raised, the nature of the HB potential well might itself change.

The acid dissociation constant  $K_a$  gives a measure of how easy it is to remove the hydrogen from an acid,  $HA \rightleftharpoons A^- + H^+$

$$\text{Equation 1.1} \quad K_a = \frac{[A^-][H^+]}{[HA]}$$

Where  $[HA]$ ,  $[A^-]$  and  $[H^+]$  are the equilibrium concentration of acid, deprotonated acid (base), and the hydrogen ion respectively. The  $pK_a$  value is  $-\log_{10} K_a$  and is a measure of the strengths of acids and bases. Large values indicate weak acids, meaning it is more difficult to remove the hydrogen atom.

The  $pK_a$  value of hydrogen bonded molecules becomes an important consideration when examining hydrogen bonding, because of its influence in the positioning of the proton in the interaction. There is a great interest in proton transfer and associated charge transfer, so being able to predict whether the proton will be on the original donor or be transferred to the acceptor atom by examining  $pK_a$  value is a useful tool. Where the  $pK_a$  of one molecule is much higher than that of the other, a strong case can be made for expecting the proton to be bound to the molecule with the higher  $pK_a$  value. Where the  $pK_a$ 's of the two molecules involved are of close or equal value the situation is not so clear and it has been postulated that H disorder, with the proton shared over two sites, is likely (double minimum potential well) this is referred to as  $pK_a$  matching. Liquid  $pK_a$  matching has been shown to be very reliable and in cases these  $pK_a$  trends can also be useful in the solid state i.e. crystals, although a lot of other factors are involved in the solid state. In strong hydrogen bonds the two minima can merge, resulting in a single flat bottomed well where temperature effects can be important, with the possibility of temperature induced hydrogen migration. This proton, and hence charge, transfer leads to potential application of materials exhibiting this phenomenon as molecular switches, thermochromic materials, temperature/pressure sensors.

### 1.3 Crystal engineering – designing and tuning intermolecular interactions

Crystal engineering is the design and synthesis of molecular solid-state structures exhibiting a desired motif or large-scale structural architecture with the aim of controlling physical and chemical properties. There are two main strategies adopted in this field; one based around non-covalent intermolecular forces with hydrogen bonding being the most important; the second, coordination complexes. Intermolecular forces can be used where combinations of functional groups on either separate or the same molecule form preferred interactions allowing the molecules to be joined together in a predetermined manner<sup>25-28</sup>. Coordination complexes can be produced with metal centres holding the complex together and/or metal clusters formed, for example metal-organic frameworks (MOFs)<sup>29,30</sup> and polyoxometalates (POMs)<sup>31,32</sup>.

Ab initio prediction of a crystal structure is extremely difficult, although some success has been achieved by computational methods working on simple single molecule systems or on simple complexes<sup>33,34</sup>. Predicting how molecules will pack, orientate and interact in complex systems is presently computationally a very demanding and time-consuming process, and currently not viable on any significant scale. To design a crystal structure with desired interactions or architecture we therefore have to use trial and error methods and construct from smaller fragments. Structural motifs can be used as building blocks (or supramolecular synthons) to try to reduce the task of crystal engineering to that of manipulating small fragments. The structural motifs that can be used are those that repeatedly reoccur and show the same interactions of particular molecules or functional groups, for instance hydrogen bonded ladder motifs displayed by amides<sup>35</sup>. Sometimes the motif can be tuned, so over a range of similar molecules a variety of systems can be arranged, for example isonicotinamide adducts. In a more complex form this could be regarded as equivalent to nucleotides forming DNA, or amino acids forming proteins, where each chain is made up of the building blocks with consistent HB or conformational properties.

### 1.3.1 Molecular complexes and supramolecular synthons

Supramolecular synthons are used as building blocks in crystal engineering, allowing either structural components or properties to be built into a material. Knowing that certain chemical groups or systems interact in a consistent way to form bigger systems allows a crystal to be designed from smaller components. Molecular complexes that contain hydrogen bonding acceptors and/or donors that form specific hydrogen bonding motifs are very useful in this manner, as they can be used to join the material together in a self-assembled way.

Strong or even bifurcated hydrogen bonds are also good for this type of application as they have geometric restraints that could be said to be predictable, although this is not always the case. One of the main materials studied in this work, chloranilic acid, forms bifurcated bonds with pyridine molecules sufficiently reliably that it has become championed by several groups for use in crystal engineering<sup>36-40</sup>.

### 1.3.2 Co-crystallisation

Crystal structures containing two types of molecule can be referred to as a co-crystal or molecular complex. There are many reasons for incorporating more than one chemical into a crystal and the process is used in a wide range of industrial and research areas.

In the pharmaceutical industry co-crystals are used to change physical properties such as solubility, melting & boiling points, taste, colour and many others. Compounds that would make potential drugs but fail to be soluble in the body, form pills or are not transported to the required area of the body, are routinely screened for co-crystals to see if their physical attributes can be altered while retaining the biological activity of the drug component. A growing area in co-crystal use is in forming polymorphs of known and patented active pharmaceutical ingredients (APIs); one reason for this is the possibility to avoid breaching patent laws if it can be proved a new preparation method is different to the documented scheme. The food industry uses co-crystallisation<sup>41</sup> for encapsulating flavours into manageable forms; this can be used for processes such as making sweets taste of orange. A range of studies have examined co-crystals that melt at low temperatures, for example pyrazine and n-alkyl

carboxylic acids<sup>42</sup> studied using *in-situ* crystal growth. Approaches such as these open up the possibilities of seemingly unlimited numbers of co-crystalline molecular materials, with varied qualities that can be exploited for many new uses.

Co-crystallisation in crystal engineering has seen a large increase in applications, where combinations of molecules can be used to create desired motifs or structures in the crystalline form. The use of multi component crystallisations for crystal engineering has increased exponentially in recent years, with attempts to form molecular materials for nanotechnology, catalysis, and as molecular complexes for storage devices for hydrogen fuel cells, along with many other applications.

Getting the right combinations of molecules is the key to successfully using multi-component crystallizations in crystal engineering. Many combinations either only produce crystals of the separate materials or no crystalline solid at all. Combinations that do interact often require the right conditions (for example temperature and solvent) before they will grow a co-crystal. Some combinations can form in stoichiometric variations containing different ratios of each component (2:1, 1:2, 3:1, 3:2, etc). Although determining the starting environments to achieve the desired product can be haphazard, trends in results can often be used in deciding compounds and conditions to gain the desired structure. The formation of such complexes also has to be reliable enough to prevent other interactions dominating and preventing the required synthon from forming, and when made, robust enough to prevent it being destroyed.<sup>35</sup>

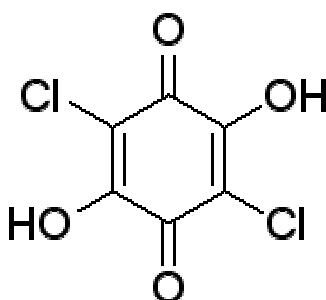


**Figure 1.9** Schematic diagram of chloranilic acid.

In this research the focus is on hydrogen bonding, with chloranilic acid (**Figure 1.9**) the main target molecule for creating new co-crystallised molecular complexes. Combining chloranilic acid with pyridine derivatives can be shown to form bifurcated

hydrogen bonds (BHBs) and hydrogen bonded units in a predictable manner. The hydrogen-bonded units can then be used as supramolecular synthons, from which large-scale structural systems can be extrapolated by the formation of chains or 2D sheets.

#### **1.4 General approach**

The number of combinations of different conditions under which crystallisation can be attempted are essentially infinite. It would be impractical to screen even a fraction of these possibilities in the search for the right conditions under which a co-crystal or polymorph will form. To reduce the number of possibilities, choices of the important or most representative conditions have to be made. Often used variables are solvent, temperature, ratios of reactants, and evaporation surface.

An initial characterization of the samples is required with many crystalline materials being grown. Screening to see if new forms of co-crystals or polymorphs are present and separating them from those already known is not always possible through visual examination. Most samples result in a powder, or a powder can be easily made, so a quick way to identify the material is to use powder diffraction or differential scanning calorimetry (DSC). Comparing the powder spectra with those of the original samples, or of known complexes of the components used, can be done using programs like polySNAP<sup>43</sup>, where similar patterns are grouped together and samples with large differences, that indicate potential new materials, are highlighted.

New complexes that are identified can then be examined using single crystal X-ray diffraction which provides accurate structural information. Multiple temperature studies can show the evolving hydrogen bond in a qualitative way and give information about the environment of the interaction. Those of interest can then be taken forward for neutron experiments to gain extra insight into the hydrogen behaviour. Computational studies are another possibility, able to examine some features that are not easily accessible through physical experimental work (extreme temperature, pressure or materials that form micro crystals).

Materials used throughout the project have been selected either because of their potential to show interesting hydrogen bonding, or their ability to co-crystallising with chloranilic acid. All the chemicals and substances were purchased from suppliers then either recrystallised individually in solvent or dissolved in solvent and combined in attempts to grow co-crystals. Whilst individual techniques provide answers on certain parts of the investigation, the combination of experiments carried out complement each other, showing a fuller picture of the materials and interactions under study.

## 2. Theory

### 2.1 Crystallography

Crystallography<sup>44,45</sup> is the analysis of crystalline solids using a beam of either electromagnetic radiation or particles to determine the structure of the material via diffraction - a form of elastic scattering. The most common type of diffraction experiment is carried out with X-rays although neutrons and electrons are also used. Neutron diffraction is less common because of the special facilities needed and electron diffraction is more of a surface probe. Each technique works on the same diffraction theory but each has different advantages and disadvantages, providing complementary information on different aspects of the crystal structure. Crystals are solids that consist of a three-dimensional lattice of a motif arranged in an ordered, repeating manner. The crystal has translational symmetry with the basic unit (unit cell) repeating essentially infinitely in all directions. The diffraction from each unit cell accumulatively amplifies the signal, allowing a diffraction pattern to be measured. Mathematical manipulation of the intensities of the diffraction pattern enables the structure to be determined.

X-ray, electron, and neutron diffraction are very different to each other mainly due to how each interacts with matter. Electrons are charged particles and interact with the electron cloud of molecule via the Coulomb force. This is a strong effect and in probing a bulky sample they do not penetrate as deeply as X-rays. X-rays are electromagnetic radiation and are also primarily scattered by the electrons of the atoms. Their wavelength is within the Ångstrom range, which is the same order of magnitude as bond lengths and therefore, ideal for studying molecules. Neutrons are neutral particles so have no electrostatic interactions with the electrons of the atoms; instead they are diffracted by the nuclei (core of protons and neutrons), mainly via the strong force. Despite being uncharged, they carry a spin and therefore can interact with magnetic moments revealing the magnetic structure. The nucleus of an atom is tiny in comparison to that of the volume covered by the electrons, so neutrons travel much further through crystals than X-rays or electrons thus probing the bulk of the material, but requiring larger samples.

X-ray diffraction is a technique that is routinely carried out with laboratory sources making it a relatively inexpensive and accessible resource. Powder diffraction is generally used for sample characterisation, although advanced techniques can allow structure determination from powder data on some occasions. Neutrons can also be used for both powder and single crystal diffraction but because of the large facilities required these are much less common, with only one source in the UK. Powerful X-ray beams can be produced at synchrotron sources. With these it is possible to do more exotic experiments or push the limit that is possible in terms of smaller crystals or larger unit cells, for example in protein crystallography. Synchrotron radiation requires large facilities, similar to the scale of neutron facilities, and again has a limited availability.

## 2.2 Theory of diffraction

Much of the theory behind crystallography and crystal structure was known well before it was measured experimentally on crystalline materials, from the diffraction of light and mathematical models of theoretical lattice packings. With the discovery of X-rays in 1895 by Röntgen<sup>46</sup>, followed by Von Laue demonstrating that crystals could diffract X-rays in 1912<sup>47</sup>, the first important stages of practical crystallography had been established. The first structure solution followed in 1913, with the structure of table salt<sup>48</sup>, but it was not until 1923 that an organic molecule was solved<sup>49</sup>. From these initial experiments the large field of crystallography has emerged, both in its own right as an important research tool, but also as a complementary technique to other work in areas such as chemistry, biology, earth sciences, and physics. Diffraction methods are often utilised to determine the crystal structure of materials, distinguish between compounds, determine purity and gain a greater insight into the bonding involved.

### 2.2.1 The lattice

A crystal can be represented by an array of identical points (lattice points) formed by applying translational symmetry, with each point the position on which a repeating pattern (the unit cell) is placed. Wallpaper is a two dimensional example, where a

flower or another pattern represents the unit cell and by repeating this horizontally and vertically the entire pattern can be produced. All unit cells have a shape of a parallelepiped defined by six parameters; the lengths  $a$ ,  $b$ ,  $c$  and angles  $\alpha$ ,  $\beta$ ,  $\gamma$ . There are seven varieties of crystal systems depending on the unit cell parameters and symmetry:

*Table 2.1 Unit cell types with length and angle associations indicated and possible Bravais lattices.*

<b>Triclinic</b>	$a \neq b \neq c$	$\alpha \neq \beta \neq \gamma \neq 90^\circ$	<b>P</b>
<b>Monoclinic</b>	$a \neq b \neq c$	$\alpha = \gamma = 90^\circ \beta \neq 90^\circ$	<b>P + C</b>
<b>Orthorhombic</b>	$a \neq b \neq c$	$\alpha = \beta = \gamma = 90^\circ$	<b>P+C+F+I</b>
<b>Tetragonal</b>	$a = b \neq c$	$\alpha = \beta = \gamma = 90^\circ$	<b>P+I</b>
<b>Cubic</b>	$a = b = c$	$\alpha = \beta = \gamma = 90^\circ$	<b>P+I+F</b>
<b>Trigonal</b>	$a = b \neq c$	$\alpha = \beta = 90^\circ \gamma = 120^\circ$	<b>R</b>
Or	$a = b = c$	$\alpha = \beta = \gamma < 120^\circ$	
<b>Hexagonal</b>	$a = b \neq c$	$\alpha = \beta = 90^\circ \gamma = 120^\circ$	<b>P</b>

**P**=primitive, **C**=centred, **I**=body-centred, **F**=face-centred, **R**=rhombohedral

In some cases it can be convenient to define the unit cell to contain more than one lattice point so as to convey the symmetry better. These come in the forms of Centred (C), Body-centred (I), Face-centred (F), and Rhombohedral (R) lattices although only certain combinations can arise, forming 14 associated Bravais lattice possibilities (*Table 2.1*). The asymmetric unit is the most basic repeat unit, and represents the smallest motif which when acted upon by a symmetry operation within the unit cell produces the unit cell contents and therefore the entire crystal when the translational symmetry is applied. 32 point groups are possible from combinations of all the internal rotation and reflection elements with the 14 Bravais lattices. These symmetry elements combined with the translational elements available in three-dimensional space leads to 230 possible space groups to which all crystals belong.

### 2.2.2 Diffraction

When atoms in a crystal diffract X-rays, the pattern produced is a series of spots, with their positions and intensities determined by the crystal symmetry and contents. The spots form from the constructive and destructive interference of the X-rays with each other, forming a 3 dimensional reciprocal space pattern through which 2 dimensional slices are measured using area detectors in a diffraction experiment. The reciprocal lattice represented in reciprocal space has dimensions of  $a^*$ ,  $b^*$  and  $c^*$  where:

$$\text{Equation 2.1} \quad a^* = (\underline{b} \times \underline{c}) / V \quad b^* = (\underline{c} \times \underline{a}) / V \quad c^* = (\underline{a} \times \underline{b}) / V$$

and  $V$  is the volume of the unit cell.

Miller indices ( $hkl$ ) representing planes through the unit cell, correspond to fractional intercepts of a plane cutting through the unit cell with the axes at  $(1/h, 1/k, 1/l)$ . Each spot in the diffraction pattern can be assigned a set of Miller indices determined from the position that the spot is located on the detector, given the knowledge of the unit cell dimensions and the diffractometer geometry. Depending on the symmetry of the system and the data collection strategy there can be several equivalent spots measured in different locations in the data set.

### 2.2.3 Bragg's law

A convenient way of visualising diffraction is through the Bragg construct. Bragg showed that the crystal could be thought of as a series of parallel planes from which the incoming beam is scattered. A diffraction spot is only produced when the diffracted beams from each layer are in phase, leading to constructive interference. It follows that the path difference between two diffracted beams must be equal to an integral number of wavelengths for a diffraction event to be detected.

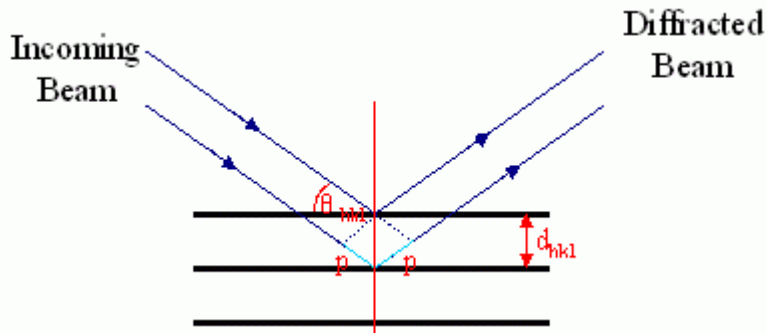


**Figure 2.1** Bragg's construct showing the additional path distance undertaken by the lower beam.

**Figure 2.1** shows that the path difference ( $2p$ ) for the two incoming beams can be calculated from the angle of incidence of the beam  $\theta_{hkl}$ , and the distance between the planes of the crystal,  $d_{hkl}$ . Hence Bragg's equation can be derived:

$$\text{Equation 2.2} \quad p + p = n\lambda = 2d_{hkl}\sin\theta_{hkl}$$

where  $n$  is an integer, and  $\lambda$  the wavelength of the incoming wave.

#### 2.2.4 The Ewald sphere

The Ewald sphere is another important visualisation tool for determining the location of the Bragg spots. A circle is drawn of radius of  $1/\lambda$  around the crystal (C) such that its edge sits on the origin of the reciprocal lattice (O). From Bragg's law a beam is scattered by the crystal as shown, and crosses at point P on the sphere. From **Figure 2.2** we see that a diffraction spot will be observed if the scattering vector is equal in length to the distance and in the same direction as a vector OP, from the origin to P the reciprocal lattice point. So to satisfy Bragg's law, the reciprocal lattice point must touch the surface of the Ewald sphere. The crystal orientation can be changed to measure the required lattice positions.

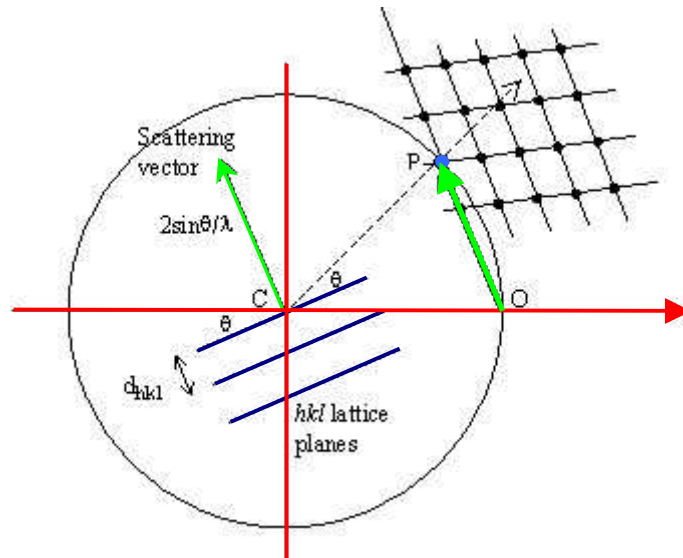


**Figure 2.2** Ewald circle with parallel planes representing Bragg's law. A reciprocal lattice point can only be observed if it occurs on the circumference of the circle and at the scattering vector from the origin. In 3 dimensions a sphere is formed. Adapted from Wilson 2000<sup>45</sup>

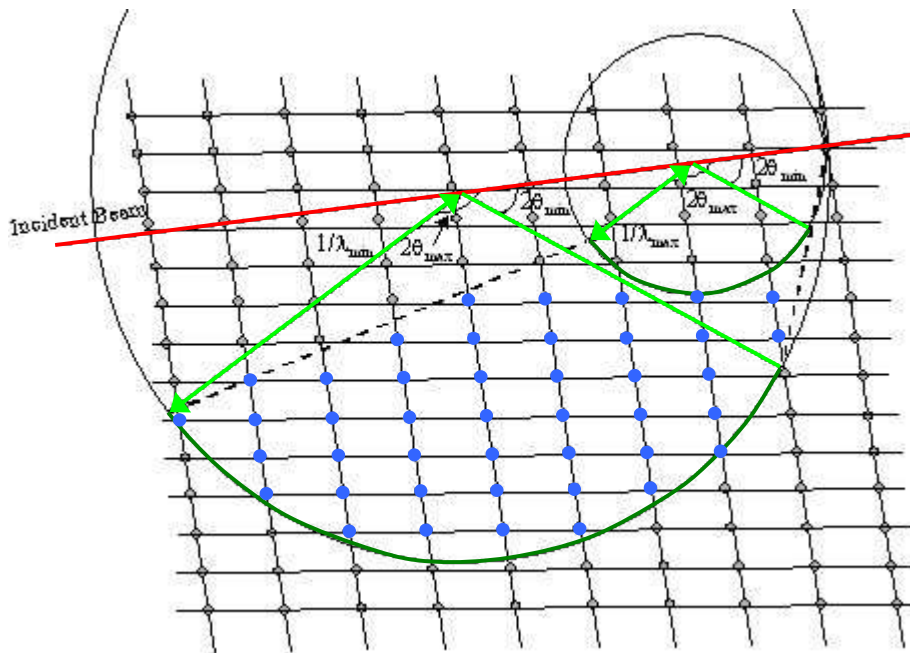


**Figure 2.3** Ewald diagram for a (time-of-flight) Laue diffraction experiment with only one detector. The observed reciprocal lattice points (marked in blue) are limited by the wavelengths used, (area between Ewald circles) and the detector coverage (for each wavelength arc marked in green and over all enclosed by dotted lines). Adapted from Wilson 2000<sup>45</sup>

If a different wavelength is used the size of the Ewald sphere will change, with larger  $\lambda$  producing smaller spheres (**Figure 2.3**). This allows experiments using a range of wavelengths to measure sections of reciprocal space (in the context of the work presented here this is especially applicable to time-of-flight Laue neutron diffraction) containing many lattice points in one image with a stationary detector and crystal.

### 2.2.5 X-ray Data collection

The collection of a data set for structure determination first requires determining the unit cell and space group of the crystal. The geometry of the reciprocal space pattern is related to the lattice and unit cell geometry, the pattern's symmetry is related to the symmetry of the Bravais lattice, and the intensity of the spots is related to the contents of the unit cell. The vectors between spots can therefore be used to work out the unit cell dimensions, with equivalent lengths, and angles of  $90^\circ$ , giving clues to the Bravais lattice. An estimation of the space group can be made by examining the symmetry of the pattern and systematic absences amongst the Bragg reflections, although if there is any doubt a lower symmetry group would be used in determining a data collection strategy as choosing too high a symmetry will lead to insufficient reflections being measured. A strategy for the data collection can be determined using the diffractometer software, positioning the detector and sample to measure the required positions using the pattern calculated from the unit cell dimensions and the geometry of the crystal mounted on the diffractometer. A diffraction pattern always has inversion symmetry so only a hemisphere of data ever has to be measured to ensure all unique reflections are accessed. Cells with more symmetry need even less; a monoclinic cell needs less data than a triclinic one, with orthorhombic and higher symmetries requiring even less.

### 2.2.6 Fourier synthesis

The intensity ( $I_{hkl}$ ) of each reflection is measured along with an error value ( $\sigma(I_{hkl})$ ) and these are written into an *hkl* file where they are all assigned Miller indices from their position. Transferring between reciprocal space, where the reflections are observed and real space (the crystal structure) can be achieved mathematically by carrying out a Fourier transform. Using Fourier transforms it is possible to transfer

between the diffraction pattern to the electron density and therefore it should be possible to produce a model of the crystal structure.

The intensities of the spots in the diffraction pattern are determined by the unit cell contents (atoms) as well as by other factors determining the diffraction quality (mosaicity, crystal quality, absorbance, size...) of the crystal and are quantified by the structure factor  $F(hkl)$ . (The intensity  $I_{hkl} \propto F_{hkl}^2$ )

$$\textbf{Equation 2.3} \quad |F_{hkl}| \propto \sqrt{I_{hkl}}$$

The structure factor can be defined as the Fourier component at each reciprocal lattice point  $hkl$ , expressed as:

$$\textbf{Equation 2.4} \quad F(hkl) = \sum_{j=1}^N f_j \exp[2\pi i(hx_j + ky_j + lz_j)]$$

where the summation is over the N atoms in the unit cell, with atom j having the atomic scattering factor  $f_j$  located at position  $x_j, y_j, z_j$ .

Several factors affect the structure factor including the atom types present in the crystal, and the Debye-Waller temperature effect. X-rays are diffracted from the electron density in the crystal and are therefore diffracted by the heavier atoms to a greater extent (this is reflected in the value of  $f_i$ , the atomic scattering factor in **Equation 2.4**). The electron density in the unit cell can be expressed as:

$$\textbf{Equation 2.5} \quad \rho(x, y, z) = (1/V) \sum_{hkl} F(hkl) \exp[-2\pi i(hx + ky + lz)]$$

where  $(x,y,z)$  represent the fractional coordinates.

The Debye-Waller factor takes into account the effect of temperature on the intensities measured for each reflection. The thermal motion/vibration of the atoms reduces the intensities, due in part to a smearing of the electron density. This effect is not equal for all reflections, with those at larger Bragg angles affected more. The thermal vibrations have a small effect on reflections at small Bragg angle, but dominate reflections at high Bragg angle. This is easily taken into account in modern

refinement programs, by refining the average amplitudes of vibration of each of the atoms in the structure.

### 2.2.7 Structure solution

The solution of a crystal structure requires the determination of the structure factors, which contain both the intensity of the reflection and the phase of the diffracted wave.

$$\text{Equation 2.6} \quad F_{hkl} = |F_{hkl}| e^{i\alpha_{hkl}}$$

#### 2.2.7.1 The phase problem

Unfortunately the phase information is lost as only the intensity is measured in the experiment (equivalent to the modulus of the structure factor squared). Therefore it is not simply an inverse Fourier transform that needs to be performed, as only half the information is available. This is referred to as the phase problem. The quantity of data, with thousands of spots measured, prevents a trial and error approach being feasible (unless the phases from a similar system are previously known), although several very effective methods have been developed to solve the phase problem. The job is made slightly easier as it is known what to expect in the unit cell, with atomic positions at bond length distances apart, even if it is not known what molecules are present.

#### 2.2.7.2 Heavy atom method

The heavy atom method relies on using phases derived from one strongly scattering atom as a start to solving the whole structure. Even without phases a very large atom can be found in a map of interatomic vectors (a Patterson map) and from its position a set of starting phases can be produced. If the atom is much more strongly scattering than the rest of the atoms its phases can be employed to the whole structure as they dominate. As the model improves the phases also improve, so better detail can be seen in the Fourier map. The better Fourier map allows a better model with better phases and so on. After a few iterations with good data the full structure can be found and refined.

### 2.2.7.3 Patterson method

The Patterson method does not require phases at all, and deals with the intensities directly. A map of the interatomic vectors, similar to a Fourier map, is created with the height of the peaks relating to the scattering powers of the two atoms that the vector is between. The positions of any heavy atom present or significant structural components can be found and added to a model. With a starting model providing approximate phases the remaining atoms can be located with Fourier maps and the structure refined to completion.

### 2.2.7.4 Direct methods

Direct methods is the most widely used technique and is built into most of the structure solution programs. The method should lead directly from the intensities of the Bragg reflections to the phases. It is based on statistical relations found between the intensities and relies on various assumptions, for example that the scattering density is positive throughout. In one of these relations the reflections are grouped into threes where triplet relationships can be established relating the values of the three phases of the reflections involved in the triplet. Multiple iterations of possible deduced phase sets are tried (often several hundred) and from this the best solution is picked and a density map generated. This results in a list of peaks from which fragments of the structure can often be seen, either by the user or with additional refinements by the program. There are several variables that can be changed for direct methods to improve the possibility of getting a better solution. The two main variables are the number of triplet reflections relations used or the number of variations of phase relationships attempted, both increasing the chances of finding a solution although the time required for the calculation gets progressively longer. Direct methods have a very high success rate in solving small molecule structures and are by far the most common method used.

## 2.2.8 Structure refinement

After the basic framework or initial fragments of the structure have been found using one of the solution methods, a combination of Fourier maps and refinement is required to produce a complete model<sup>50</sup>. Using the calculated phases with the

measured reflection intensities, a map of the electron density can be calculated, which are referred to as Fourier maps, as already mentioned in *Chapter 1*.

$$\text{Equation 2.7} \quad \rho(x, y, z) = \sum_{hkl} |F_{hkl}^o| \exp(-2\pi i(hx + ky + lz) + \alpha_{hkl}^c)$$

with each new Fourier map a better model of the structure is created and this in turn improves the phases that are used for the next Fourier calculation, creating a cycle that if repeated homes in on a complete structure. In other words this Fourier recycling is an iterative procedure.

The positions of the atoms are the peaks on the Fourier map, but to model the structure correctly the description of the atoms needs be refined to give the model that offers the best possible fit to the observed data and also to include thermal displacement. Crystallographic structure refinement, varying the atomic (positional and thermal vibrational) parameters to achieve the best model, is carried out using least square methods. Even for a small molecule the number of parameters that require refinement can be large, and the ability to rate whether a change in a parameter carried out in the least squares procedure is correct is important. The R-factor (*Equation 2.8, 2.9*) is a rating of how good the structure model is, and generally reduces when the model improves. It is a gauge for comparing the data and model during the refinement process, and is a factor in determining whether the refined structure is publishable.

$$\text{Equation 2.8} \quad R = \frac{\sum ||F_0| - |F_c||}{\sum |F_0|}$$

$$\text{Equation 2.9} \quad wR2 = \sqrt{\frac{\sum w(F_0^2 - F_c^2)^2}{\sum w(F_0^2)^2}}$$

The R-factor can be used to assess the agreement between the measured structure amplitudes, and those calculated from the atomic positions of the model being refined. If the model exactly represented the structure, the R-factor would equal zero. This never happens, as there are always inherent errors in measuring the data, a truly

complete data set cannot be collected (truncation errors) and disorder or added complexity that cannot be modelled. The higher the value of the R-factor the worse the model and data match, so the lower the better with typical published data having R (*Equation 2.8*) around 0.02-0.07. The weighted R-factor (*Equation 2.9*) works in the same way but with weighting factors for the reflections based on the  $\sigma(F^2)$  values and using the squared values of the structure factor. The cycle of improvements to the structure generally follows the rule that a better model creates a better R-factor, with consequently better phases improving the Fourier map, in turn resulting in a better overall description of the scattering density defining the structure.

Another important value used for evaluating the model and data quality is the S-value, the goodness of fit:

$$\text{Equation 2.10} \quad S = \sqrt{\frac{\sum [w(F_{hkl}^o)^2 - F_{hkl}^c]^2}{n - p}}$$

where n is the number of reflections used and p the number of parameters refined.

In general for refinement the more successfully collected reflections the better the data set, providing more information to refine the structural model. As the number of parameters refined increases, more data is required, with a good ratio in a typical least squares procedure being around 1 parameter to 10 reflections, but higher preferably. Because the S-factor is dependent on these variables it acts as a deterrent against artificially manipulating the R-value by removing data.

### 2.2.9 Difference Fourier maps (Finding hydrogen)

Difference Fourier maps are scattering density maps that only show the density not accounted for by the model. These are especially helpful when looking for the hydrogen atoms (which can be hidden in normal X-ray Fourier maps, being overwhelmed by the larger surrounding atoms) or highlighting mis-assigned atoms and atoms that are not modelled well. This is achieved by subtracting the structure factors calculated from the model away from those measured and using the resulting differences with the phases calculated from the model, producing an electron density

map (*Equation 2.11*). Atoms not accounted for will show up as peaks in this difference Fourier map; if the wrong atom is used then either a peak will show that the atom was too small, or a trough that it was too large.

$$\text{Equation 2.11} \quad \Delta\rho(x, y, z) = \sum_{hkl} (|F_{hkl}^o| - |F_{hkl}^c|) \exp(-2\pi i(hx + ky + lz) + \alpha_{hkl}^c)$$

The background noise of Fourier difference maps originates from several sources: Fourier termination errors, thermal disorder (Debye-Waller effect) and electron density which is not taken into account in the atomic model, such as bond density and lone pairs. Truncation of data is always inevitable as it is not possible to collect to infinite resolution, but it is usually possible to collect to a small enough d spacing to achieve reasonable resolution and minimise these errors. Thermal motion is present in all atoms in the structure as they oscillate around their equilibrium positions, displacing more with increasing energy; this leads to a general smearing of the electron density in the map. The atoms are normally refined using simple ellipsoid models for these displacements, that do not take into account features such as anharmonic thermal vibrations, bond density, etc; the latter means that unaccounted density peaks normally arise between atoms especially in high resolution data sets when examining the difference Fourier maps.

### 2.3 Neutron diffraction (and reasons for its use in this work)

The focus of this work is on hydrogen bonding and determining the characteristics of the hydrogen atom(s) within them as a function of temperature, crystalline environment, polymorph, complex, etc. X-ray diffraction has been shown to be an extensively useful tool towards this aim but limits in its resolution in regards to hydrogen, due to its small scattering factor often prevent definitive results<sup>22,45</sup>. Neutron diffraction, on the other hand, is excellent at detection of protons/hydrogens even in situations where there is only partial occupancy. The reason for this difference is to do with the process by which diffraction occurs (electromagnetic (X-ray) vs. strong interaction (neutron)). X-rays are scattered by the electrons in atoms, so the scattering strength of an individual atom increases with its increasing atomic number (Z). The scattering intensity of X-rays is proportional to  $Z^2$  so small atoms

like hydrogen scatter far less than a heavier atom. (*Figure 2.4 Top*) When looking at hydrogen bonds, the hydrogen has a scattering intensity of 1 whereas the other atoms present, such as carbon, nitrogen or oxygen dominate the diffraction with relative scattering factors of approx 36, 49, 64 respectively. This is only for the case where the hydrogen position is fully occupied, so where there are disordered HBs, with only partial hydrogen atoms in the model, the ratio is even worse.

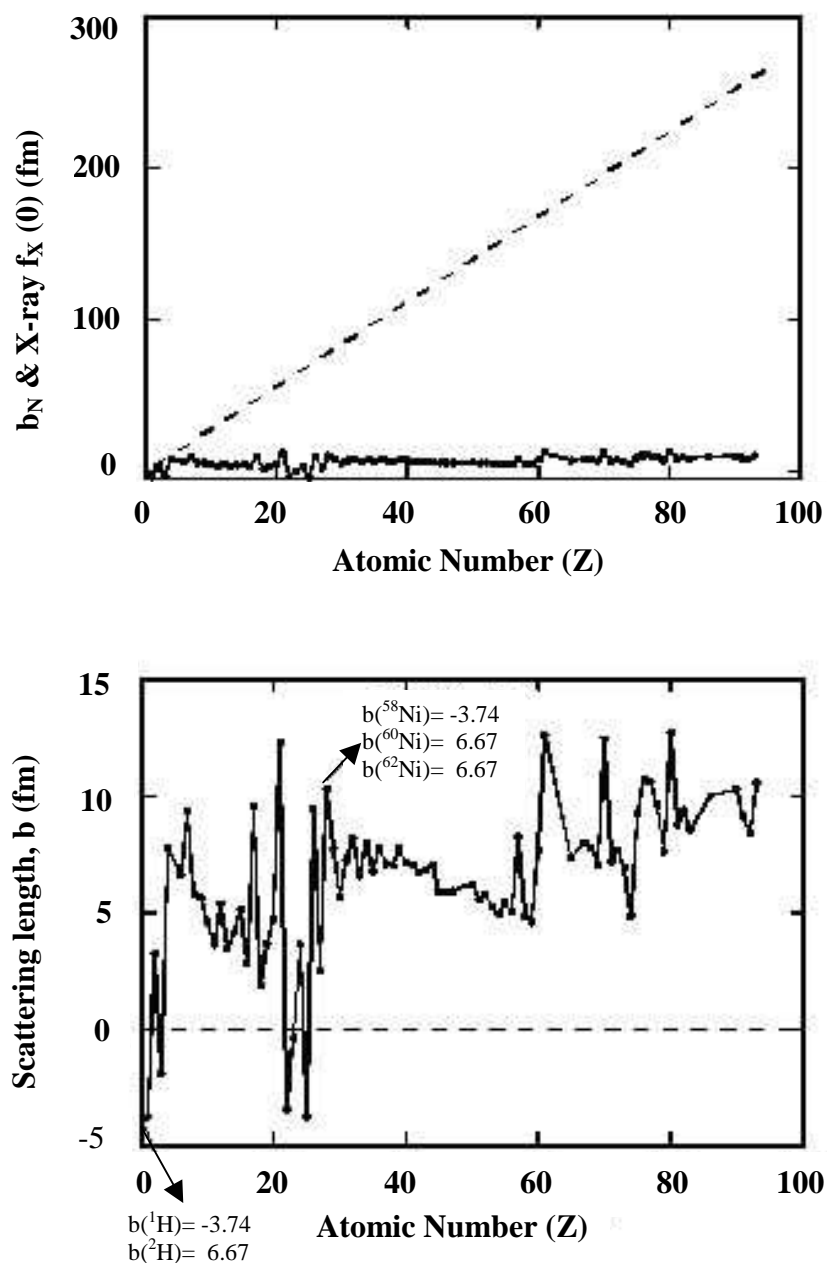


*Figure 2.4 (Top)* The X-ray scattering factors (shown with dotted line) compared with neutron scattering factors. (*Bottom*) An expanded view of the neutron scattering length versus Z (for the principal isotopes).<sup>45</sup>

The plot at the *Bottom* of *Figure 2.4* shows neutron scattering length versus  $Z$ ; of particular note is the fact that hydrogen has a negative scattering factor but is of comparable magnitude to the positive values of other elements like oxygen and carbon. The scattering factor of neutrons does not have the same systematic increase with  $Z$  as found for X-ray scattering. The neutron scattering factors do still have a dependence on  $Z$  because of the differing mixtures of protons and neutrons in the nucleus but this is a broadly random distribution of the scattering length with atomic number. (*Figure 2.4 Bottom*) This also means that the scattering length can be different (often substantially) for two isotopes which can be useful for instance when looking at hydrogen and deuterium. There is no systematic trend to the scattering length distribution but the values are of a similar order of magnitude, although this includes some negative values. For neutron diffraction studies of the type of organic molecular materials studied here, hydrogen, carbon, oxygen, and nitrogen have scattering lengths of -3.739, 6.6460, 5.803, and 9.36 fm respectively. The hydrogen atoms therefore have intensities just short of the other atoms although with a negative value. In Fourier density maps hydrogen therefore shows up as a trough of similar height (depth) to the peaks for other atoms. This results in a higher accuracy of the hydrogen position from neutron experiments (relative scattering of a hydrogen compared to a carbon with X-rays ~3%, neutrons ~32%).

Another problem with X-ray diffraction arises because there is a drop off in scattering factor with increasing scattering angle due to the large size of the electron density. Therefore it is difficult to obtain high-resolution data at large angles, which relates to short  $d$  spacing. Neutrons do not have this problem and do not show the same drop in scattering power with increasing scattering angle (although the thermal motion does effect the scattering at larger angles), making it easier to look at structures to very high resolution, although thermal effects do still have an effect on the intensity.

Neutron diffraction also has the advantage that elements that are next to each other in the periodic table can have substantially different scattering cross sections giving larger contrast than can be achieved by X-ray diffraction. A good example of this is iron +9.45 fm and manganese -3.73 fm. This also applies to isotopes, which can have very different scattering factors, allowing the use of isotopic substitution as a

technique. The most relevant in organic or biological work is hydrogen  $^1\text{H}$  and deuterium  $^2\text{H}$  with scattering factors of  $-3.74$  and  $6.67$  fm respectively. Substituting one isotope for the other can yield important structural information; this is commonly done with hydrogen and deuterium allowing a method called contrast variation to be employed.

In an ideal world, neutron diffraction would be the main diffraction technique for looking at hydrogen bonding. Unfortunately availability means that X-ray diffraction is most commonly used. X-ray diffraction is a standard technique, with in-house diffractometers common, whereas neutron facilities are large, expensive facilities of which there are a limited number worldwide. Neutron sources are normally national or even international facilities, which require very large budgets to build and run. The UK has a neutron source, ISIS, at the Rutherford Appleton Laboratory in Oxfordshire. Other facilities are available; the most relevant is the ILL in Grenoble which is partly funded by the UK as well as France, Germany and several other European countries. Despite having these two world-class facilities, it is hard to get time on the instruments with great competition especially as the low flux of neutrons requires long experiments. The utilisation is also limited by the need to grow rather large crystals, on account of the low available flux and high penetration of neutrons; crystal volumes needed for neutron diffraction are typically of order  $1\text{mm}^3$ , which it is not always possible to grow for the target sample.

Although both diffraction methods are useful in different situations, sometimes the best solution is to use a combination of both X-ray and neutron studies. A combination of both X-ray and neutron diffraction provides information on both the electron density and the nucleus position, giving a better overall picture of the structure and its interactions. The use of X-ray diffraction is essential as a precursor to neutron studies enabling the selection of materials that show promising behaviour to be chosen and reduces the number of null results (although null results can provide useful information and insight). The other benefit of having previous X-ray data is that it provides good unit cell parameters and approximate atomic positions as a starting point in processing and refining the neutron data.

## 2.4 Powder diffraction

Testing large collections of samples one by one using single crystal X-ray diffraction especially where multiple samples from the same vial need screening for the possible presence of new complexes or polymorphs, is a tedious task. A quicker method that also provides a more complete screening is powder diffraction, being able to test the material from a whole crystallisation experiment in one measurement without the need to find good quality crystals. Testing a powdered representative of the sample (including powder and crystals from all areas of the sample) can identify if new complexes and co-crystals have formed and identify new unit cells that could be of interest. Where single crystals are found their structures can then be determined using single crystal X-ray diffraction, while other techniques used to examine different aspects such as DSC, IR, and NMR, or theoretical calculations can also be used to gain additional information. If there is an interesting HB or suspected disorder in a HB, larger crystals are grown and the neutron experiment can be carried out to get a definitive answer.

X-ray powder diffraction provides a fast and reliable tool for routine identification of crystalline materials. Powder diffraction can be thought of as a reduced form of single crystal diffraction, where three dimensional reciprocal space is condensed into a one-dimensional pattern of intensity with  $2\theta$  angle. Instead of containing one crystal orientation the ideal powder sample has every possible crystallite orientation in equal quantities. The diffraction pattern for each crystal will be overlaid on to each other and therefore each Bragg reflection forms a circular band at a set  $2\theta$  angle.

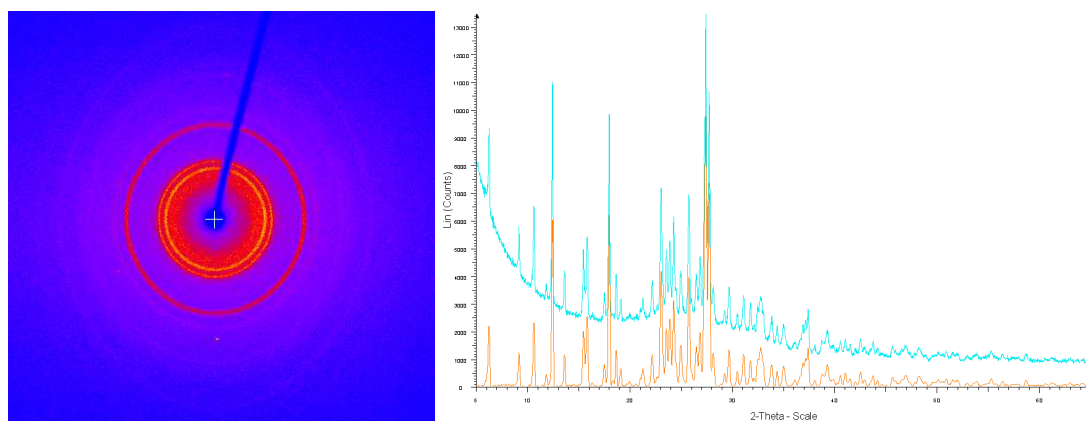


**Figure 2.5** *Left: Image of powder ring on an area detector* **Right: Powder pattern** formed integrating round the powder ring, (before (**blue**), and after (**orange**) background removed and pattern smoothed). Powder patterns can be used as a fingerprint for crystalline materials as each has a unique pattern.

Some of the problems powder data suffers from are accidental or exact peak overlap that obscures some of the peaks and finer detail as a consequence of the nature of the technique and often limited instrument resolution. The powder pattern still contains a lot of information, which can be used to characterise the sample. The peak positions are important in the 1D pattern and also their intensity and width. If the sample is of a single system (one crystal form) the peak position provides information on the crystal system, symmetry, and unit cell dimensions.

Peak intensities are affected by the unit cell contents, point group symmetry, and for multi-system samples the relative intensities give a quantitative measure of the different phases present. From the peak shape and width, information can be extracted on the size of the crystallites in the sample, and can show signs of any extended defects or strains. Broadening can be caused by instrumental effects (dispersion, divergence, detector resolution), crystal size, or strain and defects in the sample.

The majority of powder diffraction is used in fingerprinting and purity control, especially in the pharmaceutical industry where products are regularly screened to ensure each batch is the right mixture and does not contain any impurities. Programs

such as polySNAP<sup>43</sup> are able to match large quantities of powder patterns against each other or those from databases or calculated from single crystal structures.

Structure determination, refinement, and even solution is also possible from powder data, which can be important for samples where it is impossible to grow single crystals, or if they are inclined to twin. Rietveld methods have been developed that are able to reveal much structural information with relative ease in many cases<sup>51,52</sup>.

## **2.5 Differential scanning calorimetry (DSC)**

Differential scanning calorimetry is a technique to examine the thermal transitions of a compound and works according to the heat flow principle. Thermal transitions are those in which there is an energy exchange with the sample environment as it is heated. This includes glass transitions, phase transitions, melting, and recrystallisation. A few mg of the sample is placed in the sample pan and in parallel with an empty reference pan, they are then heated at a set rate. The difference in energy required to heat the sample pan compared to the reference pan is measured and plotted as the temperature is increased. The graph of the heat flow (representing the heat capacity of the sample) in relation to the temperature provides information on any endothermic or exothermic reaction or transition that the sample has undergone.

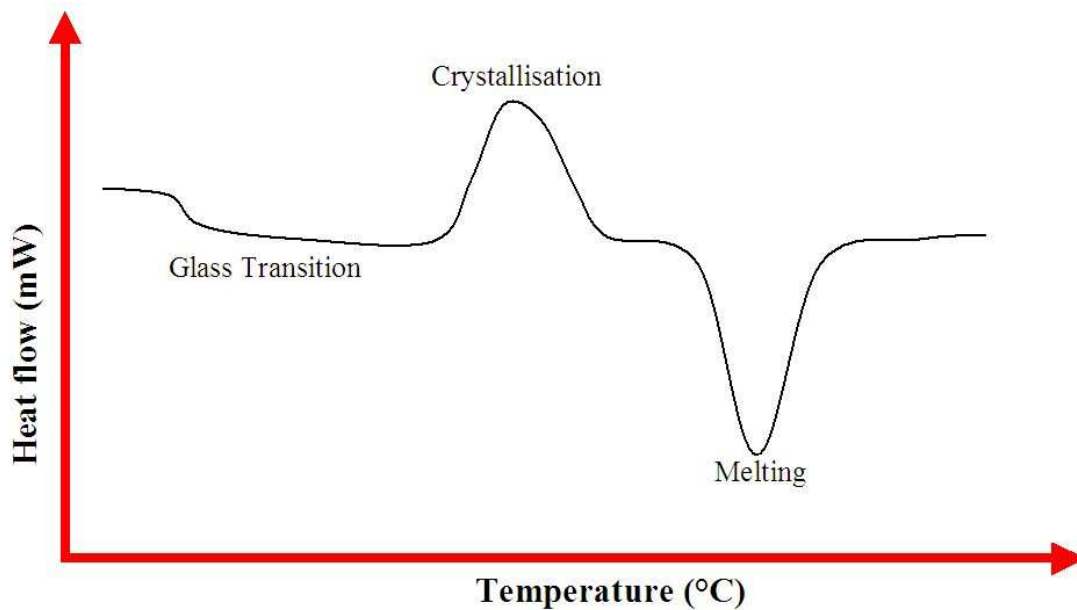


*Figure 2.6 DSC curve showing the three main types of event that can occur. A glass transition where the base level drops and remains there till another event, a crystallisation that forms an upward peak and a melting trough. A downward move shows extra energy is required, an upward move shows energy is given out.*

Where the sample under investigation undertakes an endothermic transition, for instance that of melting, the sample absorbs heat and requires an increased amount of energy to retain the same heating rate. In the plot this is represented as a trough (minimum peak). The opposite effect is seen for an exothermic transition where heat is given out by the change in the sample resulting in a peak in the DSC signal. The formation of a glass phase is neither an endothermic nor exothermic transition, instead it results in a change in the heat capacity of the sample represented as a step in the baseline of the DSC signal. The process can also occur whilst cooling the samples. When a DSC measurement is completed for heating and cooling on the same sample, the related peaks and troughs are often not aligned, as new phases can form. The area of the peak can give an indication of the quantity of each polymorph present although this is also related to the latent heat of melting or crystallisation so cannot be used as a true quantitative method unless these are known for the polymorphs involved.

DSC therefore gives the ability to determine the phase diagram of a sample as well as being useful for polymorph screening, where the different forms have different melting or crystallisation temperatures.

## 2.6 Computational chemistry

Although most of the work has been based around experimental work, theoretical calculations have been used to supply supplementary information and back-up theories. Computation can provide complementary information that is not accessible or practical experimentally. The ability to investigate compounds that have not been formed, extreme conditions like high pressure (even negative pressures), high temperature, electric, magnetic and radioactive fields or probe interactions that cannot be seen by any other means makes computational chemistry of great use and with an exciting future.

The electrons do not act like classical particles; instead these quantum particles (that travel at relativistic speeds) can be described as waves using the Schrödinger equation.

$$\textit{Equation 2.12} \quad \hat{H}\psi = E\psi$$

Where  $H$  is the Hamiltonian operator,  $E$  the total energy of the system, and the wavefunction  $\psi$ . Unfortunately any realistic sized molecule contains too many particles ( $>2$ ) for a full solution of the equation to be obtained, even with the most powerful computers available. To get around this obstacle, it is necessary to bring in some approximations that simplify the situation. The Born-Oppenheimer approximation states the nuclei can be considered as being stationary because the rapidly moving electrons can adapt to any changes in their position almost instantaneously, therefore the momentum of the nuclei can be ignored. Only the positions of the nuclei need to be considered when solving the electronic wavefunction.

It is impossible to describe the exact movement of the electrons as they are relativistic particles, so instead probability distributions of their density in the molecule are used, in other words the molecular orbitals. The molecular orbitals can be expressed as a linear combination of atomic orbitals (LCAO). In this way the molecular orbital is built from adding together of the weighted atomic orbitals. The electrons do not move independently, but are correlated (electron correlation). Three different contributions to the energies have to be considered for the electrons, the electron-electron interaction, the electron-nucleus interaction, and the exchange interaction that accounts for the spin interaction (Pauli principle).

Basis functions are usually Gaussians (which are easy to calculate), requiring a combination of them to represent single electron orbitals, which make up the molecular orbitals. Basis sets dictate the number of basis functions that are used in a calculation and thus varying in accuracy, with bigger basis set with more functions able to determine a better shape when summed together.

The two main ab-initio methods that are widely used for calculating energies are Hartree-Fock and DFT (density functional theory). Both are iterative methods that generate potentials from the wavefunction and then produce new wavefunctions from these potentials. This cycle continues until it converges and the energy is minimised (self-consistent). The way in which Hartree-Fock and DFT tackle the problem of the electron-electron interactions differs, both having associated advantages and disadvantages.

### 2.6.1 Hartree-Fock methods

The basic principle of Hartree-Fock (HF) is it produces a function (wavefunction) for each electron, based on the average potential determined from the positions of the nuclei and all the other electrons, with the electron moving independently within it. The biggest problem arises from the fact that the electron correlation is neglected, as it ignores how the motion of each electron affects the rest of the system. This means the electrons can come too close together resulting in a higher than expected energy as well as shorter bonds. This is especially important for systems with high electron

density. On the other hand the electron exchange is fully accounted for with the HF method.

### 2.6.2 Density functional Theory (DFT)

Density functional theory DFT uses the ground state electron density of the system instead of single particle wavefunctions to calculate the energy of the system. The DFT energy is written as the sum of the nuclei-electrons energy  $\int V_{ext}(r)\rho(r)dr$  and the electron-electron interactions  $F[\rho(r)]$ .

$$\text{Equation 2.13 } E[\rho(r)] = \int V_{ext}(r)\rho(r)dr + F[\rho(r)]$$

The electron-electron interaction energy can be separated into the sum of the kinetic energy of electrons ( $E_{KE}$ ), inter-electronic interactions including the Coulomb interaction ( $E_H$ ) and the exchange and electron correlation energies ( $E_{xc}$ ).

$$\text{Equation 2.14 } F[\rho(r)] = E_{KE}[\rho(r)] + E_H[\rho(r)] + E_{xc}[\rho(r)]$$

The exchange-correlation takes into account the exchange and correlation contributions, and any other interaction between the electrons not accounted for by the classical K.E. + Coulomb interactions, but cannot be calculated exactly, as no wavefunctions are produced. Therefore the exchange-correlation term is approximated using the ground state density. Two methods for calculating the exchange-correlation are the Local Density Approximation (LDA) and Generalised Gradient Approximation (GGA). Both techniques work by dividing the electron density into small volumes, with the LDA these volumes are assumed to have a uniform value determined by quantum Monte Carlo calculations of ideal gases. GGA takes into account the gradient of the electron density at each point. GGA works better for molecular systems where there are sharp density changes as a function of distance, whereas LDA works well for metallic systems.

HF calculates the exchange energy exactly but cannot calculate a value for electron correlation, whereas DFT approximates both the exchange and correlation energy. Hartree-Fock generally overestimates the energies whereas DFT normally underestimates it. Correcting the HF or DFT energies by applying a weighting factor

is one possibility, but this weighting factor would be dependent on the system under investigation. The usual method is to apply Hybrid functionals which are a mixture of both techniques using the fact that the values they provide lie on either side of the true energy. The over estimation in the Hartree-Fock energy can be countered by adding a percentage of the DFT energy.

Condensed matter calculations take into account the interactions between atoms both within the molecule(s) and within the surrounding environment of the crystal structure, based around the electron distribution. There are two approaches to modelling solid state materials, where the repeating unit imposes periodic boundary conditions, both using potentials made of Gaussian functions. The valence electrons can be modelled using a linear combination of atomic orbitals (localised basis sets) as is the case in the CRYSTAL program<sup>53</sup> or by using pseudopotentials and planewaves (CASTEP<sup>54</sup>).

A full description of condensed matter calculations and Density Functional Theory can found in *A Chemist's Guide to Density Functional Theory*<sup>55</sup>.

### **3. Techniques and apparatus**

The techniques used in the project have required a variety of apparatus from laboratory equipment and in-house X-ray diffractometers to large-scale neutron facilities. The diversity of techniques provides information into different aspects of the crystals studied, complementing each other to give a more complete picture.

#### **3.1 Sample preparation**

Sample preparation is an essential stage in the analysis process, with results dependent on the sample quality. The solid-state samples used are all obtained by crystallisation. The different techniques require different types and sizes of sample, which can be accommodated with several crystallisation methods. The optimal size of crystal required for X-ray single crystal diffraction is around 0.2 - 0.4 mm in at least two dimensions although it is possible to use samples outwith this range. Neutron single crystal diffraction needs a much larger sample, with typical volume of 1 mm<sup>3</sup> or larger (dependent on unit cell size) the normal requirement. For best results a single crystal will be pure, free of defects, with no additional material on the surface (small crystals or powder) and not include any stress and strain fractures. In samples that are inherently twinned or contain defects, good single crystals may be impossible to obtain. Twinned crystals can be used but additional processing of the data is required to separate the data sets from the different patterns and often the quality of the data is poor because of overlap of reflections. Whereas single crystal work is used to determine the structure unique to the one crystal selected for the experiment, powder data can be used to determine the identity of all the phases present throughout the crystallisation vessel.

Powder samples can naturally form in the vial while preparing the sample or can be produced from a single crystal by grinding, although grinding can induce additional reactions and these may not be desired. The desired properties in a powder sample for screening are a well-mixed sample, randomly orientated crystallites, dry and small particle size. These are important for both filling the capillaries and in the collection

of the data. For structure solution the availability of pure sample makes it easier, and a high quality data set is required.

### 3.1.1 Crystallisation methods

There are several techniques for growing crystals of small molecules and their complexes. All the crystals used during the course of these investigations were produced from evaporation from solution, although several variations were adopted around this basic method. The choice of solvent depends on the physical properties of the target materials, although often a variety of crystallisations from different solvents were used in case polymorphs or new phases arose. On some occasions a mixture of solvents were used, often where the constituents of co-crystals need to be dissolved in different solvents. Acetone, methanol, acetonitrile, ethanol, and water were commonly used, with the water solvent on several occasions becoming incorporated into the structure, forming hydrates.

In the majority of cases the solutions are prepared in small 7 mm<sup>3</sup> glass vials, with a weighed molar quantity of chemicals dissolved in the solvent. The vials are then kept somewhere where they will not be agitated and covered with pierced parafilm as a mechanism to slow the evaporation in an attempt to obtain larger single crystals. Powder samples were obtained by allowing the sample to evaporate quickly; leaving the sample uncovered and applying heat can be used for this. As a simple alternative, H-tubes allow a gradient of concentrations to be set up in one sample container (*Figure 3.1*). The two compounds are dissolved and added to the separate ends of the H-tube, as they mix into each other a diversity of concentrations is formed in which hopefully a suitable crystal-growing medium is created.

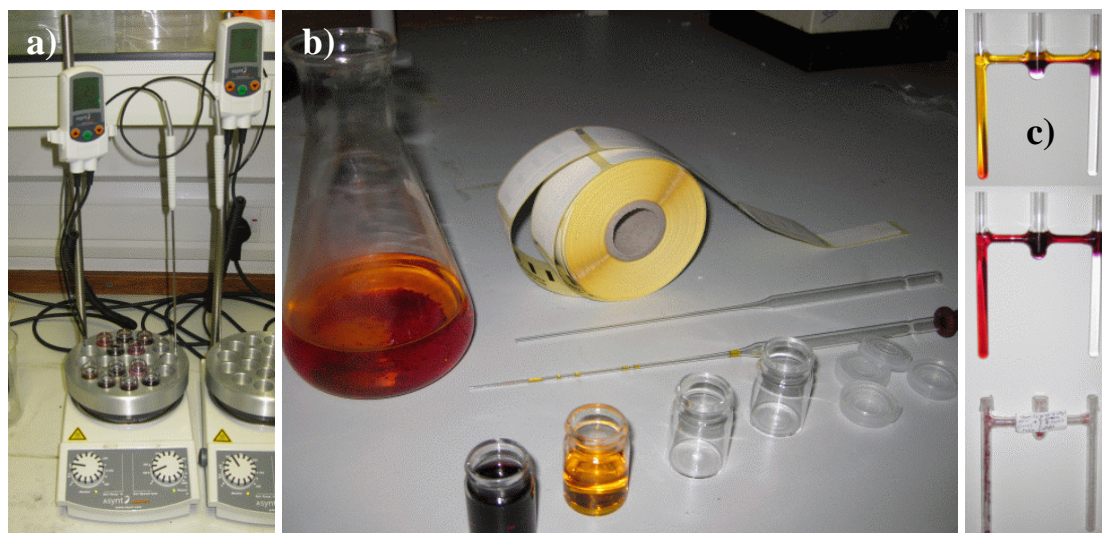


**Figure 3.1** Photo of *a)* samples in a temperature controlled hot plate, *b)* typical sample vial and equipment, *c)* H-tube crystallisation of chloranilic acid and 3,5-dimethyl pyrazole at different stages.

The temperature of the solution is also important; a large temperature gradient can cause twinning whereas heating or cooling the sample can control the rate of evaporation and therefore rate of crystal growth. Sometimes different polymorphs or structures are created at different temperatures, as different products become stable or the energies for different reaction paths vary. The use of a fridge or cold-room allowed sustained cooling over the whole crystallisation, without large temperature gradients that are often detrimental to crystal quality. Continuous Heating is achieved using either specially adapted hotplates or a ReactArray Microvate (programmable temperature controller) both of which can also hold the temperature to a specified level for prolonged times. The samples are not normally allowed to dry out as this can cause the single crystals to be encrusted or broken when they are removed. Powder samples are the exception, requiring to be dried and ground prior to filling a capillary.

### 3.2 Characterisation and screening

It is important to note that a single crystal taken from a re-crystallisation is not a reliable representation of the full contents of the entire sample jar. When working with co-crystals it is common that single crystal of more than one structure can form

as well as additional powders or oils. As well as the intended product, these can be in the form of starting materials, polymorphs, co-crystals of different ratios, and solvates.

It is therefore important to be able to examine the whole sample vial and have a system of extracting single crystals of new complexes where the presence of these may be indicated. When looking for different single crystals the morphology can give clues, often with crystals of different compositions producing differently shaped forms. Needles, blocks, plates are all common crystal forms, and of course can vary greatly in size. Colour is also another good distinguishing feature, and simply the position in the jar i.e. on the side or at the bottom can be an indication. Unfortunately the quality of the crystal is often related to the complex or crystal form adopted, making it impossible to acquire good crystals of some forms.

The unit cell can be used to recognise if the structure is already known, with a search through the CSD<sup>56</sup> using the unit cell. Powder diffraction is ideal to characterise the crystalline contents of a sample, with the powder pattern of a compound being essentially a unique fingerprint (Eva<sup>57</sup>). Mixtures can also be distinguished, and the ratios determined approximately with programs such as polySNAP<sup>43</sup>. This makes powder screening useful for determining if the required or a new complex is present, although they may not be available as single crystals.

### **3.2.1 Powder diffraction, DSC, sample identification and purity**

The identity of a crystalline material can quickly be determined through powder diffraction. The powder diffractometer used in this work is a Bruker D8 using the software Eva<sup>57</sup>, usually run at room temperature. A normal run takes about one hour with scan scans from 5- 65 degrees at a one-degree per minute rate, producing a rough pattern suitable for general comparison.

Differential scanning calorimetry DSC can also be used to distinguish whether additional structures are present or if samples are pure. Different products or reactants will melt or undergo phase transitions at varying temperatures resulting in different peaks and troughs in the DSC trace.

Other physical attributes can also be used for example chloranilic acid has a distinct red colour and co-crystals containing it have a similar colour although often a different shade. This makes it easy to identify crystals that are not co-crystals of chloranilic acid which helps prevent time being wasted screening starting materials that have not reacted. As noted above the morphology can also be a distinguishing factor between different samples.

### **3.2.2 Powder pattern analysis technique**

The powder data in this project have been analysed with EVA<sup>57</sup> by comparing the measured patterns against calculated powder patterns for the known single crystal structures. The measured patterns were corrected for background using a polynomial fit and the resulting patterns were smoothed. The relative proportions of each phase present in the sample were estimated by comparing relative peak heights.

### **3.3 Single crystal X-ray diffraction**

Although it is possible to produce a crystal structure from X-ray powder data, the resolution required to examine hydrogen bonds accurately is not in general possible. Therefore all the structures in this project have been produced using single crystal diffraction. Three different diffractometers were used. A Nonius / Bruker Kappa CCD area detector<sup>58</sup>, a Bruker APEX2<sup>59</sup> also with a CCD area detector, and an R-AXIS Rapid (Rigaku)<sup>60</sup> equipped with an image plate area detector.

To solve and refine the structures several different software packages were used. SHELXL<sup>61</sup> implemented within WinGX<sup>62</sup>, and CRYSTALS<sup>63</sup> are the two refinement programs used extensively throughout the project. SIR<sup>64</sup>, and SHELXS<sup>61</sup>, are the structure solution programs that produce the starting models these are based on.

#### **3.3.1 Unit cell determination and indexing**

On all the instruments, the primitive unit cell is determined using a preliminary set of frames. The reflections are auto-indexed to gain the primitive unit cell and crystal

orientation, which are then refined. The appropriate crystal system and Bravais lattice are then chosen, although sometimes a lower symmetry lattice is chosen where there is any doubt, to ensure sufficient data are collected.

### 3.3.2 Data collection

The data collection depends on the crystal symmetry, with all three machines able to generate a collection scheme to fit the crystal. Generally completeness to around 0.8 Å of 100% and redundancy of around four is aimed for. A typical data collection can last for a few hours to a day depending on the size of the crystal, unit cell, symmetry and how well it diffracts. The data needs to be integrated, with several correction factors (Lorentz, polarization, absorption, extinction, decay, multiplicity corrections) introduced before an *hkl* file is produced. The data is then input into a structure solution + refinement program such as CRYSTALS<sup>63</sup> or WinGX<sup>62</sup> where Direct Methods will typically be used to gain a structure solution, followed by refinement.

### 3.3.3 Variable temperature methods

Hydrogen bonds and any disorder within them are often dependent on temperature, therefore the experiments are often repeated at different temperatures so the evolution of the hydrogen bond over a temperature range can be examined. Using this method, anomalous results can also be spotted where they do not fit in with a sequence. The availability of a structure at multiple temperatures gives the results added credibility and in improving the verification of the conclusions, particularly when subtle effects are being examined. It can also yield new information, for example where a disordered site is filled with increasing temperature, a plot of the rate can be determined, rather than just a snap shot of the disorder.

All the diffractometers used have cryo-systems attached, at least capable of getting samples down to temperatures of 100 K. A common selection of temperatures used is 100 K, 200 K, and 300 K with additional temperatures possible for interesting complexes.

An additional benefit of the low temperature structure determinations comes with the reduced thermal movement of the atoms, allowing a superior structure model to be created.

### 3.4 Neutron sources

Neutron sources fit into two categories; pulsed spallation e.g. ISIS<sup>65</sup> and nuclear reactor sources e.g. ILL<sup>66</sup>, both types have been used in this project. They differ in both the way that they produce the beams of neutrons and in the characteristics of the beam itself.

Spallation sources work by smashing highly energetic protons into a heavy metal target, effectively chipping away neutrons from the target. This produces a pulsed white beam of neutrons, as the protons are accelerated in packets. This allows time of flight methods to be used, which utilise the pulsed nature of the beam to allow a large range of wavelengths to be used.

The reactor source works in a similar way to that of a fission nuclear power station with a cascade reaction producing a continuous, high flux, white beam of energetic neutrons. Different moderators slow the neutrons to produce hot and cold sources, and monochromators and collimators are used to select, tune and align the neutrons to the energies (wavelengths) required for each application.

#### 3.4.1 ISIS spallation neutron source

Spallation sources such as ISIS<sup>65</sup> at Rutherford Appleton Laboratory (Oxfordshire, UK) produce neutrons by colliding energetic protons onto a heavy metal (tantalum or tungsten) target. The impact of the protons ejects fragments (mostly neutrons) from the target, the word spallation coming from the mining term meaning to chip. The process to create the energetic protons starts with an ion source producing H<sup>-</sup> ions, which are accelerated in a pre-injector column. The hydrogen ions are then passed through several linear accelerators increasing their speed using a large potential field. They then pass through a thin sheet of aluminium oxide foil that strips them of their electrons producing a beam of protons. The protons are fed into a synchrotron where

powerful electromagnets controlled by radio frequencies are used to accelerate the protons further to very high speeds. At ISIS the synchrotron is 26 m in radius and has 10 dipole bending magnets to keep the beam travelling around the circular path as well as quadrupole magnets to keep the beam tightly focused. The process splits the beam into two packets and accelerates them to 800 MeV, ~80 % of the speed of light. The protons make approximately 10 000 revolutions of the synchrotron and the production process is repeated 50 times a second. After being accelerated to the desired velocity the protons are kicked into the extracted proton beam line that directs them to the neutron and muon targets.

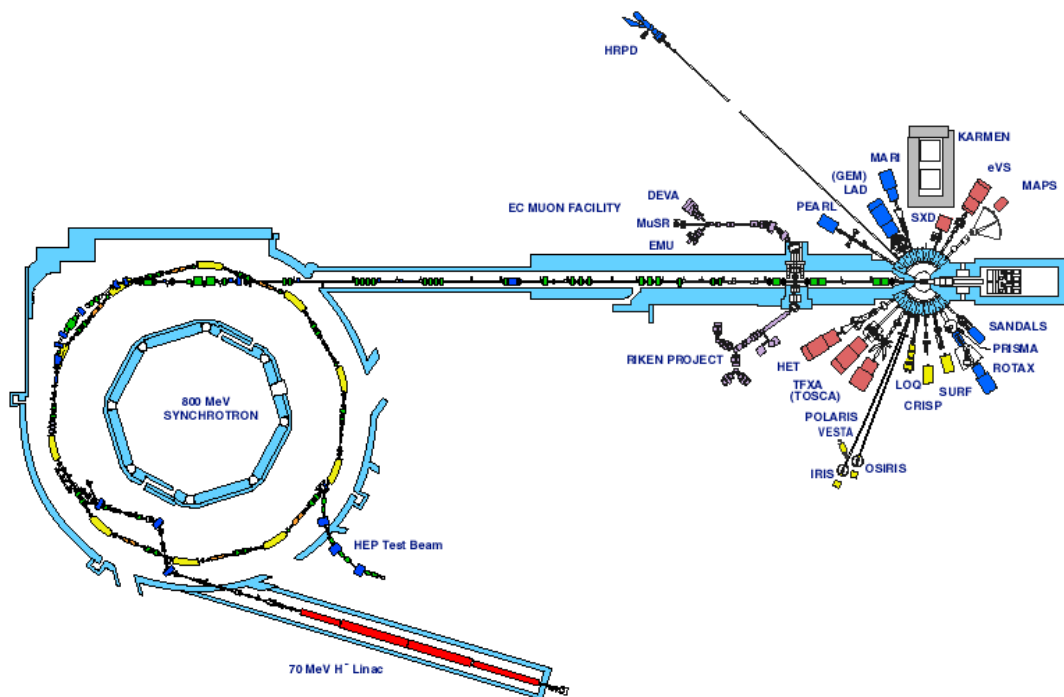


*Figure 3.2 Layout of ISIS, with the synchrotron on the left and the target with the instruments surrounding it on the right<sup>65</sup>.*

At ISIS there is a muon target made from 10mm of graphite, upstream of the neutron target. Protons colliding with the carbon produce pions, which decay into muons that can be implanted into materials in several research instruments, mostly for looking at magnetism.

The neutron target is made from a heavy metal; in the case of ISIS it is tantalum and tungsten plates although depleted uranium has also been used. The target is cooled by

water to prevent it over-heating. Each proton produces on average around 15 neutrons, which initially have high energies. Moderators are used to slow the neutrons to thermal energies for experiments. Ambient water, liquid methane and liquid hydrogen are generally used as the moderators because of their high H content, with the choice governed by the desired flux profile required by individual instruments. This feeds a wide range of instruments for varied purposes, including crystallography, spectroscopy, engineering, and materials. In the case of the single crystal diffractometer SXD used in this work, the moderator is ambient water, providing high-energy neutrons with wavelengths in the range 0.2 – 10 Å. The colder moderators produce a range of neutrons with longer wavelength/lower energies.

### 3.4.2 SXD, time-of-flight single crystal neutron diffractometer

The single crystal diffractometer<sup>67</sup> (SXD) at ISIS is able to carry out experiments on a variety of crystal samples with sizes varying from 1 mm<sup>3</sup> to larger than 100mm<sup>3</sup>. Using a Helium cryostat allows access to temperatures down to 4.2 K or below, while a furnace allows temperatures in excess of 1200K to be reached (although only part of this range can be accessed in any experiment as different set ups are required). The collection software can be programmed to change temperature as part of the overall experiment control. The layout of the instrument also permits specially designed apparatus to be fitted, for example the Paris-Edinburgh cell to allow extreme pressures to be applied to the sample. The sample is set in a vacuum tank (although this does not need to be used, for instance for fragile samples that would sublime) and can be rotated around  $\omega$  ( $\varphi$ ) as well as tilted to a 45° angle out of the plane ( $\chi$ ). The instrument has an array of 11 optically encoded ZnS scintillator area detectors **Figure 3.3**: six around the equatorial plane, four at a 45° tilt and one directly below the sample, giving a detector solid angle of  $>2\pi$  Sr.

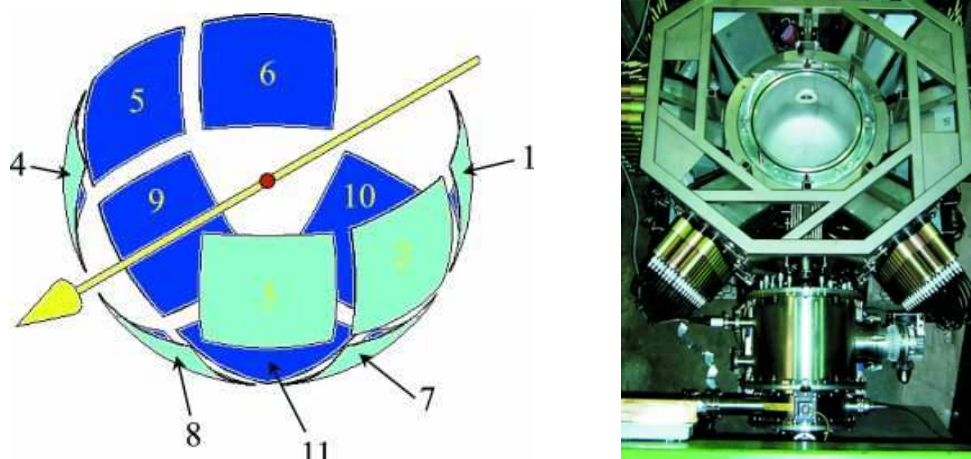


**Figure 3.3** a) Diagram representing the layout of the 11 detectors on SXD b) Photograph of SXD from the top with the inlet of the neutron beam at the bottom of the picture and 6 equatorial detectors visible<sup>67</sup>.

The pulsed nature of the neutron beam allows the time-of-flight technique to be applied. The velocity of the neutron is dependent on its energy/wavelength of the neutron, with the higher energy neutrons moving faster. With all the neutrons in a pulse being created at the same time and travelling the same distance the wavelength/energy of an individual neutron can be determined by the time it arrives at the detector. The neutron beam used by SXD therefore does not need to be monochromated and has a large range of energies, therefore having a much higher flux than if a single wavelength had to be used.

### 3.4.3 Data collection method

The data collection method for SXD, as with any other diffraction experiment, is dependent on the crystal space group, requiring fewer frames for higher symmetry systems. The crystal is wrapped in foil and mounted on an aluminium pin. The orientation of the crystal is not important although a slight tilt prevents any crystal axis being completely hidden, and the crystal dimensions in relation to its position are noted for the absorption correction. A predicted coverage for a given set of data frames can be calculated prior to the start of the collection using an inbuilt program in the SXD2001<sup>67</sup> software (**Chapter 4**). The time of exposure for each crystal orientation is dependent on unit cell size, crystal size, the property under investigation

(which determines how accurately the structure needs to be determined), and the crystal quality. A normal exposure time would be around 1-2 hours but with large well formed crystals times as short as tens of minutes are possible. If the crystal has high symmetry it is often possible to collect enough data with just a set of frames rotating the sample around the vertical,  $\omega$ , axis (e.g. -90, -45, 0, 45, 90). The crystal can be tilted up to 40° out of the plane in  $\chi$  for lower symmetry systems that require additional frames.

#### 3.4.4 ILL steady state reactor source

The ILL<sup>66</sup>, built in the 1970s (although refurbished several times since), produces the world's most intense neutron flux for condensed matter experiments. It works in the same way as a power station reactor using enriched uranium fuel to create a fission reaction producing a high flux of neutrons. The reaction is initiated by a neutron being absorbed by the nucleus of a uranium-235 atom, which splits into lighter elements as well as emitting radiation (gamma rays), other small fragments and a large amount of energy. Most of the small fragments are free neutrons, which can go on to induce fission of another uranium atom. Fission is an exothermic reaction and creates large quantities of neutrons allowing it to be a self-sustaining chain reaction. In a research reactor only a small fraction of the neutrons are required to sustain the chain reaction, with the remainder available to be used for experiments. The reactor is cooled by deuterated water (D<sub>2</sub>O) and a separate light water tank, which additionally acts as a moderating medium. The moderating region is required to slow the neutrons to energies suitable for experiments. The reactor and cooling area is surrounded by a reflector tank, which reflects fast neutrons that escape the core and can induce further fission incidents increasing the flux acquired. The set up allows the ILL to produce a high flux of neutrons for 50-day cycles, after which the fuel cell is replaced. In all, the reactor is operational for around 225 days a year.

At the ILL, the neutrons are fed to a suite of around 40 instruments for the use of diffraction, inelastic scattering, spectroscopy, and a host of other techniques including tools to investigate nuclear and particle physics. The neutrons from the reactor have a large range of energies but can be tuned for the different uses, as required, by using different moderators. Graphite at 2400 K is used as a hot source producing a beam of

very short wavelength neutrons with a Maxwellian distribution around 0.8 Å. The water moderator produces thermal neutrons with a distribution around 1.2 Å whereas materials such as liquid deuterium at 25 K can be used as a cold source where the beam of neutrons have a much larger peak wavelength around 3 Å. In the case where an instrument requires a single wavelength multilayered monochromators can be used. One hot or cold source in the reactor region provides neutrons to several different instruments, with a beam guide to direct and split the beam to the appropriate experimental area. Supermirror guides are used to ensure the most intense flux of neutrons reach the instrument.

### 3.4.5 D9 and VIVALDI single crystal diffractometers

The two important instruments at ILL with regards to this project are the single crystal diffractometers D9 and VIVALDI. These two instruments overcome the problem of the multiple wavelengths of the neutrons in very different ways. D9 is a traditional reactor neutron four-circle diffractometer, fed by a hot neutron source and is positioned very close to the reactor to achieve the highest flux possible. A multilayer monochromator is used to acquire a single wavelength from the entire spectrum of the beam. Because the neutrons of other wavelengths are discarded this dramatically reduces the flux. After the monochromator, the beam passes through a collimator to ensure the beam is parallel before it interacts with the sample thus improving resolution. A two-dimensional 64x64 mm<sup>2</sup> area detector is used to measure each reflection individually which makes the process relatively slow. The short wavelength makes D9 suited to accurate determination of very small atomic displacements and thermal motion, the instrument being able to create high-resolution nuclear density maps.

The VIVALDI (Very Intense Vertical Axis Laue Diffractometer) instrument uses a white beam from a thermal neutron source (0.8 to 3 Å) (although instruments that precede it on the same beam line affect the spectrum of wavelengths that VIVALDI receives). The multi-wavelength beam results in a Laue pattern with the different wavelengths diffracting differently (technically only quasi-Laue because a wavelength range of ~1 Å is typically used). This adds extra complication in processing the data but the greatly increased flux obtained by not monochromating speeds up data

collection by ten to a hundred-fold. The use of a cylindrical image-plate detector that wraps around the sample allows coverage of  $2\pi$  Sr solid angle of the sample. The instrument can thus scan large volumes of reciprocal space very rapidly. The image plate mounted on the detector drum is activated for neutron detection using BaFBr:Eu<sup>2+</sup> mixed with Gd<sub>2</sub>O<sub>3</sub>. The image plate has to be read and erased after each frame although this process only takes a few minutes. It is arranged vertically with an active area of 800 x 400 mm<sup>2</sup> and a radius of 159.7mm.

Whilst as on other neutron instruments the rule relating to sample size is normally “the bigger the better”, VIVALDI uses crystals of far smaller size. Both the Laue technique and the large detector coverage prevent this from being a problem in terms of long experiment times. This is of great advantage where previously crystals considered too small to be used for single crystal neutron diffraction experiments are now possible. Crystal quality has to be high to prevent deformation in spot shape in the Laue image which can lead to difficulties in integrating and overlap in spots. Other restraints on the suitable crystals are dictated by the wavelength, with primitive unit cell axes less than 25 Å preferred to prevent detrimental overlap of reflections. Sample temperatures of 1.5 to 315 K can be achieved with the cryostat or up to 1500 K with a furnace, and high-pressure cells can be inserted.

### **3.5 Examination and imaging of experimental results**

While processing data and refining the structure it is important to be able to examine the results. This is also true when the refinement is complete, to be able to draw conclusions and analyse the results, it is important to be able to represent the structural model or produce images representing or highlighting different aspects of the data. Because the results are 3 dimensional and on top of this have many different layers of information or properties that need to be viewed a wide range of imaging programs have been produced, several of which have been used throughout this project.

The main program used to view structures refined from single crystal diffraction has been Mercury<sup>68</sup>. Most of the black and white structural diagrams have been produced using the Bruker program XP<sup>69</sup>, the standard settings were ellipsoids at 50%

probability and for neutrons the hydrogens are shown with fully elliptical settings (anisotropic ADPs). Imaging electron density for normal or difference Fourier maps was achieved mostly with MapView<sup>69</sup>, taking 3x3 Å slices through the structure with resolution of 0.1 Å, with contours shown. Depending on the circumstances X-ray Fourier maps are either shown with negative values cut off or the full range; for neutron data the full range of density is always shown (since hydrogen atoms appear as troughs). MCE<sup>70</sup> is a second program used for Fourier maps that can provide a 3-dimensional structural image with slices or areas of density overlaid. Hirshfeld Surfaces have also been used to examine the hydrogen bond interactions with the program CrystalExplorer<sup>71</sup>. ChemSketch<sup>72</sup> has been used to produce some of the molecular sketches.

Programs used to view powder data have included Eva<sup>57</sup>. The DSC graphs were produced using Universal Analysis<sup>73</sup>. Dendrograms, structure overlays and cluster plots from dSNAP<sup>74</sup> have been produced using the software within the program.

### 3.6 Computational methods

Quantum chemical calculations have been carried out in parallel with several areas of the research, most noticeably in conjunction with the research into the hydrogen bonds of 2,4-dihydroxybenzoic acid, but also the picoline chloranilic acid co-crystal structures and more generally looking into the best choice of hybrid functional mixtures for carrying out solid state calculations of hydrogen bonded systems in the future. With their ability to probe the hydrogen bond potential well, quantum chemical calculations can provide complementary information as well as back up experimental work.

#### 3.6.1 CASTEP, Gaussian03, CRYSTAL06

The computational work has been carried out on several computer clusters including those local to the chemistry department (Coop, FatCat) and the University of Glasgow computer cluster. Solid state periodic calculations have used the software CASTEP<sup>54</sup>, and CRYSTAL03<sup>53</sup> whereas gas state isolated molecule calculations were run using Gaussian03<sup>75</sup>.

### 3.6.2 Hybrid functionals – mixing Hartree-Fock and DFT

Predicting energetic barriers to proton transfer in hydrogen bonds is a particularly difficult problem in theoretical structural modeling in the solid-state. The small size of the barrier height relative to the surrounding landscape of the energy surface coupled with difficulties related to the modeling of weaker interactions results in techniques tending to have large errors or uncertainties.

Although the use of high-accuracy wave function methods produces very good results it is not viable to apply these to every problem, especially for extended systems, because there are very computationally costly. From previous work comparing pure Hartree-Fock and pure DFT functional methods<sup>76</sup> it is generally believed that they overestimate or underestimate respectively the barrier height of hydrogen bonds. Using a hybrid functional that combines the characteristics of the two should enable a method that produces a reasonable result as long as the optimal proportion of each is utilised. One issue for this method is that the combination would not necessarily be the same for all situations, with studies into hydrogen bonding typically requiring a different percentage mixture than that for, say, magnetic studies or an inorganic solid.

### 3.6.3 Calculations on hydrogen peroxide, H<sub>2</sub>O<sub>2</sub>

A systematic evaluation with the aim of finding the correct mixture of Hartree-Fock and DFT for a hybrid functional to deal with calculations on small organic hydrogen bonded materials was carried out, using several basis sets within the program CRYSTAL03<sup>53</sup>. The ultimate aim was to find a method that could be adopted for such systems that is reasonably accurate without being overly computationally demanding. In the long term this could result in a significant reduction in the computational requirements for calculations into hydrogen bonded systems and increase their accuracy in assisting studies of proton disorder.

It is important that the structure used in this development work is not dependent on weak Van der Waals forces as these often result in unstable or inaccurate calculations. A simple molecule that contained a three-dimensional hydrogen bonded network was therefore chosen. Hydrogen peroxide is just such a small molecule and forms a

simple crystal structure with a three-dimensional hydrogen bonded network making it an ideal candidate for the study.

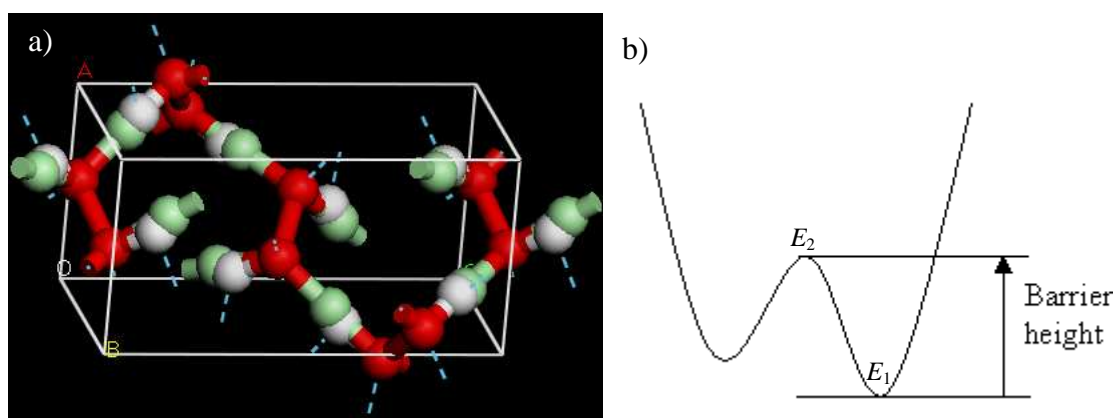


**Figure 3.4** a) Structure of  $H_2O_2$  showing the two positions of the H atom; the normal position is shown in white ( $E_1$ ), and the centred position in green ( $E_2$ ). b) The potential energy well with the barrier height and energies  $E_1$  and  $E_2$  for the normal and the centred hydrogen positions.

In each case two calculations had to be performed to calculate the energy of the potential energy barrier within the hydrogen bond: the total energy of the system with the hydrogen in its normal position (at the bottom of the potential energy well  $E_1$ ), and the total energy of the system with the hydrogen in a centred position within the HB (on top of the potential barrier  $E_2$ ) (**Figure 3.4**). The difference in the two calculated energies in the solid state would roughly show the energy of the sum of the potential barrier of the eight identical HBs in the unit cell, so dividing by eight gives the energy of one.

The calculation was carried out at the B3LYP level of theory and using several different basis sets (TZP, DZP, 6-31G\*, 6-311G\*, and 6-311G\*\*) so a comparison could be made. After the initial optimisation the resulting structure of each calculation was used as the input for the higher level basis set calculations. The percentage mixture of Hartree Fock to DFT was also altered so that for each basis set there were eleven barrier heights measured, starting with pure DFT and adding 10% HF contributions until it was pure HF. To ensure the results would be comparable with different strength HBs, calculations were also carried out with the volume of the unit cell decreased. Reducing the unit cell volume decreased all the distances

between the atoms, similar to applying a pressure to the crystal. The O...O HB lengths decreased as follows: ambient pressure = 2.718 Å, 2.5% reduction = 2.678 Å, 5% reduction = 2.628 Å, 7.5% reduction = 2.572 Å, 10% reduction = 2.511 Å.

The results can be seen in **Figure 3.5-3.11**. The first set shows for each percentage of DFT:HF mixture a plot of the HB lengths versus the barrier energy with the different lines representing the different basis sets used (**Figure 3.5, 3.6 and 3.7**). The second set shows for each basis set used, a plot of the percentage of HF versus the barrier energy with different lines representing each HB length (**Figure 3.8, 3.9 and 3.10**).

There is a linear dependence of the HB length with the energy of the barrier shown for pure DFT in **Figure 3.5** and all the tested basis sets show the same gradient. This is consistent throughout all the 11 different mixtures of DFT:HF used (50% HF **Figure 3.6** and 100% (pure) HF **Figure 3.7**). This overall trend shows that as the hydrogen bond length decreases (reduced cell size) the barrier height decreases in energy which is the expected trend (as the double potential well starts to merge towards a single minimum potential). There is a small range of energies between different basis sets, and the TZP, 6-31G\*, and 6-311G\*\* calculations are very similar, which is important as it makes it more likely that a lower level basis set could be used instead of the more computationally expensive large basis sets.

**Figure 3.8** show a close to linear dependence between the Hartree Fock exchange content of the functional and the barrier heights of the HB for all the unit cell volumes (HB lengths) in the DZP basis set. This is true for all the basis sets and was not expected (**Figure 3.9/Figure 3.10** 6-31G\* and 6-311G\*\*). For all different basis sets evaluated, the difference in the barrier energy of the different sized cells increases as the amount of HF is increased. This implies the effect of the differing DFT:HF ratios is more pronounced in longer hydrogen bonds.

To determine which mixture of DFT:HF obtains the best result for each basis set requires an exact measurement of the barrier energy for H<sub>2</sub>O<sub>2</sub>, which was beyond the scope of this project. When this value is obtained, the best ratio of DFT:HF can be extrapolated from **Figure 3.11** which is a plot of the barrier energies in H<sub>2</sub>O<sub>2</sub> at ambient pressure versus the percentage of HF with a data series for each basis set.

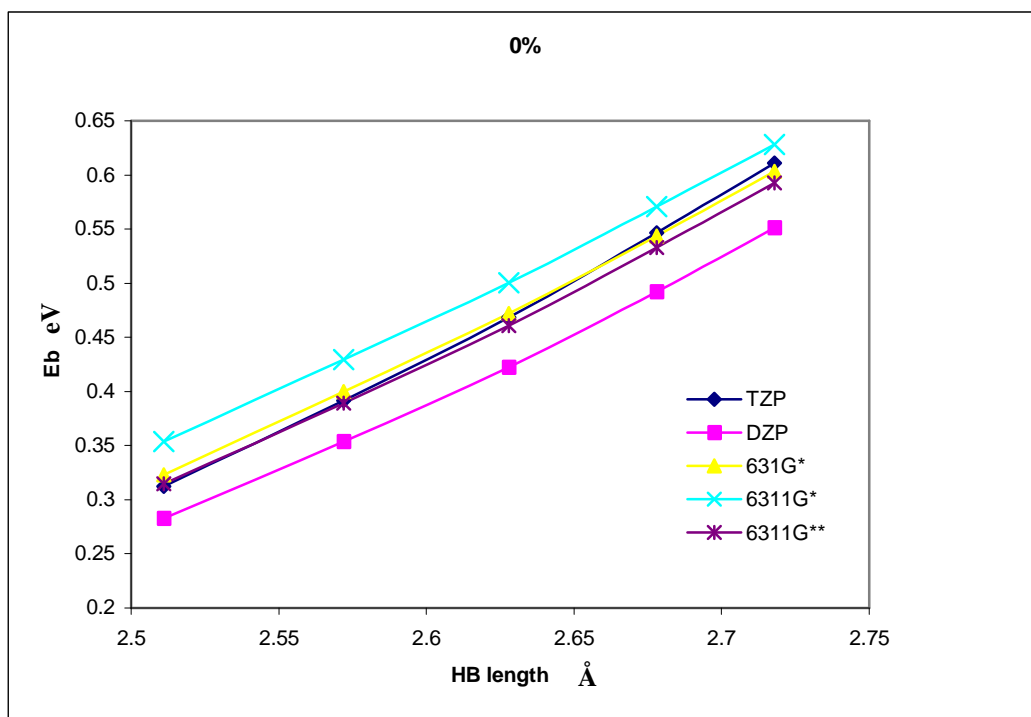


**Figure 3.5** Results of  $H_2O_2$  calculations showing variation in the energy barrier vs. HB lengths with different basis sets with pure DFT.

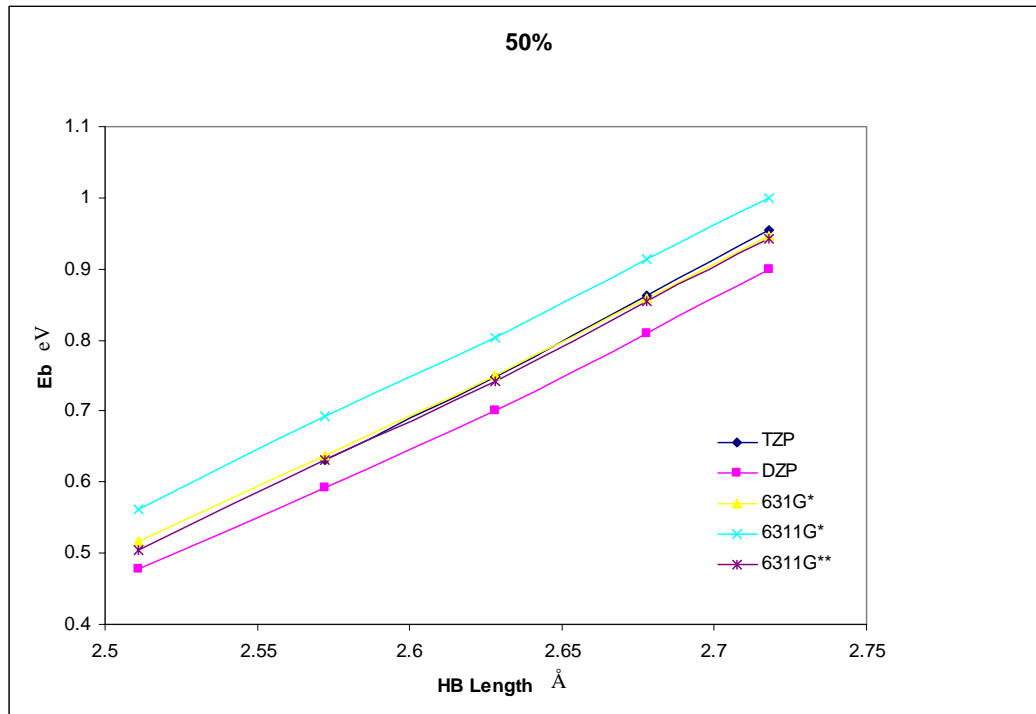


**Figure 3.6** Results of  $H_2O_2$  calculations showing variation in the energy barrier vs. HB lengths with different basis sets with 50 % mixture of HF and DFT.

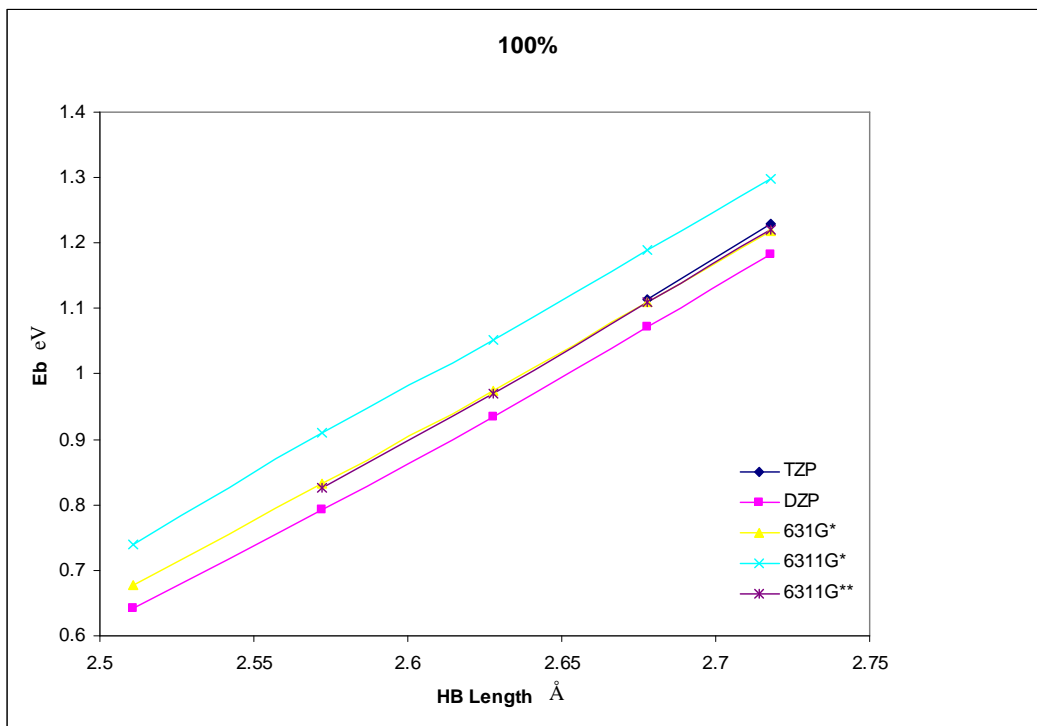


**Figure 3.7** Results of from  $H_2O_2$  calculations showing variation in the energy barrier vs. HB lengths with different basis sets with pure HF.

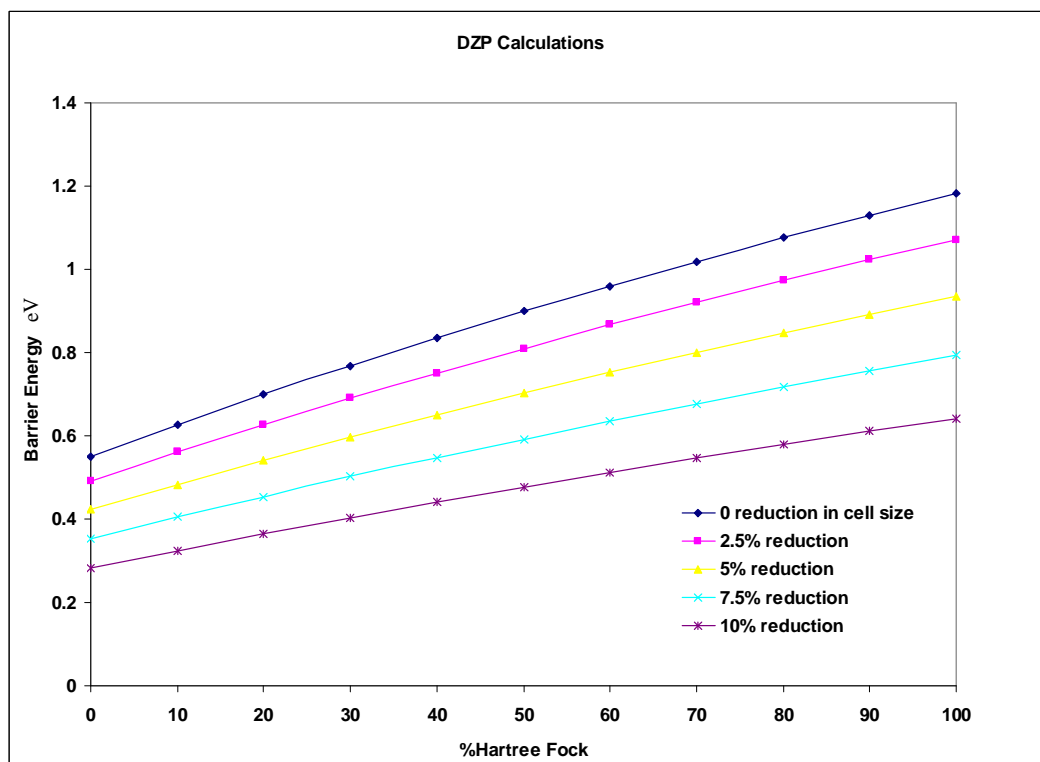


**Figure 3.8** Results of  $H_2O_2$  calculations showing variation in the energy barrier vs. % HF with different unit cell volumes for the DZP basis set.

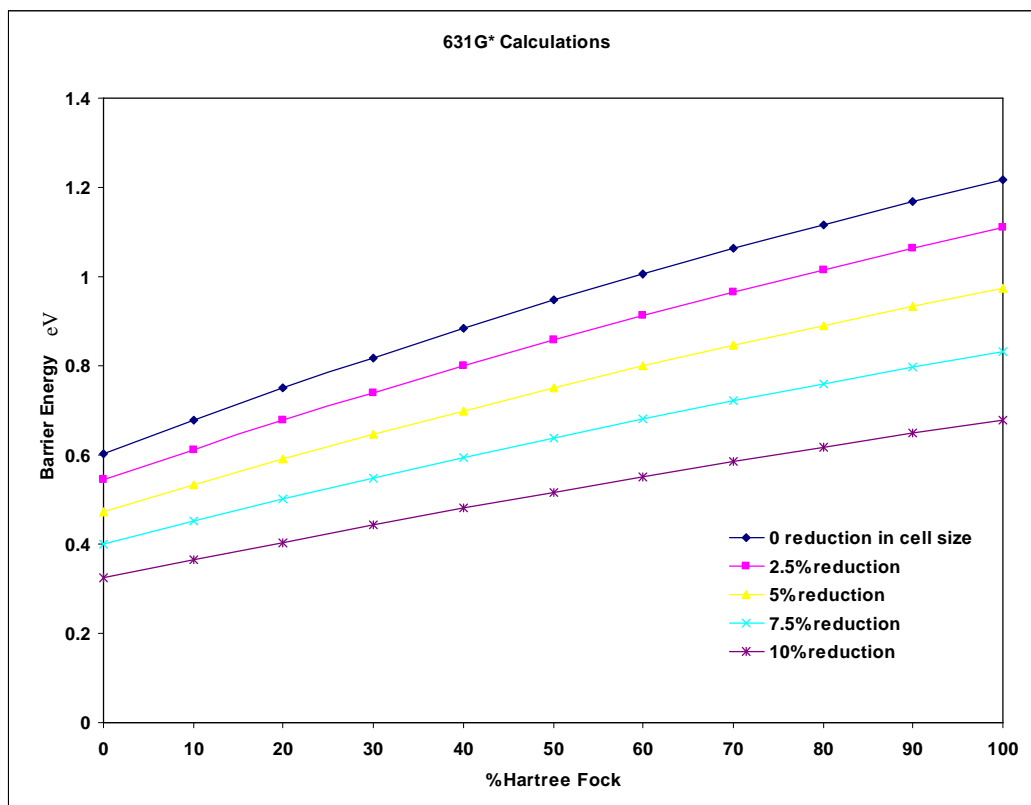


*Figure 3.9 Results of H<sub>2</sub>O<sub>2</sub> calculations showing variation in the energy barrier vs. % HF with different unit cell volumes for the 6-31G\* basis set.*

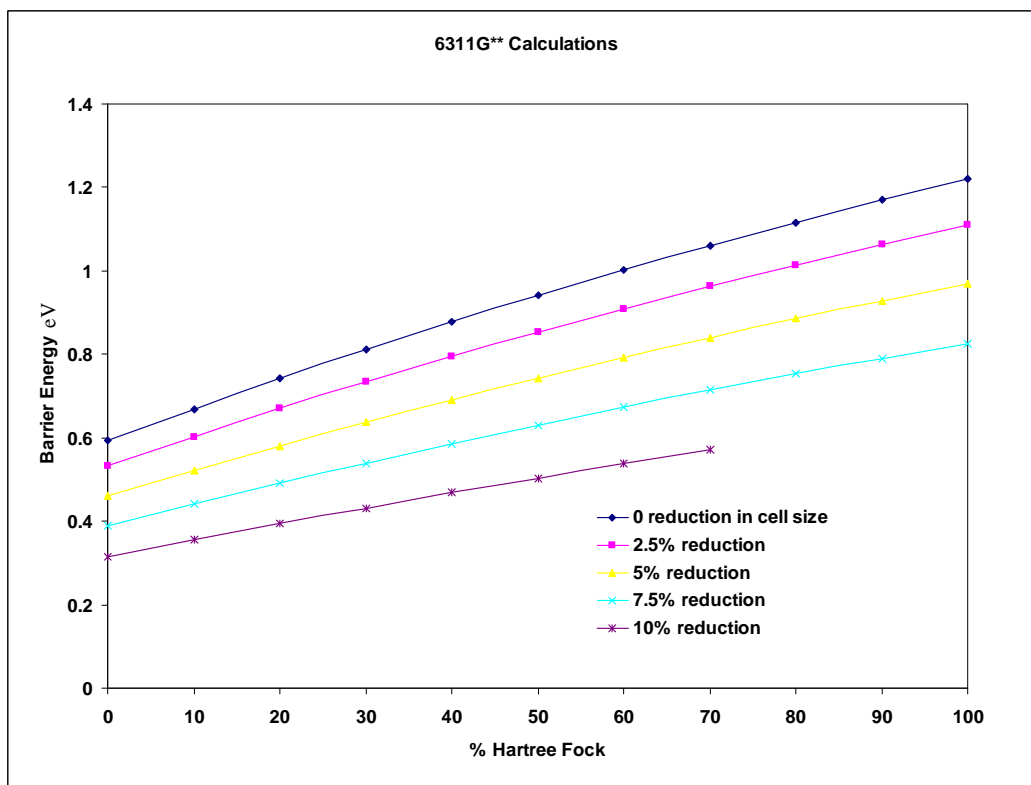


*Figure 3.10 Results of H<sub>2</sub>O<sub>2</sub> calculations showing variation in the energy barrier vs. % HF with different unit cell volumes for the 6-311G\*\* basis set.*

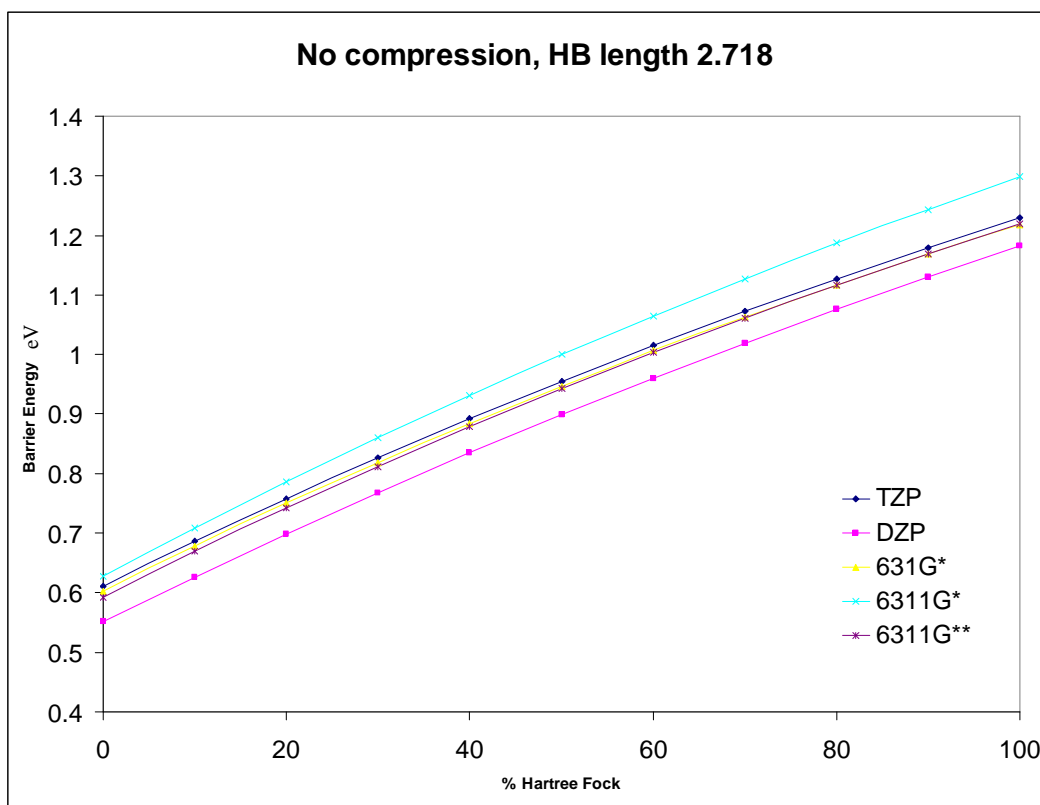


**Figure 3.11** Results of  $H_2O_2$  calculations showing the variation in the energy barrier vs. % HF with different basis sets and no compression of the cell.

## 4. SXD2001 data reduction software

The single crystal diffractometer<sup>67</sup> (SXD) at ISIS is positioned on beamline S3 on target station one (*Figure 3.2*). Over the many years that SXD has been operational it has been evolving and incorporating the latest technology especially with regards to detector design. In 2001 the instrument was completely refurbished upgrading from three detectors to 11 so that the sample position is almost completely surrounded, allowing for faster data collections. To keep up with the massive changes in the instrument new software also had to be developed.

### 4.1 SXD98, software for two position-sensitive detectors

Prior to the upgrade in 2001, SXD only had three (originally two) (*Figure 4.1*) position-sensitive detectors and was a much smaller instrument. Although the software only had to deal with data from 2 or 3 detectors there was still the time-of-flight aspect to be considered. The data reduction and analysis procedure was carried out in steps by a collection of individual programs leading into each other. Despite good results being achieved with many crystal structures solved using this equipment the software required to be upgraded to reliably handle the tilted and underneath detector banks. This upgrade also allowed for a user friendly GUI to be implemented, allowing experienced users to process the data rather than rely on the beamline scientist which was the case for the SXD98 software.

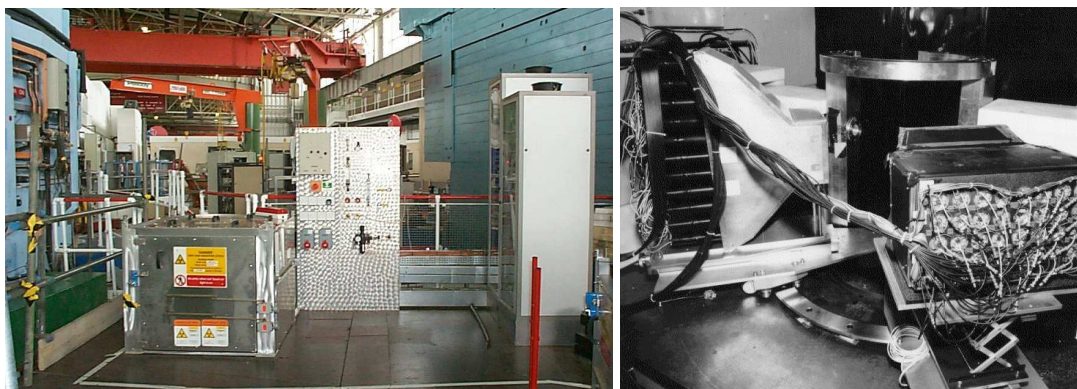


*Figure 4.1* SXD before the upgrade, **left**: instrument box and some of the controls **right**: the sample environment with the two detectors (shielding removed)

## 4.2 SXD2001, software for array of eleven position-sensitive detectors

The current SXD instrument is capable of doing experiments on crystal samples around a millimetre cubed and larger in size and is able to access temperatures below 4 K using a Helium cryostat. The instrument has an array of 11 area detectors, giving a detector solid angle of  $>2\pi$  Sr and thus increasing the data collection rate (*Figure 3.3*). In addition, SXD collects data using the time of flight method for neutrons; therefore the data needs to be normalised for the wavelength profile of the incident beam. A complex program has to be used to process the large volume of data resulting from the data collection method. From the point of view of this project, the 11 detector array makes the data processing a complicated and time-consuming task – much of the initial neutron work in this project has been spent in learning and in helping to identify bugs or inconsistencies in the software, particularly with respect to data sets for chemical crystallography. SXD2001<sup>67</sup> is the program designed specifically for the purpose, created by Dr Matthias Gutmann the station scientist for SXD.

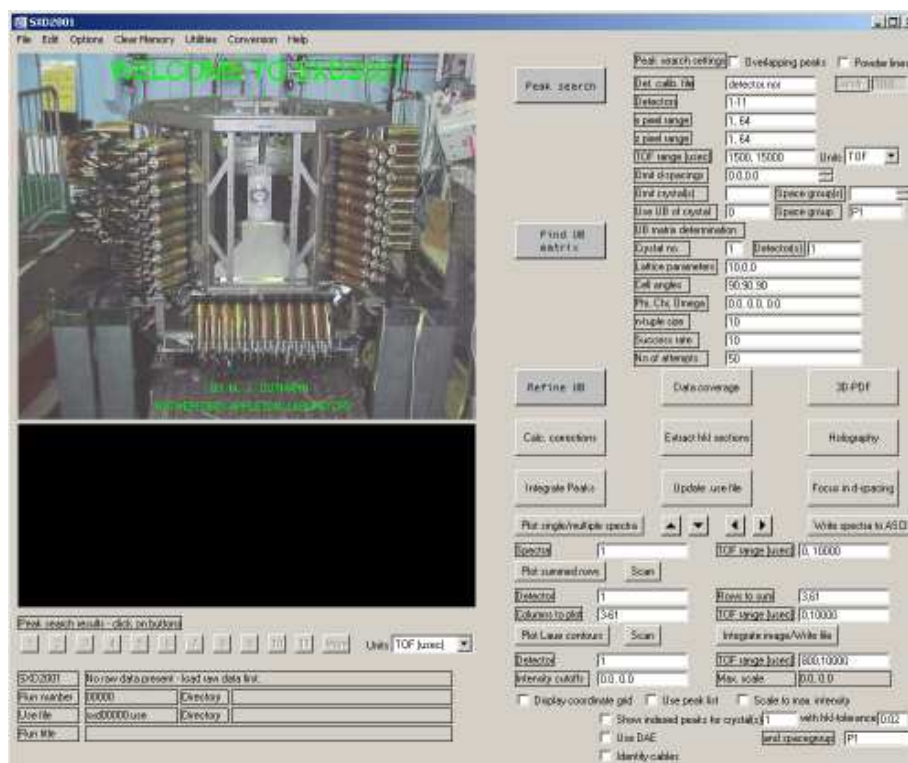


*Figure 4.2* Main display of SXD2001. From here it is possible to run all the different routines needed to process the neutron data.

The program requires at least 1Gb of memory, Windows XP, OPEN GENIE and IDL Virtual Machine v6.3. Installing the program is described in the user manual written by M. J. Gutmann<sup>77</sup>. Once started the main display window appears (*Figure 4.2*) from which all the program routines are accessible as well as being able to view the data.

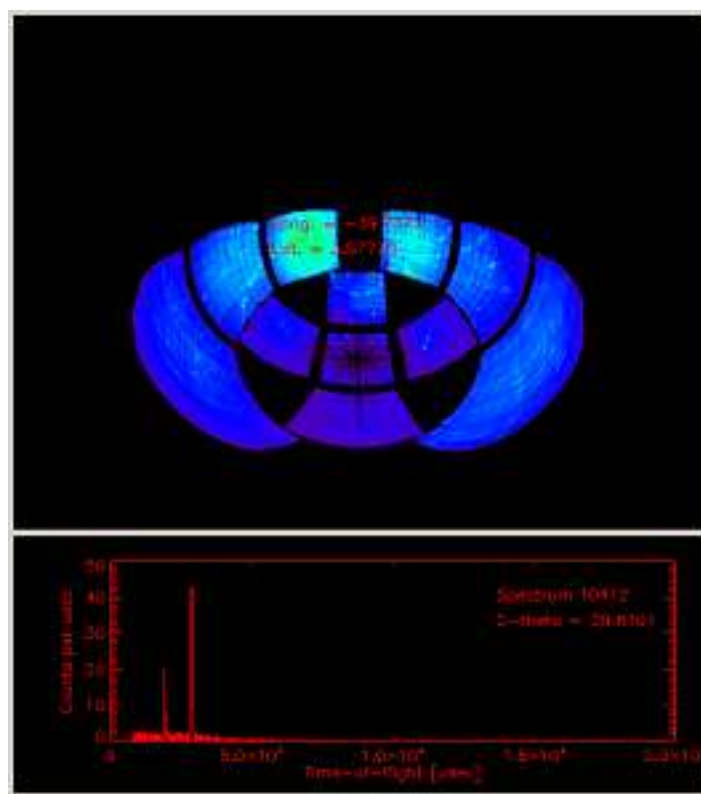


*Figure 4.3* Eleven detector display showing the diffraction pattern. Below the display a plot of the counts vs. wavelength from a selected point is shown.

A useful feature of SXD2001 is the data visualisation area (*Figure 4.3*) where it is possible to view all the 11 detectors at once as well as the time-of-flight spectrum of one pixel. As SXD has about 45000 pixels, each consisting of more than 1000 time channels, it is often wise to look at a summary of every detector rather than examine lots of individual areas.

#### 4.2.1 Flow Diagram

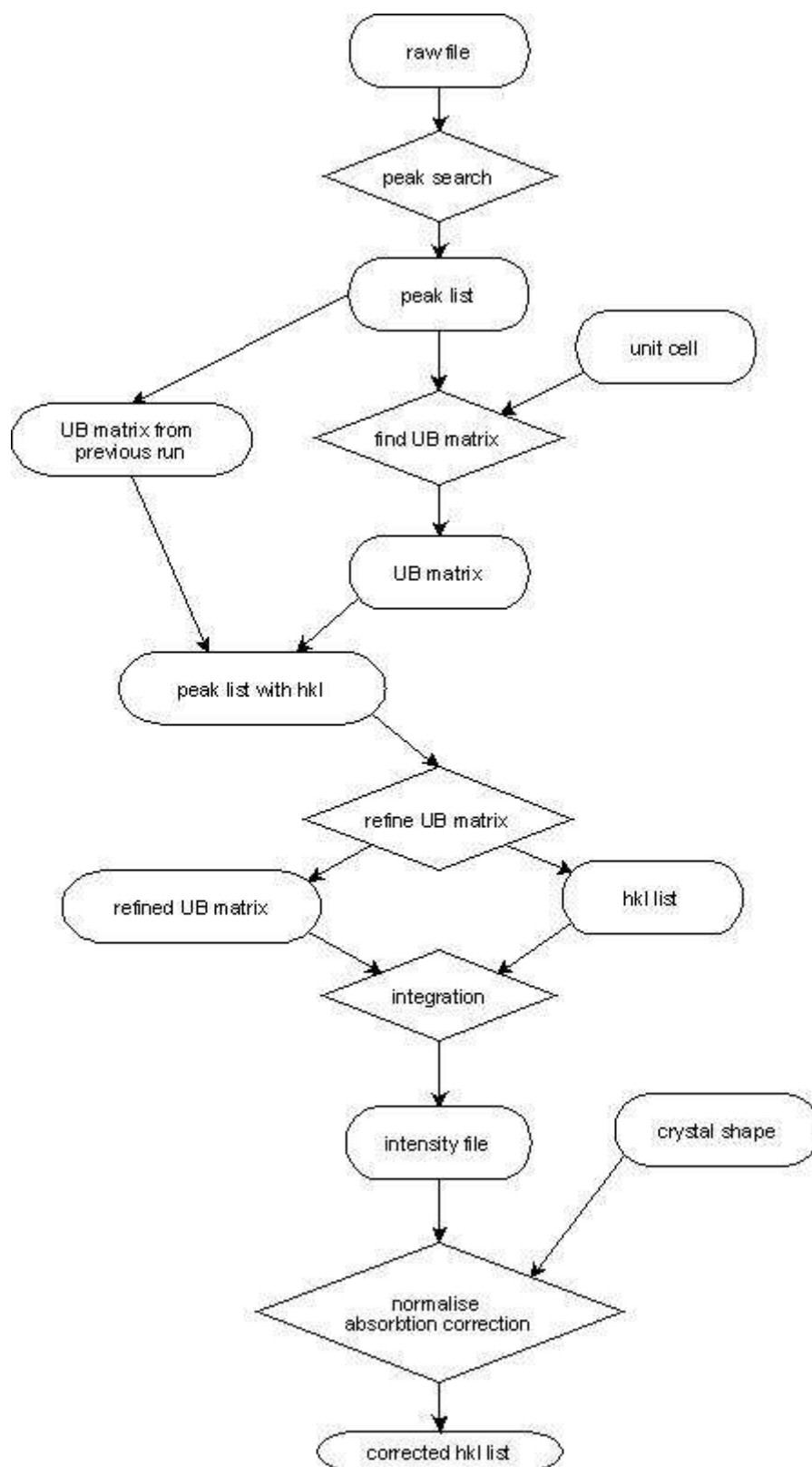


**Figure 4.4** Flow chart for processing data on SXD2001 from SXD.

The flow chart in **Figure 4.4** shows the stages which are required to process the raw data from the single neutron diffractometer at ISIS, SXD, to a format that allows a structure to be refined. A peak search is carried out of the raw data producing a list of all the observed reflections and their position on the detectors. From the strongest reflections, the program can produce a UB matrix or this can be imported from previous runs. The UB matrix is refined until a large number of the reflections are indexed and the peak list is updated with the *hkl* values for the indexed peaks. The data is integrated using the information from the peak list and the refined UB matrix, which produce intensities for all the peaks in the peak list. The data is normalised and an absorption correction applied taking into account the shape of the crystal. The output reflection file can be generated in several different forms to allow it to be used in a variety of refinement programs.

#### 4.3 Peak searching and indexing

A normal experiment on a crystal requires several different crystal orientations, normally around 10. For each position a *raw* file is produced that contains all the raw data from the eleven detectors including the time of flight profile. This *raw* file is loaded directly into SXD2001, where the data can be examined in the viewer showing a 2D image from the detector and the time of flight profile below (**Figure 4.5**).

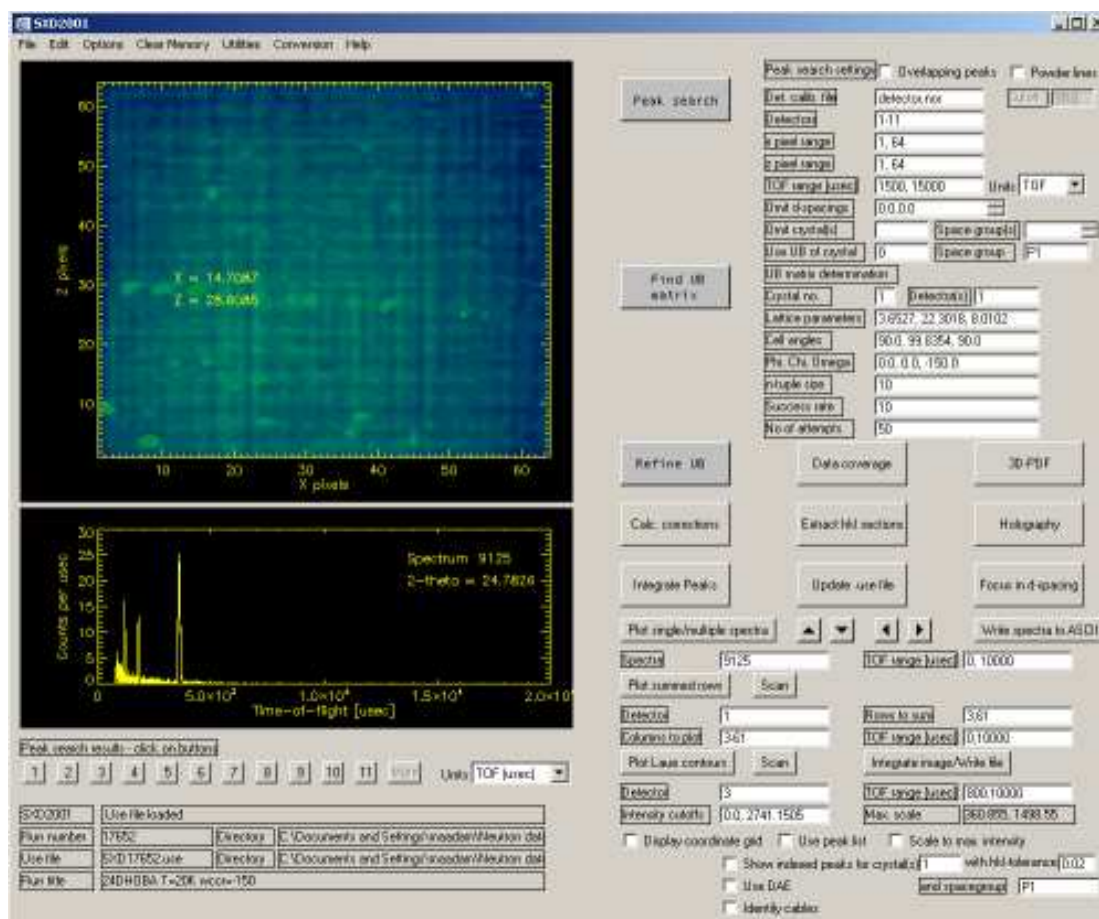


**Figure 4.5** SXD2001 with raw data loaded and displayed in the viewer.

With the raw data loaded, the first job is the peak search. All that is needed as input is the detector area and range of time-of-flight; this avoids problems with peaks close to the edge of the detectors and allows the wavelength range to be selected from the white beam of neutrons. The program will then index from the peaks found in the peak search to produce a UB matrix; alternatively, if a run from the same temperature for the crystal has been previously indexed the UB matrix can be imported from that run. If the initial attempt is not successful, data from different combinations of detectors can be tried. In a reasonable data set for a non-twinned crystal a large number of the strong reflections should be indexed, which can be assessed by checking the peak lists.

#### 4.4 Unit cell refinement

To refine the UB matrix is currently the hardest part of the process, and much harder for twinned or poor quality data sets. The refinement window (**Figure 4.6**) is an array of numerical and tick boxes, allowing the refinement of the unit cell dimensions, detector position, sample position and offsets. The system offers the ability to refine, fix or re-set selected parameters and is able to refine from 1 to all 11 detectors at once. Although the system is flexible in the way the UB matrix can be refined, due to the sheer volume of data present the process requires a level of skill to control and can be time consuming if reliable UB matrices representative of all 11 detector data sets are to be obtained.

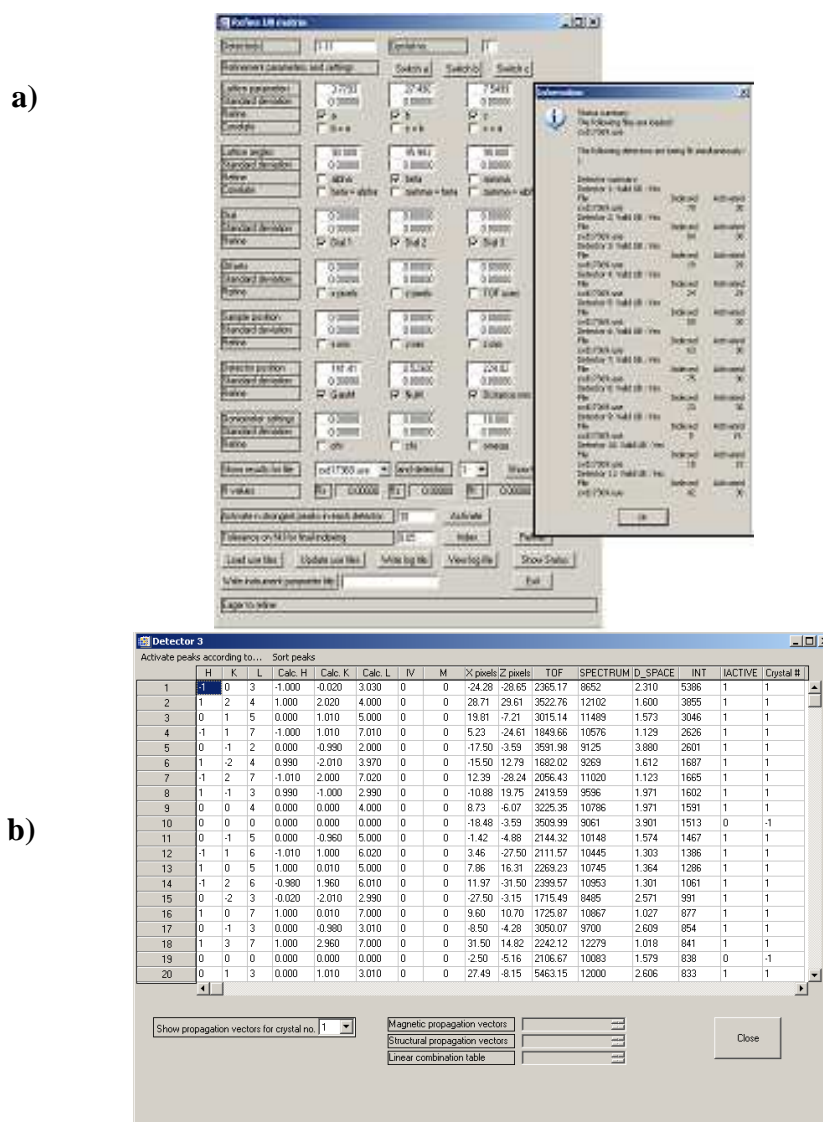


**Figure 4.6 a)** UB matrix refinement screen with added pop up screen of activated and indexed peaks. **b)** Indexed peak list from a single detector.

## 4.5 Peak integration

There are several different integration techniques available to extract the peak intensities (*Figure 4.7*). The simplest is the “shoe box” which integrates the peaks under the time of flight graph, within a certain rectangular area of pixels around the location of each peak found in the peak search. A dynamic box size can be used which varies the rectangular area of pixels integrated for each peak individually, to allow a better fit. A line integral option is also available, which only integrates a line of pixels through the peak, which it then factorises up to represent the whole peak. The 3D profile fits both the peak shape on the detector (using an area that matches the peak shape rather than a rectangular box as in the shoe boxes) and the time-of-flight profile as well. The options and required parameters are all accessible via the integration interface (*Figure 4.7*). All the data for a run at a given temperature are integrated at the same time with each run integrated using an individual UB matrix.

Manual integration is a way to check the quality of the integration, letting the user integrate individual peaks. This allows the user to select the criteria and integrate individual peaks manually, thus offering an evaluation of the different types of integration and to select the best for the specific data set. This also allows the user to replace values for peaks that they believe to be incorrect and ensuring the program is operating correctly.

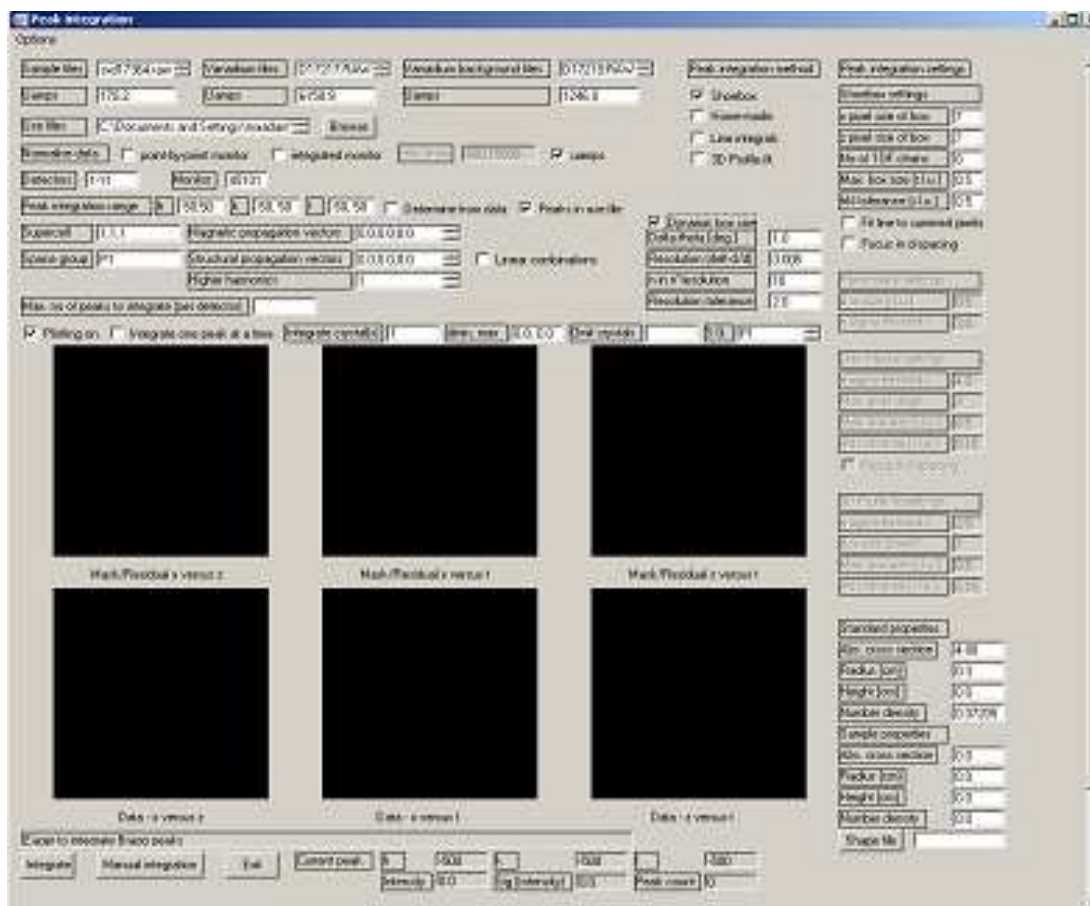


Figure 4.7 Integration window allowing a varied array of customised integration.

#### 4.6 Data correction, normalisation, absorption, extinction and refinement

To get the intensity information into a usable form it first has to be scaled to take into account the size of the crystal, the absorption of the different atoms in the unit cell, extinction and the incident flux of the data collection frame. These are calculated by the program in one step, requiring information on the crystal size, scattering and absorption cross section and the density. The SXD2001 program can then output the data in several file formats so that it is usable for different refinement programs (SHELXL (WinGX), GSAS, FULLPROF, and JANA2000).

In this project the structures from the neutron data have been refined using WinGX (SHELXL) using the *hkl* 2 data format (includes wavelengths) output by SXD2001. The atomic scattering factors need to be altered to the neutron values and the data from each detector has to be scaled to account for the difference in flux, which is done by Batch Scale Factor (BASF) values within SHELX. In a good data set the

BASF values should be around one, whereas large variation in the values can indicate a problem with the processing of the data. In the early stages of this project there were some problems arising from the integration of the data but the structures reported here all show reasonable values for the BASF, R-factors, and realistic atomic displacement parameters. Any anomalous values for any of these can be an indicator of a poor integration. SXD2001 produces reliable results and provides a flexible platform for processing data from SXD.

## 5. Hydrogen bonding in dihydroxybenzoic acids

As previously discussed neutron diffraction provides quite different information compared to X-ray diffraction regarding molecular structure, despite both techniques having a lot in common. The differences between X-ray and neutron diffraction are especially relevant when looking at hydrogen atoms and hydrogen bonding because of the relative accuracy in determination of hydrogen atoms that can be achieved. The relevance of neutron diffraction to the project has meant that it has played a large and vital role throughout. Time on two European neutron sources, ISIS at Rutherford Appleton Laboratory in the UK and the ILL in Grenoble, France, have provided useful data and results that have been integral to the research, as well as presenting several hurdles. The difference in techniques and software at the two facilities and between the instruments used, SXD (ISIS), VIVALDI and D19 (ILL) provide distinct advantages and disadvantages. Difficulties, especially in data processing, from both sites have presented problems that have required time and effort to overcome during the project. However the results have generally been well worth the effort.

Although the project has revolved round the same theme, looking at suspected disordered hydrogen bonding and hydrogen bonded systems, each time slot at the neutron sources has naturally been allocated for a specific complex or molecule or in some more recent cases a series of closely related molecules or complexes. Each experiment can therefore be considered almost separately, with each material studied by neutrons examined in collaboration with different colleagues, or as a result of other work done during the project. This section will try and convey the reasons that each target molecule or complex has been chosen, the experiment carried out in each case and the results and conclusions that can be drawn. 2,4-dihydroxybenzoic acid and 2,5-dihydroxybenzoic acid, although examined in separate experiments, will be discussed jointly because of their obvious similarities, and will form chapter 5. The collaborative experiments on compounds of isonicotinamidium formate, 2-Iodoanilinium picrate, and malonic acid will be described in *Chapter 6*. The VIVALDI neutron experiments for 2:1 2,4-lutidine chloranilic acid form I co-crystal will be discussed within *Chapter 7*, as the results should be considered in conjunction with the other research done into this complex.

## 5.1 Carboxylic acid dimer motifs in benzoic acids

Benzoic acid and its derivatives have been of longstanding interest for their hydrogen bonding networks and motifs<sup>78-82</sup> and for some derivatives showing proton disorder<sup>23,83,84</sup>; carboxylic acid dimers are well known to exhibit proton disorder in the solid state<sup>79</sup>. The benzoic acid structure is based round hydrogen bonded dimerised carboxylic acid groups, which is also a common motif in several of its derivatives. This motif can form in two configurations (**Figure 5.1**), differing by the transfer of two protons across the hydrogen bonds. Tautomerisation of the two forms results in proton disorder, with the hydrogen in each hydrogen bond having two possible locations. In the solid state the potential energy surface of the system in this situation is an asymmetric double minimum well with one configuration at a slightly lower energy than the other (**Figure 5.2**).

Neutron diffraction measurements have been performed on benzoic acid<sup>79,85</sup> allowing the occupancies of the two sites to be mapped at different temperatures. At 20 K the occupancy is 87 % to 13 %; the occupancy of the secondary site increases with rising temperatures until at 175 K the ratio is 62 % to 38 %<sup>79</sup>. Increased hydrogen disorder with increasing temperature is a common trend and agrees with the results of IR and NMR studies which have been used to examine benzoic acid previously<sup>82</sup>. Proton tunnelling, which dominates the transfer rate at low temperatures, is of great interest in this material, and has been studied by NMR experiments<sup>80,82</sup>. Ab initio quantum mechanical calculations (described in **Section 5.5**)<sup>86</sup> and molecular dynamics simulations<sup>87</sup> fit well with the experimental results, and were able to predict the energy barriers and different conformations, as well as model the tautomerism.

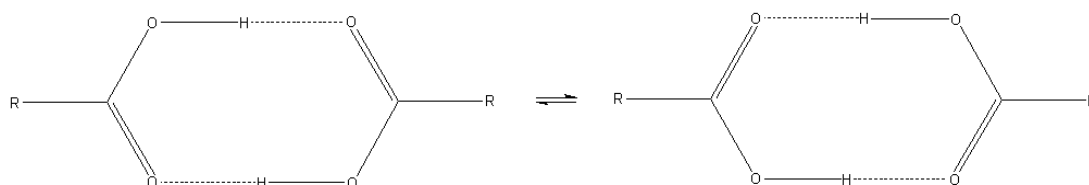


**Figure 5.1** The two possible tautomers for benzoic acid carboxylic acid dimer.

4-Iodobenzoic acid is a derivative of benzoic acid that also shows signs of dynamic proton disorder in a similar manner to that seen in benzoic acid itself (**Figure 5.1**)<sup>83</sup>. The X-ray difference Fourier maps show clear secondary peaks that grow in population with increasing temperature. These are clearly present at 100K, and at around room temperature are almost as occupied as the original positions.

A halo-substituted benzoic acid that shows proton transfer is 4-chlorobenzoic acid. Wilson et al <sup>84</sup> used neutron diffraction to show the temperature-dependence of the two dimer configurations and compare it with that of benzoic acid. The results backed up previous NMR relaxometry measurement estimates for the energy asymmetry associated with the proton transfer <sup>81</sup>, and similar studies have been carried out on other halo-benzoic acids. The energy asymmetry of the two wells of the potential energy surface is significantly larger for the halo-substituted molecule than for benzoic acid itself (around 2.6 times greater).

### 2,4- and 2,5-dihydroxybenzoic acid, cooperative hydrogen bonding

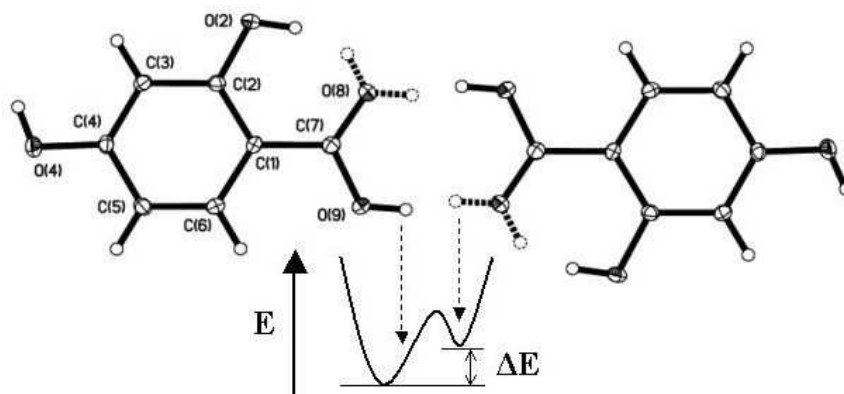


**Figure 5.2** The dimerised structure of 2,4-dihydroxybenzoic acid with the classical representation of an unsymmetrical double well minimum indicating the possibility for proton disorder by thermal population of the slightly higher energy configuration. The dotted line indicates the alternative locations for the disordered protons.

2,4-dihydroxybenzoic acid and 2,5-dihydroxybenzoic acid both form structures incorporating carboxylic acid dimers: they are of extra interest because of their additional hydroxyl groups that can also act as hydrogen bond donors and acceptors

(*Figure 5.2*) in potential intramolecular hydrogen bonds. The carboxylic acid group and the two hydroxyl groups thus have great potential for forming interesting hydrogen bonding networks in the solid state. Both molecules have hydroxyl groups in the ortho-position, adjacent to the carboxylic acid group, and these have a strong tendency to form an intramolecular hydrogen bond with the hydroxyl of the carboxylic acid group. The other (para) hydroxyl group in both structures usually forms an intermolecular hydrogen bond.

As both the intramolecular and dimer hydrogen bonds share the same oxygen as an acceptor atom, a change in one will most likely trigger an effect in the other. This leads to the idea of a cooperative effect. Several different tautomeric layouts, with the hydrogens taking up different positions, are possible.

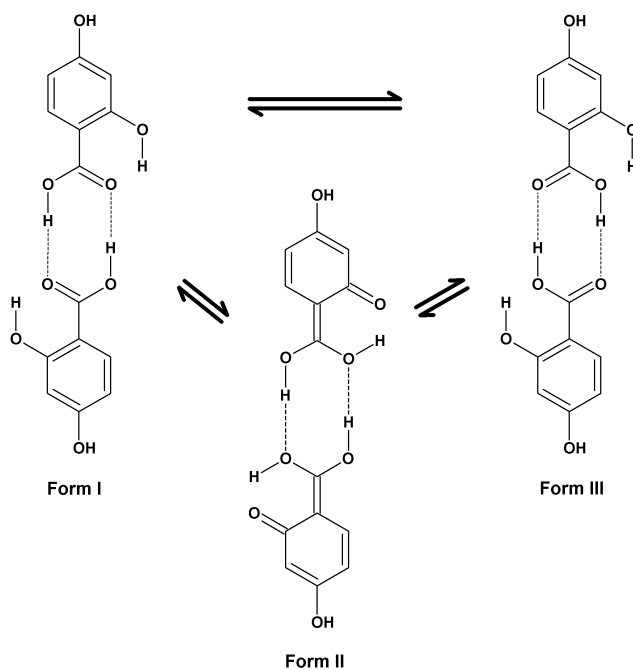


*Figure 5.3* Scheme showing three possible tautomers of 2,4-dihydroxybenzoic acid.

In *Figure 5.3* the three likely end-point tautomers in the isomer 2,4-dihydroxy benzoic acid are shown. There are only three of these as the other combinations would have two hydrogens on the same donor atom or the two hydrogens of the dimer on the same side, both of which are energetically disfavoured. Although these alternative configurations do not exist as long-lived stable conformers, it is not to say they do not exist as excited states or transition states with respect to the three main tautomeric dimer configurations. A cooperative relationship between the

intermolecular carboxylic acid dimer and the intramolecular hydrogen bond can therefore be imagined where they interchange between the three forms (*Figure 5.3*). In the solid state, this can be manifest by the presence of partially occupied alternative hydrogen sites in the determined structure.

## 5.2 2,4-dihydroxybenzoic acid

The original structure of 2,4-dihydroxybenzoic acid ( $C_7H_6O_4$ ) was solved in  $P\bar{1}$ <sup>88</sup> as part of a programme aimed at finding a suitable matrix-assisted laser desorption/ionisation matrix molecule. Work carried out as part of the present project found a new polymorph in a monoclinic space group, which from initial indications appeared to show cooperative temperature dependent disorder among the hydrogen bonding configuration<sup>18</sup>.

The structure of the new polymorph was characterised by multiple-temperature X-ray diffraction and followed up with preliminary solid-state DFT computations. Because of the possibility of a cooperative disordered hydrogen-bonded system, neutron diffraction was then carried out to provide an accurate and unambiguous description of the material. Additional comprehensive periodic quantum chemical calculations, both static and dynamic, were run, allowing the determination of the energy differences between the potential hydrogen-bonded configurations.

### 5.2.1 Experimental

Crystals of 2,4-dihydroxybenzoic acid were grown from acetone solution by slow evaporation in a vial covered with pierced parafilm at room temperature. Large single crystals suitable for neutron diffraction studies were obtained in the same way although in this case the vial was sealed to slow the rate of evaporation.

### 5.2.2 Comprehensive variable temperature X-ray studies

An initial X-ray study of the new polymorph of 2,4-dihydroxybenzoic acid was carried out in order to examine the hydrogen bonding involved in the material. The structure of the new polymorph consists of centrosymmetric dimers (*Figure 5.4, labelled A*) linked by hydrogen bonds between the carboxylic groups as shown in

**Figure 5.2.** An additional intramolecular hydrogen bond is formed between the hydroxyl group on the ortho-position and the hydroxyl of the carboxylic acid group (**Figure 5.4, labelled B**). The oxygen on the ortho-position also acts as an acceptor for an intermolecular hydrogen bond with the hydroxyl group at the para-position (**Figure 5.4, labelled C**). All the hydrogen bonds are therefore connected, sharing donor and acceptor atoms. The molecules form hydrogen bonded layers which interact with each other by  $\pi$ - $\pi$  interaction (**Figure 5.4**). The layers have a slight undulation and are comprised of tautomer Form I configuration (**Figure 5.3**).

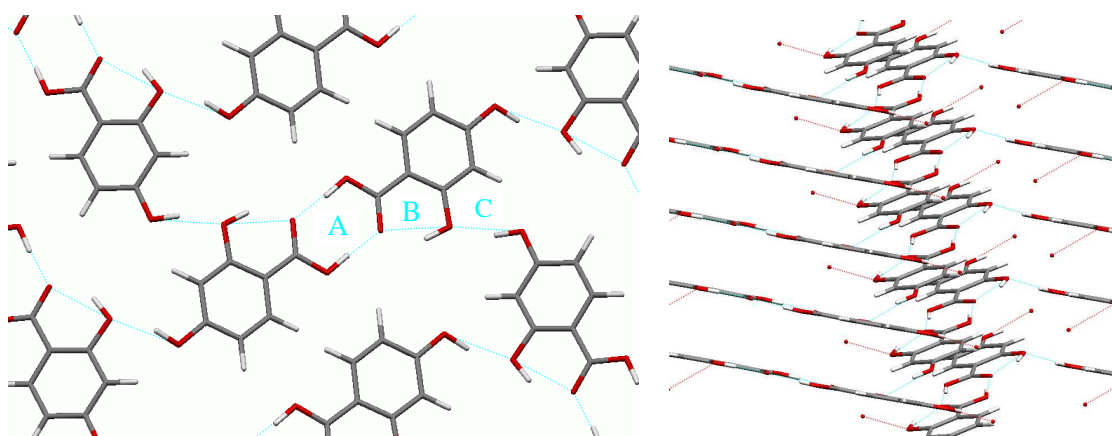


**Figure 5.4** Structure of 2,4-dihydroxybenzoic acid showing a layer (viewed along the *a*-axis) that is held together by three hydrogen-bonding motifs: (A) intermolecular dimer; (B) intramolecular; (C) intermolecular. The view on the right shows the staggered  $\pi$ - $\pi$  stacking.

Initial analysis of the hydrogen bonding showed signs of potentially anomalous behaviour of the hydrogen atoms within the carboxylic acid dimer and intramolecular hydrogen bonds. In the refined model the isotropic thermal parameters are larger than would be expected for normal hydrogens. The difference Fourier maps revealed possible extra density peaks suggesting hydrogen disorder (**Figure 5.6**). In light of this further multiple temperature X-ray studies were undertaken.

A variable temperature X-ray experiment allows changes to be tracked over the temperature range. In the case of hydrogen disorder occupancy level of the second site would be expected to increase with increasing temperature as more energy is available for the proton to move across the barrier and fill the excited states. Visible

signs of this would be that the refinement thermal parameters of the hydrogens under investigation become enlarged at higher temperatures (in neutron studies where anisotropic refinement is possible, disfiguration or elongation across the bond can be seen). Another indication would be that in the difference Fourier maps the electron density for hydrogen would deviate from a smooth spherical shape, or additional peaks appear in case of hydrogen disorder.

**Table 5.1** Crystallographic data for 2,4-dihydroxybenzoic acid at 90 K.

a(Å)	3.6686 (5)	V(Å <sup>3</sup> )	646.58 (15)
b(Å)	22.333 (3)	N <sub>total</sub>	5714
c(Å)	8.0046 (11)	N <sub>unique</sub>	2022
α(°)	90	N <sub>param</sub>	125
β(°)	99.630 (3)	R <sub>f</sub> I>2σ(I)	0.0560
γ(°)	90	WR <sub>2</sub> (all data)	0.1449

The hydrogen positions were refined for all the temperatures from the X-ray data. In the refinement shown in **Figure 5.5**, the hydrogen atoms were allowed to refine isotropically to highlight any possible signs of disorder. In **Table 5.1** the refinement details are summarised for the 90K data and in **Table 9.7** the refinement details for all the published variable temperature data.

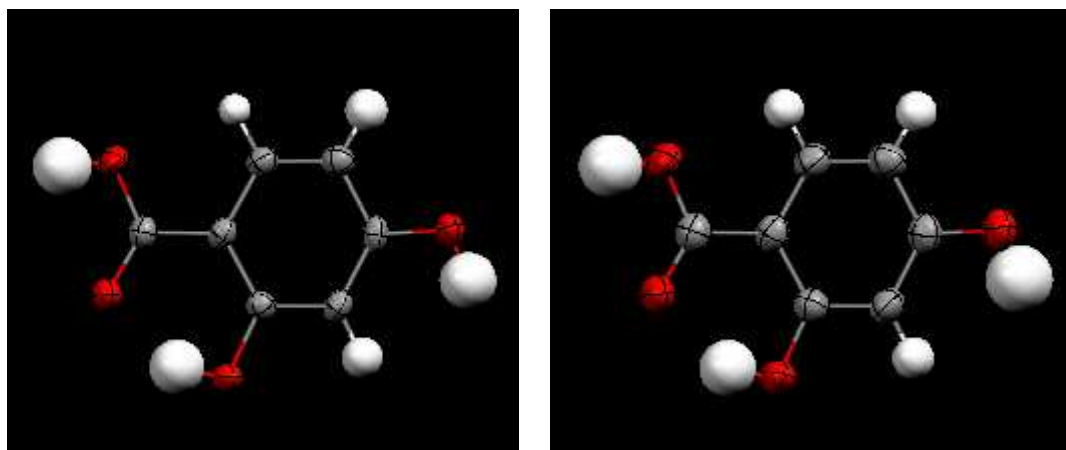


**Figure 5.5** Structure 2,4-dihydroxybenzoic acid determined from X-ray data at (**left**) 90 K and (**right**) 150K with hydrogens allowed to refined isotropically.

Two of the structures from the multiple temperature X-ray experiment are shown in **Figure 5.5**. The large isotropic thermal parameters for the three hydrogen bonded

atoms are an indication that disorder could be present. The expected increase in thermal parameters by going from 90 K to 150 K is pronounced for the H atoms involved in the intermolecular HB (**A** and **C** *Figure 5.4*).

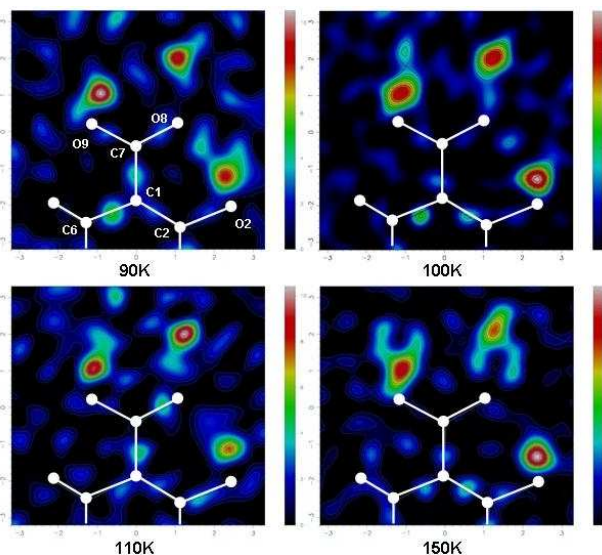


**Figure 5.6** Difference Fourier maps of 2,4-dihydroxybenzoic acid at 90 K, 100 K, 110 K, and 150 K in the plane of C7, O8, and O9. RMS = 0.09 e/Å<sup>3</sup>, 0.09 e/Å<sup>3</sup>, 0.09 e/Å<sup>3</sup>, 0.09 e/Å<sup>3</sup>

Difference Fourier maps, in the plane of the carbon and two oxygens of the carboxylic group, for four temperatures are shown in *Figure 5.6*. An initial low temperature of 90 K is shown with three higher temperatures of 100 K, 110 K, and 150 K revealing how the bonds evolve with a temperature increase. At 90 K the peaks in the dimer (**A**) do not show much sign of disorder but in the intramolecular bond (**B**) indications of a secondary peak around a third of the height of the main peak of the hydrogen is seen close to O8. This would suggest at 90 K there is no disorder in **A** but possible disorder in **B**. The other relatively large peaks correspond to bonding electron density between the atoms and is normal in good data where the refinement model does not take into account the density involved in the covalent bonds.

At 100 K the secondary peak in **B** is reduced to around a quarter of the main peak height; the dimer (**A**) has now developed a secondary peak just less than half the relevant hydrogen peak height beside O8. At 110 K the intramolecular hydrogen bond (**B**) disorder is all but disappeared with only a diffuse patch of electron density

present beside the original hydrogen position. The disorder peak in **A** appears to have grown in area but not height and shows a greater affiliation with the original peak. At the highest temperature shown, 150 K, any indication of disorder in the intramolecular bond (**B**) is totally gone, and the hydrogen peak is circular. The peaks representing the hydrogen in the dimer (**A**) are irregular and misshapen along the length of the bond.

The difference Fourier maps suggest that at low temperatures H disorder may be present in the intramolecular hydrogen bond **B** and as the temperature rises that this decreases and disappears. On the other hand the carboxylic acid dimer initially has no disorder but as the temperature increases, possible indications of a second position of electron density appears and the electron density for H becomes more irregular in shape. This would be consistent with a pattern of hydrogen bonding cooperativity between the intermolecular carboxylic acid dimer and intramolecular hydrogen bonds. A tentative theory that the disorder started in the intramolecular bond but was then transferred to the dimer due to the shared oxygen acceptor atom was thus hypothesized.

Further X-ray experiments were carried out with different crystals and on different instruments to check that this was not a specific crystal effect, and to demonstrate a repeatable experiment. Not all results showed the secondary density peaks possibly indicative of disorder, although it was present in a significant number. The X-ray studies thus did not fully rule out the cooperative hydrogen bonding disorder making further experiments necessary. Both neutron experiments and computational studies were then used to determine whether any disorder was in fact present in this system.

### 5.2.3 SXD variable temperature neutron studies

Since the results from the X-ray experiment did not rule out the possibility of disorder, neutron diffraction experiments were carried out. Four days of data collection on the material were obtained on the SXD instrument at the ISIS spallation neutron source. The neutron data would be able to give an unambiguous answer to whether there was disorder present and on any cooperative hydrogen bonding effect due to the more reliable imaging of proton positions from neutron diffraction data.

Initial aims were to obtain data for a range of temperatures from 20 K to 300 K but due to technical difficulties, crystal degradation, and loss of beam, data sets at only three temperatures were fully collected. The helium cryostat allows temperatures below 4 K to be achieved but 20 K was chosen as the lowest temperature as no significant gain would be achieved by going lower in T and this was the most effective use of time. Data at two further temperatures of 90 K and 150 K were also collected. These temperatures were chosen to allow for direct comparison with the X-ray data. At 90 K the disorder was expected in the intramolecular hydrogen bond (**B**) from the results of the X-ray experiment, whereas at 150 K the disorder should have transferred across to the carboxylic acid dimer (**A**) if the cooperative model was correct. The 20 K structure provides a good reference to compare with the other temperatures and also allows the low temperature region to be explored.

The structure models of 2,4-dihydroxybenzoic acid refined from the neutron data are shown in *Figure 5.7*. At 20 K the data refines well, the hydrogens show some lateral motion in the slant of the ring but this is in line with their relative mobility and they show reasonable anisotropic displacement parameters. The two hydrogens most suspected of disorder in **A** and **C** (H1 and H2) show no abnormal behaviour at this temperature.

The X-ray refinement and the neutron refinement are both very similar with all the bond lengths and angles comparable, apart from the bond lengths involving hydrogen that are inevitably shorter in the X-ray model; a consequence of the electron density being drawn into the bond.

There is a gradual increase in the size of the atomic displacement parameters for all atoms as the temperature is increased due to the larger displacements at higher temperature (*Figure 5.7*). As expected, this is most marked in the hydrogen atoms, but the overall shapes stay close to spherical. No deformation in shape is observed for the hydrogens under investigation.

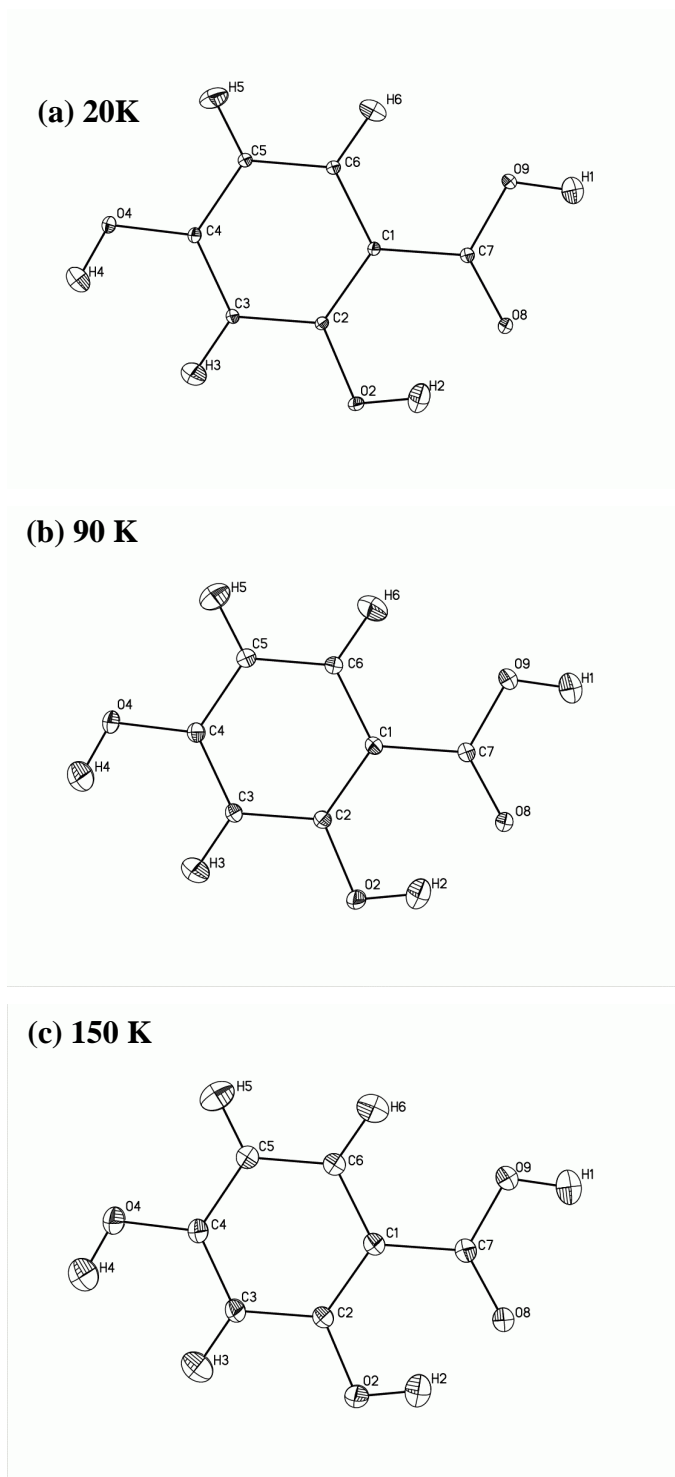


*Figure 5.7* The structure of 2,4-dihydroxybenzoic acid refined from neutron data at (a) 20 K, (b) 90 K, and (c) 150 K

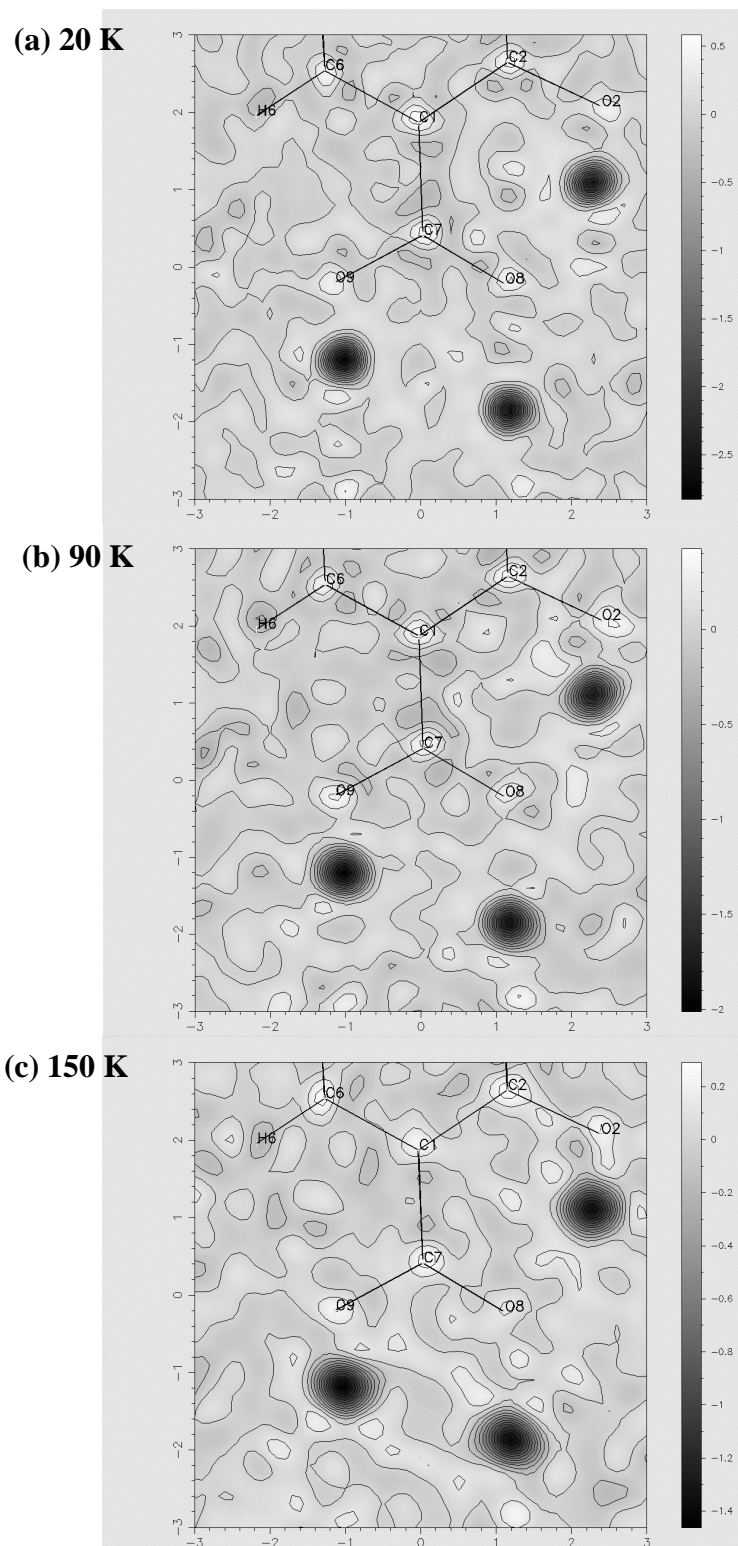


**Figure 5.8** Difference Fourier maps for 2,4-Dihydroxybenzoic acid at (a) 20 K, (b) 90 K, and (c) 150 K produced from neutron data collected on SXD, in the plane of C7, O8, and O9. The well-defined H atom density is apparent at all temperatures. The scale is in fm and the respective RMS on these values are (a) 0.07 fm/Å<sup>3</sup>, (b) 0.05 fm/Å<sup>3</sup>, and (c) 0.04 fm/Å<sup>3</sup>.

**Table 5.2** Bond lengths and angles for the hydrogen bonds in 2,4-dihydroxybenzoic acid from the neutron refinements.

	<i>D-H</i>	<i>H...A</i>	<i>D...A</i>	$\angle$ <i>D-H...A</i>
20K <b>A</b>	1.003(2)	1.653(2)	2.6539(17)	175.1(3)
<b>B</b>	0.985(2)	1.756(3)	2.6270(19)	145.40(19)
<b>C</b>	0.976(2)	1.831(3)	2.776(2)	162.13(19)
90K <b>A</b>	0.996(3)	1.659(3)	2.653(2)	174.9(4)
<b>B</b>	0.979(3)	1.762(4)	2.628(2)	145.5(3)
<b>C</b>	0.973(3)	1.835(3)	2.776(2)	162.1(3)
150K <b>A</b>	0.999(4)	1.657(4)	2.654(3)	175.2(4)
<b>B</b>	0.977(4)	1.762(4)	2.626(3)	145.4(3)
<b>C</b>	0.979(4)	1.837(4)	2.785(3)	161.9(3)

**A:** O9-H1...O8, **B:** O2-H2...O8, **C:** O4-H4...O2

The neutron difference Fourier maps of 2,4-dihydroxybenzoic acid in the plane of C7, O8 and O9 (carboxylic acid group), show well shaped hydrogen positions and it is evident that there is no proton disorder in any of the hydrogen bonds (**Figure 5.8**). Even at the highest temperature measured in the neutron experiments (150 K) both the dimer (**A**) and intramolecular (**B**) proton densities are spherical with no evidence for a second position.

There is a gradual increase in the size of the atomic displacement parameters of the hydrogen atoms with increasing temperature relating to their increasing mobility, but the overall shapes stay close to spherical and no second (disordered) positions for the hydrogen atoms are observed.

The bond lengths for all the non-hydrogen atoms are in good agreement with those of the X-ray structure, they differ only slightly and are within the experimental error. The length of bonds to hydrogens cannot be compared directly between the X-ray and neutron structures unless the associated shift is taken into account. Both change very little as the temperature increases with a slight fluctuation in the position of the hydrogen in some of the bonds and the donor-acceptor length virtually the same throughout. Examining the three temperatures of the neutron experiment the three bonds have only slight differences in hydrogen position throughout. The changes in bond **A** and **C** are random, the changes in **B** follow a progression of the donor hydrogen bond reducing in length and the acceptor hydrogen increasing in size as the temperature rises but these are so small that it is probably incidental.

This is an important “null” finding; with no disorder observed in the definitive neutron diffraction experiments, there is no evidence of cooperative behaviour between hydrogen bonds in this system.

#### 5.2.4 Conclusions on 2,4-dihydroxybenzoic acid

The neutron diffraction data give a decisive conclusion that the protons within the three hydrogen bonds are not disordered. This would appear to contradict the initial X-ray diffraction experiment that showed possible secondary density peaks that could have indicated hydrogen disorder in at least two of the hydrogen bonds, and cooperation between these. The results from the X-ray experiment were only providing an indication of possible disorder derived from small secondary density peaks and these alone were obviously insufficient clear to prove disorder in the hydrogen bond. However, it was, important to use neutron diffraction to ensure no proton disorder existed.

A further possibility is that although the proton of the hydrogens doesn't show any sign of a second position, the electron density could still show anomalous effects. The neutron diffraction only observes the hydrogen nucleus so any abnormal behaviour in the electrons can not be detected. The electrons are far more mobile than the proton, so it is possible that even if the proton is in a stable state the electron density around it could show anomalous behaviour.

#### 5.3 2,5-Dihydroxybenzoic acid

The closely related structure of the isomer 2,5-dihydroxybenzoic acid<sup>89</sup> has a very similar hydrogen bonding motif to that of 2,4-dihydroxybenzoic acid. With 2,4-dihydroxybenzoic acid suspected of containing proton disorder, 2,5-dihydroxybenzoic acid, because of its similarity in structure, was then also a candidate for investigation. A study using variable temperature X-ray and neutron single crystal diffraction as well as theoretical calculations was undertaken in parallel with that of 2,4-dihydroxybenzoic acid.

2,5-dihydroxybenzoic acid (**Figure 5.9**) contains a carboxylic acid group (labelled C7, O8, O9, H1) and two hydroxyl groups (O5, H2, and O2, H5), which are involved in hydrogen bonding in the crystal structure.

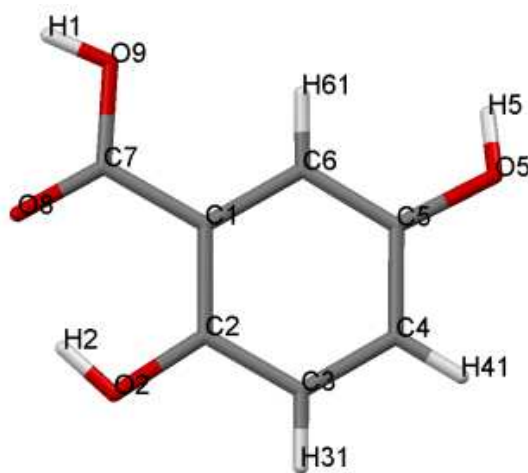


**Figure 5.9** Molecule of 2,5-dihydroxybenzoic acid showing atom labels

Crystals of the material can easily be grown by slow evaporation from acetone solution, normally forming white opaque flat blocks.

### 5.3.1 Variable temperature X-ray diffraction

X-ray diffraction data for 2,5-dihydroxybenzoic acid were collected from 100 K to 350 K at 50 K intervals to chart the evolution of the hydrogen bonds. 2,5-dihydroxybenzoic acid forms planar ribbons that stack flat on each other forming layers with adjacent layers having the ribbons running perpendicular to each other. It also contains three crystallographic unique hydrogen bonds (HBs), two intermolecular (**A** and **C**) and one intramolecular (**B**) (**Figure 5.10**). The carboxylic acid group (C7, O8, O9) forms an intermolecular HB dimer (**A**) with the centre of the dimer located on an inversion centre. O8, the non-protonated oxygen of the carboxylic acid group, also acts as the acceptor atom with the hydroxyl group (O2-H2) forming an intramolecular HB (**B**). The other hydroxyl group (O5-H5) forms an intermolecular HB (**C**) with its symmetry equivalent on a neighbouring molecule, forming a continuous hydrogen bonded chain along the b-axis.

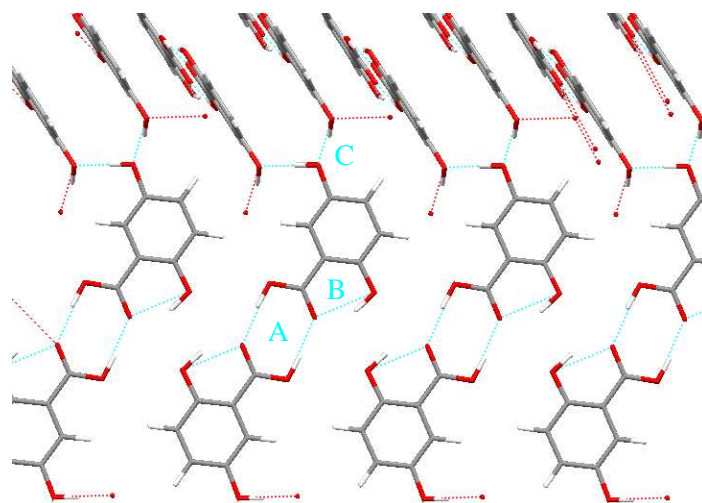


**Figure 5.10** Structure of 2,5-dihydroxybenzoic acid in the plane of one of the flat ribbons also showing the perpendicular ribbons it is bonded to. The three hydrogen-bonding motifs are labelled: (A) intermolecular carboxylic acid dimer, (B) intramolecular, (C) intermolecular chain involving O5 and H5.

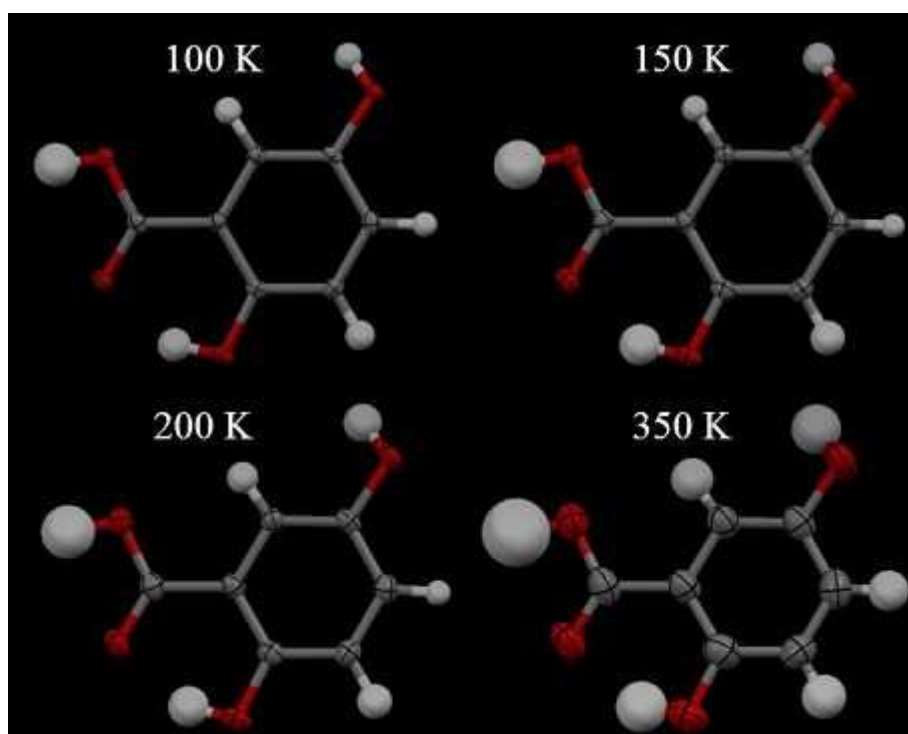


**Figure 5.11** Structure models of 2,5-dihydroxybenzoic acid from the multiple temperature X-ray experiment.

**Table 5.3** The crystallographic data for 2,5-dihydroxybenzoic acid. At 100 K all H positions were fully refined.

<b>a</b> (Å)	5.5591(2)	<b>V</b> (Å <sup>3</sup> )	631.23(4)
<b>b</b> (Å)	4.8698(2)	<b>N<sub>total</sub></b>	11756
<b>c</b> (Å)	23.3593(9)	<b>N<sub>unique</sub></b>	1463
<b>α</b> (°)	90.00	<b>N<sub>param</sub></b>	120
<b>β</b> (°)	93.448(2)	<b>R<sub>f</sub>I&gt;2σ(I)</b>	0.0391
<b>γ</b> (°)	90.00	<b>WR<sub>2</sub>(all data)</b>	0.1302

The structure refinement of 2,5-dihydroxybenzoic acid was carried out using CRYSTALS<sup>63</sup>. The refinement data for the 100 K experiment are summarised in **Table 5.3** and the refinement data for all temperatures are in **Table 9.7**. In **Figure 5.11** the structures at four of the temperatures measured are shown (100 K, 150 K, 200 K, 350 K), with the hydrogens allowed to refine isotropically. The progression in increase of the size in the thermal ellipsoids (spheres for the isotropic thermal parameters of the H atoms) is visible concluding with large ellipsoids at 350 K. Even at 100 K the size of the thermal motions of H1 (in bond **A**), and to a lesser extent the other two hydrogens in hydrogen bonds (**B** and **C**), are larger than those for the other hydrogens. This could suggest either disorder or a more extensive thermal motion of the H atoms involved in H bonding with the thermal parameter increasing to accommodate the more diffuse nature of the H atoms and thus the associated electron densities.

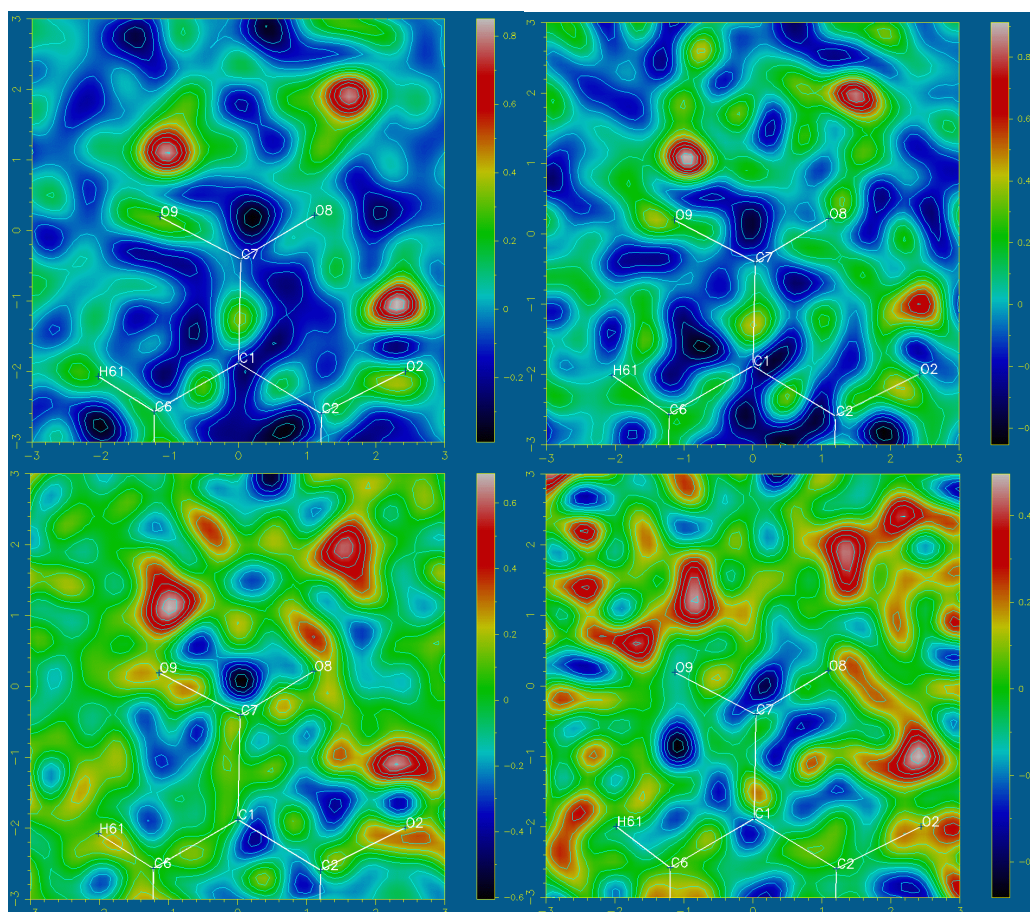


**Figure 5.12** Difference Fourier maps of 2,5-dihydroxybenzoic acid at 100 K, 150 K, 200 K, 350 K in the plane of C7, O8, and O9. RMS =  $0.08 e/\text{\AA}^3$ ,  $0.09 e/\text{\AA}^3$ ,  $0.08 e/\text{\AA}^3$ ,  $0.08 e/\text{\AA}^3$

The difference Fourier maps from the X-ray study on 2,5-dihydroxybenzoic acid compared with those for the 2,4-dihydroxybenzoic acid do not give any particular indication of any possible secondary density peaks. At 100 K the electron density peaks representing the hydrogens in question are very prominent. Although the dimer (**A**) hydrogen has additional areas of density attached to the main peak both in the direction of the bond and to the side of it, those are weak and are comparable with the level of the noise therefore not supportive of the presence of a secondary occupied site. The intermolecular bond (**B**) has an elongated shape along the direction of the bond; this could be a sign of proton migration, with the hydrogen and electron density being transferred towards the middle of the hydrogen bond as the temperature rises.

The temperature trends in these hydrogen atom density peaks again do not provide a consistent picture of any significant disorder indications. However, while this is

compelling, the X-ray difference Fourier maps for the 2,5-dihydroxybenzoic acid do not necessarily conclusively rule out the possibility of disorder or migration in the hydrogen bonds. Neutron data were used to investigate this system further both to eliminate conclusively this possibility and to offer direct comparison with the structure of the 2,4-dihydroxybenzoic acid.

### 5.3.2 SXD multiple temperature neutron studies

A separate but similar experiment to that carried out for its isomer, 2,4-dihydroxybenzoic acid, was thus scheduled to investigate the hydrogen bonding network in this material. Three days on SXD were allocated to allow a multiple temperature neutron study on 2,5-dihydroxybenzoic acid.

Complete data sets were collected for three temperatures, 20 K, 100 K and 200 K. Diagrams of the structures at the three temperatures for 2,5- dihydroxybenzoic acid are shown below in *Figure 5.13* and Fourier difference maps are shown in *Figure 5.14*.

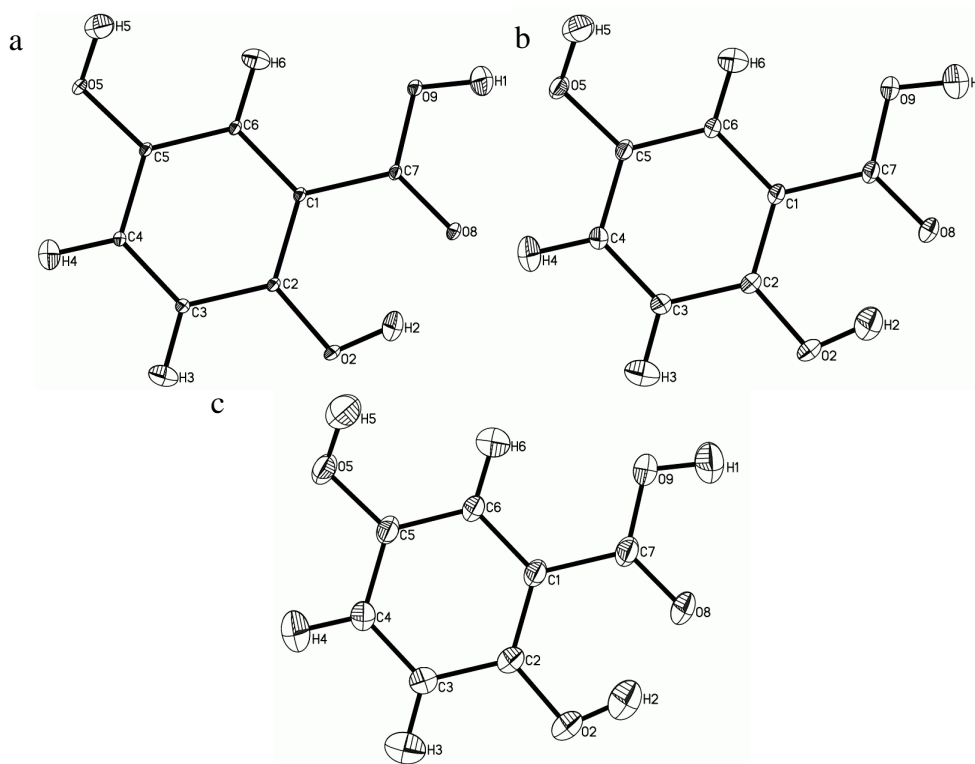


*Figure 5.13* The structure of 2,5-dihydroxybenzoic acid determined from neutron diffraction data at (a) 20 K, (b) 100 K, and (c) 200 K.

At 20 K (**Figure 5.13 a**), all the carbon atoms and oxygen atoms show small and reasonably spherical ellipsoids, as would be expected at this temperature because of the lack of thermal motion. The protons have larger ellipsoids in line with their larger freedom to explore the hydrogen bond potential, and their shapes reveal no indication of any unusual behaviour. With increasing temperature to 100 K and 200 K (**Figure 5.13 b and c**) the ellipsoids expand at the same relative rate.

The bond lengths and angles for the three hydrogen bonds (D-H, H $\cdots$ A, D $\cdots$ A and  $\angle$  D-H $\cdots$ A) remain constant, apart from small deviation, with increasing temperature.

	<i>D-H</i>	<i>H<math>\cdots</math>A</i>	<i>D<math>\cdots</math>A</i>	$\angle$ <i>D-H<math>\cdots</math>A</i>
20K <b>A</b>	1.000(2)	1.715(2)	2.7097(16)	172.81(18)
<b>B</b>	0.988(2)	1.691(2)	2.5761(17)	147.09(18)
<b>C</b>	0.989(3)	1.772(3)	2.7506(13)	169.8(2)
100K <b>A</b>	0.997(3)	1.712(3)	2.7049(17)	173.4(2)
<b>B</b>	0.984(3)	1.689(3)	2.573(2)	147.4(2)
<b>C</b>	0.981(3)	1.784(3)	2.7540(15)	169.6(2)
200K <b>A</b>	1.000(3)	1.713(3)	2.709(2)	173.8(2)
<b>B</b>	0.984(4)	1.691(3)	2.573(2)	146.9(2)
<b>C</b>	0.980(3)	1.792(3)	2.7619(16)	169.7(2)

**A:**  $O^9-H^1 \cdots O^8$ , **B:**  $O^2-H^2 \cdots O^8$ , **C:**  $O^5-H^5 \cdots O^5$

**Figure 5.14** Bond lengths and angles for the hydrogen bonds in 2,5-dihydroxybenzoic acid from the neutron refinements.

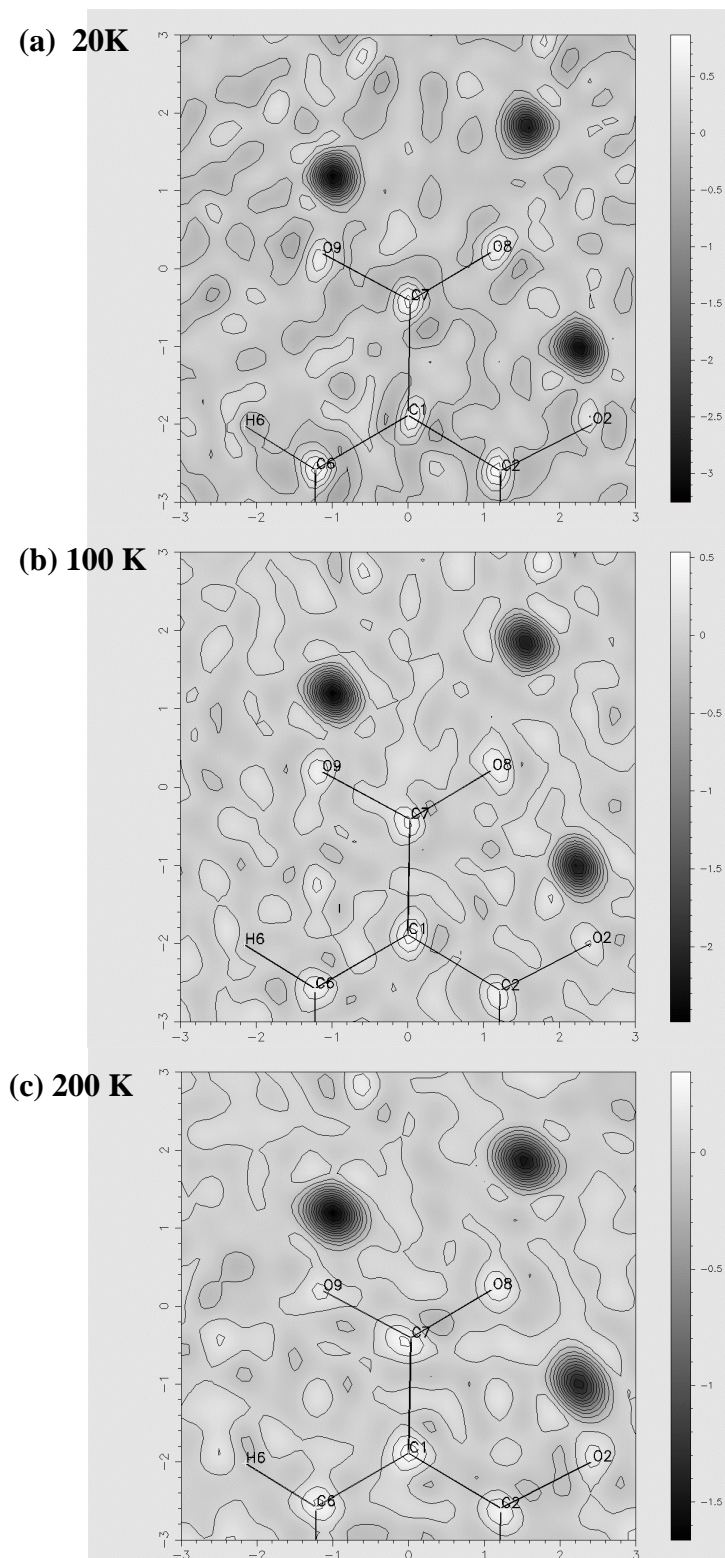


**Figure 5.15** Difference Fourier maps of 2,5-dihydroxybenzoic acid shown at (a) 20 K, (b) 100 K, and (c) 200 K, produced from neutron data collected on SXD, in the plane of C7, O8, and O9. The well-defined H atom density is apparent at all temperatures. The scale is in fm and the respective RMS on these values are (a) 0.09 fm/Å<sup>3</sup>, (b) 0.06 fm/Å<sup>3</sup>, and (c) 0.04 fm/Å<sup>3</sup>.

### 5.3.3 Conclusions on 2,5-dihydroxybenzoic acid

The similarity of the difference Fourier maps to those found for 2,4-dihydroxybenzoic acid is evident with no proton disorder observed within any of the HBs. Only the thermal ellipsoid sizes increase with increasing temperature as expected. The shape of the electron density for H2 in the intramolecular HB diverts slightly from spherical but this is a minor effect and is unlikely to be significant and not a sign of proton disorder.

The neutron experiment conclusively rules out the possibility of proton disorder but because of the nature of the experiment it gives no indication of the characteristics of the electron density involved in the interaction. While this leaves the possibility that although the proton is not disordered the electron density of the atoms involved in the hydrogen bond could show some anomalous behaviour, with more diffuse arrangement where the density is spread across the bond and not fixed to the positions of the protons; there, however, is little evidence for any such effect in this case. Any effect is more likely caused by the general distortion of the electron density present in hydrogen bonds<sup>22</sup>.

The neutron experiment was able to rule out conclusively any disorder of the protons in any of the hydrogen bonds up to a temperature of 200 K. This result is again important in ruling out cooperative hydrogen bond in this system involving an interchange of tautomers.

### 5.4 Computational studies of dihydroxybenzoic acids

After the initial discovery by X-ray diffraction experiment of characteristics potentially indicative of hydrogen bond disorder 2,4-dihydroxybenzoic acid, it was clear that further methods were necessary to clarify the picture. The time needed to arrange and carry out neutron experiments is typically in the range of months and so although this was the best route to give a definitive result, computational studies were also carried out in the interim.

To obtain the energy difference between the three possible end point tautomeric forms (*Figure 5.3*), total energy periodic quantum chemical calculations were carried out using the CASTEP code<sup>54</sup>. The unit cell was fixed to the 90 K X-ray data, and the initial atomic positions were taken from the refinement model. The HB configurations of the three tautomeric forms were set manually. Subsequently the geometries were optimised until all atomic forces were less than 0.01 eV Å<sup>-1</sup>. The unit cell was fixed to the experimental values as current gradient-corrected functionals are known to be poor for describing weak, long-range interactions.

Tautomer form II was not stable in the optimisation and reverted back to form I (the dominant crystallographically observed configuration) by transferring the hydrogen back across the intramolecular HB. Form III was stable but had a higher energy than form I. The calculated energy difference of 8.64 kJ mol<sup>-1</sup> between the two optimized tautomers (forms I and III) is larger than similar systems that have shown unambiguous proton disorder<sup>82,86,90,91</sup>. One explanation could be that this large energy difference is caused by the asymmetry imposed on the dimer interaction by the intramolecular HB. The presence of a hydrogen on O8 makes it a less effective acceptor, weakening the intramolecular bond. It cannot, however, be fully ruled out as a possible conformation.

A further calculation to estimate the energy of form II was carried out. By moving the proton across the intramolecular HB along the line of the two oxygens a rough relative energy was obtained of 90 kJ mol<sup>-1</sup>. A correction was applied to account for the overestimation in energy due to the heavy-atom positions remaining fixed using the stretching frequencies of the relevant bonds. An approximate value of 51 kJ mol<sup>-1</sup> was obtained for the difference in energies between forms I and II. This was later a value of 51 kJ mol<sup>-1</sup> for the difference in energy compared to form I is significantly large making it improbable that any thermal population of form II will be observed. A fuller description of these experiments can be seen in the paper by Parkin et al.<sup>18</sup>

Further calculations were carried out to probe deeper into the two possible stable forms of 2,4-dihydroxybenzoic acid (I & III), examining the difference in energies in several environments<sup>92</sup>. The relative energies of the isolated dimer and the isolated molecule were determined by first principle electronic structure calculations to add to

the previously calculated relative energies of the molecule in the crystal environment. The energy of formation of the intermolecular dimer HB (*Figure 5.16 b*, labelled **A**) can be worked out from the difference in the isolated dimer and isolated molecule (*Table 5.4*). Similarly the stabilisation of the dimers arising from their interaction with the crystalline environment was obtained by taking the difference between the total energies per molecule of the isolated dimer and the total energy of the crystal system. *Table 5.4* shows that tautomer I has a lower energy than tautomer III in all the environments presented. Previously this energy difference was attributed to the presence of the intramolecular HB (*Figure 5.16 b*, labelled **B**) but this was ruled out when the calculation showed that O9 had a higher electronic population than O8 by 0.14e, which should lead to a strengthening of the intramolecular HB (**B**) and therefore an increase in the stability.

**Table 5.4** Results from calculations on forms I and III of 2,4-dihydroxybenzoic acid in various environments as well as the energy of the dimer HB (**A**) and the stabilisation energy **A** gains from the crystalline environment. All energies in  $\text{kJmol}^{-1}$ .

Environment	E (Form I)	E (Form III)	$\Delta E_{\text{FormIII-FormI}}$
Crystal	0.00	8.64	8.64
Isolated dimer	19.65	29.23	9.58
Isolated molecule	55.12	76.67	21.55
Intermolecular dimer HB ( <b>A</b> )	35.47	47.44	—
Stabilisation energies of <b>A</b> in lattice	19.65	20.60	—

The deformation electron density map (*Figure 5.16 a*), generated from the isolated molecule calculations on Form I, shows that another possibility is that the O in the carboxylic acid group has a less favourable orientation of the lone pairs in form III. The O9-H1 and C7=O8 groups have tetrahedral and planar orientations respectively due to the  $\text{sp}^3$  and  $\text{sp}^2$  hybridization of orbitals. In the deformation electron density map the planar orientation of O8 can be seen to have the lone pair also lying in the plane of the molecule making it a better hydrogen bond acceptor than O9 which has the lone pairs pointing out of the plane.

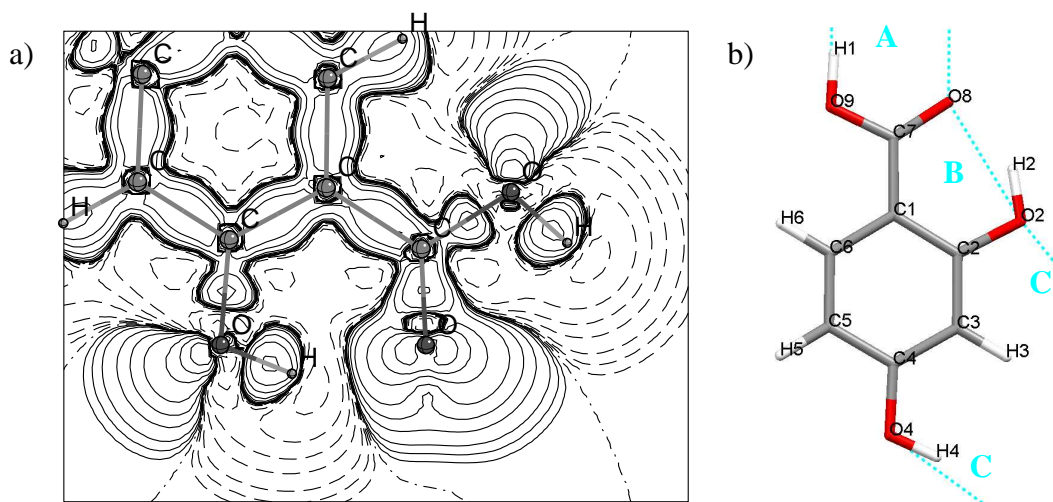


**Figure 5.16** a) The deformation electron density  $\rho_{def}(r) = \rho_{molecule}(r) - \sum \rho_{atoms}(r)$  of the isolated form I monomer of 2,4-dihydroxybenzoic acid. Solid, dashed and dot-dashed lines indicate positive-, negative- and zero-valued contours respectively<sup>92</sup>, b) The atomic numbering and hydrogen bond labelling for 2,4-dihydroxybenzoic acid.

The difference in energy between forms I and III reduces with the formation of the dimer bond (**A**) as seen in **Table 5.4**. This can be attributed to fact that O8 (referring to the O atom involved in the intramolecular HB **B** and protonated) lone pairs in form III will be able to relax from the tetrahedral configuration therefore increasing the strength of the intramolecular HB (**B**) whereas the other monomer has no equivalent energy reduction mechanism. The relaxation happens because of the formation of the dimer HB, which redistributes the electron density to the bond and lengthens the O8-H1 distance. The packing of the dimer into the crystalline state does not significantly change the energy difference showing that the differences are mostly due to intradimer effects.

### 5.5.1 Computational Conclusions

For more detailed and fuller computational details refer to the paper<sup>18</sup>. Overall the calculations agree with the neutron results, showing that form I has the lowest energy which is the tautomer found in the neutron experiments. They also begin to explain why this is the case, showing that the two oxygens of the dimer **A** (O8,O9) take up different orientations which affect the lone pairs and their abilities to be the acceptor for the intramolecular bond **B**.

## 6. Neutron Structures Determined on SXD

### 6.1 Isonicotinamidium Formate

The first neutron experiment of the project was carried out on isonicotinamidium formate, an organic co-crystal that showed promise of disorder effects within its hydrogen bond system. The initial X-ray work on this system was carried out by Dr Ian Oswald, from the Parsons group (Edinburgh), in collaboration with the Wilson group. X-ray structures and Fourier maps carried out as part of the original work provided enough evidence to show the complex had a suspected migrating proton and potential hydrogen bond disorder.

#### 6.1.1 X-ray studies

The crystal structure of the 1:1 molecular complex of isonicotinamide and formic acid contains three crystallographically unique N...O hydrogen bonds through which it forms ribbons perpendicular to the a-axis. These ribbons are stacked above and below each other, and extend in the third direction so the stacks of ribbons are interlocked at their edges. The ribbons are constructed from the two isonicotinamide molecules end on; the amide groups form a dimer around the inversion centre, such that the pyridyl nitrogens are hydrogen bonded to an oxygen of the formic acid (**Figure 6.1**). This four molecule unit is then connected to the next unit through hydrogen bonds between the free oxygen of the formic acid and the nitrogen from the amide group which is involved in the dimer (**Figure 6.1**).

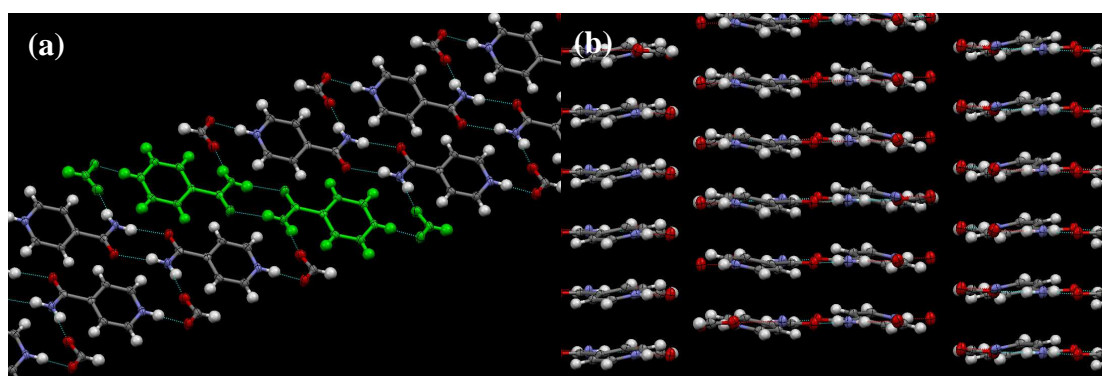


**Figure 6.1** (a) The X-ray structure of isonicotinamidium formate showing the ribbon structure with one dimer unit highlighted in green and the hydrogen bonds shown. (b) The ribbons stack in a staggered fashion as shown.

From the X-ray data, the complex, at least at low temperatures, exists in the salt form with the hydrogen in the intra-molecular hydrogen bond between the pyridyl nitrogen and the formic acid observed to be on the nitrogen. This is also the shortest of the three hydrogen bonds with a N...O separation of 2.544(2) Å at 100 K, due most likely to these being the most basic and acidic atoms in the structure. In some of the neutron refinements the oxygen-hydrogen (acceptor-hydrogen) distance is relatively short because of the strong nature of the hydrogen bond; the classification of this as a strong hydrogen bond is supported by the position of the hydrogen being relatively central. This leaves an ambiguous situation as to whether this should be represented as a quasi-covalent bond. To avoid confusion in all diagrams and figures such a strong potentially covalent HB it will be represented in the same manner as the other hydrogen bonds. The other two hydrogen bonds in the complex are medium in length with the dimer N...O distance 2.908(2) Å at 100 K, and the amide nitrogen formate hydrogen bond having a distance of 2.823(3) Å at 100 K. In both cases the hydrogen is located on the nitrogen as is necessary for it to be an amide.

X-ray diffraction data were collected from a crystal of isonicotinamidium formate at multiple temperatures to allow trends in the behaviour of the hydrogen atoms to be studied systematically. Details of the X-ray refinements for all temperatures are in **Table 9.8**. The results showed that the most significant observation regarding the hydrogen atoms is that the short pyridyl formate hydrogen bond has signs of disorder. Difference Fourier maps of the pyridyl formate bond with the hydrogen removed can be seen in **Figure 6.2**, from 100 K to 300 K; these show secondary electron density that could indicate a second proton site at the higher temperatures. This is a potentially exciting result as such proton disorder is normally only seen where both the donor and acceptor are oxygen atoms; this is an unusual example of a N-H...O hydrogen bond possibly exhibiting temperature-dependent hydrogen atom disorder. The dimer hydrogen bond (**Figure 6.3**) has slightly deformed peak shapes but a single hydrogen site is indicated. The third hydrogen bond in the complex has well defined peaks indicating the location of the hydrogen atom, for the whole temperature range studied.

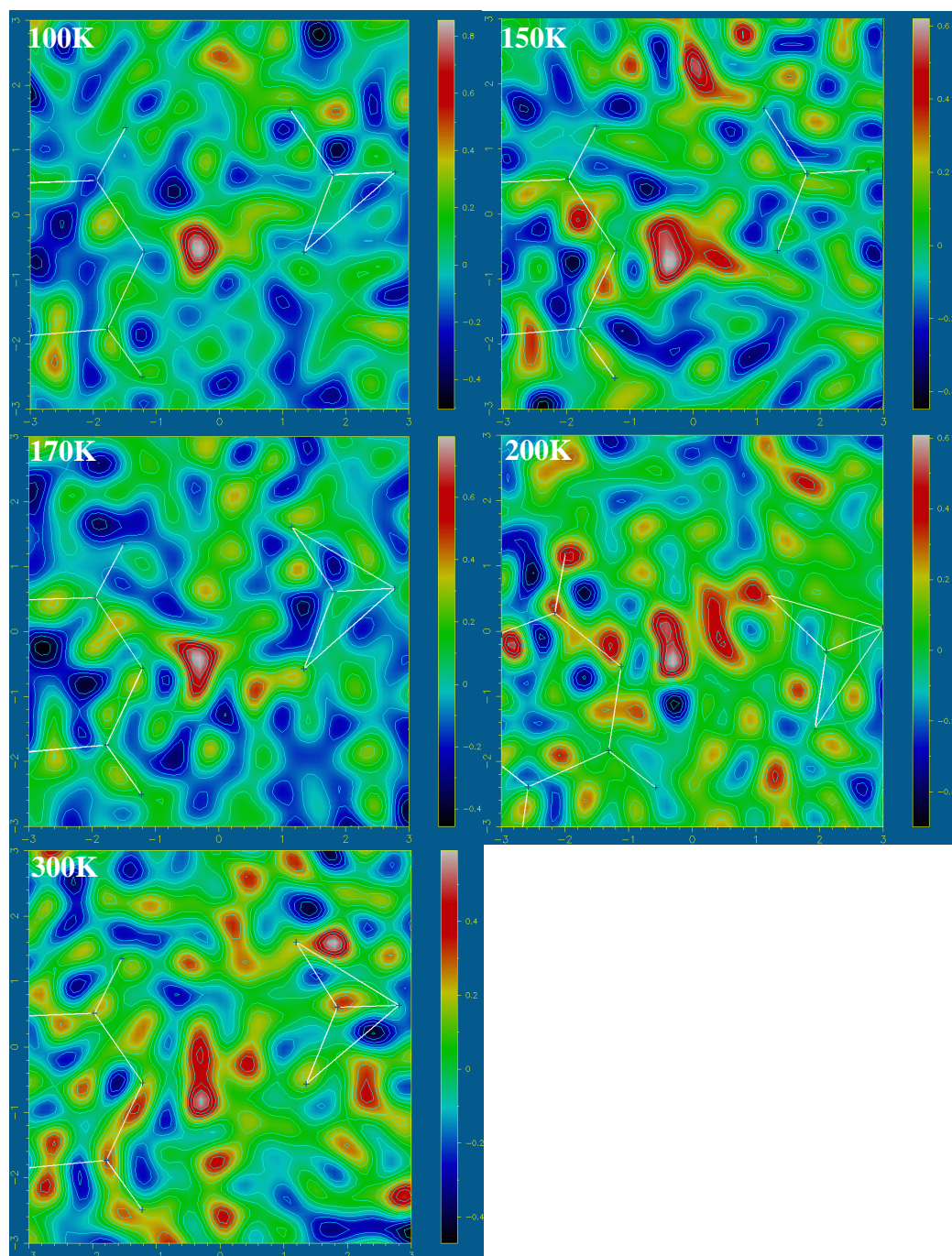


**Figure 6.2** Multiple temperature difference Fourier maps of isonicotinamidium formate showing the pyridyl formate hydrogen bond where the H has been removed from the model. RMS respectively =  $0.10 e/\text{\AA}^3$ ,  $0.09 e/\text{\AA}^3$ ,  $0.09 e/\text{\AA}^3$ ,  $0.08 e/\text{\AA}^3$  and  $0.07 e/\text{\AA}^3$

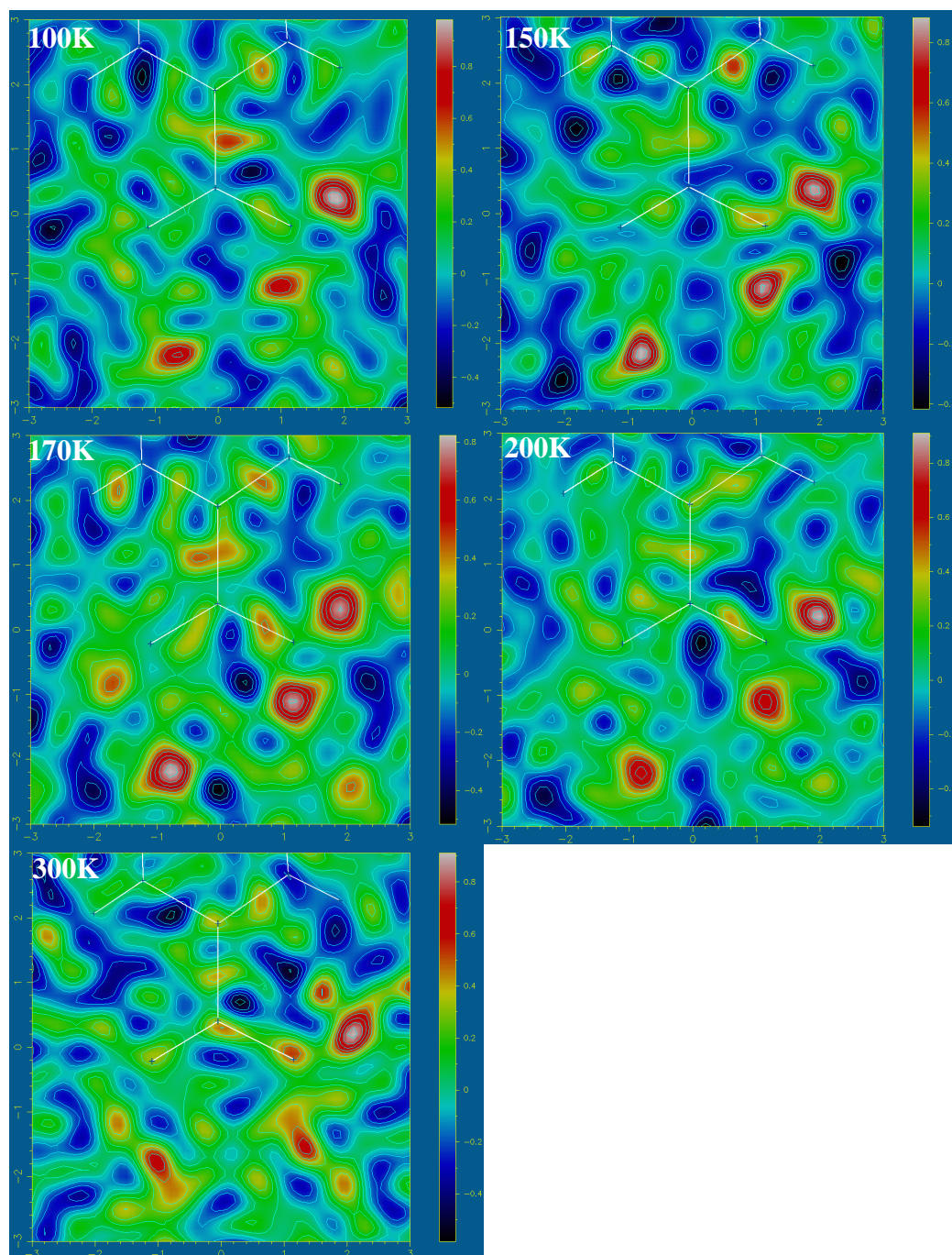


**Figure 6.3** Multiple temperature difference Fourier maps of isonicotinamidium formate showing the dimer and amide formate hydrogen bonds where the hydrogen has been removed from the model. RMS respectively =  $0.10 e/\text{\AA}^3$ ,  $0.09 e/\text{\AA}^3$ ,  $0.09 e/\text{\AA}^3$ ,  $0.08 e/\text{\AA}^3$  and  $0.07 e/\text{\AA}^3$

The X-ray experiments were also repeated using separate crystals and on different diffractometers in Glasgow and Edinburgh with similar results. This was a

reassurance that the indications of possible disorder in the short N-H...O hydrogen bond wasn't a crystal or diffractometer specific result or just a one off occurrence.

### 6.1.2 Variable temperature neutron data

The neutron experiment on isonicotinamidium formate was allocated four days at the single crystal diffractometer SXD, at ISIS, using a helium cryostat for low temperatures. The lowest temperature was set at 40K as the X-ray data indicated that the interesting behaviour occurred at a much higher temperature, removing the extra time and difficulties associated with getting to the extremely low temperatures. The data collection at 40 K was required to provide a good quality structure and reference point when examining the proton positions at the other, higher, temperatures. Data were also collected at 100 K, 150 K, and 200 K. Details of the refinements for all temperatures are in *Table 9.9* and *Table 9.10*. As discussed previously there are several reasons to collect the data at multiple temperatures. The X-ray data indicates that both migration and split protons between double potential wells may be present in this complex and this can be quantified fully from the X-ray experiment. Full data runs of 10 data frames for 40 K, 100 K, 150 K and 200 K were collected; the images on examination looked good apart from slight splitting on some of the diffraction spots. The splitting is most likely due to a small secondary crystallites or twin that always seemed to be present, possibly fragmented from the main body of the crystal on cooling, where the crystal is being put under stress because of the contractions involved.

Initial attempts at processing the data using SXD2001 proved to be difficult. After the integration section of the program was improved by the ISIS team, the data for all four temperatures were integrated successfully even with the slightly fragmented diffraction spots using the 3D profile fit option.

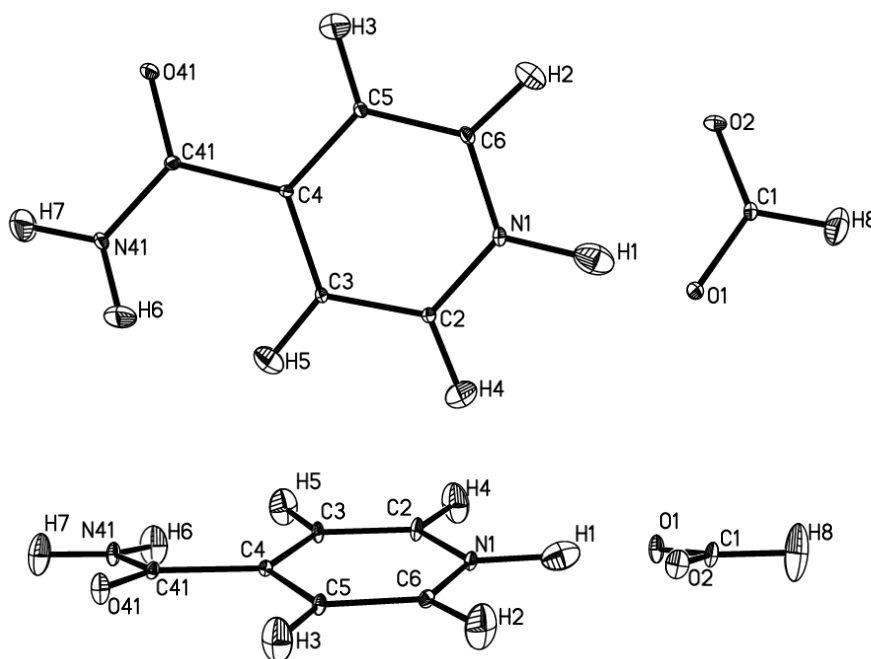


**Figure 6.4** Structure of isonicotinamidium formate as refined from the 40 K neutron diffraction data.

Refinement of the 40 K data produces a structure (**Figure 6.4**) that looks reasonable with all the ellipsoids having dimensions in the expected range. The R-value is 0.0764, which is good for multiple wavelength neutron data, and other factors that might indicate a bad data set, for instance the BASF values, all look reasonable. The majority of the atoms, especially the hydrogen, have an ellipsoid with a long dimension out of the plane of the molecule. This observation is not against reason as slight flexing in this direction is expected with the hydrogen having the greatest freedom of movement.

**Table 6.1** The hydrogen distances and angles for the three crystallographically unique hydrogen bonds in the 40 K structure of isonicotinamidium.

	D...A	D-H	H...A	D-H...A
$N_1-H_1 \cdots O_1$	2.560(2)	1.224(6)	1.337(6)	176.1(5)
$N_{41}-H_7 \cdots O_{41}$	2.922(2)	1.031(4)	1.893(5)	175.8(5)
$N_{41}-H_6 \cdots O_2$	2.827(3)	1.013(5)	1.839(5)	164.2(4)

The N1-H1...O1 hydrogen bond is short at 2.560(2) Å, which is close to the X-ray value of 2.544(2) Å; the slight difference may be due to the difference in temperature (40 K vs. 100 K). Even at low temperature the proton is found to be near the centre of the bond.

At 40 K the refinement (*Figure 6.4*) looks to show the hydrogen (H1) between the pyridyl nitrogen and the formic acid to have an ellipsoid that is slightly elongated along the direction of the hydrogen bond as often observed. The difference Fourier map (*Figure 6.5*), with H1 removed, plotted in the plane of C6, N1, O1 and C1, shows the peak for the proton is well rounded with no sign of a second position. This is expected at low temperature. This is also the case for the hydrogen bond involved in the dimer and the third hydrogen bond between the two molecules, which can be seen in *Figure 6.6*. In *Figure 6.6* the difference Fourier map is calculated in the plane of O41, N41, and C41 with hydrogens H6 and H7 removed from the models. H7 appears twice in *Figure 6.6* because of the symmetry of the dimer, and shows a very well located position without disorder. The same can be said for H6, which also has a well-located position and no disorder. This is perhaps unsurprising with the low temperature data where the lack of energy in the system reduces the likelihood of proton disorder.

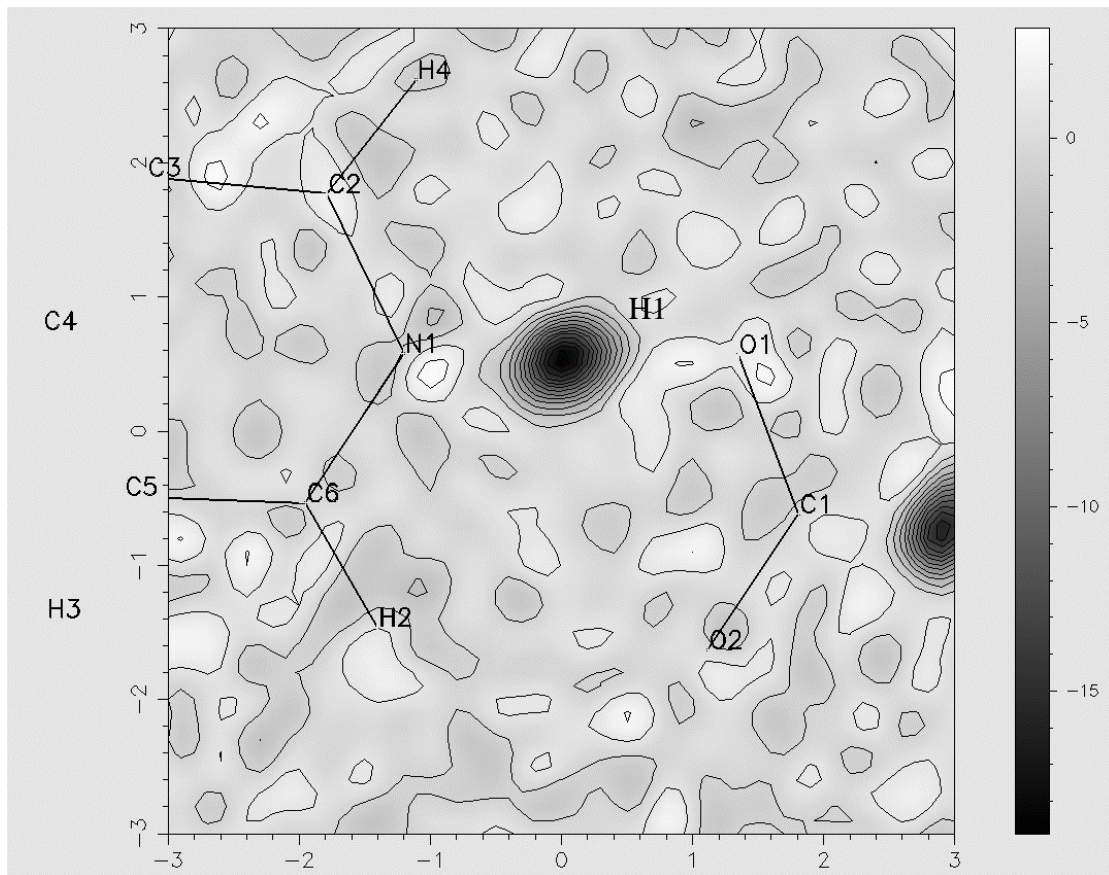


**Figure 6.5** Difference Fourier map of isonicotinamidium formate with H1 removed in the plane of O1,C1,N1 and C6, for neutron data collected at 40 K on SXD. RMS =  $1.33 \text{ fm}/\text{\AA}^3$

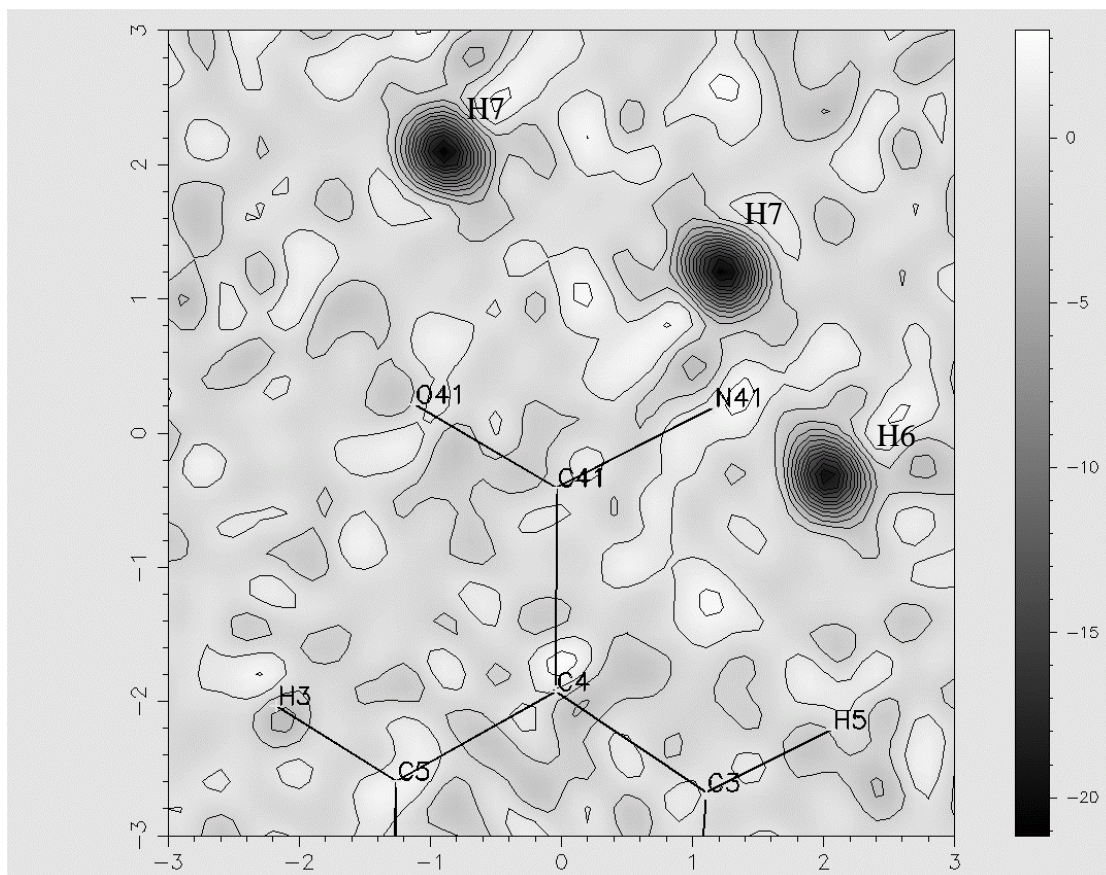


**Figure 6.6** Difference Fourier map of isonicotinamidium formate with H7 and H6 removed in the plane of O41, C41, and N41, for neutron data collected at 40 K on SXD.  $RMS = 1.33 \text{ fm}/\text{\AA}^3$

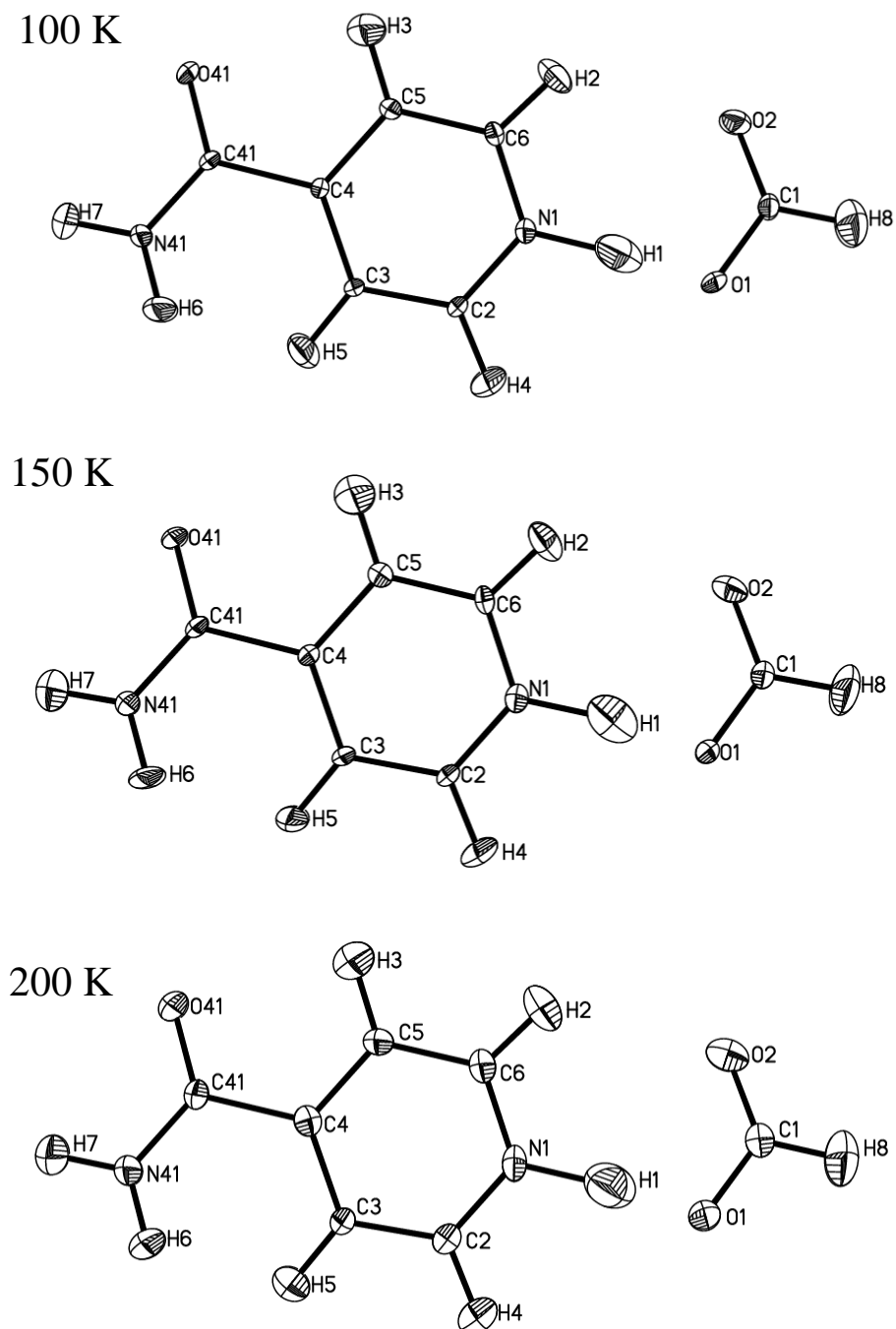


**Figure 6.7** Refined neutron structures of isonicotinamidium formate at 100 K, 150 K, & 200 K.

The data collected at the other three neutron temperatures were also successfully refined to produce structures with ADP's that fit with the freedoms of the molecules (realistic characteristics) and no major background noise (**Figure 6.7**). As the temperature increases the ellipsoid sizes for the atoms increase consistently as would be expected but the overall shape stays close to spherical.

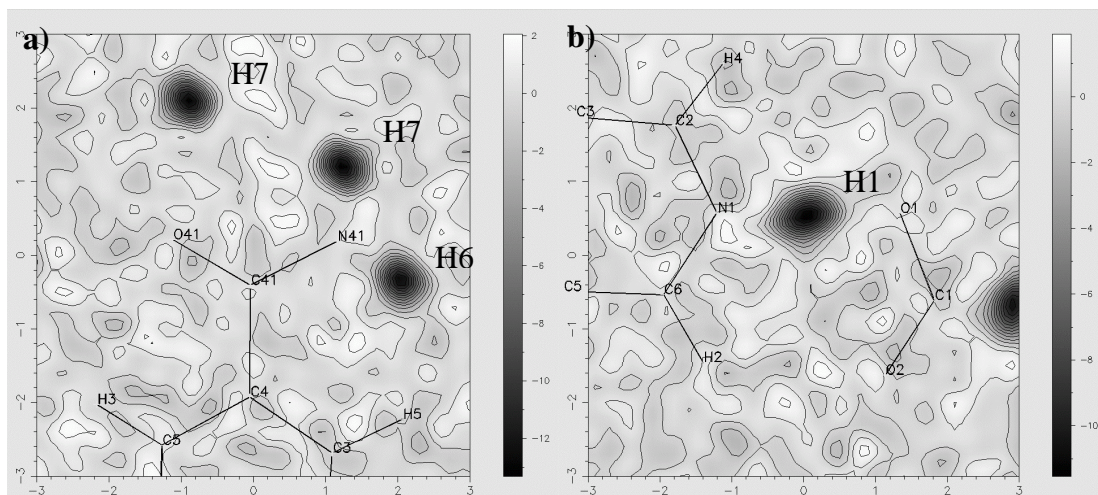


**Figure 6.8** 100K difference Fourier maps of isonicotinamidium formate, showing the HB hydrogen atom density. RMS =  $0.80 \text{ fm}/\text{\AA}^3$

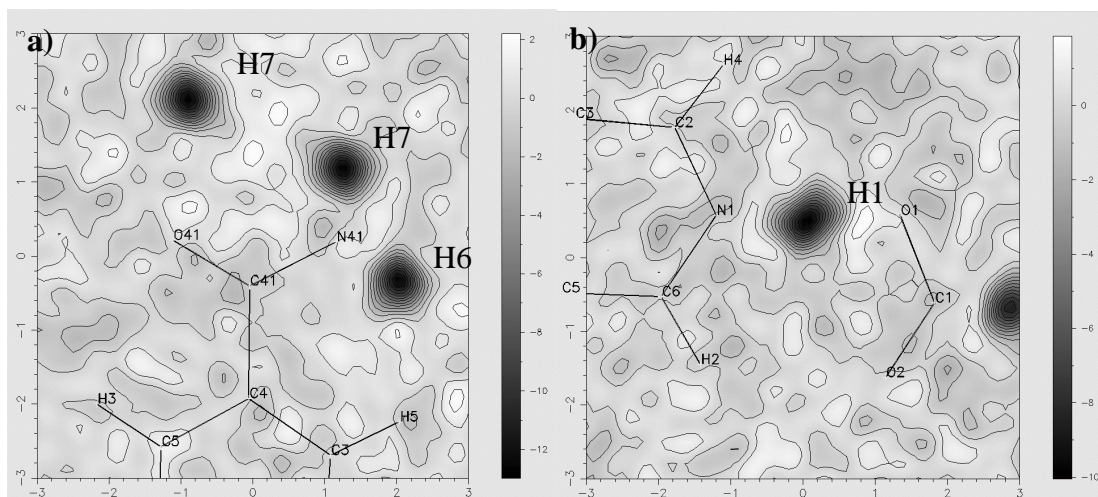


**Figure 6.9** 150K difference Fourier maps of isonicotinamidium formate, showing the HB hydrogen atom density. RMS =  $0.72 \text{ fm}/\text{\AA}^3$

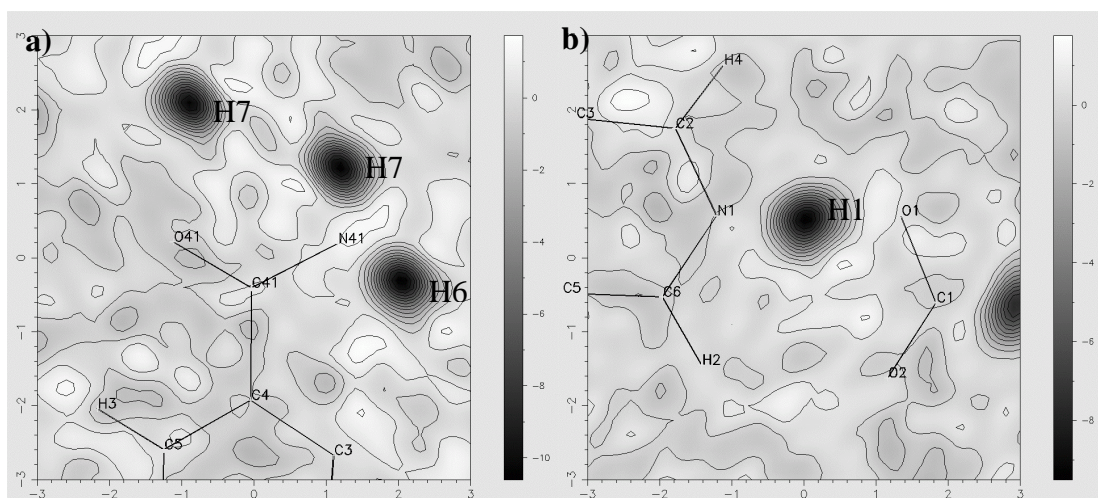


**Figure 6.10** 200K difference Fourier maps of isonicotinamidium formate, showing the HB hydrogen atom density. RMS =  $0.40 \text{ fm}/\text{\AA}^3$

The difference Fourier maps collected at 100 K, 150 K and 200 K, (**Figure 6.8a**, **Figure 6.9a**, **Figure 6.10a**) respectively, show that the hydrogens H6 and H7 have well defined single location proton positions. The neutron data thus shows that at these temperatures there is no hydrogen bond disorder, although H7 does have a slightly deformed shape in the higher temperatures. In contradiction to the indications of the X-ray Fourier, H1 also shows no significant disorder with a well defined shape (**Figure 6.8b**, **Figure 6.9b**, **Figure 6.10b**). Although there is no second site indicated H1 is still of interest as after examination of the bond lengths the proton appears to show the second potential effect of small migration across the hydrogen bond in this material.

**Table 6.2** Hydrogen bond geometry in isonicotinamidium formate as a function of temperature. (The values showing the migrating proton are highlighted in grey, and show the proton to migrate by up to 0.06 Å in this short, strong HB)

Temperature	Type	D-H (Å)	H...A (Å)	D...A (Å)	Angle (°)
40K	N1-H1...O1	1.224(6)	1.337(6)	2.560(2)	176.1(5)
	N41-H6...O2	1.013(5)	1.839(5)	2.827(3)	164.2(4)
	N41-H7...O41	1.033(5)	1.893(5)	2.922(2)	175.8(5)
100K	N1-H1...O1	1.254(6)	1.254(6)	2.551(3)	176.2(5)
	N41-H6...O2	1.029(5)	1.840(5)	2.842(3)	163.5(4)
	N41-H7...O41	1.033(5)	1.887(5)	2.919(3)	176.1(4)
150K	N1-H1...O1	1.261(8)	1.297(8)	2.553(3)	173.0(6)
	N41-H6...O2	1.016(5)	1.858(6)	2.847(4)	163.7(4)
	N41-H7...O41	1.016(6)	1.904(6)	2.919(3)	176.9(6)
200K	N1-H1...O1	1.274(7)	1.290(8)	2.562(4)	175.4(6)
	N41-H6...O2	1.015(8)	1.863(7)	2.854(5)	164.8(5)
	N41-H7...O41	1.037(6)	1.882(6)	2.916(4)	174.7(6)

The proton (H1) can be seen to move away from the nitrogen (to which it is covalently bonded although always with a substantially elongated bond distance) and closer to the centre of the hydrogen bond as the temperature increases. As can be seen in **Table 6.2**, the change in hydrogen position between 40 K and 200 K is significantly larger than three sigma. This effect can therefore be regarded as real. In the difference Fourier map the effect is not obvious but this is not surprising because of the scale of the move and the changing shape of the peak. The earlier X-ray data had suggested that this could be dual site disorder but the presence of migration is equally exciting and significant, Schmidtman *et al* have discussed at length the possible

sources of such ambiguities in X-ray Fourier maps<sup>93,94</sup>. The difference in results from the X-ray and neutron experiments could be due to several different factors; the hydrogen determination from the X-ray data is intrinsically poor, further reduced by the fact that the electrons involved may be diffuse or disordered, and the presence of nitrogen lone pairs can also lead to ambiguity. A second issue is that the two techniques measure different properties, X-rays are diffracted from the electrons and the neutrons diffract from the atom nuclei. The effects on the electron density are quite likely to be different to the migration of the proton so therefore the difference in results is not surprising and indeed is an interesting aspect of complementary diffraction studies of hydrogen bonds<sup>22</sup>.

## 6.2 2-Iodoanilinium Picrate

The co-crystal complex 2-iodoanilinium picrate has three forms<sup>95</sup>, although only two are stable with form III (red plates) changing to form I over time. Form I (yellow needles) and form II (dark green platelets) have both been studied by X-ray diffraction, polarized IR absorption, DSC thermal analysis, and the visible absorption spectra of the single crystal taken using a polarized absorption microspectrophotometer<sup>95</sup>. The investigation was prompted because of the interesting optical properties and thermochromism that the complex exhibits. Form I crystals change from a light yellow colour to red crystals as the temperature is increased from room temperature to around 60 °C. This is postulated to be caused by charge transfer, with the proton in the hydrogen bond between the two molecules being transferred (*Figure 6.11*). At room temperature and below the crystal is a salt with the hydrogen of the OH group on the picrate transferred over to the N of the 2-iodoaniline; when the temperature is increased the hydrogen is transferred back on to the picrate reforming the neutral molecules (*Figure 6.11*).

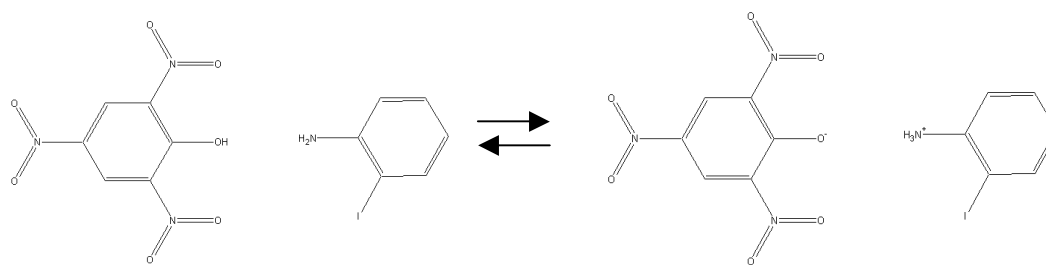


**Figure 6.11** Thermochromism, in 2-iodoanilinium picrate and associated proton transfer, salt to molecular. (For the 2<sup>nd</sup> polymorph this happens between 330-360 K.)

2-Chloroanilinium picrate<sup>96</sup> is the only other example of a co-crystal between a halo-aniline and a picrate reported in the CSD. It does not show any thermochromism as seen in the iodine equivalent, although it does have the proton transferred from the OH group of the picric acid to the amino group of the 2-chloroaniline. Proton transfer in picrate salts is common. Interestingly, the structure of 2-chloroanilinium picrate is not isomorphous with either of the polymorphs of 2-iodoanilinium picrate, instead having a similar structure to one of the anilinium picrate structures<sup>97</sup>. This is an unexpected result as chlorine and iodine are more similar than hydrogen with respect to their size and properties.

Chris Spanswick from the Pulham group at the University of Edinburgh, in collaboration with the Wilson group, has been working with 2-iodoanilinium and other halo-anilines as well as co-crystals derived from them. The main focus of the research was to examine the hydrogen bonding systems and any effects related to it. They reported<sup>98</sup> on the crystal structure of 2-iodoanilinium, a colourless compound with a low melting point, measured just above room temperature (it forms needle crystals from a solution of benzene). The packing involves an interesting helix of a weak hydrogen bond N-H...N network as well as two other distinct helices involving the iodine and C-H... $\pi$  interaction respectively. The amino nitrogen does not adopt the usual planar formation because of the hydrogen bonding. In the picrate co-crystal this is taken one step further with the transfer of the proton forming a tetrahedral nitrogen, whereas in the (homogenous) picrate structure the nitrogen has a pyramidal character. There is only one other isolated 2-halo-aniline with a structure in the CSD, 2-fluoroaniline, which had to be grown in situ from a liquid because it has a low

melting point of  $-73\text{ }^{\circ}\text{C}$ . The 2-fluoroaniline structure is interesting in itself as it shows static disorder of the position of the fluorine<sup>99</sup>. The fluorine can occupy the 2- and 6- position on the ring. The asymmetric unit cell contains one and a half molecules, with the occupancies of the possible fluorine positions at 0.73, 0.25 and 0.5 for the half molecule. The molecules stack in a way that allows N-H...F, N-H... N and C-H...F interactions.

Neutron time was obtained at ISIS on SXD to investigate further the structure of 2-iodoanilinium picrate co-crystals. The previous X-ray diffraction experiments are limited in their ability to detect the hydrogen, which is further hindered by the presence of possible partial occupied sites and the heavy atom iodine. High quality multiple temperature neutron diffraction data allows high resolution mapping of the proton providing information on the site occupancies of the two possible positions of the proton. This will allow any proton transfer across the hydrogen bond to be followed, with the effect probably happening gradually over a temperature range, or any sign of disorder of the proton to be observed.

The original proposal was intended to study form I of the co-crystal as this shows the colour change as well as the proton/charge transfer. However form I crystals of the 2-iodoanilinium picrate form in long yellow crystalline needles, which present a real challenge when aiming for the size required for neutron samples. The low flux at a neutron source requires large sample size to achieve sufficient diffraction in a suitable time frame. Despite several attempts Spanswick was unable to obtain crystals of sufficient size, with growth primarily only in one dimension. Crystals of the second polymorph of 2-iodoanilinium picrate were grown as a substitute and this second polymorph forms into blocks. With the right conditions large samples were successfully produced in the mm scale required for neutron diffraction. Although form II does not exhibit a dramatic colour change it is still believed to undergo migration of a proton causing charge transfer. A multiple temperature neutron experiment was feasible on form II crystals.

The X-ray experiments for the second polymorph reported in the literature show that the thermochromic effect happens somewhere between 330 K and 360 K<sup>95</sup> but also from experiment the crystal was found to deteriorate around 350 K to 360 K. Despite

the low (triclinic) symmetry of the structure, with 4 days of beam time in which to carry out the experiment, collection of several temperatures was feasible. After evaluating the crystal with a quick collection it was calculated that it would be possible to collect between 5 and 6 good quality data sets. Therefore the experiment was designed to start at 300 K and measure the structure at increasing 10 K intervals until 340 K, with an attempt at 350 K to be made if time were available. Although this would not cover the whole temperature region of the phenomenon, the beginning of the proton transfer should be visible without major risk of sample decomposition.

The crystal diffracted well providing round diffraction spots. To achieve a full data set 10 frames per temperature were required. This included 6 at the original mounting position with changing omega of 90, 30, -30, -60, -90, and -150, followed by 4 in the tilted position at omega settings of -45, 0, 45, and -90.

Good quality data was collected for 300 K, 310 K and 320 K, from which reliable structures were produced. When examining the 330 K diffraction images it became clear that the crystal had begun to decompose as the spot shape was deformed and the background noise had increased to a much greater extent than would be expected for the slight temperature rise. After some assessment it was determined that this has been down to the crystal being over-heated when reaching the desired temperature, combined with the vacuum in the sample area. The computer controller that regulates the heater uses an algorithm to calculate the power required to home in on the temperature, with the normal range of experiments below 300 K, the controller is calibrated for that temperature range. Unfortunately this meant the heater required a longer period to stabilise at temperatures above 300 K and consistently over-shoots the target. The higher temperature and extra strain caused by the vacuum resulted in the crystal decomposing when attaining the stable temperature at 330 K. A full data set was still measured for 330 K in the hope that there would be sufficient observed data to produce a structure, as the crystal did not decay further after it had stabilised at 330 K. When processing the 330 K data it became evident, however, that the quality of the images was too poor to achieve a structure. On heating to 340 K the crystal decayed further and it was obvious that there was no further use in continuing.

The initial three temperatures produced structures with anisotropic thermal parameters that reflect the freedoms of the molecule and R-values that are reasonable for neutron data: 7.2 %, 10.6 % and 9.3 % for the 300 K, 310 K and 320 K respectively. The unit cell was refined for each temperature with the initial setting taken from the data available in the CSD.

**Table 6.3** Unit cell dimensions for the co-crystal of 2-iodoanilinium picrate for both the published X-ray structure and the neutron structure for the three temperatures.

	a	b	c	$\alpha$	$\beta$	$\gamma$
X-ray CSD unit cell	7.323	8.245	13.656	75.71	74.05	75.64
300 K Neutron cell	7.345(4)	8.272(3)	13.688(8)	75.84(3)	74.15(3)	75.72(7)
310 K Neutron cell	7.339(5)	8.268(5)	13.696(10)	75.73(4)	74.06(4)	75.66(9)
320 K Neutron cell	7.349(5)	8.323(5)	13.707(6)	75.75(4)	74.04(4)	75.69(8)

The cell sizes determined from the X-ray and neutron experiments (**Table 6.3**) vary marginally, which could be a temperature effect but is also likely to be due to the larger errors associated with neutron cell determination.

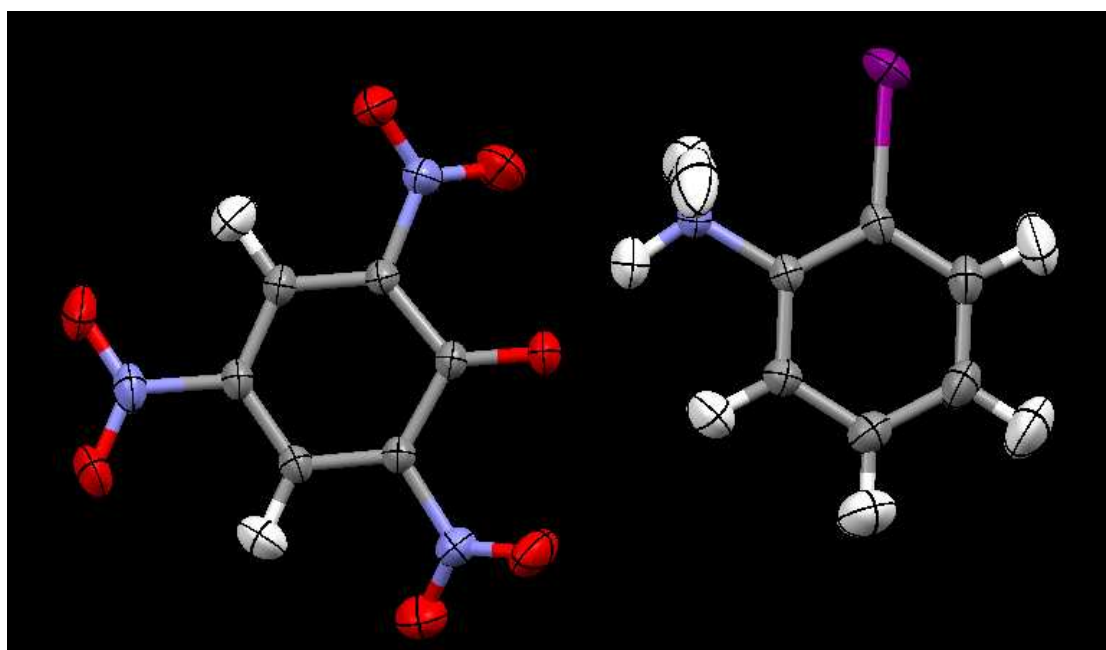


**Figure 6.12** Refined neutron structure of 2-iodoanilinium picrate at 300K.

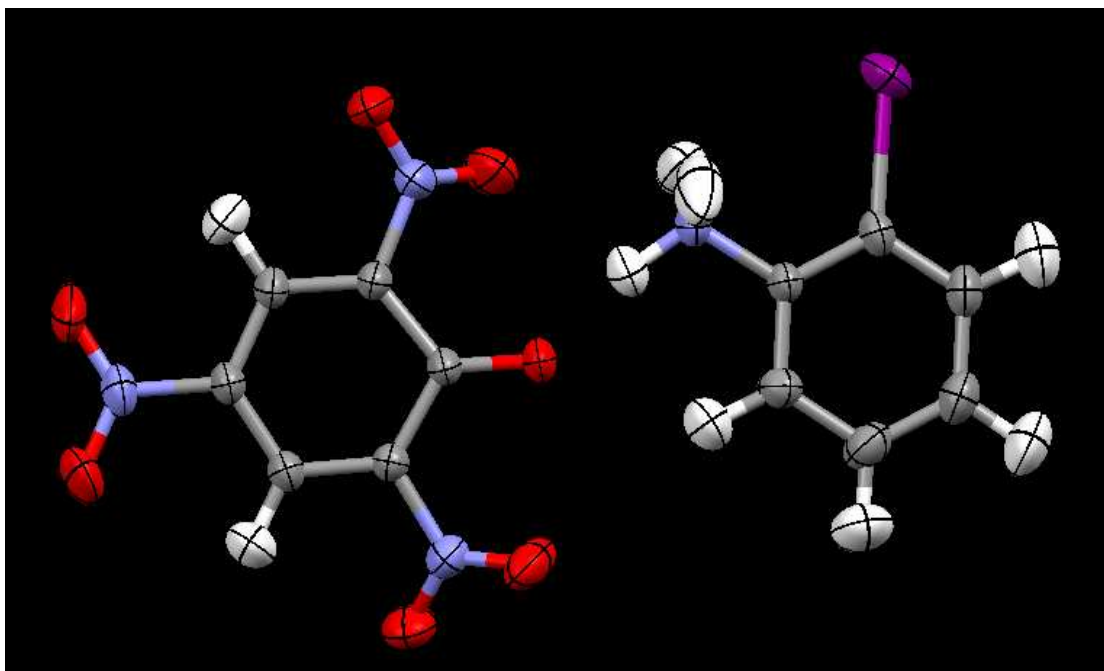


**Figure 6.13** Refined neutron structure of 2-iodoanilinium picrate at 320 K.

In the structure the amino group forms several hydrogen bond interactions with the oxygens of the picrate. Although the major intermolecular bond is that where the proton is transferred, the nitrogen also interacts with an additional oxygen in the same picrate molecule and with a second picrate molecule in the same plane. The N-H that is pointing out of the plane of the 2-iodoanilinium molecule forms a hydrogen bond with a picrate above it. To accommodate this complex hydrogen bonded network centred round the 2-iodoanilinium nitrogen, the molecules are stacked alternately, which also results in  $\pi$ - $\pi$  interactions between the aromatic rings.

The structures over the three temperatures look almost identical apart from a slight increase in the size of the thermal ellipsoids, which is normal for a temperature increase. Movement or disorder in the hydrogen which is under investigation is not evident from the refinement although the data collection temperature is still 30-40 K away from the temperature at which the thermochromism occurs. However, the best way to examine the proton is to construct a difference Fourier map with the proton of interest removed as this will allow any features in the density associated with this atom to be imaged.

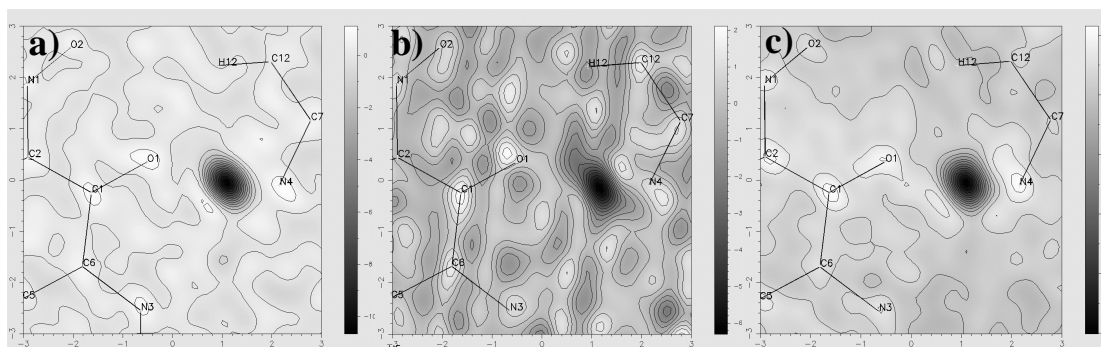


**Figure 6.14** Difference Fourier map in the plane of the complex, containing the hydrogen bond calculated from the **a)** 300 K, **b)** 310 K and **c)** 320 K neutron data of 2-iodoanilinium picrate.  $RMS = 0.30 \text{ fm}/\text{\AA}^3$ ,  $0.27 \text{ fm}/\text{\AA}^3$ ,  $0.58 \text{ fm}/\text{\AA}^3$

**Figure 6.14** shows the difference Fourier maps calculated from the neutron data in the plane set by the nitrogen N4, O1 and C1 with the proton H1 removed. The proton position in the 300 K data clearly has a single site, which has a well-defined shape. There is no sign of disorder or a second site next to the oxygen. At 310 K there is slight deformation of the proton peak shape in the difference Fourier map. This presents as an elongation towards the oxygen and could be the result of the start of the migration of the proton. Unfortunately the map at 310 K has a very noisy background, and as the movement is within the range of the noise level no conclusive answer is possible. At 320 K the structure shows no sign of disorder, which suggests the signs of disorder on the previous temperature are artificial.

The neutron data suggests that there is no disorder in 2-iodoanilinium picrate at the temperature range of 300 K to 320 K. It does not rule out the possibility of such a change being associated with thermochromism for temperatures above this where the X-ray diffraction experiment suggested the effect occurred. Unfortunately because of the crystal degrading the experiment was not able to provide any definite answers to whether the 2<sup>nd</sup> polymorph of 2-iodoanilinium picrate undergoes thermochromism, but has shown that there is no disorder or unusual behaviour in the temperature range of 300 K to 320K.

### 6.3 Malonic acid

To study the effects of temperature change on the intermolecular hydrogen bonds of malonic acid, a five-day experiment was carried out at SXD (in September 2005). This was then followed up by a four days experiment on VIVALDI providing additional temperatures and a comparison of the data collected for the two machines.

The SXD experiment, in collaboration with Dr A. J. Horsewill of the University of Nottingham, was to characterise the proton disorder within the hydrogen bond of the malonic acid structure. The structure had already been determined in the past using single crystal X-ray diffraction, examined by X-ray and neutron powder diffraction<sup>100,101</sup> and also extensive NMR<sup>102,103</sup> experiments as well as techniques such as vibrational spectroscopy, Raman spectroscopy<sup>104</sup>, inelastic neutron scattering and DFT calculations. The addition of single crystal neutron diffraction to this already long list of techniques will allow the hydrogen atoms to be visualised, using difference Fourier maps and site occupancy refinement to assess the population ratios between the two available proton-transfer tautomers.

#### 6.3.1 Background on Malonic Acid

The data from the experiment are intended to allow verification of the theory predicting the occupation of the proton positions using NMR experiments and allow a more complete quantification of the proton transfer and phonon-assisted tunnelling within the carboxylic acid dimers. The NMR experiment used partially deuterated molecules to observe the dynamics of the bonds. The transfer of population to the second site was postulated to fit on to a curve relating to temperature, with the occupancy of the second site expected to be greater at higher temperatures. Malonic acid is of particular interest when looking at the carboxylic acid dimers because of a large energy asymmetry, which leads to a proton transfer rate around three times faster than observed in the model system benzoic acid. The proton transfer involves a simultaneous displacement of the two protons in the two bridging hydrogen bonds across a multi-dimensional potential energy surface

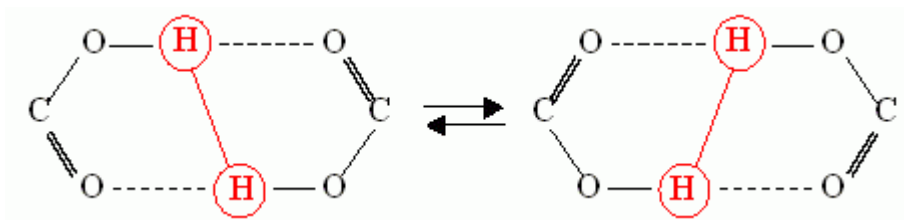


**Figure 6.15** Alternating positions of the hydrogen atoms in carboxylic acid dimers such as in malonic acid.

The ambient temperature triclinic crystal structure of malonic acid was published in 1956<sup>105</sup> and has since been redetermined<sup>106</sup> but this is only one of three phases the molecule forms. The phase adopted between 360 K and 40 K is termed the beta phase. Malonic acid also has an alpha phase that forms at temperatures above 360 K and a gamma phase at lower temperatures lower than 48 K. The beta phase has several entries in the CSD as well as the two previously mentioned<sup>105,106</sup> these are isostructural<sup>107,108</sup>. The alpha phase has been determined from an ab initio neutron powder diffraction<sup>100,109</sup> study, and found to have an orthorhombic unit cell. Interestingly the two dimers of the malonic acid structure become equivalent in the alpha phase which is not the case for the beta phase.

The first of the dicarboxylic acid family, malonic acid  $\text{CH}_2(\text{COOH})_2$  has been of interest because of its proton migration but also dicarboxylic acids are known to be substrates of a large number of enzymes<sup>103</sup> and have a role in biological metabolism. Unlike the rest of the dicarboxylic acid family, malonic acid, with only three carbon atoms, doesn't contain any symmetry within the molecule in the crystal structure because of the rotation of one of the carboxylic acid groups. The other dicarboxylic acids with odd numbered chains of carbons have a 2-fold rotational axis and the even numbered have a inversion symmetry<sup>108</sup>. The lack of symmetry in malonic acids means that the two dimer carboxyl groups are non-equivalent showing different vibrational frequencies in both Raman and infrared investigations<sup>104,110</sup>. Although each dimer is crystallographically distinct, they are both planar and close to orthogonal relative to each other. The beta structure has the same carboxyl groups from adjacent malonic acids interacting to form the dimer hydrogen bond (**Figure 6.16 a**). The malonic acids arrange in infinitely long chains via the hydrogen-bonded dimers. The chains have a zigzag shape because of the bend in the molecule (**Figure**

**6.16 b).** In the a-axis direction the chains are held together by oxygen-oxygen close contacts and Van der Waals forces hold the rest.

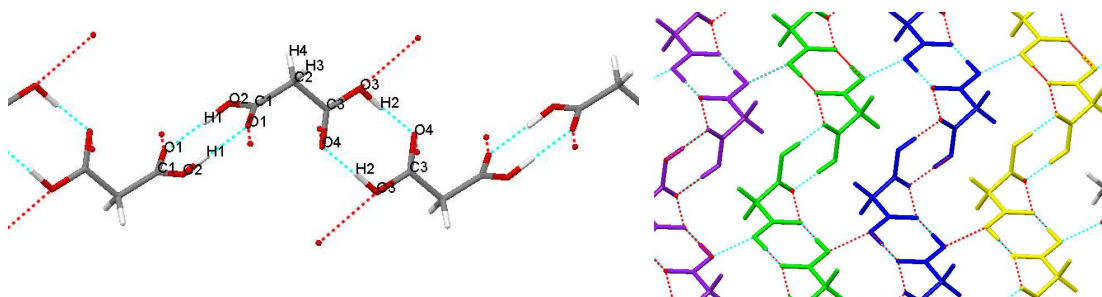


**Figure 6.16 a)** Chain of malonic acid molecules, **b)** representation of how the chains form into layers held together by O-O close contacts.

### 6.3.2 SXD Neutron Experiment for Malonic Acid

Examining the hydrogen bonding and quantifying the proton occupancies was the main aim of the experiment although a data set allowing the refinement of the low temperature structure would also be interesting.

The triclinic unit cell of malonic acid make it necessary to run additional runs with the crystal tilted out of the equatorial plane to collect a sufficient amount of reciprocal space for a stable structure refinement. The runs carried out for each temperature were at omega angles of  $-150^\circ$ ,  $-120^\circ$ ,  $-60^\circ$ ,  $-30^\circ$ , and  $90^\circ$  with tilted runs at  $-150^\circ$ ,  $-90^\circ$ ,  $40^\circ$ , and  $90^\circ$ .

Initially it was hoped to be able to take measurements at small temperature intervals of around 25 K starting at 75 K, increasing to around 350 K. After some problems with mounting the crystal it was decided instead to limit the measurements to 5 temperatures (75 K, 140 K, 200 K, 270 K, 350 K) and then, if time permitted, to carry out low temperature structure determination to see if the low T phase could be obtained. Unfortunately after the first three temperatures the degradation of the crystal, combined with significant beam downtime prevented the remaining measurements from being completed. The destruction of the single crystal is thought to have been caused by a combination of the vacuum applied within the cryostat and the increased temperature of 350 K. Although the experiment proceeded

systematically, the 270 K experiment following the 200 K experiment, the sample was heated to 350 K in case problems in the accelerator ended the experiment prematurely, skipping the 270 K data run. The 350 K data should show a higher population in the second site of the hydrogen bond because of the increased energy allowing the proton to occupy the higher energy state. Unfortunately the raised temperature combined with the vacuum was found to cause non-reversible damage to the sample. After the first scan it was evident that the images were unusable. On removal of the sample it was clear that it had become polycrystalline although maintaining its original volume.

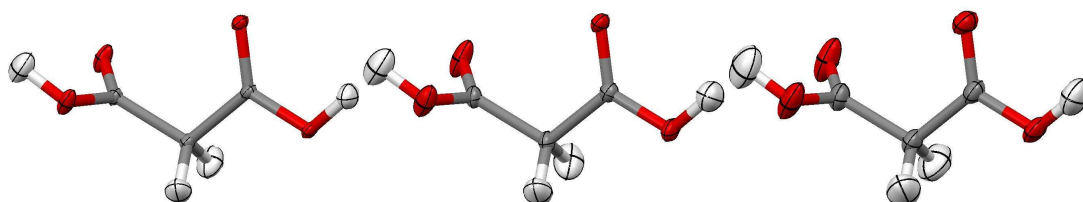


**Figure 6.17** The structure of malonic acid at 75 K, 140 K, and 200 K.

Looking at the 75 K structure it would appear to have refined well with reasonable thermal parameters determined. The three carbons have spherical ellipsoids, whereas the oxygens, which have a greater freedom, are elongated out of the plane of their respective carboxyl groups. The hydrogen atoms on the carboxyl group are elongated in the same direction as the oxygen as would be expected. Looking at the three temperatures the expected thermal ellipsoids expansion is observed and the shape of each is similar to that at 75 K. Although the structures look reasonable the R values tell a different story. The 75 K data refined to a R value just below 7%, the 140 K data is just over 10%, both these are reasonable. The 140 K data, however, has a very high R value of around 36% making it unreliable. The BASF commands, the scale factor that indicate the relative intensities between detectors and runs, also reflect the quality of data. The 75 K BASF numbers are mostly around 1 which relates to the each data run being similar in intensity and is normally a good sign. The 200 K data on the other hand has several values above 500, which is totally unrealistic, and cause for concern. Whether this is to do with the refinement or the quality of the data is not certain, although the fact that the refinements are good at other temperature makes it

most likely that the data quality is poor. Further processing may result in more useable results, but these attempts are on going.

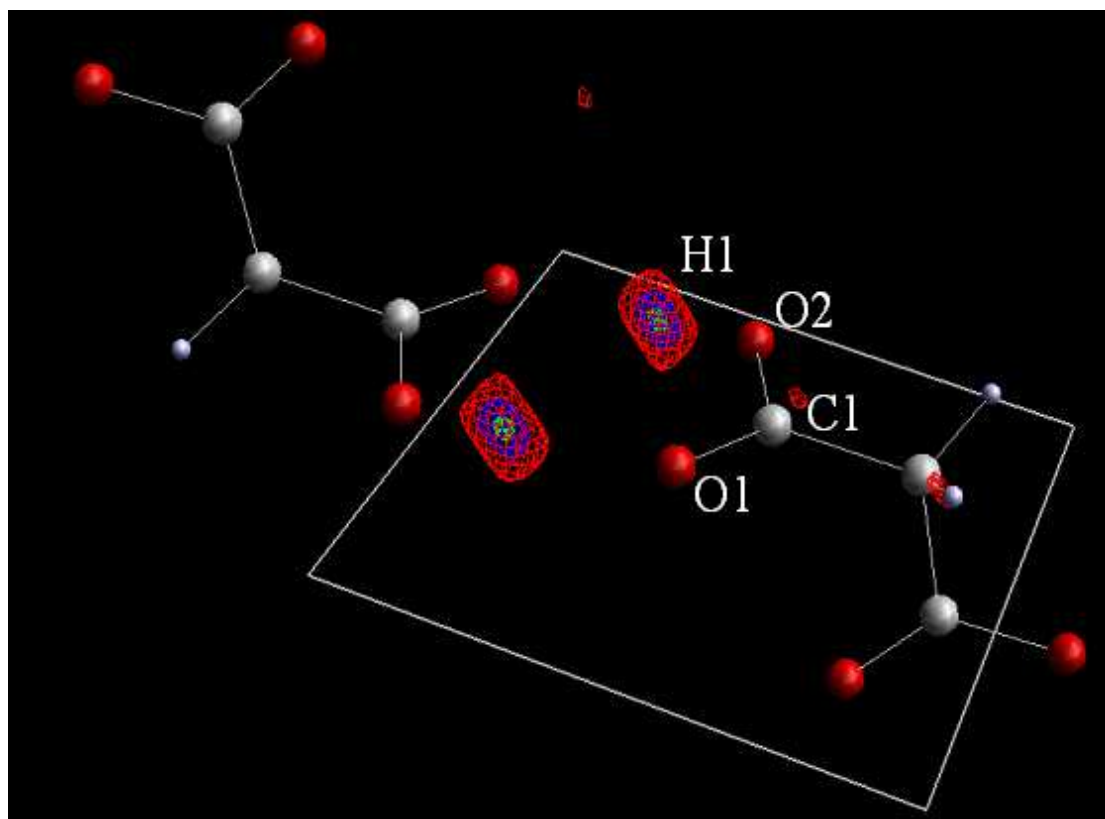


*Figure 6.18* 3D image of the difference Fourier map for O1/O2 hydrogen-bonded dimer of malonic acid at 75 K.

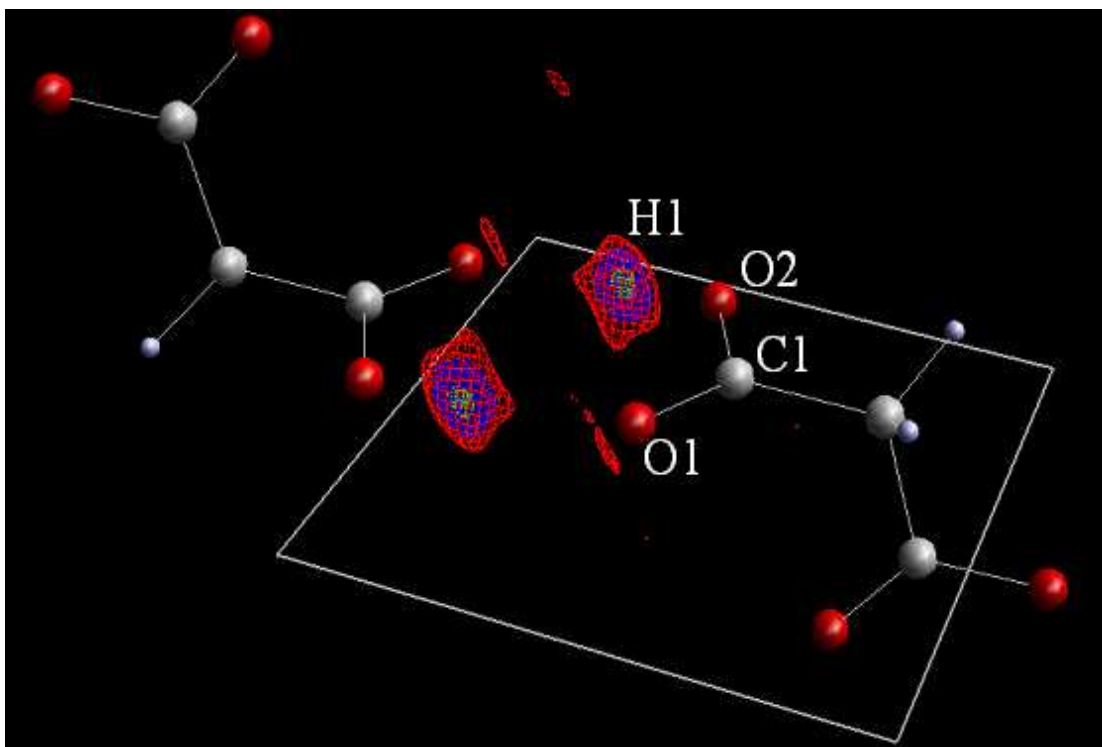


*Figure 6.19* 3D image of the difference Fourier map for O1/O2 hydrogen-bonded dimer of malonic acid at 140 K.

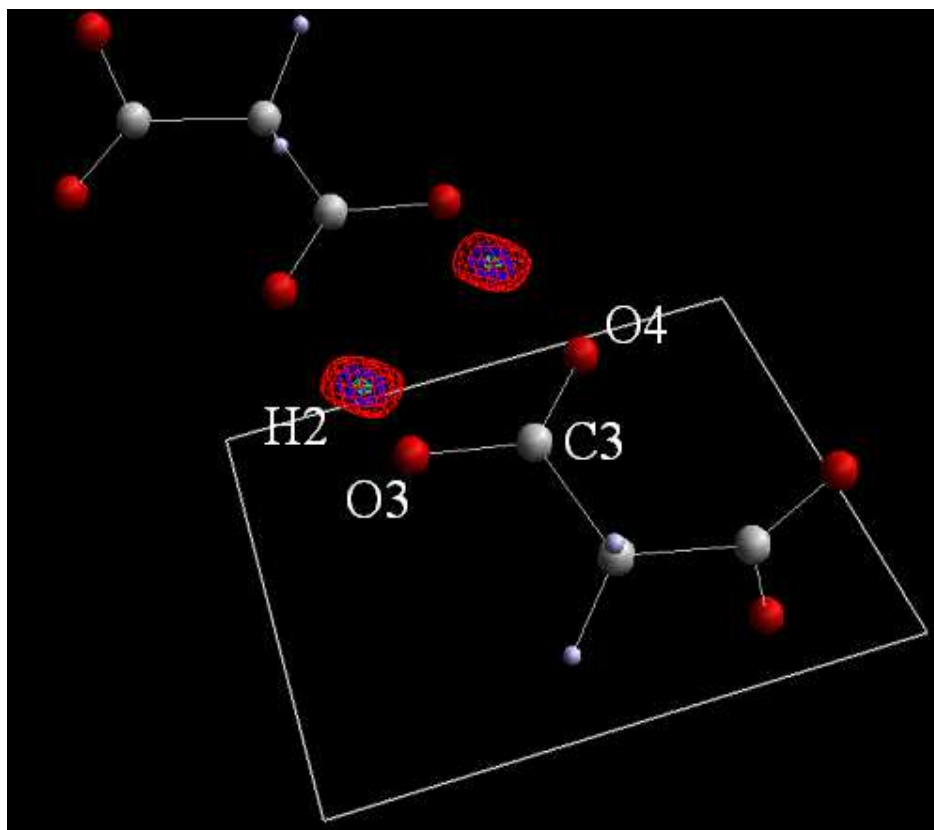


*Figure 6.20* 3D image of the difference Fourier map for O3/O4 hydrogen-bonded dimer of malonic acid at 75 K.

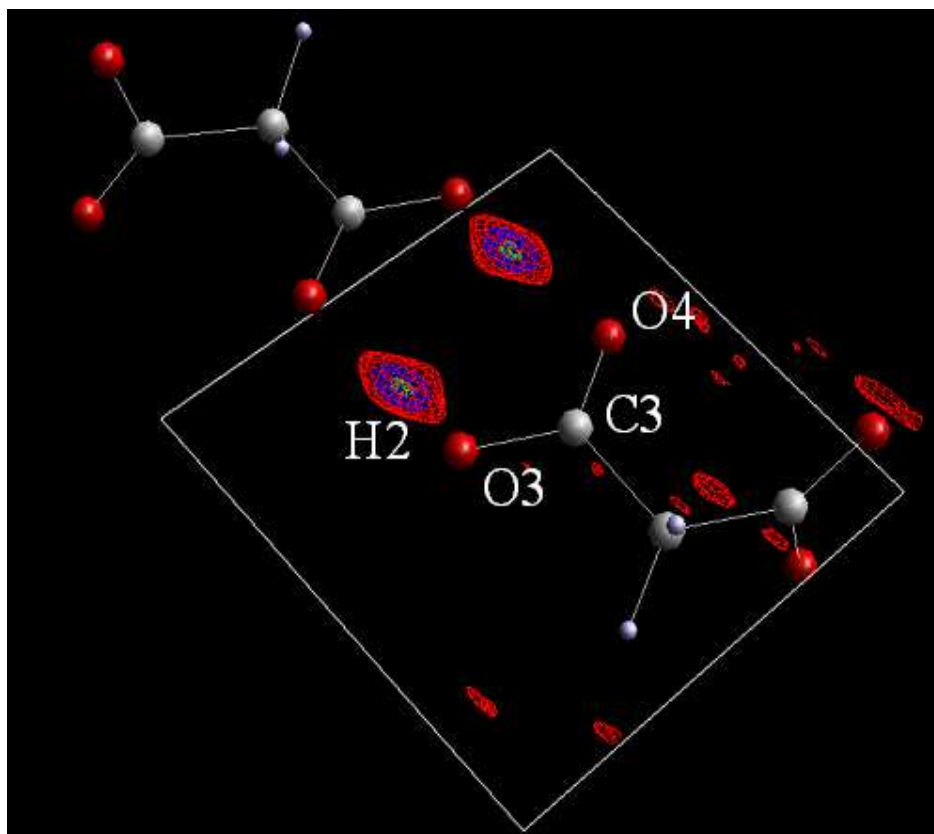


*Figure 6.21 3D image of the difference Fourier map for O3/O4 hydrogen-bonded dimer of malonic acid at 140 K.*

The 75 K and 140 K 3D Fourier maps show that H1 and H2 have single positions, and there is no sign of a second proton peak. The peak for H1 in both the 75 K and the 140 K has a spherical shape without any major disorder. H2 at 75 K also looks spherical but at 140 K it would appear to elongate along the hydrogen bond. This could just be an effect of noise or could be a start to the proton disorder expected in this material. Unfortunately the difference Fourier maps from the 200 K data has very large amounts of systematic background noise because of the poor quality of data. The lack of data at higher temperatures makes it impossible to tell if the indicators of disorder at 140 K of H2 is a real effect.

### 6.3.3 VIVALDI measurements on malonic acid

Having only achieved data collection at three temperatures in the initial experiments on SXD an allocation of a further 4 days on VIVALDI at the ILL was awarded. The aim of the VIVALDI experiment was to try and verify the SXD results and take data

at additional higher temperatures. It was also an opportunity to directly compare the quality of data obtained from the two instruments.

A reactor shut down caused by a structural failure in the fuel cell and container resulted in a delay in the experiment. Large crystals grown for the original time had degraded (the surface appeared frosted) in the time they were out of solution prior to the rescheduled time. Instead crystals from the original ISIS experiment were used that although significantly smaller where of reasonable neutron size and formed well shaped diffraction spots. The delay in carrying out the experiment as well as problems in processing the data (which is currently ongoing) has prevented the results of this experiment from being presented here. A preliminary non-optimised integration has been carried out, but the refinement produced unsatisfactory results in the form of non-positive definite anisotropic displacement parameters and a very large R-factor. The quality of the images (the data collection frames) is good so it is hoped a better integration will help resolve the problems.

## 7. Complexes of Chloranilic Acid with Lutidines

Chloranilic acid has a wide range of uses both in research and as a starting product for larger complexes. Relatively recently it has been found to be a useful molecule for crystal engineering, as well as having more historical physical chemistry uses. Throughout this project co-crystals of chloranilic acid have been generated to examine both the fundamental aspects of bifurcated hydrogen bonded systems and to expand previous studies into the possible motifs towards crystal engineering.

### 7.1 Introduction to chloranilic acid

Chloranilic acid or 2,5-Dichloro-3,6-dihydroxy-*p*-benzoquinone is a member of the anilic acid or benzoquinone family of compounds, (**Figure 7.1**).

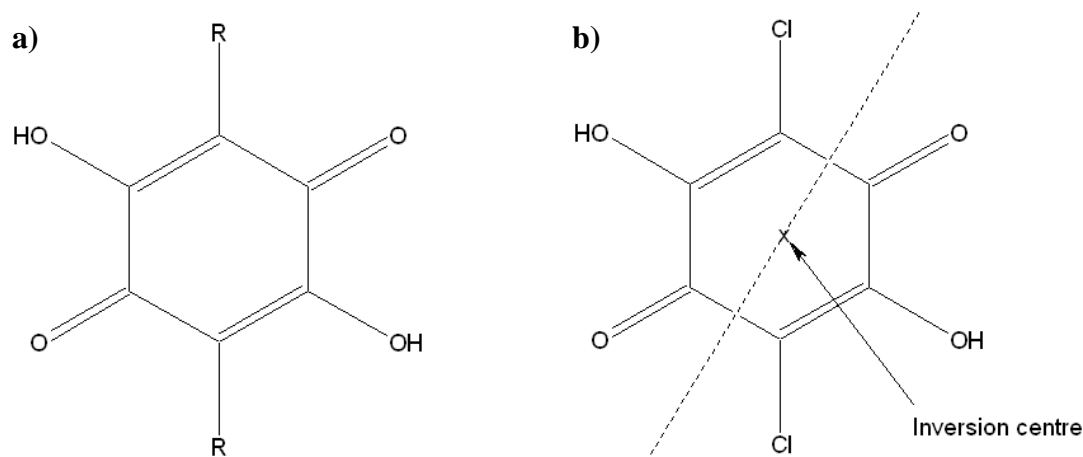


**Figure 7.1** a) The general structure for the anilic acid family of molecules, where *R* represents a range of elements or chemical groups (Cl, Br, NO<sub>2</sub>, O, H...). b) Chloranilic acid has a inversion centre because of the symmetry of the molecule - it is therefore common for only half to be present in the asymmetric unit cell.

With a distinct red colour, chloranilic acid can crystallise in several morphologies, including hexagonal blocks, needles and most commonly rectangular blocks. In acid base reactions and crystallisations, its two hydrogens can be lost making it a strong dibasic acid, but it also possesses proton-accepting capabilities. It can deprotonate either fully or partially (losing one and retaining one) creating three possible charged

states (this is also true for other anilic acids like bromanilic acid) (**Figure 7.2**), ( $pK_{a1}=0.58$ ,  $pK_{a2}=3.18$ )<sup>38</sup>.

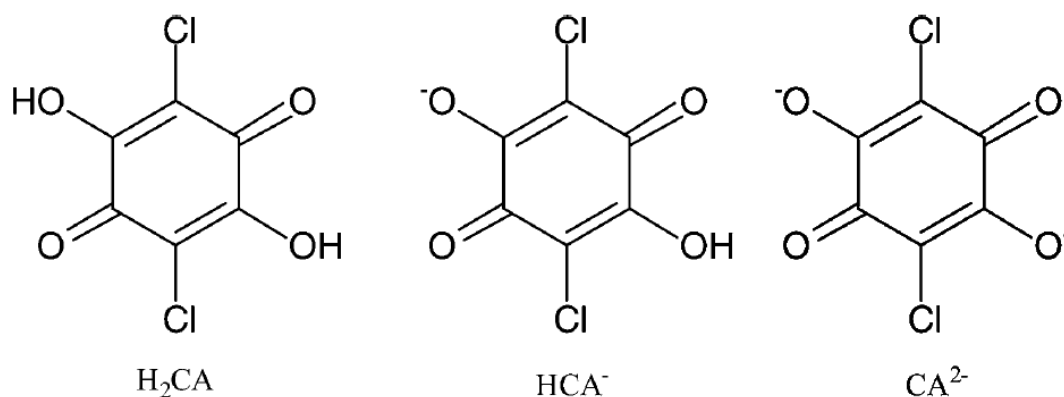


**Figure 7.2** The three charged forms of chloranilic acid, its neutral state H<sub>2</sub>CA, partially deprotonated HCA<sup>-</sup>(monoanion) and fully deprotonated, CA<sup>2-</sup>(dianion)<sup>38</sup>.

The initial crystal structure of chloranilic acid was determined by X-ray diffraction in 1966<sup>111</sup> although this has since been updated; the use of the molecule in techniques such as chromatography dates back much further. The structure of chloranilic acid dihydrate was also subsequently published by E.K.Andersen<sup>112</sup>.

This varied degree of protonation and oxidation is ideal for donor-accepter complexes and allows chloranilic acid to form neutral adducts and proton-transfer monovalent or divalent salts, depending on the basicity and molar ratio of the co-molecule<sup>113</sup>. Although not aromatic, the ring is able to form in  $\pi$ - $\pi$  stacks, and with the presence of chlorine, halogen-halogen interactions are also common. The molecule also contains a  $\pi$ -conjugated fragment (HO-C=C-C=O) that can be involved in resonance-assisted hydrogen bonding.

In the presence of metal centres, chloranilic acid is able to coordinate in either a bidentate (has two points at which it can attach to the central atom) or di-bidentate mode (contains two separate bidentate ligand binding groups)<sup>38</sup>. Just under half of the chloranilic acid complexes or co-crystals in the CSD contain a metal, mostly directly coordinating with the chloranilic acid molecule. The remaining entries are mostly co-crystals of chloranilic acid with small organic molecules particularly amides.

Chloranilic acid has limited solubility in most commonly used solvents such as acetone and alcohols but significant amounts dissolve in acetonitrile or DMSO especially when heated gently. Acetonitrile was the solvent of choice for most of the work, with DMSO requiring extremely long evaporation times. The solution was not always taken to saturation to prevent the solid crashing out when cooled. Although only small quantities are dissolvable in water, where water is present hydrates are often formed preventing the formation of more desirable complexes, chloranilic acid often forming 2:1 chloranilic acid hydrate. Chloranilic acid commonly forms co-crystals with molecules containing amine groups especially with pyridine groups where the nitrogen is involved in an aromatic ring, as well as heterocyclic rings containing multiple nitrogens<sup>37-40,114-120</sup>. The symmetry of the molecule allows for ratios of 2:1 in co-crystals although 1:1 complexes are also common with other ratios also produced depending on the substance and quantities. Co-crystals containing the same compounds in different ratios often arise, as well as polymorphism. Multiple examples of both have been found for the compound throughout this project. Solvates (mostly hydrates) of the co-crystals have also been common adding to the diversity of products. The resulting colours for the co-crystals of chloranilic acid are in a range from dark purple to several shades of red and orange.

The crystal structure of chloranilic acid determined in 1966<sup>111</sup> contains medium strength O-H...O hydrogen bonds from each oxygen (O...O distance 2.769 Å, O-H...O angle 157.54°). These form layers of hydrogen bonded chloranilic acid molecules in planes perpendicular to the a-axis; the planes are held together by Cl...Cl close contacts of distance 3.335 Å (**Figure 7.3**). The layers have a netting structure, made up of loops each containing 4 molecules.

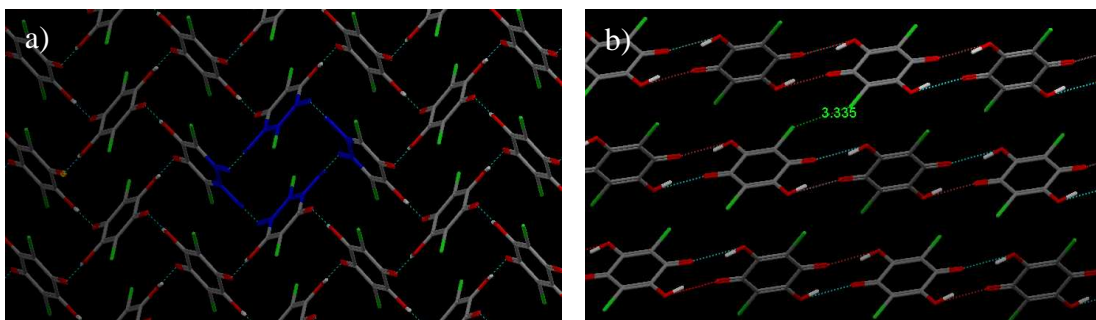


**Figure 7.3** a) The netting structure of the hydrogen bonded layer within the chloranilic acid structure (with one of the hydrogen bonded four molecule loops highlighted in blue), and b) an illustration of the layers with the Cl···Cl close contact of 3.335 Å indicated<sup>111</sup>.

The chloranilic acid dihydrate subsequently published by Andersen<sup>112</sup> has a three-dimensional hydrogen bonded network. The chloranilic acid is bound to water molecules symmetrically on either side with bifurcated hydrogen bonds (BHB) (**Figure 7.4**). Unlike the situation in the amide co-crystals of chloranilic acid the hydrogen remains on the chloranilic oxygen resulting in both an intramolecular and intermolecular part to the BHB. The ketone oxygen of the chloranilic acid is also an acceptor for a single HB with a different water. The water molecules also hydrogen bond with themselves to form chains throughout the crystal and combined with the HBs to the chloranilic acid produce a 3-dimensional structure.

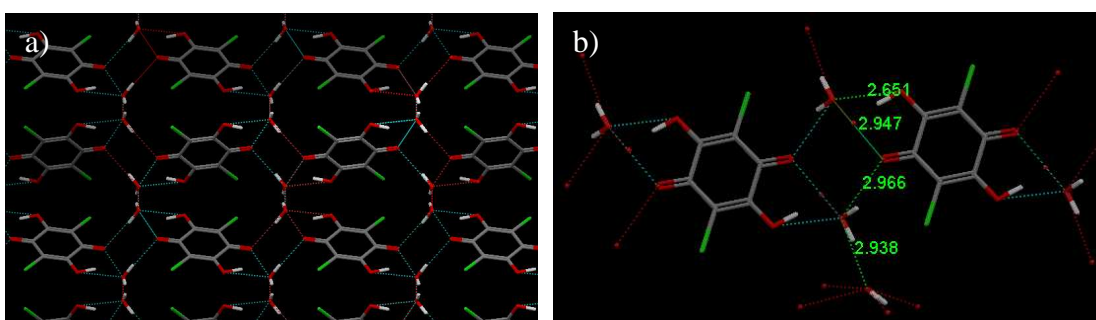


**Figure 7.4** a) 3-dimensional hydrogen bonded structure of chloranilic acid dihydrate. b) Hydrogen bonded unit of chloranilic acid with water molecules on either side and acceptor-donor lengths shown<sup>112</sup>.

## 7.2 Historical and recent uses of chloranilic acid

Chloranilic acid is not just a research chemical but has had various historical practical uses; a reagent for micro analysis<sup>121</sup>, spectrophotometry<sup>122</sup>, staining calcium in cell tissues<sup>123</sup> and even techniques like paper chromatography<sup>124</sup>.

In micro analysis chloranilic acid salts can be used in determination of the ion concentration of aluminium salts, sulphides, thiosulphates, cyanides and fluorides<sup>121</sup>. The chloranilate reacts with the ion under investigation forming an insoluble precipitate. The quantity of surplus chloranilic acid can be found from the colour of the solution and from this the amount used is determined. The amount of chloranilic acid is not necessarily directly proportional to the amount of ion present, but tables of related volumes are available to consult to allow the ion content to be determined. This provides a procedure that is simple and rapid.

In paper chromatography, chloranilic acid has been used as a reagent, with good results for alkali earth metals as well as some other heavier metals<sup>124,125</sup>. Its main advantages in paper chromatography of inorganic compounds are its low specificity and high sensitivity, allowing it to be used for a wide range of samples.

Modern uses of chloranilic acid focus around multiple component systems. The neutral co-crystal complex of chloranilic acid and phenazine has been shown to exhibit ferroelectricity<sup>113</sup> with a large dielectric constant, that provide interest to the area of electronic devices. The use of chloranilic acid-amine co-crystals in crystal engineering will be discussed in **Section 8.3** as well as the predictable supramolecular synthons they contain. Chloranilic acid has the potential to be involved in intermolecular electron transfer interactions through the hydrogen bonding motifs it produces. Such interactions are seen as important in proteins, and have potential for future electronics development.

### 7.3 Hydrogen bonding motifs, and $pK_a$ matching for proton transfer

One of the ultimate goals of modern day crystallography is the ability to be able to predict and design crystal structures to give the substance the properties desired. Crystal engineering could allow materials to be designed with a purpose in mind allowing substances with the desired physical properties such as physical strength, conductivity, solubility, etc. to be built in. Although several complex computational techniques are being developed to try to allow prediction of properties of crystalline molecular materials, there is a lot that can be learned from simple studies of systems and previous work done with the materials. The use of co-crystals where one molecule with additional functionality can be substituted in the complex is one of the simplest forms of crystal engineering, and allows the target structure to be reached using the separate molecules like Lego<sup>™</sup> blocks. The added advantage of this idea is that it can be designed so that the complex is relatively easy to self assemble, where each unit joins onto the next in a predetermined way because of the favoured interactions. Understanding and controlling the non-covalent forces, especially hydrogen bonding, is key to structural design, as they will provide the means to link and stabilise the different components<sup>38</sup>.

Co-crystal complexes of chloranilic acid almost always produce hydrogen-bonded systems. Where the second molecule is an amide, a bifurcated hydrogen bond between the nitrogen and a pair of the oxygens is usually observed. This reliable interaction can be referred to as a motif for the system. Using the motif as a foundation, larger structural units can be built by varying the amide and the ratios of reagents. Previous work by H. Ishida and S. Klashino<sup>37,125</sup> into lutidine chloranilates and other related structures deposited in the CSD revealed that the hydrogen bonded pattern in 1:1 complexes of chloranilic acid-amine systems can be classified into 3 main types (**Figure 7.5**). From the following examples in this project, and entries deposited in the CSD, it would appear similar broad classifications can be made for 2:1 ratios. This is an example of another form of control and prediction that can be exerted on the resultant crystal structure with the choice of co-molecule determining the final composition and form of the complex. The design of the amine dictates the topology of the system, for example two pyridyl rings joined by a carbon backbone in

a 1:1 ratio with chloranilic acid is likely to make a chain network with alternating threads of molecules.

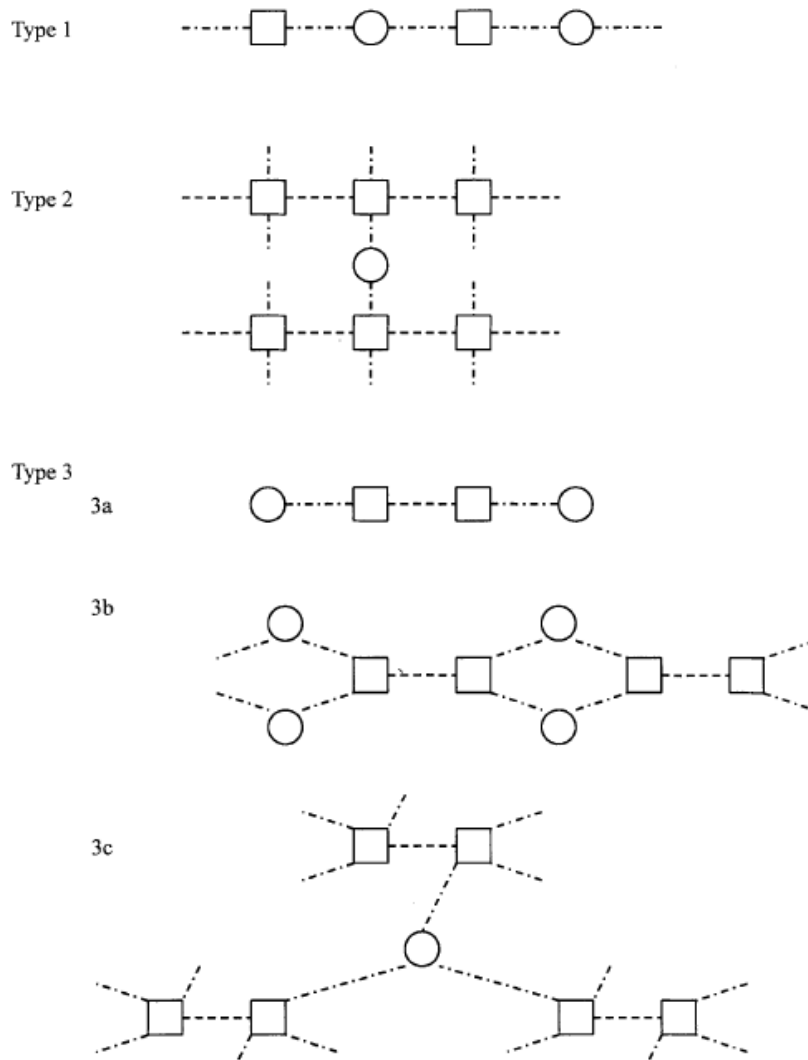


**Figure 7.5** Classification of 1:1 chloranilic acid-amine systems, showing the three types of hydrogen bond patterns<sup>37</sup>.

As well as being a useful motif for crystal engineering, the bifurcated hydrogen bond is an interesting interaction in itself. The presence of three centres brings with it the possibility of varying ratios of acceptor distance/strength and unlike the classical strong hydrogen bond which is essentially linear, the proton has a plane on which it can be found. This added “freedom” allows possibilities for a more complex structure, or for potential hydrogen disorder and migration effects.

The crystal structure of chloranilic acid has the molecule fully protonated and therefore possesses two OH groups. In many of the chloranilic acid co-crystals, proton transfer occurs where one or both of the hydrogens exchange across the hydrogen bond. In the case of the amines, the hydrogen usually transfers from the oxygen of the chloranilic acid to the nitrogen of the amine forming the salt. Also known as charge transfer (due to the resulting charges on the acceptor and donor atoms), proton transfer has been of interest in many scientific areas and can be attributed as the cause of several effects such as fluorescence, acid base reactions, charge transfer, and salt formation.

Discussions about the position of the hydrogen in the hydrogen bond have often focused on the relation of the  $pK_a$  of the co-molecule pyridine species to that of the chloranilic acid<sup>19,20,37</sup>. This leads to the idea that the hydrogen position can be tuned using the  $pK_a$  value. In the case where the  $pK_a$ s of two molecules are matched it has been suggested that the proton could be centred or disordered in the hydrogen bond<sup>19,20</sup>. Issa et al.<sup>126</sup> have suggested that such a centred hydrogen bond does exist in a molecular complex of a lutidine derivative with chloranilic acid based on solid-state NMR measurements, whereas Ishida et al.<sup>37</sup> did not observe it using X-ray crystallographic methods. However, Ishida et al. have focussed solely on refined X-ray hydrogen positions for their conclusions, which are known to give less reliable information than direct visualisation of the Fourier difference maps, particularly in the case of systems exhibiting solid-state proton migration or transfer<sup>45</sup>. In the general case of strong hydrogen bonds it has been shown that temperature regulated migration of the proton can occur in other systems<sup>22</sup>, with the proton moving to the centre of the bond with increasing temperature. This is believed to be due to a wide flat bottom to the potential well of the hydrogen bond. Disordered hydrogen bonds have also been seen, with secondary positions for the proton present next to the acceptor atom, in this case the potential well is thought to have a double well formation with a low barrier between them. In bifurcated hydrogen bonds similar effects to the migration and disorder could be possible although these could occur in a much wider variety because of the increased geometric freedom and a more complex 2D potential surface defining the BHB. With the use of multi-temperature X-ray diffraction experiments combined

with visualisation of the Fourier difference maps it is possible to investigate in detail the possibility of temperature-dependent proton disorder and migration.

#### 7.4 Structure determinations of chloranilic acid-lutidine complexes

Lutidine or dimethylpyridine of formula  $C_7H_9N$  comes in six different forms, 2,3-, 2,4-, 2,5-, 2,6-, 3,4- and 3,5- substituted, most of which can be obtained from bone oil, coal tar, or other natural sources. They are all clear colourless liquids with a pungent odour, some are toxic or irritants. Lutidines have a high affinity for protons and act as a  $H^+$  ion absorber, with 2,6-lutidine commonly used in organic synthesis as a sterically hindered mild base.

Co-crystals of lutidine and chloranilic acid have previously been studied by H. Ishida and S. Klashino<sup>126</sup>, who published the structures of 1:1 chloranilic acid, with 2,4-, 2,5-, 2,6- and 3,4- lutidine crystals<sup>37</sup>. These all produced the same hydrogen bonded unit made from the supramolecular synthons that are common throughout the chloranilic acid amide co-crystals. The chloranilic acid forms centrosymmetric dimers joined by two  $O-H\cdots O$  hydrogen bonds (*Figure 7.6 a*). The dimers are linked to the lutidine via  $N-H\cdots O(O)$  bifurcated bonds on either side, forming a four molecule unit. The  $N-H\cdots O(O)$  bifurcated hydrogen bond and  $O-H\cdots O$  single hydrogen bond pair represents the two motifs exhibited throughout the amine/chloranilic acid co-crystal series.

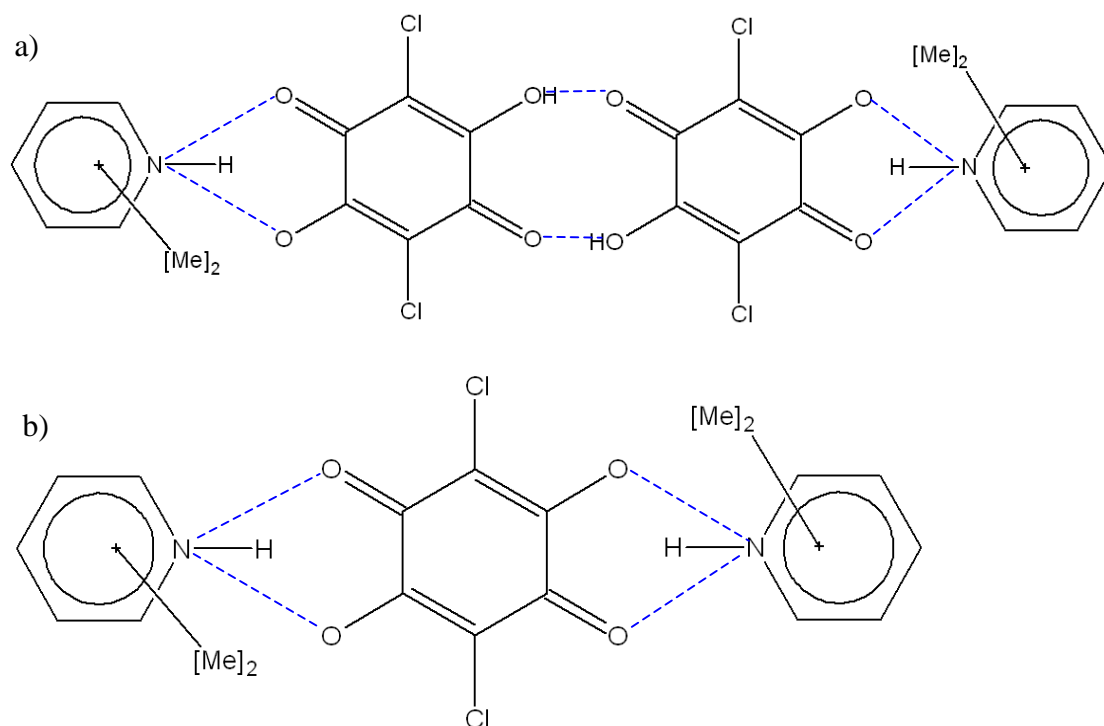


**Figure 7.6** Representation of the **a) 1:1** and **b) 1:2** chloranilic acid lutidine hydrogen bonded supramolecular synthon units.

The four structures all had the hydrogen transferred to the lutidine, which is expected because the  $pK_a$  values of the lutidines are significantly higher than any of the other reported co-molecules which resulted in no proton transfer. Any new co-crystals grown in this series were therefore expected to exhibit proton transfer.

Lutidine provides an ideal set of six relatively simple molecules with which to examine the bifurcated hydrogen bond and from the literature it is known reliably to form supramolecular synthons that are created in chloranilic acid-amine co-crystals. By studying simple molecules, information pertaining to complex systems or interactions may be obtained.

In an attempt to produce new forms of lutidinium chloranilates, a screening trial of different crystallisation conditions including different ratios of components and temperatures was undertaken. Solvent choice is often used as a variable in searches for different polymorphs or crystallisation screening but in the case of chloranilic acid, the choice of solvent is limited as chloranilic acid does not dissolve in many solvents. Acetonitrile was used for the majority of the crystallisations because it

dissolves chloranilic acid fairly well and also evaporates in a reasonable time span because of its low boiling point. A mixture of water and acetonitrile was occasionally used in an attempt to form hydrates. In these cases the chloranilic acid and lutidine were dissolved in acetonitrile and the water added subsequently to reduce the likelihood of chloranilic acid dihydrate forming. In the cases where water was added prior to the lutidine, chloranilic acid dihydrate was almost always the exclusive product even in cases where co-crystal hydrates were formed if the mixture was created in the opposite order. This suggests even in solution the molecules form into the hydrogen bonded units which are stable prior to the crystal formation. The ratios of chloranilic acid to lutidine crystallisations set up were either roughly 1:1 or with lutidine in excess, which effectively acted to allow 1:2 complexes to form. In crystallisations where chloranilic acid was in dominance, pure chloranilic acid crystals were a major product which meant that the co-crystals were hard to find. All the lutidines produced at least one single crystal of a new complex with chloranilic acid; 2,3-, 2,4-, 2,5-, and 2,6- lutidine formed a 2:1 co-crystal, with 2,4- forming a polymorph (i.e. two forms); the 3,4- and 3,5- formed hydrates. The structures of these will be described and discussed below.

Powder diffraction was used to assess if any additional complexes were present, and as a rough guide to the ratio of the different products. Differences in ratios of the products from the three different crystallisation conditions (1:1, 2:1 and 2:1 with added water) were examined to allow a determination of the predominant products for each or what conditions are necessary for a certain form.

Hydrogen bonds are directional interactions, as seen in single HB's by the difference in range of angles ( $\angle$  D-H...A) between the strong ( $\sim 180^\circ$ ) and weak cases ( $> 90^\circ$ ). The variation in the positioning of the co-molecule in relation to the chloranilic acid, discussing the angles between the rings, ring tilts, and the positions of the protons will feature throughout this section in an attempt to rationalise the "level of bifurcation" and other features of the hydrogen bonded system. The use of the phrase "level of bifurcation" is in reference to the amount the second acceptor oxygen is involved. For instance a case where the nitrogen hydrogen bond is directed between the two oxygens such that the angles and distances for the major and minor parts are equal,

could be referred to as being more bifurcated than the case for the 2,3-lutidine complex for example, where N-H...O1 is stronger than the minor N-H...O2 part.

#### 7.4.1 2,3-lutidine chloranilic acid 2:1 co-crystals

As 2,3-lutidine chloranilic acid was missing from the series of co-crystals previously reported by H. Ishida and S. Klashino several attempts were made to grow 1:1 crystals chloranilic acid with 2,3-lutidine to fill the gap. No 1:1 crystals were found although a 2:1 2,3-lutidine chloranilic acid was produced. The 2:1 co-crystal complex was grown from a mixture of chloranilic acid dissolved in acetonitrile and an excess of lutidine. Crystals were also formed when the starting ratio was 1:1 but with less abundance.

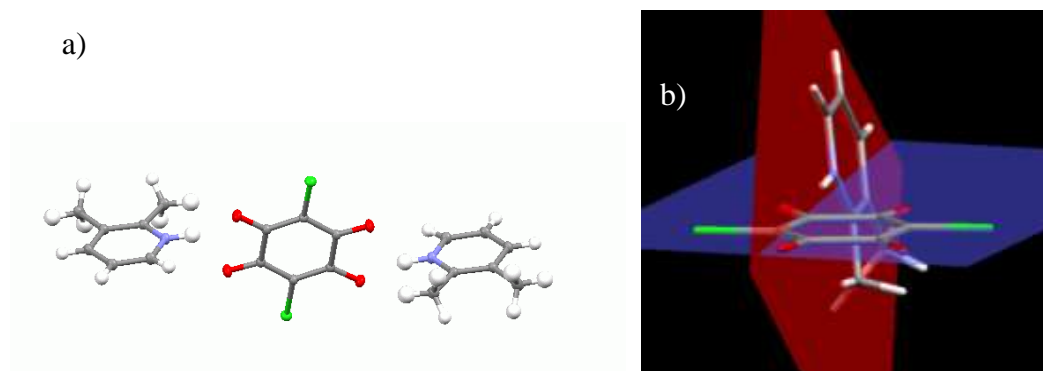


**Figure 7.7** a) 2:1 hydrogen bonded unit of 2,3-lutidine-chloranilic acid. b) Planes of the rings are near perpendicular but the lutidine is rotated so the N-H is directed towards one of the oxygens.

The structure of the 2:1 2,3-lutidine chloranilic acid co-crystal (**Figure 7.7 a**) is formed around bifurcated hydrogen bonds similar to the motif and the molecular synthon described previously (**Figure 7.6**). The four oxygens on the chloranilic acid allows it to form two separate bifurcated bonds whereas the lutidine only contains one nitrogen and therefore is only able to participate in one bifurcated bond. The 2:1 ratio of the crystal is therefore determined by the chloranilic acid making bifurcated hydrogen bonds with two separate lutidines.

The hydrogen bonded unit for the 2,3-lutidine contains two asymmetric units (each containing one lutidine and half a chloranilic acid,  $Z'=0.5$ ) as the two lutidines are in

symmetry related positions (**Figure 7.7 a**), although this is not always necessarily the case for all the co-crystals studied here. The 2,3-lutidine is near perpendicular to the plane of the chloranilic acid (**Figure 7.7 b**) but although the centre of the molecule is positioned between the oxygens a slight tilt in its position directs the hydrogen bond towards O1. N-H...O1 will be referred to as the main interaction of the bifurcated bond (the donor-acceptor interaction with the most influence over the proton position) and the minor part of the interaction will refer to the donor-acceptor interaction which is not as influential, in this case N-H...O2.

It should be noted that for the 2,3-lutidine co-crystal and for all the lutidine and picoline structures with chloranilic acid reported below, the hydrogen has been transferred across from the oxygen to protonate the nitrogen which is expected because of the higher  $pK_a$  values for the lutidines and picolines relative to the chloranilic acid.

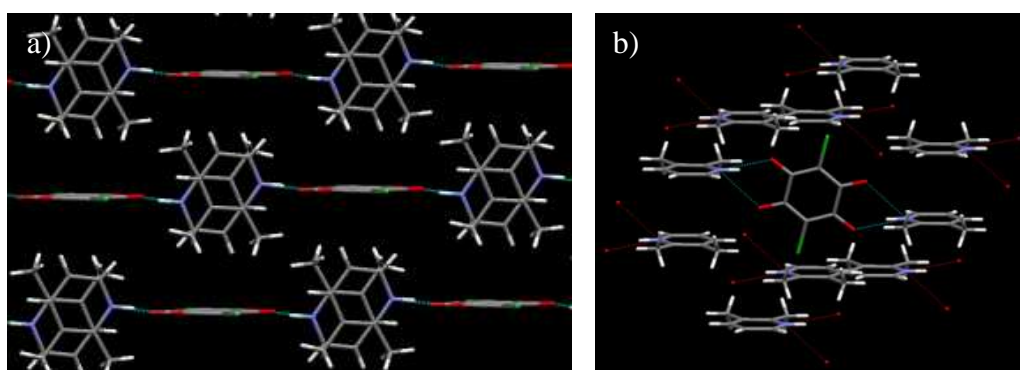


**Figure 7.8 a)** Hydrogen bonded units in the 2:1 2,3-lutidine chloranilic acid complex stack with overlapping lutidines, **b)** Chloranilic acid surrounded by lutidines.

The hydrogen bonded unit is repeated throughout the crystal with overlap of the lutidine allowing staggered stacking (**Figure 7.8 a**). The 2,3-lutidine molecule has the two methyl groups on the same side of the ring and these stack so that they are “head to foot” with the adjacent molecules, so the methyl groups are adjacent to the ring below. The chloranilic acid is surrounded by the 2,3-lutidines (**Figure 7.8 b**).

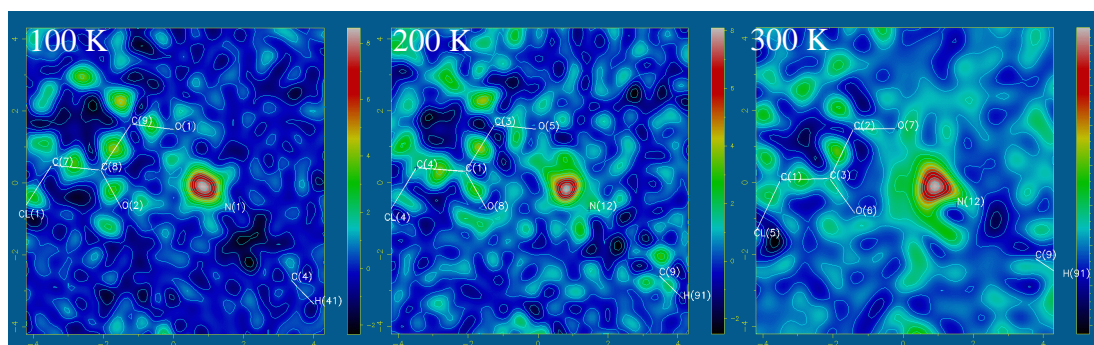


**Figure 7.9** Fourier maps of 2,3-lutidine chloranilic acid co-crystal at 100 K, 200 K and 300K taken in the plane of the N and two O involved in the bond. RMS= 0.06  $e/\text{Å}^3$ , 0.06  $e/\text{Å}^3$  and 0.05  $e/\text{Å}^3$

The structure of the 2,3-lutidine chloranilic acid co-crystal was determined at 100 K, 200 K and, 300 K allowing the calculations of Fourier maps showing how the hydrogen in the bifurcated bond was positioned over this range (**Figure 7.9**). At 100 K there is a round shaped peak with well-defined position present indicating no disorder. As the temperature increases the peak shape distorts but compared with the background this is a minor effect and does not indicate disorder.

#### 7.4.2 2:1 2,4-lutidine chloranilic acid polymorphs

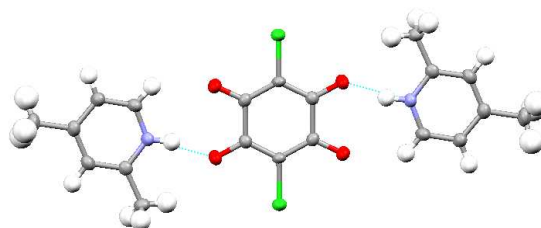


**Figure 7.10** Form I of 2,4-lutidine-chloranilic acid showing the 2:1 hydrogen bonded unit.

Two new forms of 2,4-lutidine-chloranilic acid co-crystals were produced, both in 2:1 ratios and therefore polymorphs, to add to the previously published 1:1 structure<sup>126</sup>. Form I (**Figure 7.10**) of the 2:1 structures fits the molecular synthon seen for the 2,3-lutidine structure with  $Z'=0.5$  and the two lutidines on either side of the chloranilic acid interacting via bifurcated HBs. Although the rings of the chloranilic acid and lutidines are parallel, the 2,4-lutidine is rotated so that the major interaction of the HB

is much more important than the minor part (**Figure 7.11 a**). The stacking allows  $\pi$ - $\pi$  interactions between the chloranilic acid and the lutidines, with each chloranilic acid having a lutidine above and below it (**Figure 7.11 b**). There is also a zigzag motif where the columns of  $\pi$  stacked hydrogen bonded units meet.

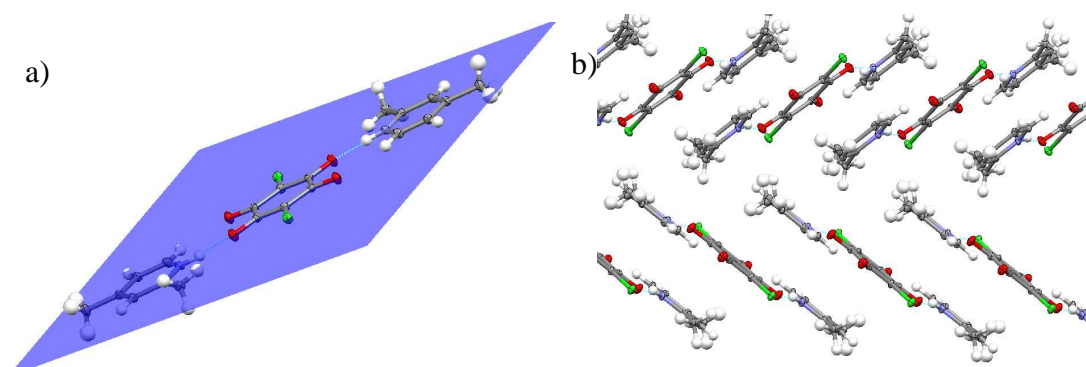


**Figure 7.11 a)** A parallel hydrogen bonded unit of the form I 2,4-lutidine chloranilic acid with the three molecules in the plane. **b)** zig-zag structure and  $\pi$ - $\pi$  interactions form between the rings .

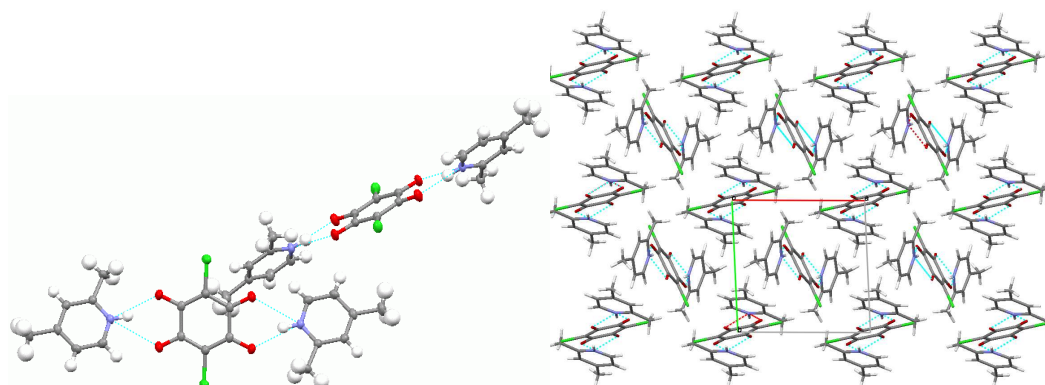


**Figure 7.12 a)** 2,4-lutidine-chloranilic acid Form II with two separate 2:1 hydrogen bonded units. **b)** Packing of the structure.

Form II (**Figure 7.12**), of the 2:1 2,4-lutidine chloranilic acid co-crystals, has  $Z'=1$  but this is made up of two non-equivalent pairings. Individually similar to the first form, of a lutidine and half a chloranilic acid, the angles between the rings of the picoline and chloranilic acid do, however differ ( $39.81^\circ$  and  $28.93^\circ$ ). Both of the chloranilic acid lutidine pairings have the rings near parallel to each other and the N-H tilted towards O1. The stacking is not similar to Form I, forming a pseudo cubic

close packed structure. The tilting of the molecules in relation to each other provides space for the methyl groups.

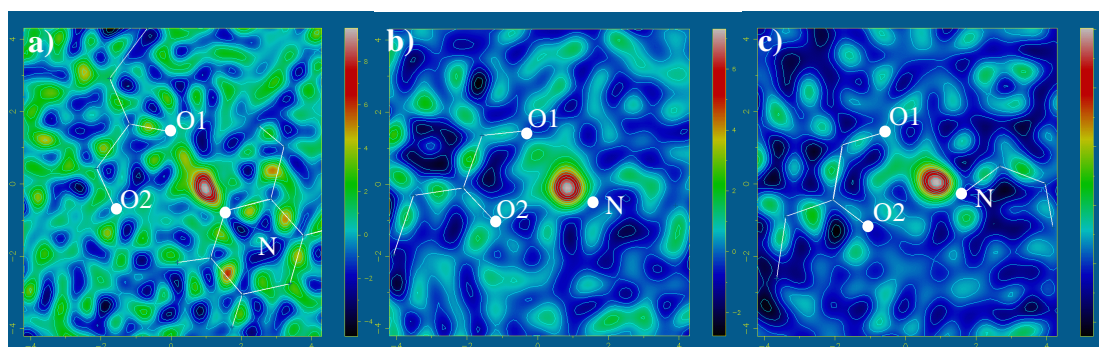


**Figure 7.13** a) Difference Fourier map for the Form I 2,4-lutidine chloranilic acid at 100 K. RMS= 0.08 e/A<sup>3</sup> b,c) Difference Fourier maps for the two independent BHBs in Form II of 2,4-lutidine chloranilic acid at 100 K, b) H1 c) H2. RMS= 0.06 e/A<sup>3</sup>

The two difference Fourier maps for Form II (**Figure 7.13 b and c**) show the two H atoms to be well defined with no clear signs of disorder. The hydrogen peak in the difference Fourier map for Form I (**Figure 7.13 a**) is elongated along the direction of the bond but this is often observed in hydrogen bonds showing no disorder and may also be contributed to by background noise.

#### 7.4.3 2:1 2,5-lutidine chloranilic acid

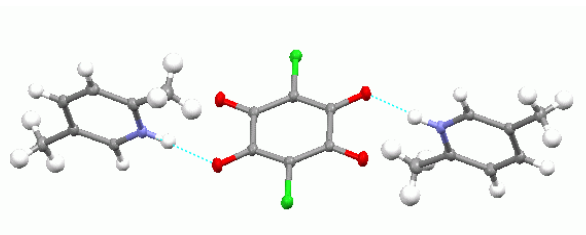


**Figure 7.14** The 2:1 HB unit of the 2:1 2,5-lutidine chloranilic acid co-crystal.

The 2:1 2,5-lutidine chloranilic acid structures follow the same pattern for the hydrogen-bonded synthon unit. The rings of the two molecules are perpendicular to each other and the tilt of the lutidine out the plane of the chloranilic acid is so large that the minor part of the hydrogen bond between the molecules is very long even to the extent that the HB appears not to truly be a bifurcated interaction. The HB

synthon unit has a zig-zag arrangement and forms into layers so the lutidine can form  $\pi$ - $\pi$  interactions (*Figure 7.15 b*).

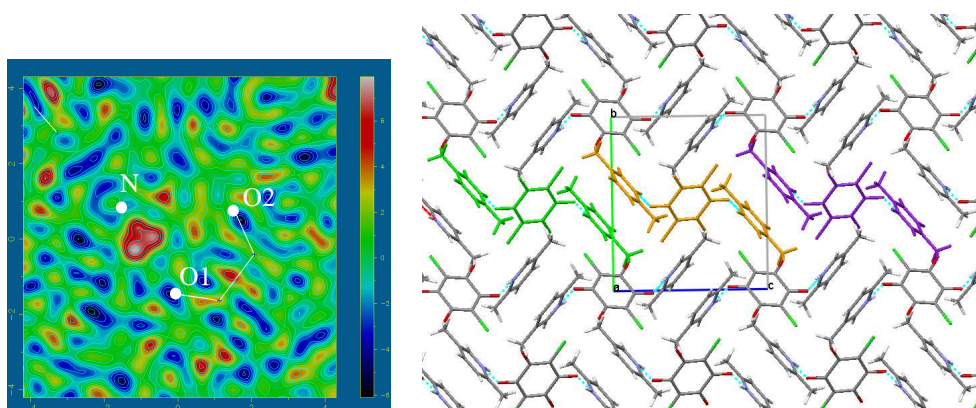


**Figure 7.15** a) Difference Fourier map of 2:1 2,5-lutidine chloranilic acid at 100 K,  $RMS = 0.08 \text{ e}/\text{Å}^3$  b) view down the *a*-axis showing the packing of the zig-zag shaped synthon units.

The shape of the peak representing the hydrogen in the difference Fourier map of 2:1 2,5-lutidine chloranilic acid (*Figure 7.15 a*) is irregular in shape but this can be attributed to poor resolution data for the refinement due to a poor crystal quality. No signs of disorder are present.

#### 7.4.4 2:1 2,6-lutidine chloranilic acid

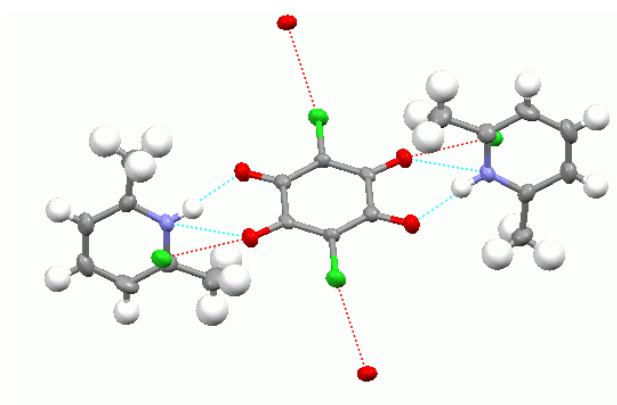


**Figure 7.16** 2:1 hydrogen bonded unit of 2:1 2,6-lutidine chloranilic acid.

The 2:1 2,6-lutidine chloranilic acid co-crystal is very similar to the 2:1 2,5-lutidine chloranilic acid, with the rings of the molecules perpendicular to each other and a large tilt in the equivalent molecular synthon. Within the bifurcated hydrogen bond

the minor part is very long in length. There is no  $\pi$ - $\pi$  stacking but there is a close contact between the chlorine and O2 of 3.128 Å which is smaller than the normal Van der Waals radii of 3.27 Å (O = 1.52 Å, and Cl = 1.75 Å) probably contributing to the weakening of the minor part of the bifurcated HB. The Cl-O close contacts connect the chloranilic acids into layered net structure (**Figure 7.17**), with the HB units sticking diagonally out of the plane.

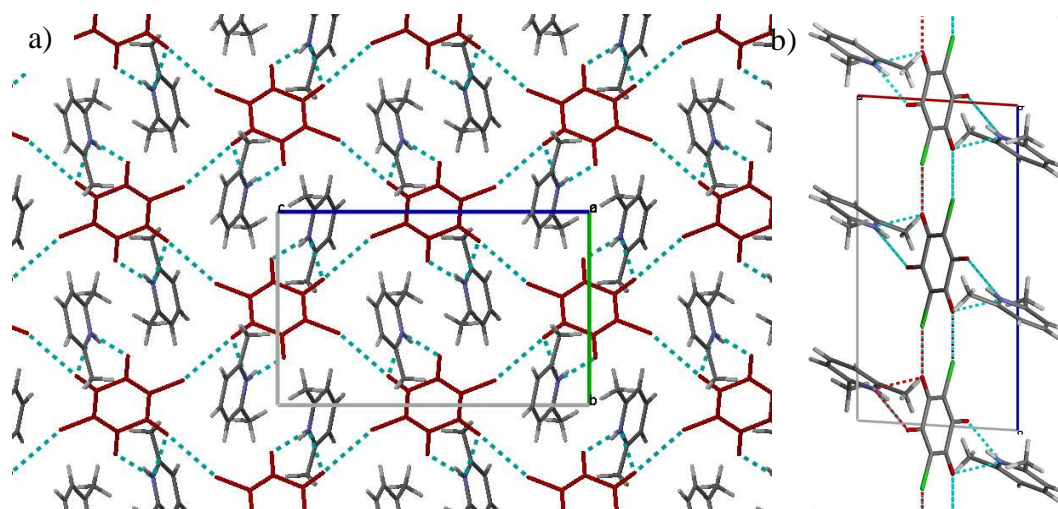


**Figure 7.17** *a*) view down the *a*-axis of the lattice of chloranilic acid (red) forming a layer via Cl-O close contact in the structure of 2:1 2,6-lutidine chloranilic acid, *b*) view down the *c*-axis of the layer.

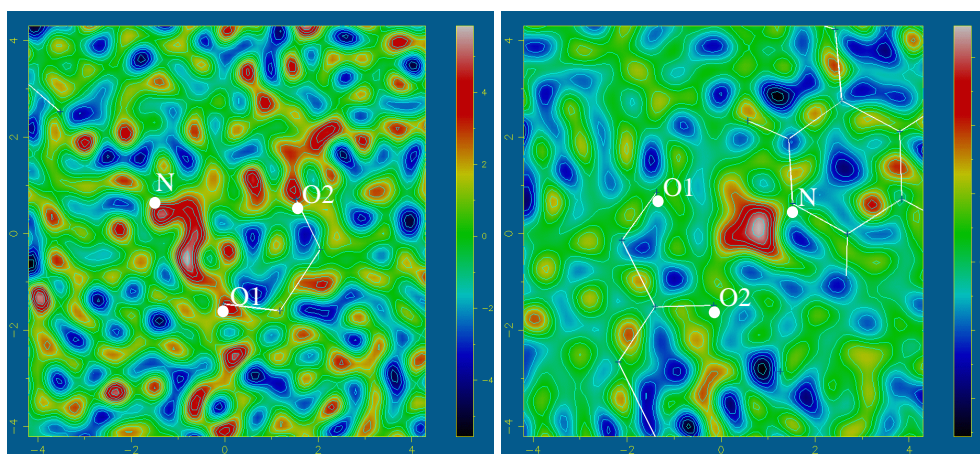


**Figure 7.18** *a*) Difference Fourier map of 2:1 2,6-lutidine chloranilic acid at 100 K, RMS = 0.08 e/Å<sup>3</sup> *b*) Difference Fourier map of 2:1 3,4-lutidine chloranilic acid dihydrate at 100 K. RMS = 0.07 e/Å<sup>3</sup>

The difference Fourier map of 2:1 2,6-lutidine chloranilic acid (**Figure 7.18 a**) has background peaks which are comparable in size to any effect that would be expected which makes it impossible to make any definite conclusions, although the peak formation between N and O1 is worth further investigation with X-ray diffraction data on a different crystal or to a higher resolution which might produce a better result.

#### 7.4.5 2:1 3,4-lutidine chloranilic acid dihydrate

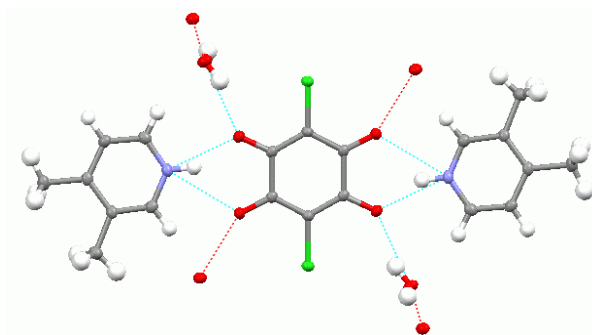


**Figure 7.19** The 2:1 hydrogen bonded unit of 3,4-lutidine chloranilic acid dihydrate.

With the 3,4-lutidine 1:1 structure already existing, it was hoped a 2:1 structure could be found in our approaches to synthesis of molecular complexes in this series. No pure 3,4-lutidine chloranilic acid 2:1 structure emerged although a hydrate form did. In the hydrate, the 2:1 hydrogen bonded unit seen in the other structures is present, and these units are interconnected by the water molecules. In the hydrogen-bonded unit the rings of the lutidine and chloranilic acid molecules are parallel, and the bifurcated bond has only a slight asymmetry towards O1. The water forms hydrogen bonds through the oxygens of the chloranilic acids, therefore each HB unit is attached to four others via the waters forming layers in the a-b plane (**Figure 7.20 a**). The fact that the HB units are flat, combined with the zig-zag structure of the layers, allows  $\pi$ - $\pi$  interactions between the rings of the chloranilic acid and lutidine (**Figure 7.20 b**).

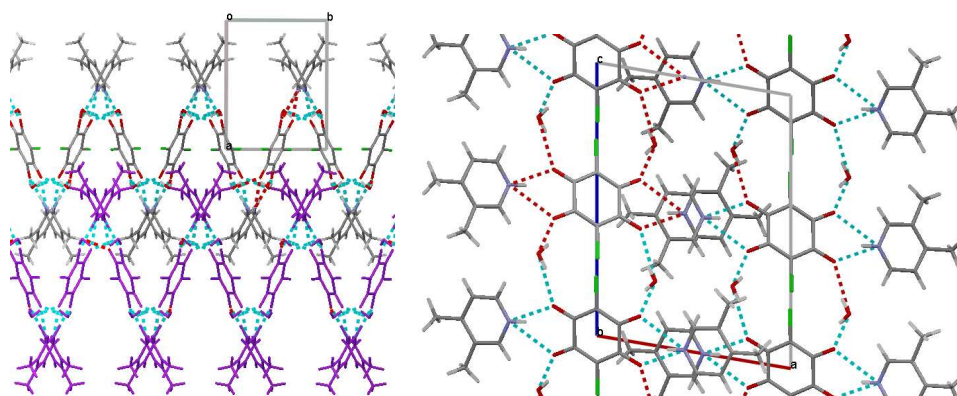


**Figure 7.20** The structure of 2:1 3,4-lutidine chloranilic acid dihydrate viewed along the **a**) *c*-axis (showing HB layer in purple) and the **b**) *a*-axis, shows a zig-zag layered HB structure with the water molecules connecting the 2:1 units via HB to the oxygens of the chloranilic acid.

The difference Fourier map for 2:1 3,4-lutidine chloranilic acid dihydrate is shown in **Figure 7.18 b** and the hydrogen is represented by a well defined peak with no disorder present.

#### 7.4.6 2:1 3,5-lutidine chloranilic acid hydrate trihydrate (100K)

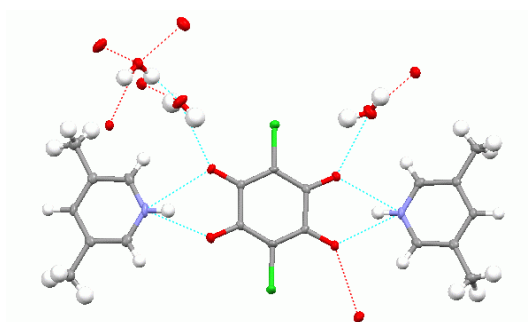


**Figure 7.21** 2:1 hydrogen bonded unit of 3,5-lutidine chloranilic acid, and three water molecules.

A 2:1 3,5-lutidine chloranilic acid hydrate was grown with three waters for every chloranilic acid molecule. No unsolvated 3,5-lutidine chloranilic acid co-crystals have been found or have been published despite multiple attempts, although contamination with water of the 3,5-lutidine stock used in the crystallisation experiments has not been ruled out. The familiar 2:1 hydrogen bonded synthon is present and it is almost flat apart from a slight bend of the lutidine away from the

plane of the chloranilic acid. The interactions that form the bifurcated bond are almost equal for O<sup>1</sup> and O<sup>2</sup> providing a highly bifurcated (symmetric) BHB. The water molecules join the synthon units together through hydrogen bonding although with a more complex network compared to the 3,4-lutidine case (discussed in *Section 8.4.5*). The water molecules form a square motif (*Figure 7.22 c*) with waters joining onto the chloranilic acid molecules via O-H... O HBs. The 2:1 HB synthon units stack on top of each other with half a unit displacement (*Figure 7.22 a*), held together by the network of water molecules (*Figure 7.22 b*).

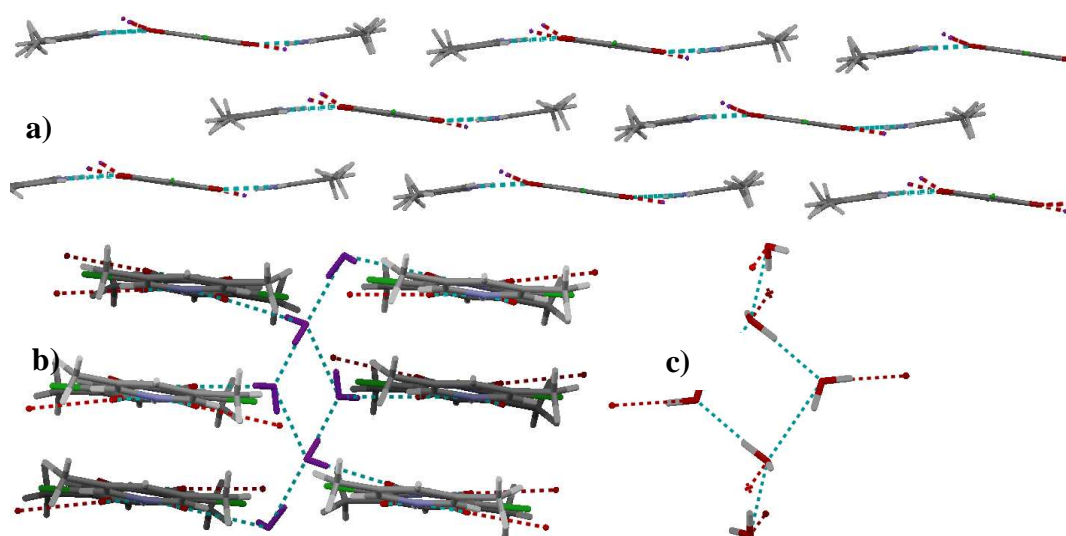


*Figure 7.22 a) The 2:1 HB units stack on top of each other displaced by half a unit, b) and are held together by a network of water molecules (shown in purple), c) Formation of water molecule network.*

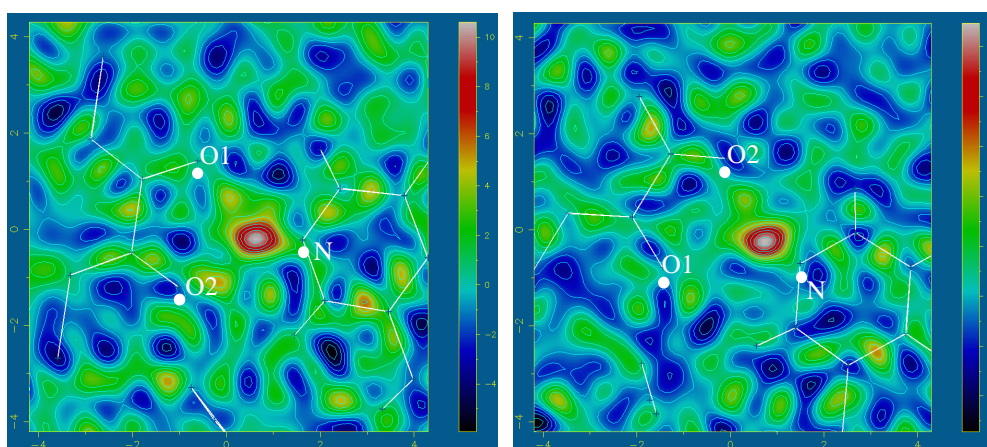


*Figure 7.23 Difference Fourier maps for 2:1 3,5-lutidine chloranilic acid trihydrate, a) hydrogen 1, b) hydrogen 2. RMS = 0.07 e/A<sup>3</sup>*

## 7.5 Powder patterns for chloranilic acid lutidine co-crystal crystallisations

### Chloranilic 23Lutidine

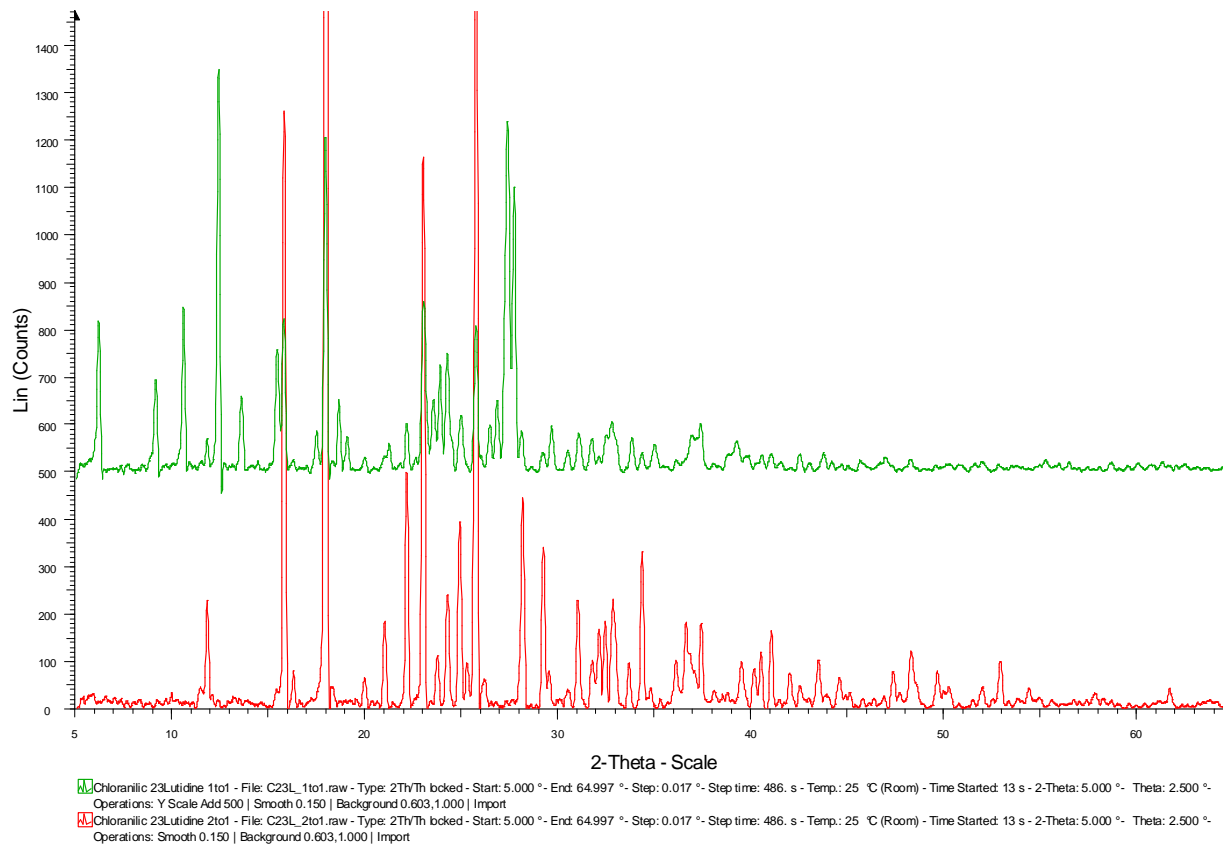


**Figure 7.24** Powder pattern for the crystallisations of 2,3-lutidine and chloranilic acid, *Green-1:1*, and *Red-2:1*.

## Chloranilic 24Lutidine

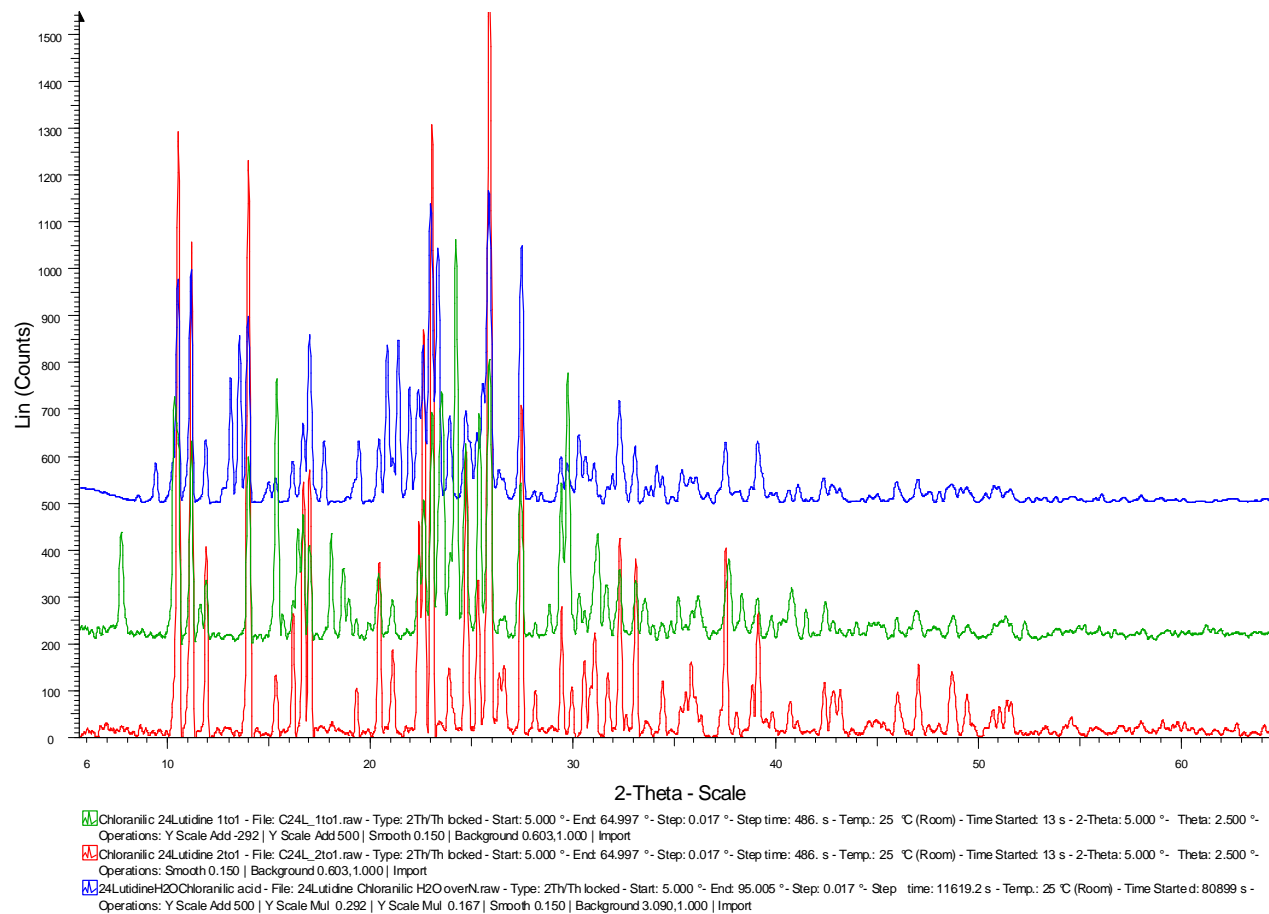
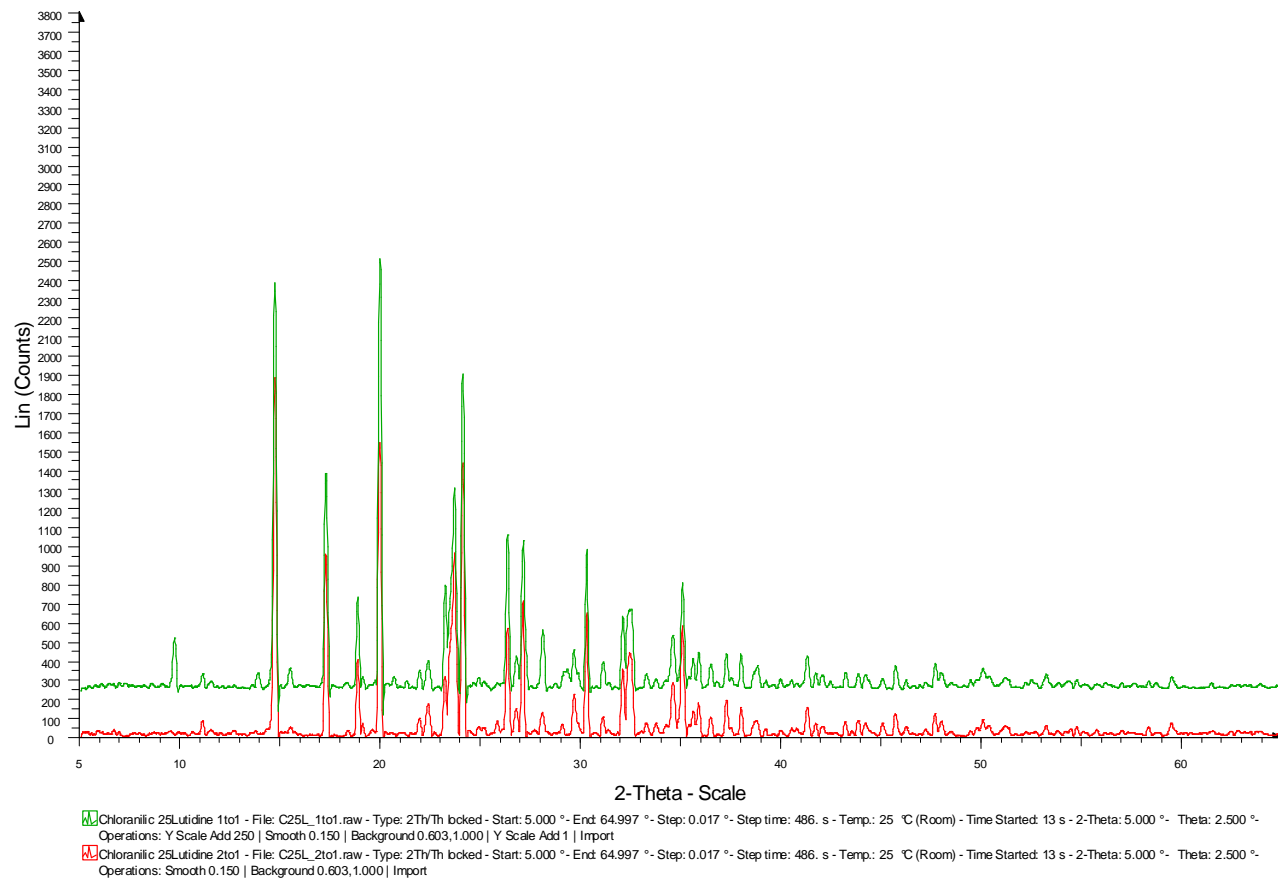


Figure 7.25 Powder pattern for the crystallisations of 2,4-lutidine and chloranilic acid, *Green-1:1*, *Red-2:1* and *Blue-water*

## Chloranilic 25Lutidine



**Figure 7.26** Powder pattern for the crystallisations of 2,5-lutidine and chloranilic acid, *Green-1:1* and, *Red-2:1*.

## Chloranilic 26Lutidine

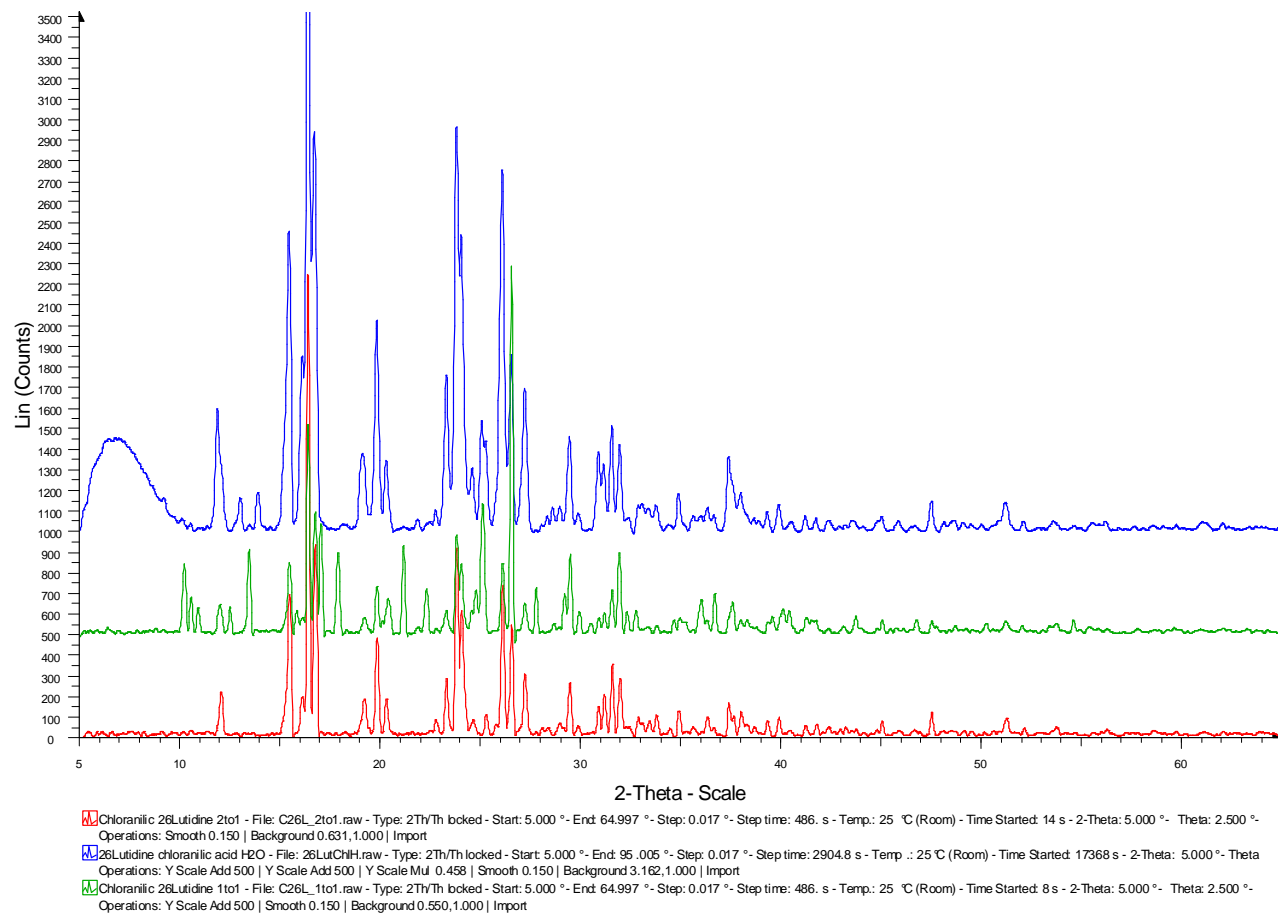


Figure 7.27 Powder pattern for the crystallisations of 2,6-lutidine and chloranilic acid, Green -1:1, Red-2:1 and Blue-water

## Chloranilic 34Lutidine

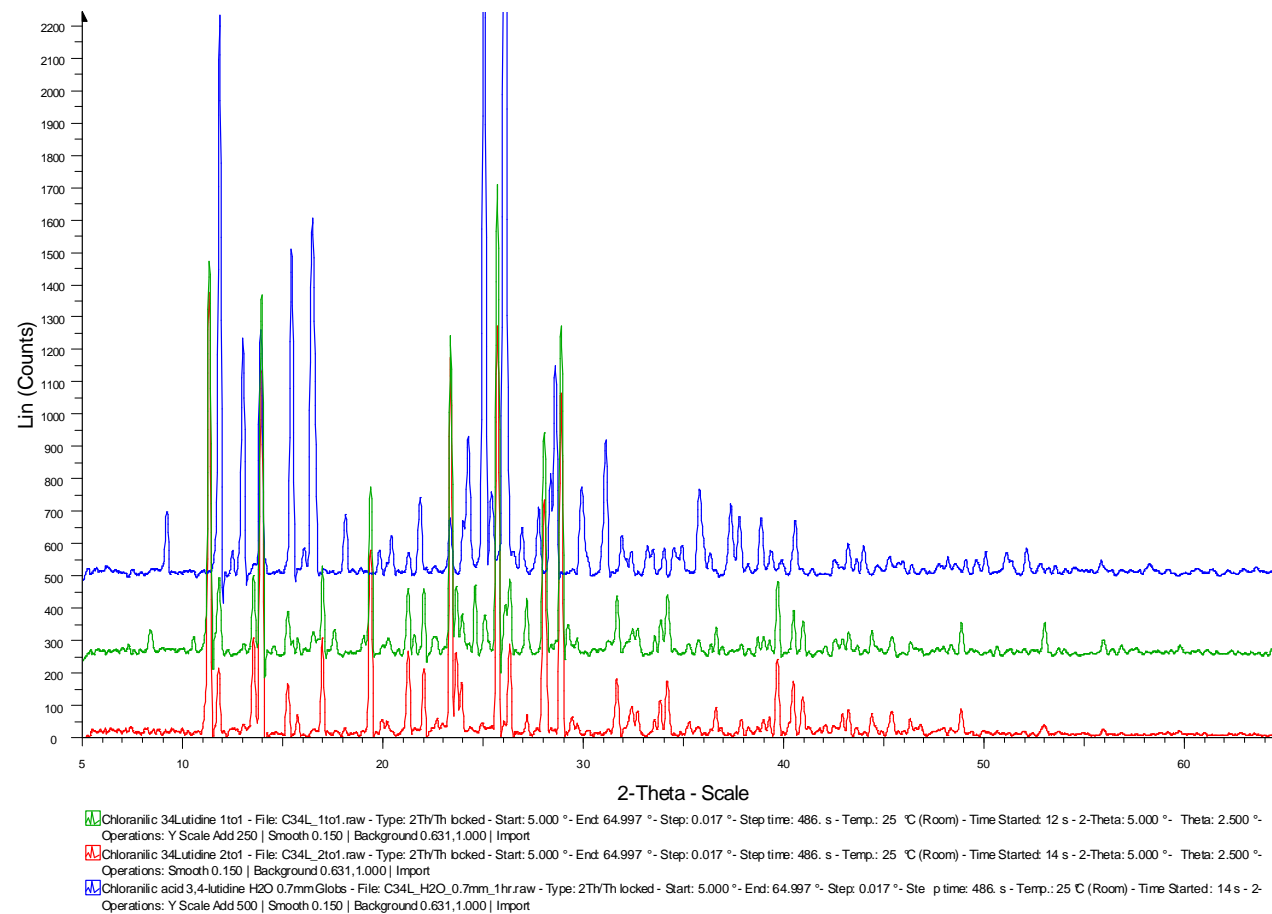


Figure 7.28 Powder pattern for the crystallisations of 3,4-lutidine and chloranilic acid, Green -1:1, Red-2:1 and Blue-water

## Chloranilic 35Lutidine

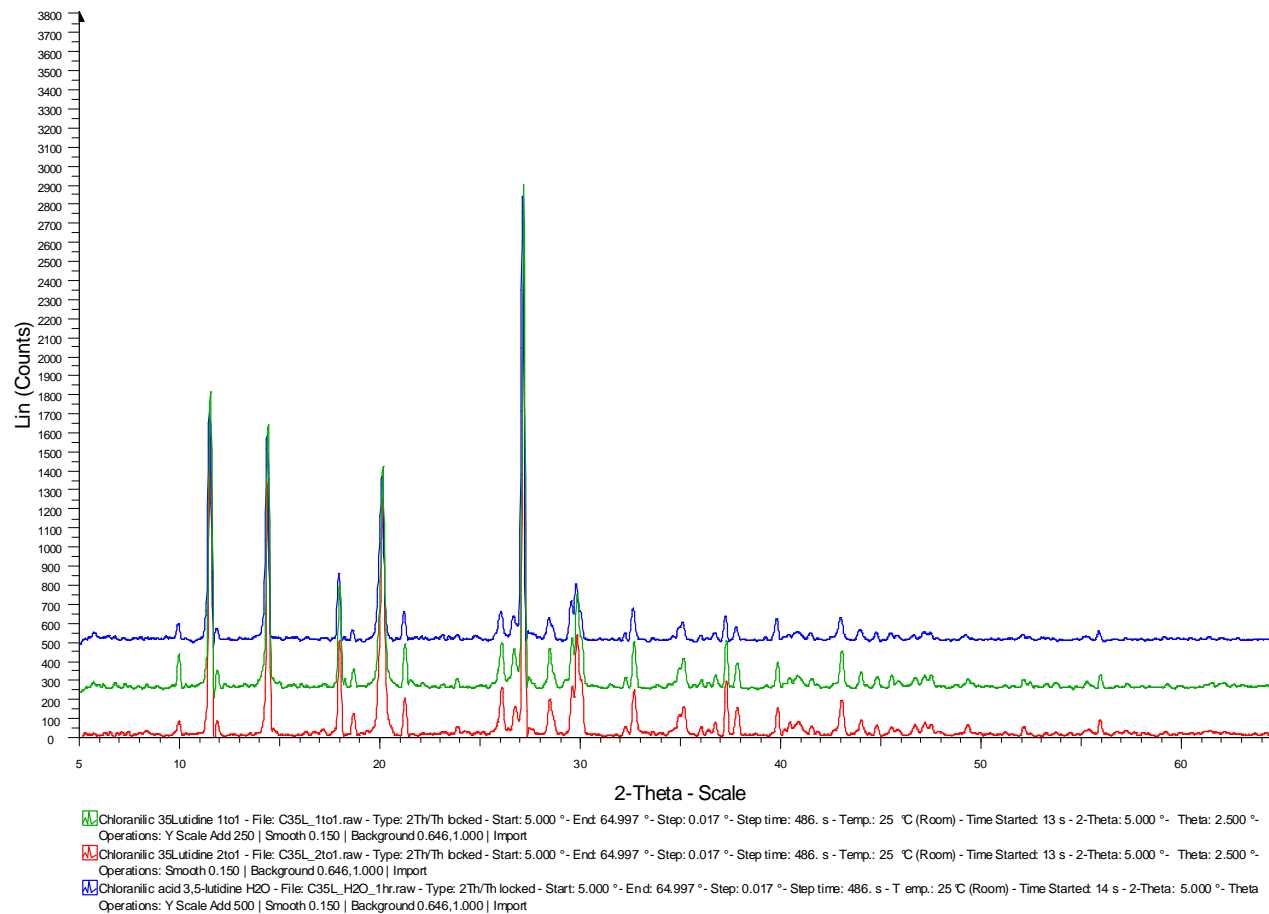


Figure 7.29 Powder pattern for the crystallisations of 3,5-lutidine and chloranilic acid, Green-1:1, Red-2:1 and Blue-water

Shown in *Figure 7.24* to *Figure 7.29* are the powder patterns for sample crystallisation experiments for mixtures of lutidine and chloranilic acid. Three samples were set up for each of the six lutidines, a 1:1, a 2:1 (lutidine in excess) and a 2:1 with water added (testing for hydrate forms). Unfortunately the 2,3-lutidine and 2,5-lutidine samples with water added cannot be presented as the powder patterns are not available.

The two powder patterns for the 2,3-lutidine chloranilic acid (*Figure 7.24*) are different although the 1:1 pattern contains all of the peaks for the 2:1 pattern. The 2:1 matches the calculated pattern for the 2:1 2,3-lutidine chloranilic acid almost exactly with no other products beyond small traces. Part of the 1:1 pattern are the peaks from the 2:1 structure but the majority does not fit any of the known structures, although a small trace of pure chloranilic acid is present. This suggests there is a possible new 1:1 structure that was not found in the single crystal experiments.

The three powder patterns for the 2,4-lutidine chloranilic acid (*Figure 7.25*) crystallisation have a large amount of similarity but have some significant peaks that are different. The 2:1 pattern matches the calculated structure of 2:1 2,4-lutidine chloranilic acid Form I with no extra peaks; there is no additional crystalline material. The calculated pattern for 1:1 2,4-lutidine chloranilic acid matches the major peaks of the 1:1 graph but the 2:1 Form I structure is also present in a smaller amount. The 2:1 with water added graph is a mixture of the two forms of the 2:1 co-crystals. The major features of all the graphs are accounted for, showing no new crystalline material was produced in significant quantities in the sample crystallisation although the possibility of a hydrate being formed in other conditions cannot be ruled out.

There are only 2:1 and 1:1 crystallisation powder patterns for the 2,5-lutidine chloranilic acid which are very similar to each other apart from some additional peaks in the 1:1. The calculated pattern for 2:1 2,5-lutidine chloranilic acid matches the 2:1 pattern and the majority of the 1:1 pattern, with the remainder fitting the calculated pattern of the 1:1 structure and a small amount of chloranilic acid.

The powder data for the 2,6-lutidine chloranilic acid (*Figure 7.27*) show different patterns for the three sample crystallisation environments. The calculated pattern of

2:1 2,6-lutidine chloranilic acid forms the major part of the 2:1 with added water, a minor part of the 1:1 samples patterns, and the entire 2:1 sample pattern, therefore representing the sole crystalline product of the 2:1 sample crystallisation. The 1:1 2,6-lutidine chloranilic acid structure forms the remaining peaks of the 1:1 sample pattern and is in more abundance than the 2:1 form. The large broad hump at the start of the water added powder graph is due to the instrument and not a peak caused by the sample. The majority of the powder pattern for the 2:1 with added water is from the 2:1 structure but this does not account for all the peaks, these non-referenced peaks don't match the structures of chloranilic acid or its hydrate. This leaves the possibility that there is a hydrated version of the 2,6-lutidine chloranilic acid co-crystal.

In the powder patterns for the 3,4-lutidine chloranilic acid (*Figure 7.28*) the majority of the large peaks from all three sample crystallisations cannot be assigned to the two known 3,4-lutidine chloranilic acid co-crystals or the structures of chloranilic acid or its hydrate. This makes it likely that there is another form (maybe even a 2:1 form) that has not been found in the single crystal experiments. Small peaks in the 1:1 sample pattern matched with the calculated pattern for 1:1 3,4-lutidine chloranilic acid and some peaks in the 2:1 with added water were assigned to the 2:1 3,4-lutidine dihydrate structure found in the single crystal work.

The three powder patterns for the 3,5-lutidine chloranilic acid crystallisation (*Figure 7.29*) are almost identical. Only a hydrate structure for 3,5-lutidine with chloranilic acid was found and no previous structures have been published. The 3,5-lutidine chloranilic acid hydrate structure only accounts for some of the small peaks in the sample powder patterns, with chloranilic acid and its hydrate accounting for some others, but this still leaves several peaks unassigned. The fact all three starting conditions, including the two dry samples, grow the 3,5-lutidine hydrate crystal suggests that the sample of 3,5-lutidine was contaminated with water prior to being used for the crystallisations. This and the unassigned peaks leaves the possibility of 1:1, or 2:1 co-crystals of 3,5-lutidine and chloranilic acid being possible to obtain.

## 7.6 Hydrogen-bonded supramolecular synthon; comparison of hydrogen bonding schemes

All six lutidines produced at least one new co-crystal complex with chloranilic acid, with 2,4-lutidine producing two. The seven co-crystals all contain the same bifurcated hydrogen bond motif and either the 1:1 or 2:1 lutidine chloranilic acid hydrogen bonded supramolecular synthon established and discussed during this work. **Figure 7.30** shows the bifurcated hydrogen bonds of all the structures roughly overlaid using the chloranilic acid plane as the constant geometrical reference.

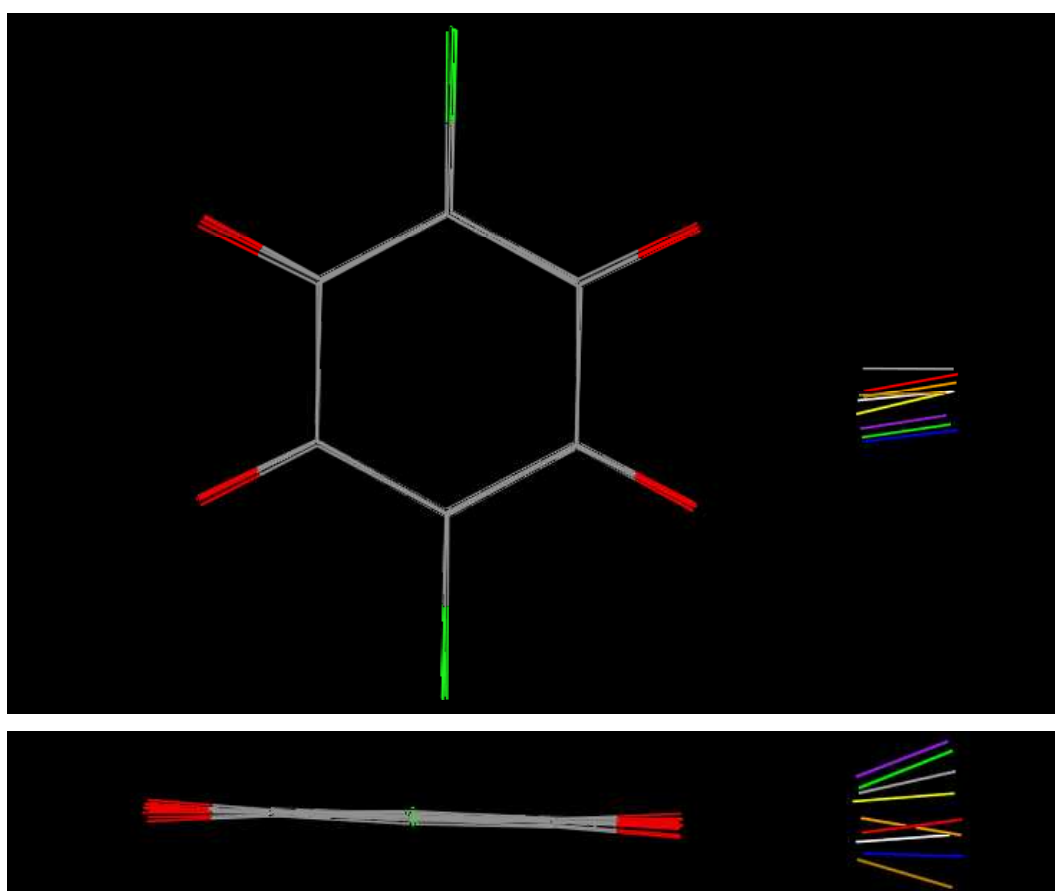


**Figure 7.30** Structure of the nitrogen, hydrogen and chloranilic acid fragments of the lutidine chloranilic acid co-crystals complexes studied, roughly overlaying the chloranilic acid to line up the structures. The nitrogen and hydrogen of the bifurcated hydrogen bond have been coloured for each co-crystal, 2,3-lutidine (yellow), 2,4-lutidine form I (blue), 2,4-lutidine form II H1 (orange), 2,4-lutidine form II H2 (red), 2,5-lutidine (green), 2,6-lutidine (purple), 3,4-lutidine (white), 3,5-lutidine H1 (brown), 3,5-lutidine H2 (grey).

All the complexes have the proton transferred from the chloranilic acid across to the lutidine which was expected due to the high  $pK_a$  values for the lutidines. In **Figure 7.30** there is a clear visual representation of the level of bifurcation of the BHB in comparison to the other structures. It appears that only one of the nine crystallographically unique BHB shows a high level of bifurcation, which is the 2:1 3,5-lutidine hydrogen 2 represented in grey. This can also be seen in the  $H\cdots O1$  and  $H\cdots O2$  lengths shown in **Table 7.1** where it has a difference of 0.01 Å whereas the rest have larger values the biggest being 0.81 Å. Although the variation in the  $H\cdots O1$  and  $H\cdots O2$  lengths of the BHB of the different structures is quite large, when the two lengths are combined ( $H\cdots O1 + H\cdots O2$ ) the difference between the structures is quite small. This suggests no matter what the level of bifurcation the overall strength of the BHB interaction is reasonably constant.

Despite the variation in the BHB motif the spread of the N-H bonds in comparison to the chloranilic acid is relatively small. Looking at the bond lengths (**Table 7.1**) some of the minor parts ( $N-H\cdots O2$ ) could be discounted as HB as they are weak, therefore changing the BHB into a single HB. The best example is 2:1 2,4-lutidine chloranilic acid Form II, which has a  $N\cdots O2$  length of 3.138(2) and  $N-H\cdots O2$  length of 2.56(3), the former is very long for a  $N\cdots O$  HB. However, looking at the spread in **Figure 7.30** the 2:1 2,4-lutidine chloranilic acid structure fits in well with the other BHB in the lutidines and therefore is better described as a weak BHB. The level of bifurcation of the BHB motifs does not seem have a direct link to the position of the methyl groups in the lutidine, as in **Figure 7.30** form I of the 2:1 2,4-lutidine chloranilic acid structure is the weakest bifurcated BHB and form II contains one of the highly bifurcated BHB.

The overall sum of angles in the BHB, (shows the planarity of the BHB **Figure 1.2**) for all the complexes is greater than 355°. This shows the hydrogen remains close to the plane of the donor and two acceptors and is probably an indication that the BHBs are overall quite strong even if some of their components are relatively weak. Surprisingly there does not seem to be any relation between the level of bifurcation and the overall angle.

The angle between the planes of the chloranilic acid and the lutidine rings varies from nearly perpendicular to almost parallel but this doesn't seem to follow any trends with regards to the level of bifurcation or the position of the methyl groups. The 2:1 structures of 2,3-, 2,5- and 2,6-lutidine have large angles at  $79.1^\circ$ ,  $86.33^\circ$  and  $72.04^\circ$  respectively whereas the 2:1 2,4-lutidine structure has an almost flat HB synthon unit with an angle of  $1.64^\circ$ . It is interesting to note that the two hydrate forms have reasonably small angles between the planes in the three BHB.

**Table 7.1** Distances and angles for the bifurcated hydrogen bond in the lutidine chloranilic acid complexes studied, and angles between planes of the rings of the two molecules.

	N-O <sub>1</sub> (Å)	N-O <sub>2</sub> (Å)	N-H (Å)	H···O <sub>1</sub> (Å)	H···O <sub>2</sub> (Å)	N-H···O <sub>1</sub> (°)	N-H···O <sub>2</sub> (°)	O <sub>1</sub> ··H··O <sub>2</sub> (°)	Overall (°)	Between planes (°)
<b>2,3-lutidine</b>	2.663(4)	2.940(4)	0.98(5)	1.72(5)	2.36(5)	163(4)	117(3)	79.96	359.96	79.10
<b>2,4-lutidine Form 1</b>	2.644(2)	3.138(2)	0.92(4)	1.75(4)	2.56(3)	164(3)	122(2)	73.08	359.08	1.64
<b>2,4-lutidine Form 2 H1</b>	2.742(3)	2.879(3)	0.89(3)	1.91(3)	2.29(3)	156(3)	124(3)	77.76	357.76	39.83
<b>2,4-lutidine Form 2 H2</b>	2.782(3)	2.848(3)	0.89(3)	1.95(3)	2.24(3)	155(3)	125(2)	78.15	358.15	28.94
<b>2,5-lutidine</b>	2.652(2)	3.072(2)	0.95(4)	1.73(4)	2.50(3)	162(3)	119(3)	74.55	355.55	86.33
<b>2,6-lutidine</b>	2.655(5)	3.036(5)	0.85(6)	1.83(6)	2.51(6)	163(5)	121(5)	74.82	358.82	72.04
<b>3,4-lutidine Hydrate</b>	2.694(4)	2.901(4)	0.97(4)	1.79(4)	2.24(4)	154(4)	125(3)	79.05	358.05	8.86
<b>3,5-lutidine Hydrate H1</b>	2.681(4)	2.942(4)	0.93(5)	1.84(4)	2.25(4)	149(3)	131(3)	78.04	358.04	16.41
<b>3,5-lutidine Hydrate H2</b>	2.769(3)	2.819(3)	0.88(4)	2.07(4)	2.06(4)	144(3)	136(3)	79.30	359.3	16.34

## 7.7 ILL neutron experiment on 2:1 2,4-lutidine chloranilic acid form 1

Although most of the structures refined from neutron data presented here have been from data collected on SXD at ISIS, several experiments have been carried out at the reactor neutron source (ILL) on the machine VIVALDI. Unfortunately due to difficulties processing the VIVALDI data only the structure of 2:12,4-lutidine chloranilic acid form I has been fully refined with reliable results.

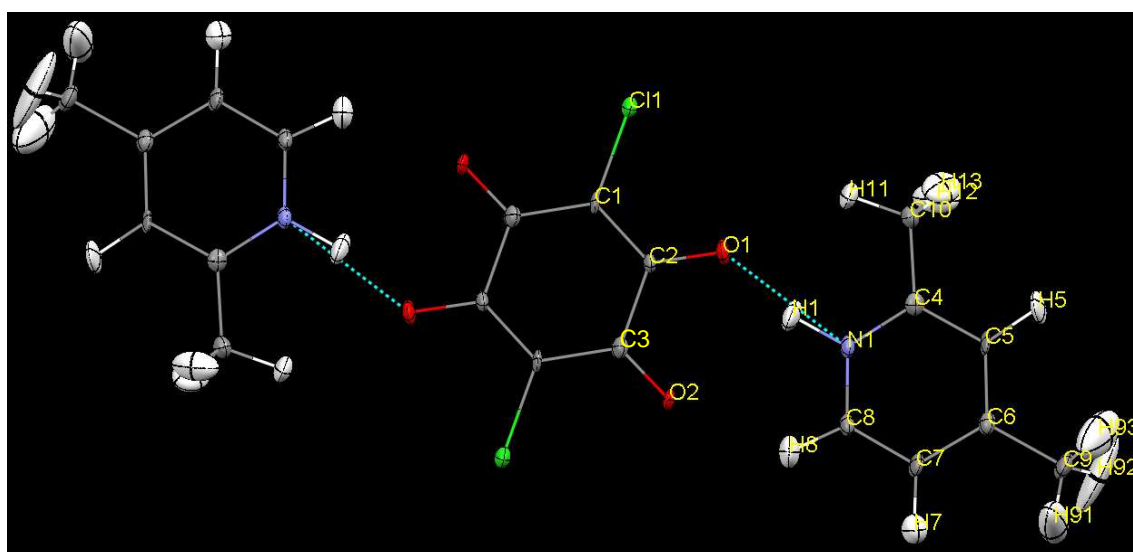


**Figure 7.31** The 2:1 HB synthon unit from the neutron refinement of 2:1 2,4-lutidine chloranilic acid form I at 40 K.

The X-ray structure for 2,4-lutidine chloranilic acid has already been described in **Chapter 7.4.2** and it forms a nearly flat 2:1 HB synthon unit. An image of the refinement for the VIVALDI neutron data can be seen in **Figure 7.31** and the refinement data in **Table 9.8**.

The refinement is not as good quality as the experiments on SXD, which is mostly due to the difficulty in integrating the data from VIVALDI. The multiple wavelength data (in combination with possible problems with crystal quality) leads to peak overlap, streaky spots, and background noise, which cannot always be corrected for. The refinement is also not helped by the limited data (1602) to parameter (218) ratio which is below the accepted 10:1 ratio generally preferred for a good refinement.

This is reflected in the R-value, which is larger than desired although for neutron data this is acceptable, and good enough to provide reliable H-positions and anisotropic thermal parameters. The ellipsoid shapes of some of the atoms are not as spherical as expected from a constrained ring, especially C1, and C5 which show flat thermal ellipsoids (small ADP values in the b-axis). The C9 methyl group shows large atomic displacement parameters for the hydrogens (H91, H92 and H93) resulting from the rotation but this is not abnormal and is a result of a rotation of the methyl group.

**Table 7.2** The HB lengths of 2:1 2,4-lutidine chloranilic acid form I for the 100 K X-ray and the 40 K neutron refinements.

Neutron	D-H (Å)	H...A (Å)	D...A (Å)	Angle (°)
N1-H1...O1	1.087(9)	1.573(9)	2.638(6)	164.9(8)
N1-H1...O2	-	2.501(10)	3.136(5)	116.2(6)
X-ray	D-H (Å)	H...A (Å)	D...A (Å)	Angle (°)
N1-H1...O1	0.92(4)	1.75(4)	2.644(2)	164(3)
N1-H1...O2	-	2.56(3)	3.138(2)	122(2)

The BHB lengths for the X-ray and neutron data can be found in **Table 7.2**. A comparison of the position of the hydrogen atom in the BHB shows the expected difference between the X-ray and neutron experiments. This is because the electron density associated with the hydrogen is shifted towards the donor, therefore shortening the D-H bond length of the X-ray data compared to that resulting from the nuclear positions seen in the neutron experiment. With this taken into account all the HB lengths and angles compare well, and the same conclusion of a low level of bifurcation in the HB is reached with the neutron data.

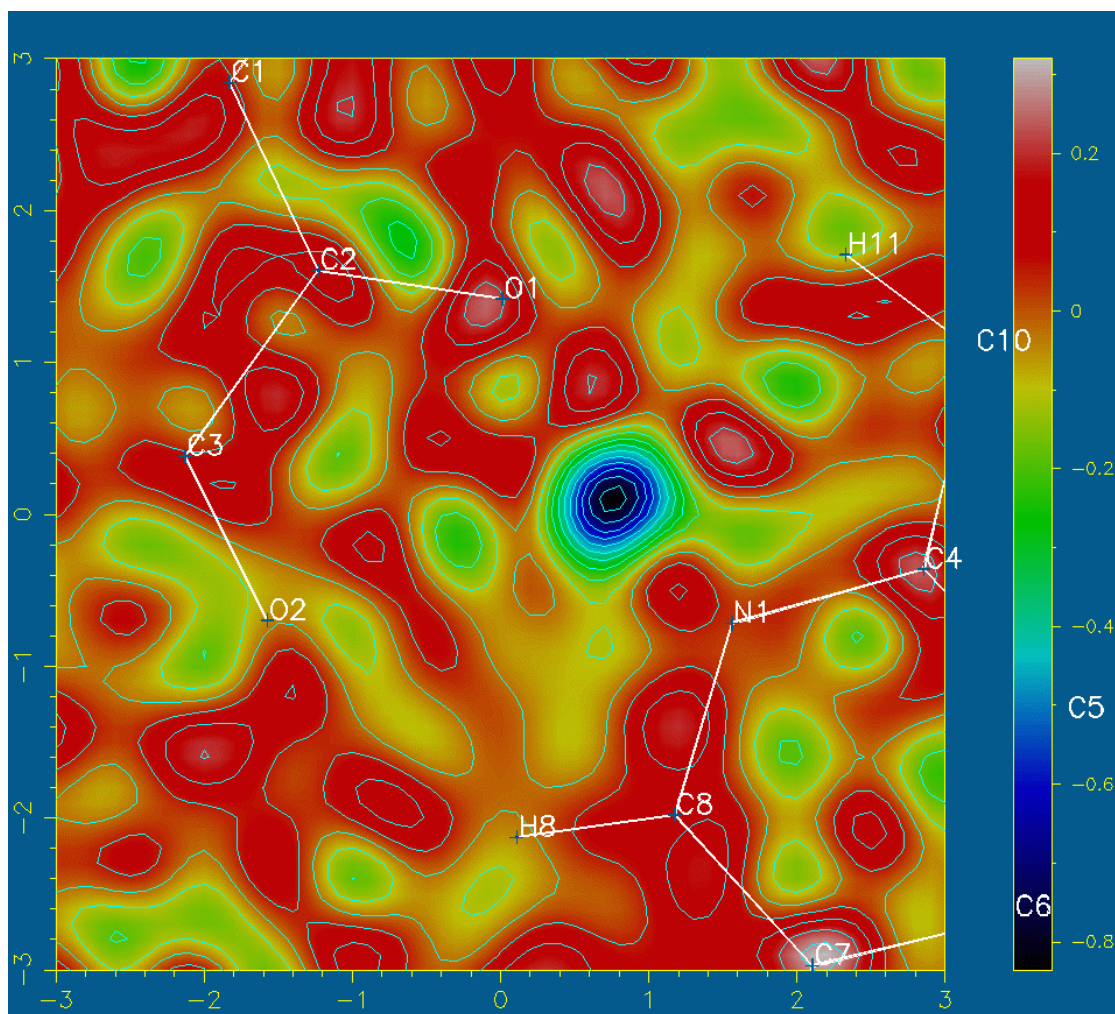


**Figure 7.32** Difference Fourier map of 2:1 2,4-lutidine chloranilic acid form I at 40 K. RMS =  $0.04 \text{ fm}\text{\AA}^3$

The difference Fourier map **Figure 7.32** shows a well positioned peak representing the proton within the BHB and no signs of disorder are present. In the X-ray difference Fourier map the peak was slightly elongated which was thought to arise from the high background. This is backed up by the neutron data.

## 7.8 Conclusions

A new co-crystal with chloranilic acid has been found for the six lutidines, and two polymorphs for 2,4-lutidine. The seven new and four previously determined chloranilic acid lutidine co-crystals contain one of the two larger supramolecular synthon units in either a 1:1 or 2:1 ratio, shown in **Figure 7.6**. The two synthons share a common BHB motif formed between two of the O atoms of the chloranilic acid and the N atom from the lutidine.

The hydrogen atom in the BHB is located on the nitrogen of the lutidine in all of the structures meaning that it has transferred across from the chloranilic acid. From examining the difference Fourier maps none of the structures shown any clear signs of disorder although the 2:1 2,4-lutidine chloranilic acid form I structure has an elongated peak and the 2:1 2,6-lutidine chloranilic acid structure has a unusual pattern, but both have large background noise that could account at least in part for the effects.

The powder patterns showed that the starting ratio of the crystallisation is important in determining the product. In many of the crystallisation attempts on the four lutidines that 2:1 structures have been found: the powder pattern showed that it was the main product formed for the 2:1 (lutidine in excess) crystallisation, and the 1:1 crystallisation always produced some of the 1:1 but not always as the main product. The addition of water was also a determining factor, with some forming hydrates. It is suspected that the 3,5-lutidine sample was contaminated with water as all the crystallisations produced some of the hydrate even where the lutidine starting material was meant to be dry. Unassigned peaks in some of the 2,3-, 2,6-, 3,4- and 3,5-lutidine sample powder patterns make it likely that there are further chloranilic acid complex crystals being produced in the crystallisations but these have not been picked up in the single crystal work either because these phases are powder in nature or not enough crystals have been screened.

An experiment on VIVALDI at the ILL has provided sufficient data to provide a refinement of the structure of 2:1 2,4-lutidine chloranilic acid form I, although this is not to the same standard seen in the structures from SXD. This was not the only experiment run on VIVALDI but it is the only data set in this project to be fully refined due to both technical problems and difficulties integrating the data, although other data is expected to provide useful results in the near future. The results of this experiment showed the proton position in the BHB to be well defined with no disorder present, backing up the X-ray diffraction refinement described in **Section 7.4.2**. The structure from the refinement has two atoms (C1 and C5) with atomic displacement parameters that are anomalous but otherwise was stable and matched the structure defined by the X-ray experiment described earlier.

## 8. Complexes of Chloranilic Acid with Picolines

The work on the lutidine chloranilic acid co-crystals (presented in *Chapter 7*) found many new compounds that show similar motifs and hydrogen-bonded units. Using these findings as a basis the study was followed up with further co-crystallisation experiments using the knowledge gained from the lutidines. The three picolines (methylpyridine isomers) are very simple amide molecules, ideal for the present investigations into chloranilic acid co-crystals and their hydrogen bond motifs. Comprising of a pyridine ring with a methyl group at the either the 2-, 3-, or 4-position (also referred to as  $\alpha$ ,  $\beta$ ,  $\gamma$ ), the picoline isomers are all colourless, strong-smelling liquids at room temperature with a chemical formula  $C_6H_7N$  and molar mass of  $93.13 \text{ g mol}^{-1}$ . They are obtained from coal tar, horse urine or petroleum and are useful as solvents and raw materials for various chemical products used in the polymer, textiles, fuels, agrochemicals, pharmaceuticals and colorants industries.

### 8.1 Hydrogen bonding motifs, proton transfer and $pK_a$ matching

In the case of the lutidine chloranilic acid co-crystals discussed previously, the bifurcated hydrogen bonded motif was shown to be reliable, forming in all the structures. This interaction was then used to hold hydrogen bonded supramolecular synthon units together in both 2:1 and 1:1 molecular complex stoichiometry. Although seven new structures are reported it is most likely this is not an exhaustive collection of the possible complexes and hydrates that could be produced from the six lutidines in combination with chloranilic acid. The related study of picoline (and additional molecules) presented here will make it possible to see whether the same bifurcated hydrogen bonded motif and associated hydrogen bonded supramolecular synthon is as prominent in other chloranilic acid containing systems. An intensive screening of a large number of distinct crystallisation environments will test whether the motif and synthon is as exclusive as indicated or if, under the right conditions, co-crystals not containing them will form.

Although one of the methods suggested to tune or affect the hydrogen position within a short hydrogen bond is varying  $pK_a$ , like the lutidines the picolines have  $pK_a$  higher

than chloranilic acid and will therefore most likely produce structures where the hydrogen is on the side of the nitrogen. Despite this indication, and with the awareness that conclusions from solution-state  $pK_a$  values will not always translate across to the solid state, several other molecules with a variety of  $pK_a$ s have also been crystallised with chloranilic acid and should result in some cases where the hydrogen is not transferred.

## 8.2 Structure determinations of CA-picoline complexes

The aim with the new crystallisations presented in this chapter is to obtain complexes of these compositions as seen for the lutidines with the picolines but with better control due to the experience gained in the previous investigations. As will be seen, the end result was good with success in gaining almost all the target structures.

### 8.2.1 Picoline chloranilic acid 1:1 structures

All three picolines form 1:1 complexes with chloranilic acid. The 2-picoline and 4-picoline molecules form similar hydrogen bonded units to those found in the 1:1 lutidines in the paper by Ishida et al<sup>37</sup> (*Figure 7.6 a*). Two chloranilic acid molecules are linked through two hydrogen bonds and on either side, a picoline forms a bifurcated hydrogen bond, which results in a four molecule hydrogen bonded unit with centrosymmetric symmetry. The 3-picoline 1:1 structure with chloranilic acid has more in common with the 2:1 structures of the lutidines (*Figure 7.6 b*) and the 2:1 picolines (*Section 8.2.2*), than the other two 1:1 structures. In the 3-picoline chloranilic acid structure, the chloranilic acid molecule is directly bonded to two picolines with bifurcated HBs as seen for the 2:1 co-crystal complexes of lutidine with chloranilic acid. Additional chloranilic acid molecules then connect the units together with O-H...O single hydrogen bonds and chlorine-oxygen close contacts.

In all three structures the hydrogen in the bifurcated bonds has been transferred across to the nitrogen of the picoline, although some are still semi-protonated as they form bonds between two chloranilic acid hydrogen molecules.

#### 8.2.1.1 2-picoline chloranilic acid complex

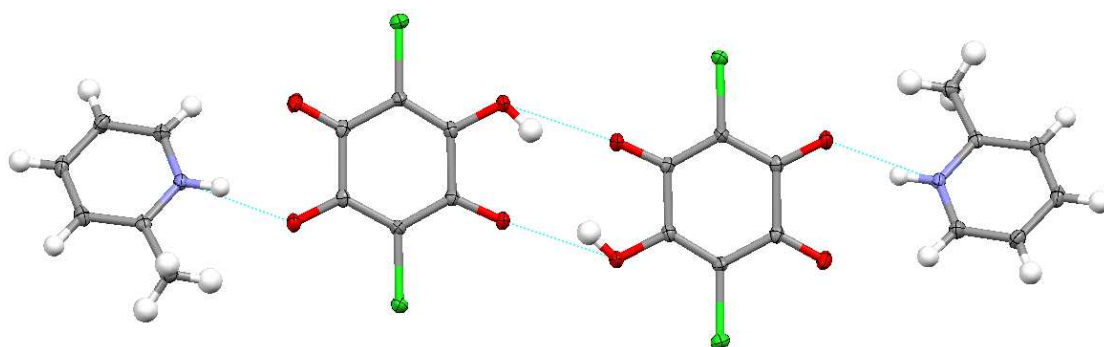


**Figure 8.1** The 1:1 hydrogen bonded unit from the 2-picoline chloranilic acid structure.

In the 2-picoline complex, the picoline chloranilic acid 1:1 hydrogen bonded units (**Figure 8.1**) are almost flat with the two chloranilic acid molecules in the same plane and the picoline only slightly out of this plane. The tilt aligns the N-H with the one oxygen and makes the minor part of the bifurcated hydrogen bond almost non-existent. The HB units are packed in staggered fashion with adjacent picolines head to tail, this allows for some  $\pi$ - $\pi$  interactions between chloranilic acid molecules (**Figure 8.2**).

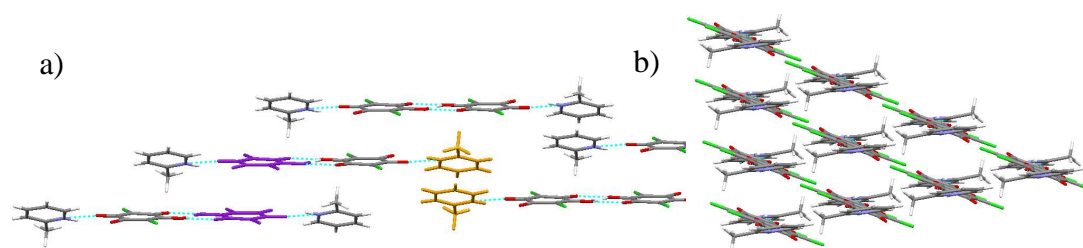


**Figure 8.2 a)** Stacked HB units showing  $\pi$ - $\pi$  interactions (purple) and adjacent rotated picolines (orange), **b)** stacked HB units end on.

### 8.2.1.2 3-picoline chloranilic acid

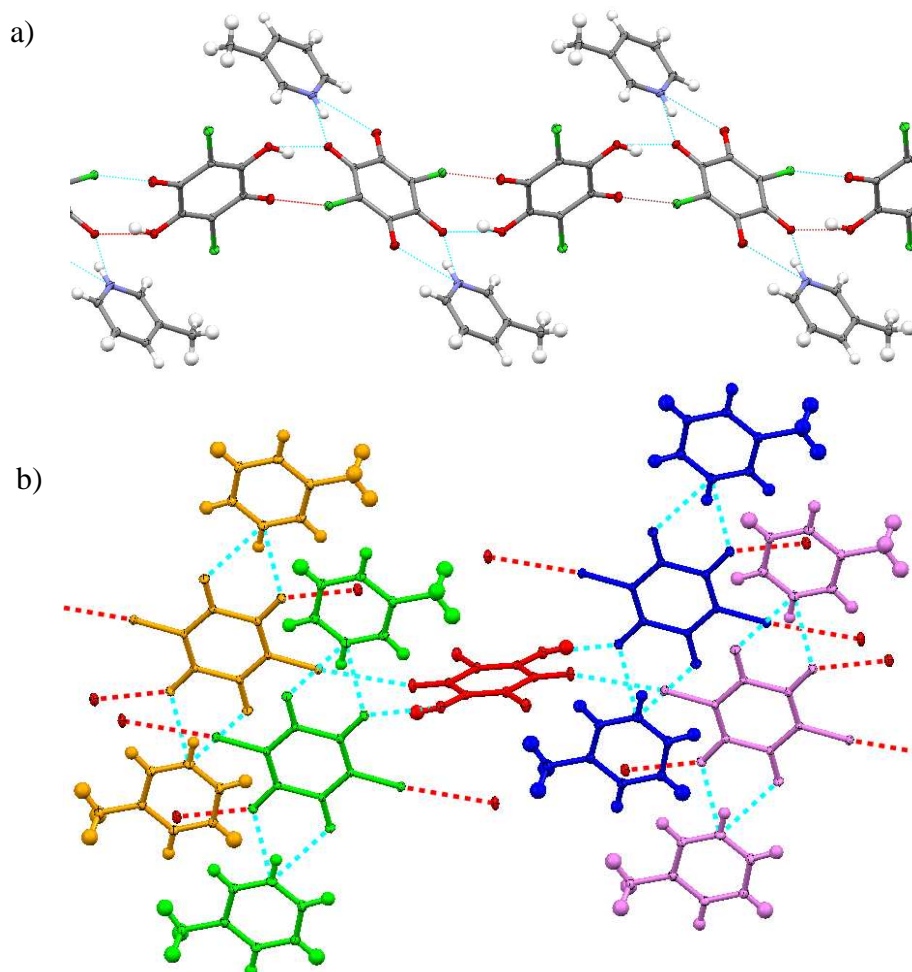


**Figure 8.3** The 1:1 structure of 3-picoline chloranilic acid, **a)** showing the 2:1 HB units connected via single O-H...O bonds and oxygen-chloride close contacts, **b)** the connector chloranilic acid (red) joining 4 separately coloured 2:1 HB units.

Although a crystal of 1:1 3-picoline chloranilic acid was successfully grown the structure has more in common with the 2:1 units than the other 1:1 structures (**Figure 8.3 a**). One 3-picoline molecule is hydrogen bonded to either side of the chloranilic acid forming the 2:1 HB synthon (**Figure 7.6 b**). These hydrogen bonded units are then joined via an additional chloranilic acid molecule that forms O-H...O hydrogen bonds and Cl-O close contacts (3.244Å) with the chloranilic acid between the picolines (**Figure 8.3 b**). The combination of the HB units and the connecting chloranilic acid molecules make 2-dimensional planes that stack in layers. The bridging chloranilic acid retains its protons whereas the other is de-protonated, with the protons transferring across the bifurcated HB to the picoline nitrogens.

### 8.2.1.3 4-picoline chloranilic acid complex

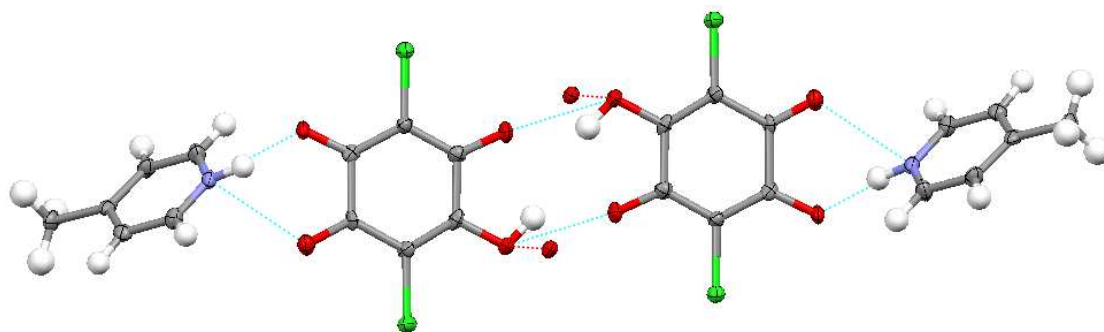


**Figure 8.4** Hydrogen bonded unit from the 1:1 4-picoline chloranilic acid.

As with the 2-picoline case the two chloranilic acids in the 1:1 HB unit in the 4-picoline chloranilic acid co-crystal are in the same plane but the 4-picoline is severely rotated and tilted off this plane giving the 1:1 HB unit a zig-zag shape. Additional close O...O contacts between the chloranilic acid molecules connect the hydrogen-bonded units on either side, forming a stack along the b axis (**Figure 8.5 a**). The stacks of the 1:1 HB units pack together in a regular array, with the tilt in the picoline (relative to the chloranilic acid) probably present to allow the methyl groups to move apart from each other, with the HB units end on.

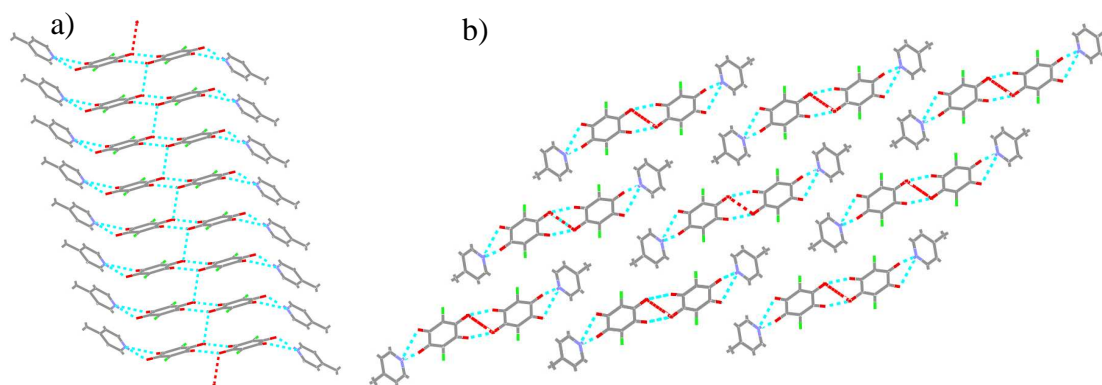


**Figure 8.5 a)** HB units form chains in the structure of 1:1 4-picoline chloranilic acid, **b)** the packing together of these, here viewed down the b-axis.

## 8.2.2 Picoline chloranilic acid 2:1 structures

The three picolines produce very similar structures when forming 2:1 molecular complexes with chloranilic acid. Grown from mixtures of chloranilic acid and the respective picoline in excess, the majority of crystals grown were 2:1 although a small proportion of the respective 1:1 structures (*Section 8.2.1*) were also produced. In the case of the 3-picoline, two forms of 2:1 co-crystal were formed. The structures have the supramolecular synthon already seen in the chloranilic acid lutidine co-crystals with 2:1 picoline-chloranilic acid forming blocks held together by bifurcated N-H...O(O) hydrogen bonds. The centre of the chloranilic acid unit is located on an inversion centre and the picoline ring is positioned so the nitrogen is between the two oxygen atoms of the chloranilic acid (*Figure 7.6 b*). Similar again to the lutidine case, the chloranilic acid is totally de-protonated with the hydrogen being transferred to the nitrogen.

### 8.2.2.1 2-picoline chloranilic acid

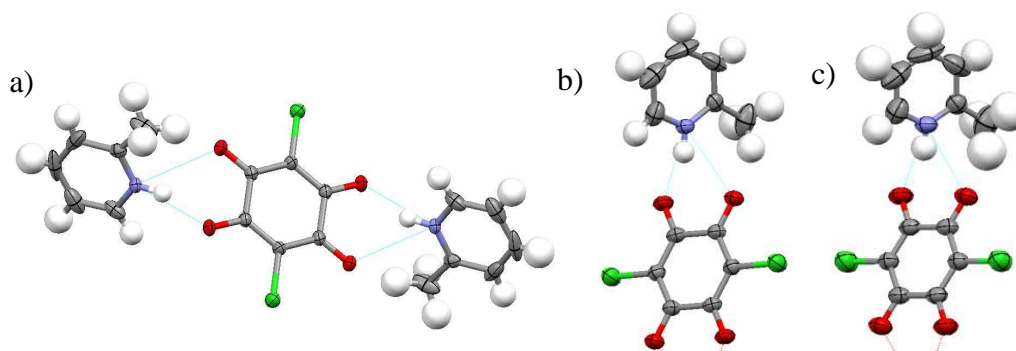


**Figure 8.6** a) Hydrogen bonded unit of the 2:1 2-picoline chloranilic acid co-crystal at 100 K, the ellipsoids on the picoline show large values indicative of disorder, b) The two molecules shown at 200 K and, c) 300 K.

The carbons of the picoline show large and anisotropic thermal displacements, from the direction of the elongation it would appear that this is due to pivoting of the molecule around the bifurcated HB (*Figure 8.6*). This could be due to static or dynamic disorder and is present at all the temperatures. In the 2-picoline complex (*Figure 8.7*) the hydrogen bonded blocks are orientated along the long *c*-axis forming stacks in the *a*-direction. In the *b*-direction the hydrogen-bonded blocks are tilted by

90° shifted along by half a block each layer to accommodate the bulk of the methyl group.

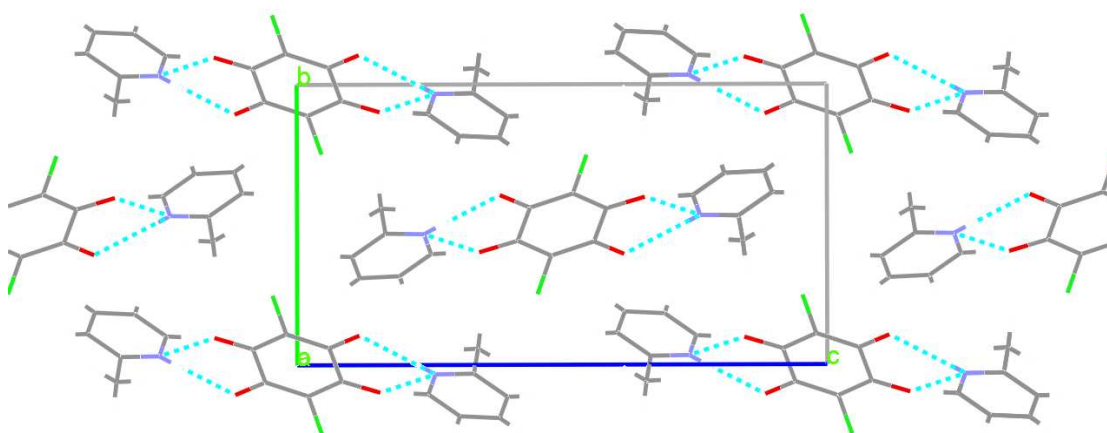


**Figure 8.7** View of the 2:1 2-picoline chloranilic acid structure along the b-c plane showing the stacking of the hydrogen bonded units allowing space for the methyl groups.

#### 8.2.2.2 3-picoline chloranilic acid complex, forms 1 and 2

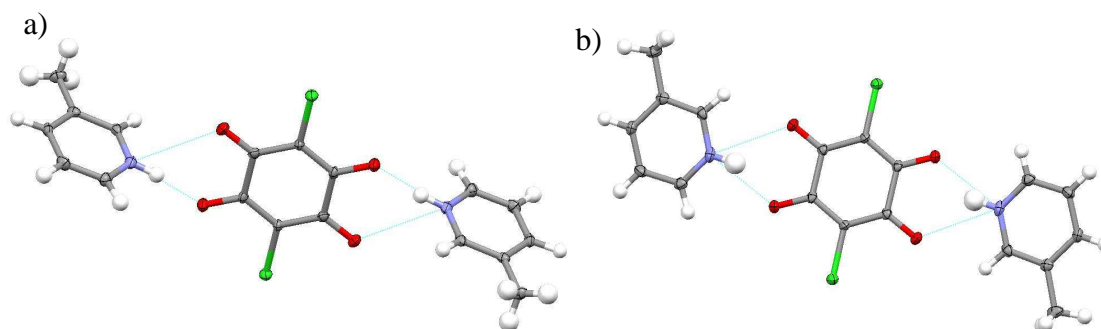


**Figure 8.8** The hydrogen bonded units from the structures of the two polymorphic forms of the 2:1 3-picoline chloranilic acid co-crystal complex **a)** Form 1 **b)** Form 2.

The crystallisations of excess 3-picoline with chloranilic acid produced two polymorphs of the 2:1 complex. Form 1 of the 2:1 3-picoline chloranilic acid complex is the more common of the two forms growing in a much higher abundance and generally producing crystals that are larger in size, although both polymorphs form rectangular blocks. Form 1 has the ring of the picoline perpendicular to the chloranilic acid (**Figure 8.9 b**) with a slight tilt lining up the N-H with O1. The stacking has to accommodate the methyl groups of the picoline, as the molecule is at

right angles to the plane of the chloranilic acid (**Figure 8.9 c**). The packing seems less favourable; there are no  $\pi$ - $\pi$  interactions and the methyl group of one picoline is directed towards the ring of a second picoline.

Although form 2 produces the same HB synthon as form 1 (**Figure 7.6 b**) they are different in the way the two molecules are orientated, with form 2 having almost parallel rings between the picoline and chloranilic acid (**Figure 8.9 a**). The nitrogen hydrogen bond is also directed between the two oxygens of the chloranilic acid making the bond in form 2 much more bifurcated in nature. The hydrogen-bonded blocks are orientated along the *a-c* plane and in contrast to the stacking of form 1, the flat HB units lie on top of each other in slanting rows (**Figure 8.10**). The rows are then stacked with a half a unit offset.

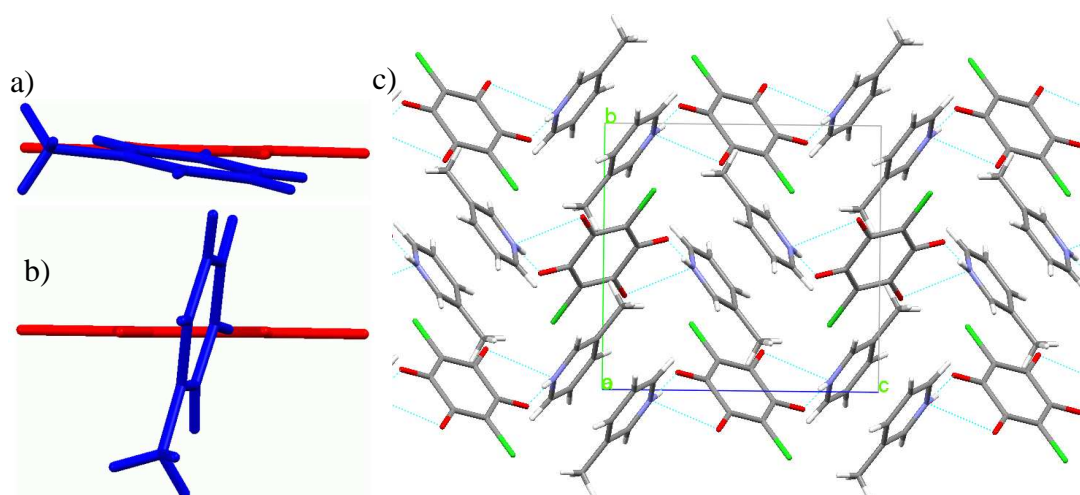


**Figure 8.9** View showing different angles between the chloranilic acid (red) and 3-picoline (blue) for **a**) form 2, and **b**) form 1 of the 2:1 3-picoline chloranilic acid complex, **c**) the stacking present in form 1 viewed down the *a*-axis.

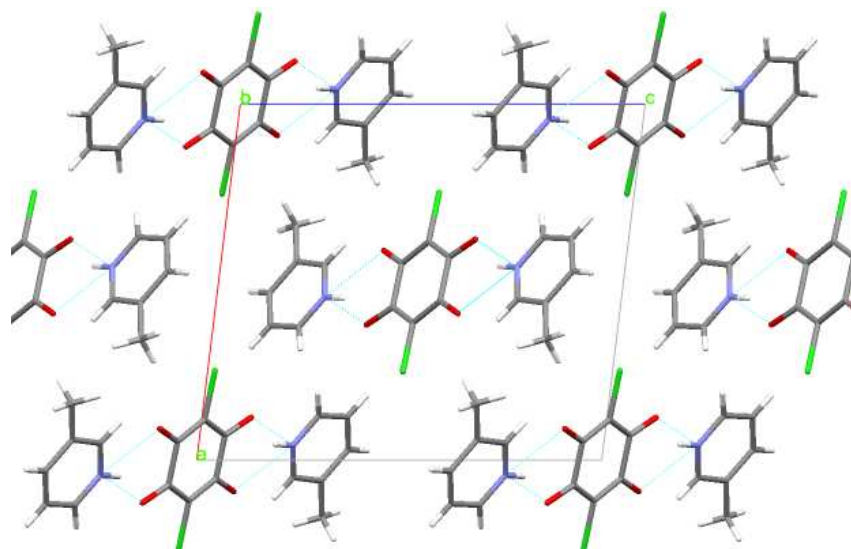


**Figure 8.10** The stacking viewed along the *b*-axis in 2:1 3-picoline chloranilic acid form 2.

#### 8.2.2.3 4-picoline chloranilic acid complex

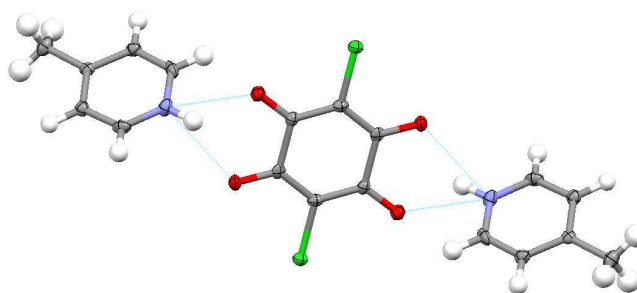


**Figure 8.11** 4-picoline chloranilic acid 2:1 co-crystal hydrogen bonded unit.

The structure of the 4-picoline complex is very similar to that of the 2-picoline, and has the HB units orientated close to the *c*-axis (**Figure 8.12**). In the *b*-direction they are stacked above and below each other. The picolines have a tilt away from the plane of the chloranilic acid presumably to accommodate the methyl groups as the stacking involves them being end to end with each other.

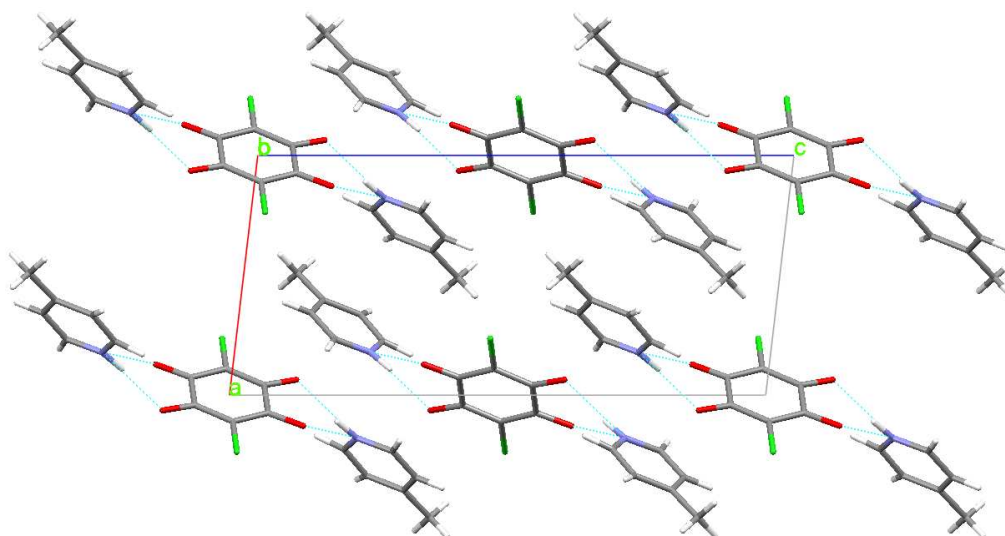


*Figure 8.12* The stack viewed along the *b*-axis in 2:1 4-picoline chloranilic acid.

### 8.2.3 Picoline chloranilic acid solvates

As well as the pure co-crystals between the picolines and chloranilic acid several hydrates were produced during the crystallisation attempts, including the previously known structure of 2:1 3-picoline chloranilic acid dihydrate<sup>114</sup>. There was also a new hydrate of 3-picoline chloranilic acid formed which incorporates the 2:1 HB units in a more complex system. The ratio in this complex was 4:3:2 of 3-picoline, chloranilic acid and water respectively. Another new hydrate formed involved 4-picoline and chloranilic acid in the ratio 2:1, with four waters present. This was similar to the previously known 3-picoline chloranilic acid hydrate with the simple 2:1 HB units connected by the water molecules via HB, and forming a layered structure. The 2-picoline did not form any hydrated forms of chloranilic acid co-crystal, although a red thick oil was created at the bottom of some of the vials. This suggests a hydrated form was produced (but its melting point was below room temperature) as none of the samples without water formed oil.

### 8.2.3.1 2:1 3-picoline chloranilic acid dihydrate

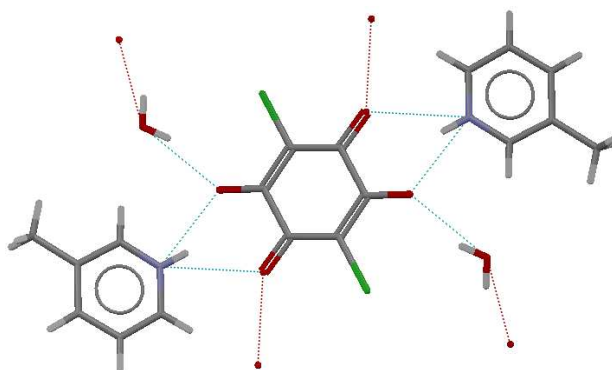


**Figure 8.13** Flat hydrogen bonded unit within the 2:1 3-picoline chloranilic acid dihydrate.

Although already in the CSD the structure of 2:1 3-picoline chloranilic acid dihydrate<sup>114</sup> is relevant to the series of co-crystals studied in this chapter so will be briefly described here. The 2:1 hydrogen bonded unit (**Figure 8.13**) is clear in the structure and is flat with the picoline and chloranilic acid rings in the same plane. The water molecules form additional hydrogen bonds with the oxygens of the chloranilic acid joining them into saw tooth layers that interlock with each other as shown in **Figure 8.14**.

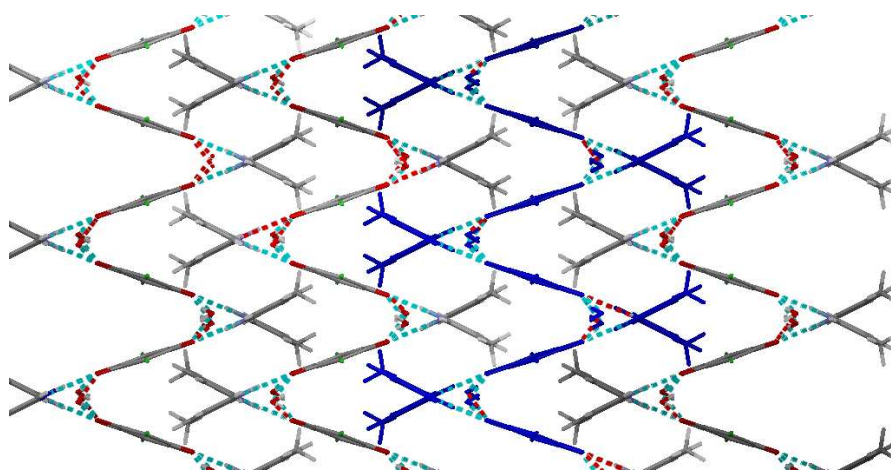


**Figure 8.14** Interlocking hydrogen bonded saw-tooth layers within the 3-picoline chloranilic acid dihydrate.

### 8.2.3.2 3-picoline chloranilic acid hydrate 4:3:2 complex

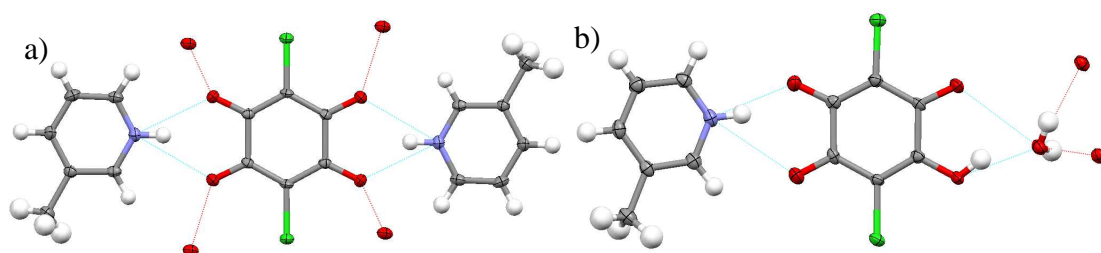


**Figure 8.15** The HB units contained in the structure of **a)** the 2:1 unit, **b)** the offshoot unit, in the 4:3:2 complex.

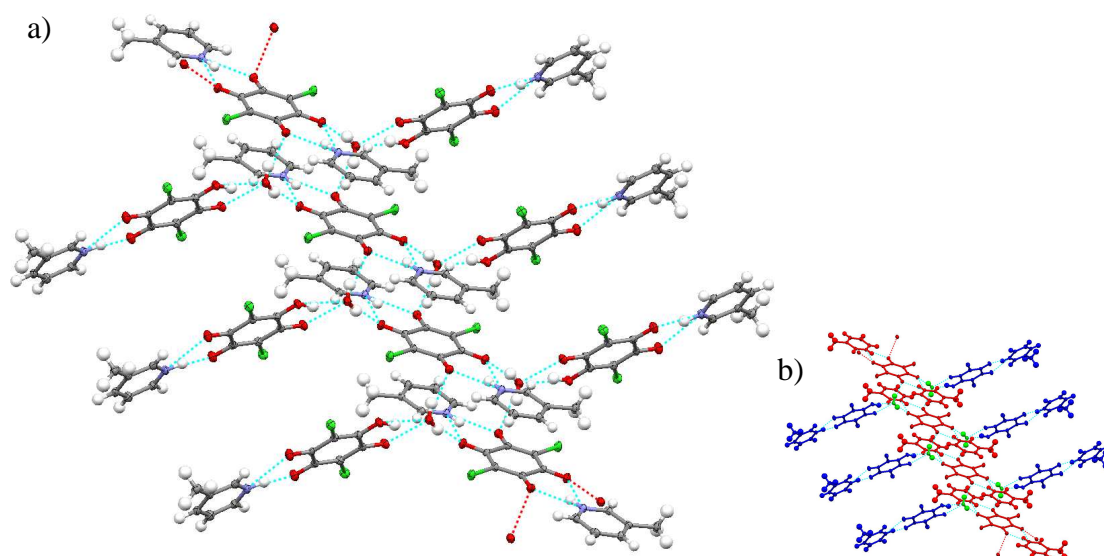


**Figure 8.16 a)** 2:1 HB units in the complex hydrate of 3-picoline with chloranilic acid are formed into hydrogen bonded chains through links made by water molecules, and additional chloranilic picoline groups stick out from this, forming BHB to the water **b)** colour coded version highlighting the chain of stacked 2:1 3-picoline chloranilic acid HB units (**red**), the HB unit bifurcated to the water molecules (**blue**), and the waters connecting the structure (**green**).

The new hydrate of the 3-picoline chloranilic acid synthesised in this work is a mixture of the 2:1 HB units (**Figure 8.15 a**) seen several times already and a new unit involving the water (**Figure 8.15 b**). The water molecules do not simply act as links between the blocks, but also replace some of the picolines forming bifurcated hydrogen bonds. The 2:1 hydrogen bond units comprising one chloranilic acid molecule with two picolines, are formed into a one-dimensional HB chain via the

water molecules. Each water molecule is also involved in a bifurcated hydrogen bond with another chloranilic acid, which is itself hydrogen bonded to a picoline; these stick out perpendicular to the chain (*Figure 8.16*).

#### 8.2.3.3 2:1 4-picoline chloranilic acid tetra-hydrate

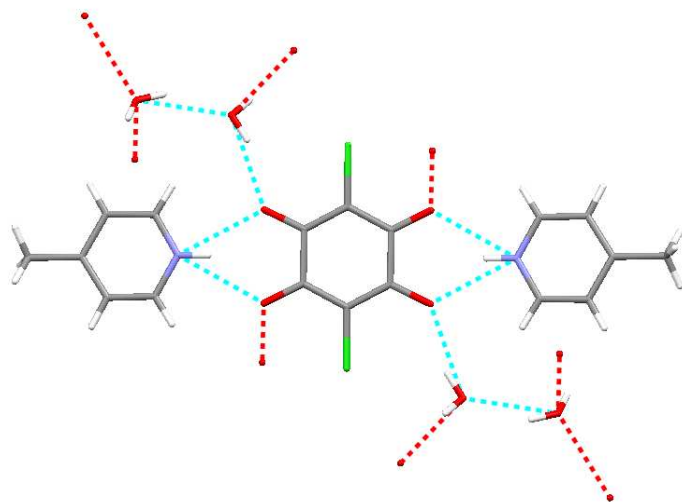


*Figure 8.17* Hydrogen bonded unit with water molecules from the 2:1 4-picoline chloranilic acid tetrahydrate structure

In the structure of 2:1 4-picoline chloranilic acid tetrahydrate the 2:1 hydrogen bonded units (*Figure 8.17*) are very flat. Each chloranilic acid, in addition to making bifurcated hydrogen bonds on either side with the picolines, hydrogen bonds with four waters. When viewed down the b-axis it can be seen that this forms hydrogen bonded layers that interlock with each other (*Figure 8.18*). Each chloranilic acid is connected to the next by a link of two hydrogen bonded waters (this gives a similarity to the 3,4-lutidine structure *Figure 7.19*). The water linkage provides the space for the picolines from the layers above and below to fit in between each HB unit, producing a saw blade effect.

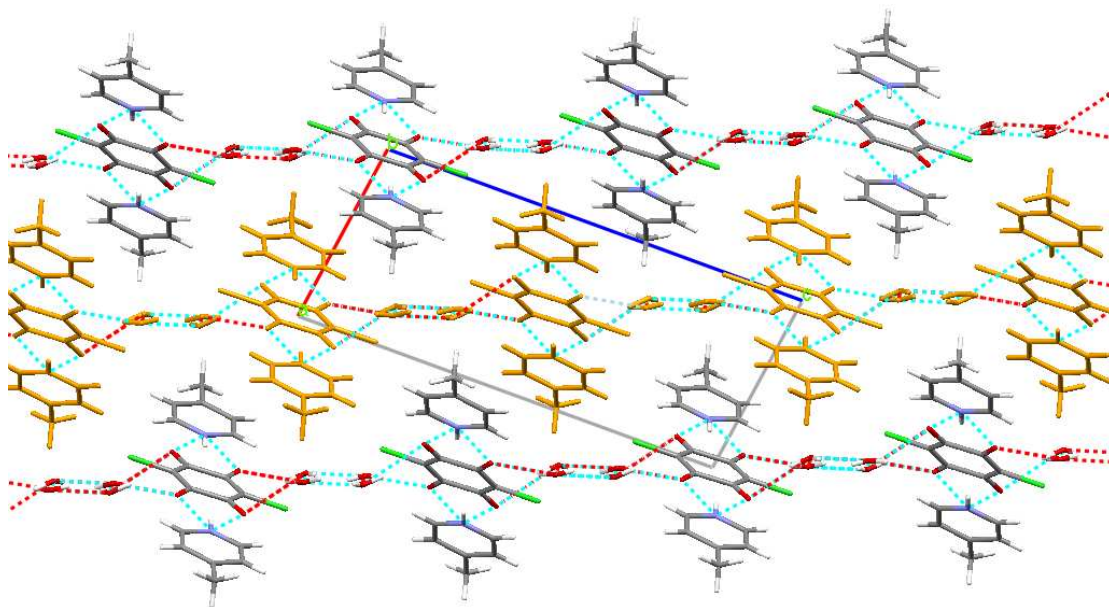


**Figure 8.18** Interlocking HB layers of 4-picoline chloranilic acid tetrahydrate viewed down the *b*-axis.

### 8.3 Hydrogen-bonded supramolecular synthon

All the picoline chloranilic co-crystal complexes studied here contain either the 1:1 or 2:1 hydrogen bonded supramolecular synthon previously described for the lutidine case (**Figure 7.6**). Eight contain the 2:1 HB unit (including the previously studied 3-picoline chloranilic acid dihydrate) although several of these contained additional interactions building them into more complex structures. Only two 1:1 HB units were found but these are in exactly the same style as several lutidine chloranilic acid complexes seen in the literature<sup>37</sup>. The fact that the synthon formed without exception in both the picoline and lutidine co-crystals shows that it is of a reliable and robust nature, which could be used as the starting point to construct more complex structures such as chains, planar, or three dimensional networks involving molecules with multiple pyridine groups.

The way in which the molecules that make up the HB synthons orientate with respect to each other varies greatly, with some of the HB units entirely flat to others having nearly perpendicular picolines in relation to the chloranilic acid. It is interesting to note that all the hydrates have flat HB units, this could be because the extra space

provided by the water connections allows the HB units to take the arrangement they would adopt if unconstrained.

### 8.3.1 Comparison of hydrogen bonding schemes

Although all the structures contain the same HB synthon unit there is variation within the HBs and hydrogen bonding schemes. The bifurcated bonds can vary in arrangement and in the dominance of the different parts, and there is additional hydrogen bonding, especially in the hydrate forms, holding the structures together. Comparing the hydrogen bond dimensions can provide a lot of useful information about the nature of the HBs present in the structures but a good way to visualise the interaction to provide additional detail on the HBs is via Fourier maps (as shown in the neutron work), while a second visual aid is the Hirshfeld surface, which shows the proximity of different atoms to the core molecule and therefore the interactions.

A Hirshfeld surface is a useful visualisation tool, representing the interaction of the electron density of selected molecule with that of the surrounding crystal structure. The surface is defined around the selected molecule at the point where contribution to the calculated electron density from molecule and the rest of the structure is equal, i.e. 50% of the density is from the molecule. This provides a smooth surface that encloses the molecule on which different properties can be displayed showing how the molecule interacts with the crystal (nearest contact distances to internal/external nuclei, curvature of surface, and difference between contact and the sum of the Van der Waals radii). The property projected on to the surfaces presented here is the distance from the surface to the nearest external atom (intermolecular contact distance), with the shorter the distance being shown in red and longer in green. The surfaces are produced by the program CrystalExplorer<sup>71</sup>, and all that is required is a *cif* file from the refinement of the crystal structure.

### 8.3.2 Fourier maps and Hirshfeld surfaces

A large variation can be seen in the bifurcated hydrogen bond motif in the picoline chloranilic acid co-crystal structures, but to examine the position of the hydrogen and look for indications of unusual behaviour with in the hydrogen bond, difference

Fourier maps are required. Difference Fourier maps for all the unique bifurcated hydrogen bonds found in all the picoline structure are shown below, in some cases this includes multiple temperature data.

The maps are all taken in the plane of the two oxygens of the chloranilic acid and the nitrogen of the picoline, which are indicated on the images. O1 and O2 are named in reference to the major and minor parts of the BHB and may differ to the names given in the *cif*.

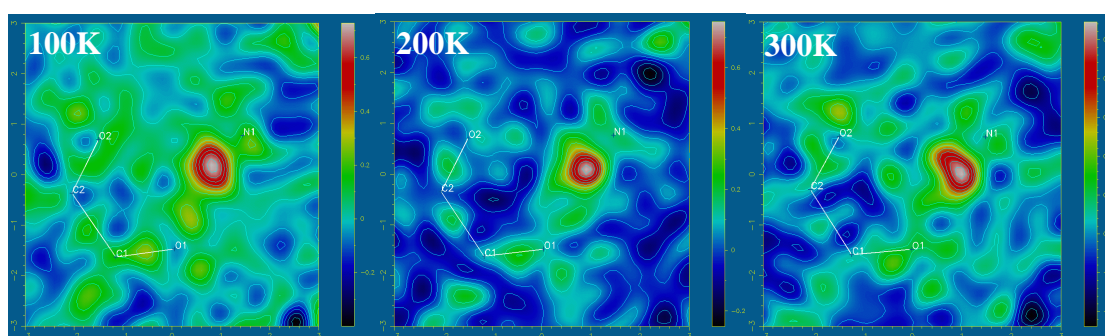


**Figure 8.19** Difference Fourier maps for the 2:1 2-picoline chloranilic acid at 100 K, 200 K and 300K.  $RMS = 0.07 e/\text{\AA}^3$ ,  $0.06 e/\text{\AA}^3$ ,  $0.05 e/\text{\AA}^3$

The 100 K, 200 K, and 300 K difference Fourier maps of the 2:1 2-picoline chloranilic acid are presented in **Figure 8.19** showing a reasonably clear map with a well defined hydrogen position. The peak is slightly elongated and positioned in the line between N and O1.

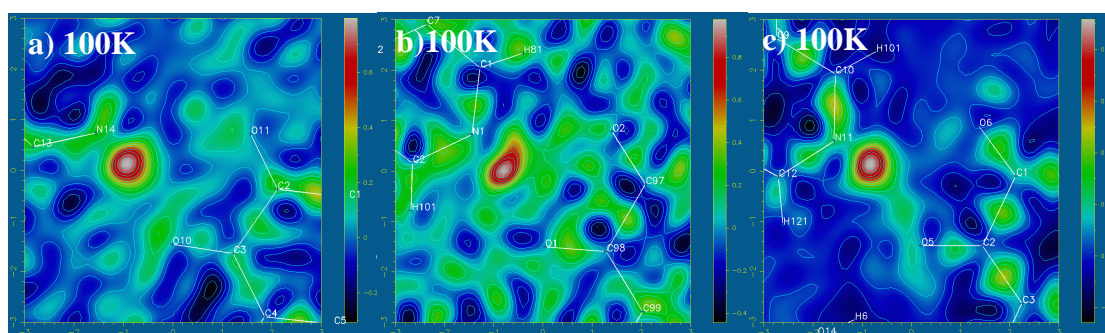


**Figure 8.20** Difference Fourier maps for the 100 K refinements of **a)** 1:1 2-picoline chloranilic acid,  $RMS = 0.06 e/\text{\AA}^3$  **b)** 2:1 3-picoline chloranilic acid form 2,  $RMS = 0.09 e/\text{\AA}^3$  **c)** 2:1 3-picoline chloranilic acid dihydrate.  $RMS = 0.06 e/\text{\AA}^3$

**Figure 8.20** shows well defined peaks representing the hydrogen positioned between the N and O1 in the BHB for three structures studied at 100 K. The 2:1 3-picoline chloranilic acid map form 2 (**Figure 8.20 b**) has significant background noise, due to limited data quality. The 2:1 3-picoline chloranilic acid dihydrate map shows a slight secondary peak beside O1 in a position whose geometry would be consistent with a disordered hydrogen, but this is small enough to be accounted for by the bonding density of the hydrogen bond.

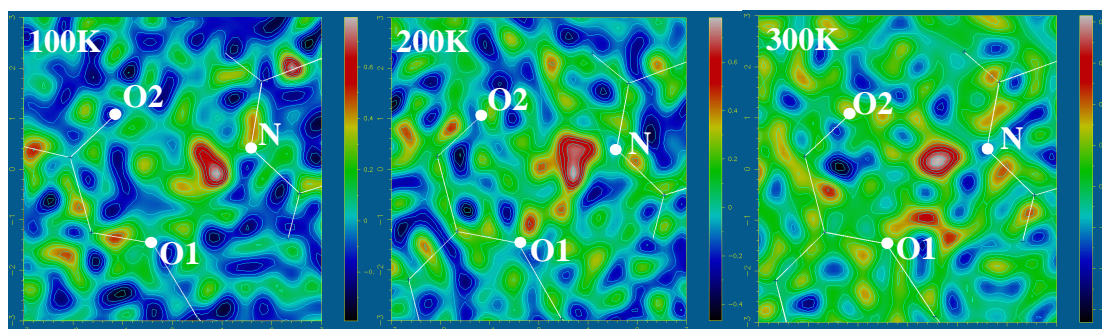


**Figure 8.21** Difference Fourier maps for the 1:1 3-picoline chloranilic acid at 100 K, 200 K, and 300K. RMS =  $0.09 e/\text{\AA}^3$ ,  $0.08 e/\text{\AA}^3$ ,  $0.07 e/\text{\AA}^3$

The 1:1 3-picoline chloranilic acid co-crystal difference Fourier maps (**Figure 8.21**) at all temperatures show a significant amount of noise but a clear singular peak representing the hydrogen can be seen. On the 200 K map (**Figure 8.21 b**) an additional peak directly next to the N is seen although this is too close to the N to be a realistic position for a disordered hydrogen position, instead this is most likely electron density from the N and the bond to the hydrogen accumulated with noisy background to the map. With the hydrogen positioned nearly equidistant between O1 and O2 the HB shows a high “level” of bifurcation.

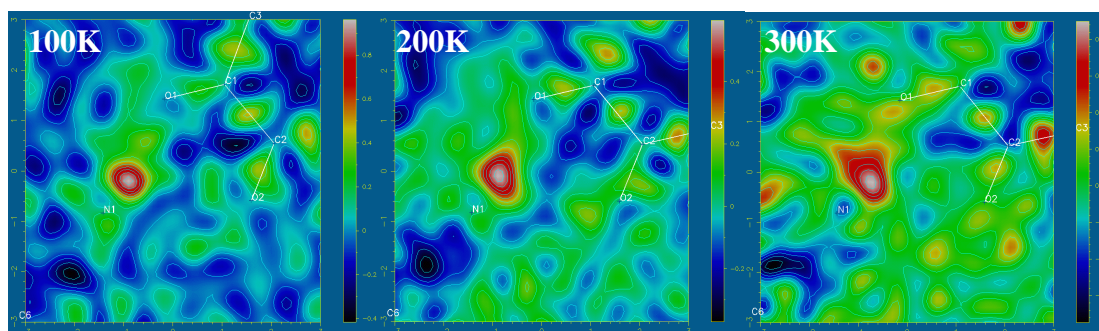


**Figure 8.22** Difference Fourier maps for the 2:1 3-picoline chloranilic acid form 1 at 100 K, 200 K, and 300 K. RMS =  $0.10 e/\text{Å}^3$ ,  $0.08 e/\text{Å}^3$ ,  $0.07 e/\text{Å}^3$

The 2:1 3-picoline chloranilic acid form 1 difference Fourier map (**Figure 8.22**) has a well defined peak positioned between N and O1, with slight elongation as the temperature is increased.

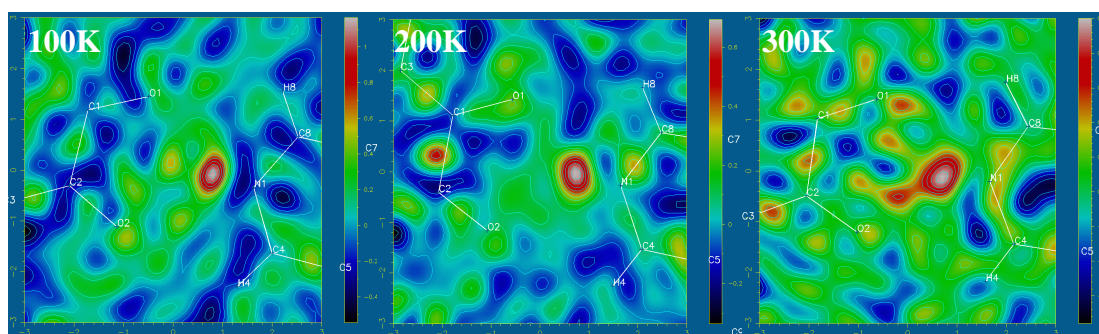


**Figure 8.23** Difference Fourier maps for the stacked chain HB units of the 3-picoline chloranilic acid new hydrate. RMS =  $0.13 e/\text{Å}^3$ ,  $0.06 e/\text{Å}^3$ ,  $0.06 e/\text{Å}^3$

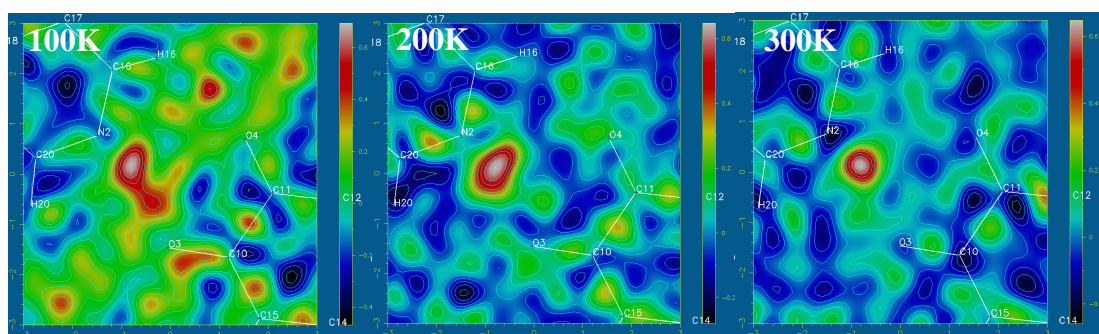


**Figure 8.24** Difference Fourier maps for the offshoot HB units of the 3-picoline chloranilic acid new hydrate. RMS =  $0.13 e/\text{Å}^3$ ,  $0.06 e/\text{Å}^3$ ,  $0.06 e/\text{Å}^3$

Both of the BHB present in the new hydrate of 3-picoline chloranilic acid show well-located hydrogens in the multiple temperature difference Fourier maps (**Figure 8.23**, **Figure 8.24**). The hydrogen in the offshoot HB unit is directed towards O1 whereas the stacked chain HB has a more bifurcated HB.

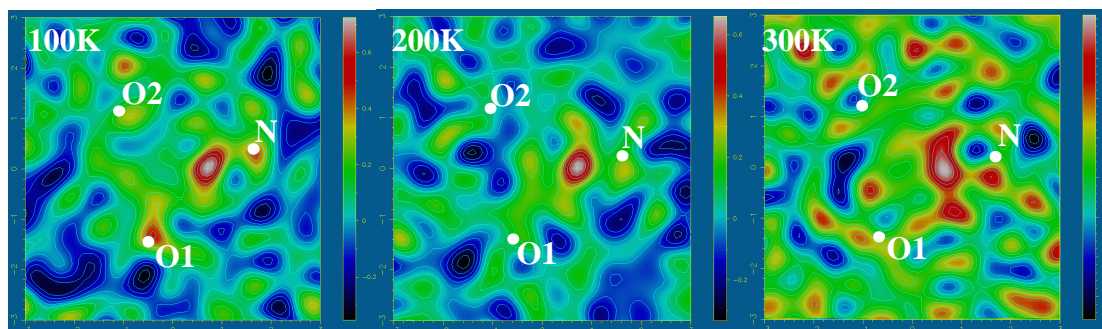


**Figure 8.25** Difference Fourier maps for the 2:1 4-picoline chloranilic acid at 100 K, 200 K, and 300K. RMS =  $0.10 e/\text{\AA}^3$ ,  $0.06 e/\text{\AA}^3$ ,  $0.05 e/\text{\AA}^3$

Despite a noisy set of difference Fourier maps, 2:1 4-picoline chloranilic acid (**Figure 8.25**) appears to have a well located hydrogen atom in the BHB positioned between O1 and O2 with a high level of bifurcation.

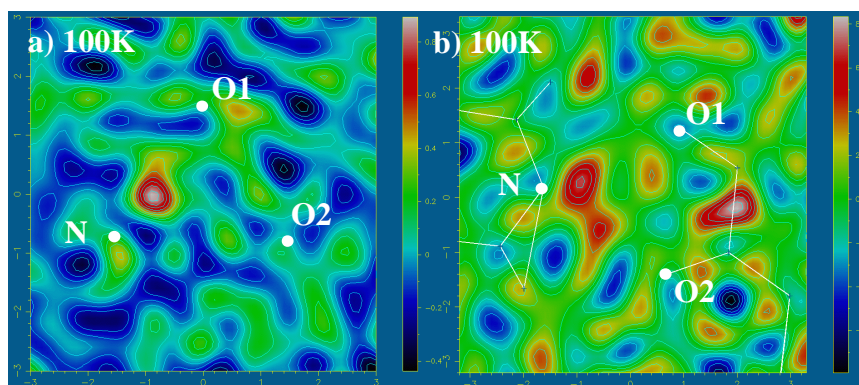


**Figure 8.26** Difference Fourier maps for the 100 K refinements of **a)** 1:1 4-picoline chloranilic acid RMS =  $0.11 e/\text{\AA}^3$  **b)** 2:1 4-picoline chloranilic acid dihydrate. RMS =  $0.12 e/\text{\AA}^3$

The other two refinements of 4-picoline chloranilic acid complexes, the 1:1 and dihydrate structures, have noisy difference Fourier maps as seen in **Figure 8.26 a** and **b** respectively. Both appear to have small secondary peaks within the BHB. In the 1:1 map a reasonable sized secondary peak is positioned in the middle of the dominant part of the bond (N-H...O1) which is worth further study, but due to the

poor quality of the crystals the collection of multiple temperature or higher quality data was not possible. Without this it is unreasonable to reach any conclusions at this time. In the dihydrate there is a small secondary peak positioned between N and O2 but its size is comparable with that of background noise elsewhere in the Fourier map so is unlikely to be a significant feature.

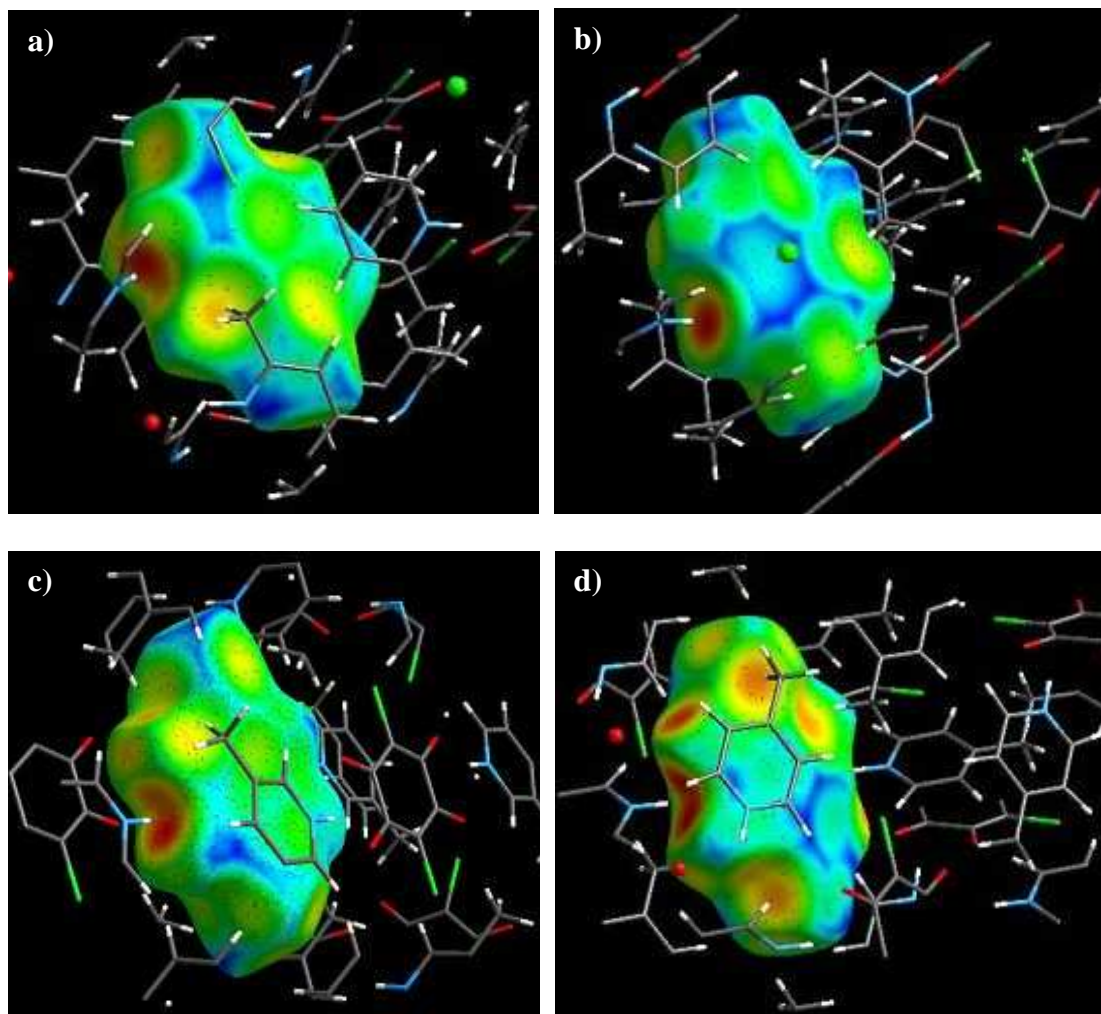


**Figure 8.27** The Hirshfeld surface of the chloranilic acid in the 2:1 co-crystals complexes with **a)** 2-picoline **b)** 3-picoline form 1 **c)** 3-picoline form 2 **d)** 4-picoline. A sphere of atoms is also included to show the packing round the molecule.

The Hirshfeld surfaces are a useful tool to show the orientation of the BHB, giving some indication to the “level” of bifurcation and strength of the two D-H...A parts. The Hirshfeld surface of the chloranilic acid molecules in the four different 2:1 picoline chloranilic acid structures are shown in **Figure 8.27**. The part of the surface that relates to the discussion is the red patch on the left hand side where the picoline

interacts with the chloranilic acid in the BHB interaction. In the 2:1 3-picoline chloranilic acid structure (*Figure 8.27 b*) the spot is circular indicating that the interaction is almost entirely with only one of the oxygens. The complex involving 4-picoline (*Figure 8.27 d*) shows the opposite with a red patch stretched across the area of both oxygens indicating a very high level of bifurcation in the BHB. The other two structures (*Figure 8.27 a and c*) represent intermediate cases with a red patch that covers both oxygens but with one side much darker than the other; this indicates a situation where both oxygens are involved but there is an asymmetry to the strength of this interaction. The Hirshfeld surface plots reveal a further trend in the intermolecular interactions: it can be seen from the visual plots that part of the reason for this could be the other interactions involving the oxygens, as it appears the more bifurcated the bond the more intense the other interactions are with the oxygens.

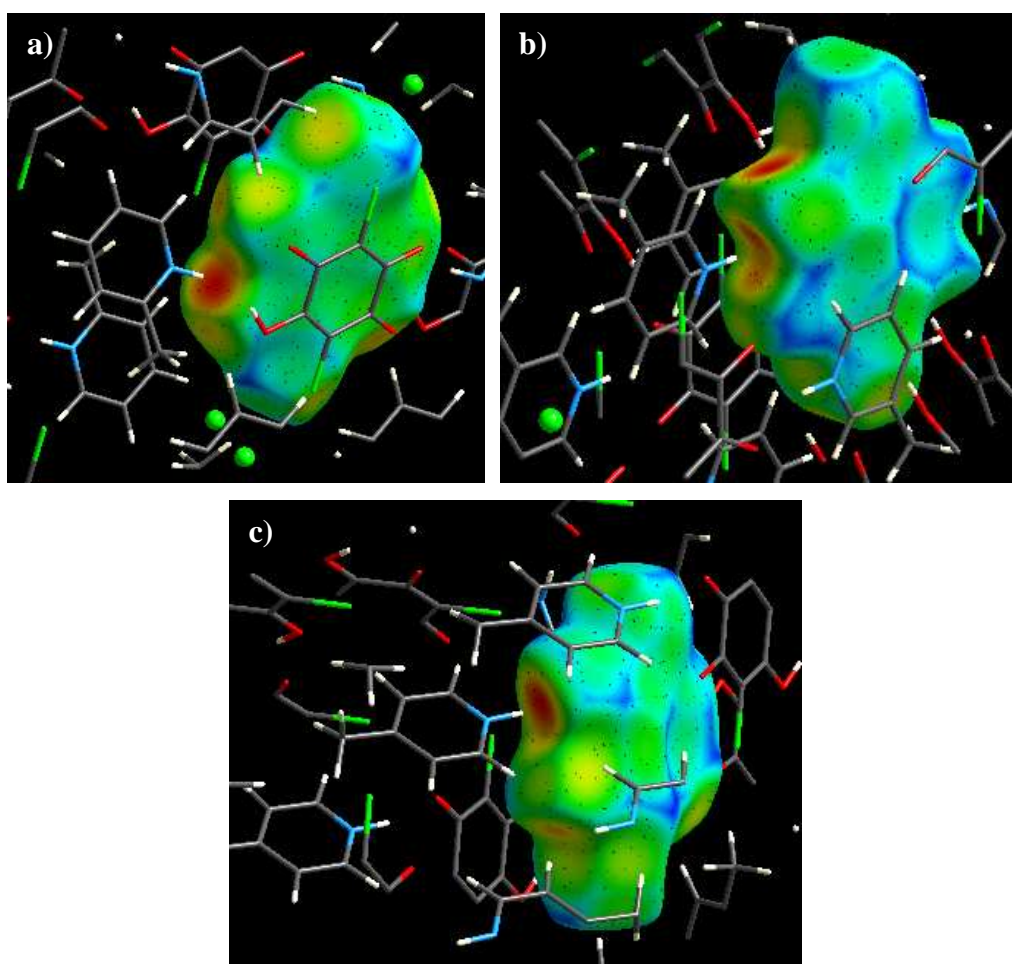


*Figure 8.28* The Hirshfeld surface of the chloranilic acid in the 1:1 co-crystals complexes with **a)** 2-picoline, **b)** 3-picoline, **c)** 4-picoline. A sphere of atoms is also included to show the packing round the molecule.

The Hirshfeld surface of the chloranilic acid molecules in the four different 1:1 picoline chloranilic acid structures are shown in *Figure 8.28*. The 2- and 4-picoline forms of the 1:1 chloranilic acid complex produce Hirshfeld surfaces (*Figure 8.28 a, c*) where the red patch, representing the BHB, is positioned on one of the oxygens and only a small yellow fringe spreads across to the second oxygen. This represents an interaction that is almost entirely interacting towards one of the oxygen acceptors and only weakly with the second. The 1:1 3-picoline chloranilic acid (*Figure 8.28 b*) on the other hand has a red patch that is spread quite evenly between the two oxygens, representing a high level of bifurcation within the hydrogen bond.

These observations follow the trend seen in the 2:1 complexes where the structures that have a more symmetrical BHB (red patch spread across both oxygens) have stronger additional interactions. This can be seen in *Figure 8.28 b*, which is a highly bifurcated HB, where there is a strong additional hydrogen bond contact from another chloranilic acid onto one of the oxygen acceptors, compared to the *Figure 8.28 a, c* that have much weaker additional interactions and are far less bifurcated.

### 8.3.3 Bifurcated hydrogen bond lengths and angles

*Table 8.1 Bond lengths and angles for the BHB in the picoline (P) chloranilic acid (CA) complexes and angles between planes of their rings.*

	N-O <sub>1</sub> (Å)	N-O <sub>2</sub> (Å)	N-H (Å)	H···O <sub>1</sub> (Å)	H···O <sub>2</sub> (Å)	N-H···O <sub>1</sub> (°)	N-H···O <sub>2</sub> (°)	O <sub>1</sub> ··H··O <sub>2</sub> (°)	Overall (°)	Between planes (°)
<b>1:1 2-P CA</b>	2.688(2)	3.129(2)	0.88(3)	1.85(3)	2.56(3)	159(3)	123(2)	73.34	355.34	28.07
<b>2:1 2-P CA</b>	2.658(2)	2.952(2)	0.90(2)	1.89(2)	2.41(2)	159.1(19)	118.9(14)	76.70	354.7	68.69
<b>1:1 3-P CA</b>	2.7246(18)	2.8101(18)	0.91(4)	1.93(4)	2.13(3)	146(3)	131(3)	79.93	356.93	3.88
<b>2:1 3-P CA Form1</b>	2.583(3)	3.017(3)	0.88(3)	1.71(3)	2.57(3)	171(3)	113(2)	74.15	358.15	78.78
<b>2:1 3-P CA Form 2</b>	2.671(3)	2.848(3)	0.89(5)	1.86(5)	2.22(5)	151(5)	128(4)	80.15	359.15	11.40
<b>3-P CA new hydrate H1</b>	2.776(4)	2.873(4)	0.83(4)	2.06(4)	2.19(4)	141(4)	139(3)	79.43	359.43	3.86
<b>3-P CA new hydrate H2</b>	2.651(4)	3.016(4)	0.90(5)	1.81(4)	2.40(5)	156(4)	125(3)	78.14	359.14	7.87
<b>1:1 4-P CA</b>	2.695(6)	3.016(6)	1.01(9)	1.71(9)	2.47(8)	165(8)	114(6)	76.34	355.34	61.22
<b>2:1 4-P CA</b>	2.847(5)	2.768(5)	1.02(5)	1.98(5)	2.00(5)	141(4)	130(4)	79.97	350.97	62.13
<b>2:1 4-P CA hydrate</b>	2.777(9)	2.808(9)	0.83(10)	2.11(10)	2.10(10)	137(9)	143(9)	79.93	359.93	6.73

**Table 8.1** shows the bond lengths and angles for the BHB at 100 K in all the new picoline chloranilic acid complexes as well as the angle between the planes of the rings of the picoline and chloranilic acid. As already said the hydrogen in all the complexes is transferred across to the nitrogen of the picoline, which was expected because of the higher  $pK_a$  value of the picolines than the chloranilic acid. The N-H distances are all within what would be considered normal, and although there is almost a 0.2 Å difference between some of the values this is still within the error for hydrogen position determination with X-rays. The 1:1 and 2:1 4-picoline chloranilic acid structures have the longest N-H distances at just over 1 Å, whereas the shortest are the 2:1 4-picoline chloranilic acid hydrate and the H1 part of the new 3-picoline chloranilic hydrate.

From the Hirshfeld surfaces the 2:1 4-picoline and 1:1 3-picoline chloranilic acid complexes were shown to be the most highly bifurcated closely followed by the 2:1 3-picoline chloranilic acid complex. The bond lengths and angles reflect this with the values for the N-O and H $\cdots$ O lengths and the N-H $\cdots$ O angles in these complexes being similar for O1 and O2. The complexes that were highlighted as having weakly bifurcated bonds are seen to have large differences for O1 and O2 for these values. The most notable is 2:1 3-picoline chloranilic acid Form I which has a very weak bifurcated bond with a strong major component and weak minor component with large differences of 0.434 Å, 0.86 Å and 58 ° for N-O, H $\cdots$ O and angle N-H $\cdots$ O. The major component may equally be thought of as a strong-medium single HB, but in this case the weak BHB description is more appropriate as the second oxygen appears to have some influence holding the N-H in a similar motif as the other structures. A Hirshfeld surface was not presented for 2:1 4-picoline chloranilic acid hydrate but from **Table 8.1** it appears to contain the most symmetrical BHB.

The overall angle in the BHB unit (which shows the planarity of the BHB **Figure 1.2**) for all the complexes is greater than 350°. This shows that the hydrogen remains close to the plane of the donor and two acceptors and is probably an indication that the BHBs are overall quite strong even if some of their components are relatively weak. Surprisingly there doesn't seem to be any correlation between the level of bifurcation and the overall angle.

The last column in the table is the angle between the planes of the ring of the chloranilic acid and the ring of the picoline. Some of the complexes have the two molecules almost in the same plane with low values for this angle, these include the 1:1 3-picoline, the two parts of the 3-picoline new hydrate and the 2:1 4-picoline hydrate. These correspond to the highly bifurcated bonds apart from the H2 part of the new 3-picoline hydrate, which is weakly bifurcated. Four of the other weakly bifurcated BHB complexes have large angles ( $>60$ ) between the planes, and the 1:1 2-picoline complex which also has a weakly bifurcated BHB has a moderate angle of 28.07. The only highly (symmetrical) BHB with a large angle (62.13) is found in the 2:1 4-picoline chloranilic acid complex.

#### 8.4 Powder patterns

Powder diffraction data have been collected for crystallisations of chloranilic acid with the three picolines. Three different conditions have been prepared for picoline and chloranilic acid; an approximately 1:1 sample (Black), a sample with the picoline in excess representing the conditions that have produced 2:1 complexes (Red), and a 2:1 sample with water added (Blue). The powder samples were prepared separately from the single crystal experiments, gently heated throughout the whole crystallisation until the sample was dry. This encouraged fast evaporation of the solvent and dried the sample. The sample was ground making sure that powder was taken from all areas of the vial to ensure that all possible complexes and polymorphs present were represented. The powder patterns are shown in *Figure 8.29* for the 2-picoline, *Figure 8.30* for the 3-picoline and *Figure 8.31* for 4-picoline.

The 2-picoline powder patterns (*Figure 8.29*) are almost identical apart from small insignificant artefacts and a difference in intensity due to different exposure times. Comparing with calculated patterns this common pattern appears to be from the 1:1 2-picoline chloranilic acid structure. Although only the 1:1 structure is present in the powder patterns, a single crystal 2:1 structure was collected which suggests that either the 2:1 sample crystallisation created for the powder pattern had the wrong starting conditions (insufficient picoline, wrong temperature, for example) or that only a very small amount of the 2:1 complex is produced (the 1:1 dominated the single crystal samples) which is masked by the 1:1 majority polymorph. The sample with water

added being the same as the other patterns fits with the fact there was no hydrate form for 2-picoline chloranilic acid discovered.

The three powder patterns of 3-picoline appear to be mixtures of different structures (*Figure 8.30*). The 2:1 with water added powder sample appears to be almost all the new 3-picoline chloranilic acid hydrate but with a small amount of the 1:1 structure. The 3-picoline chloranilic acid dihydrate did not appear in any significant amount although a bigger yield of the dihydrate is expected for a sample with less picoline. The majority of the 1:1 powder pattern matches the 3-picoline 1:1 chloranilic acid structure although a small amount of the 2:1 3-picoline chloranilic acid form I and traces of the new hydrate are also seen. The majority of the 2:1 powder pattern is the 2:1 3-picoline chloranilic acid Form I, but also a small amount of the new 3-picoline chloranilic acid hydrate and small traces of the form II 2:1 structure. The three powder samples all have a small amount of one of the hydrate which suggests a small amount of water was present in the crystallisations.

The 4-picoline sample powder patterns (*Figure 8.31*) are all similar because they all show a majority of the 2:1 4-picoline chloranilic acid structure. The 2:1 pattern is entirely the 2:1 structure whereas there is a large part of the 1:1 4-picoline chloranilic acid structure on the 1:1 pattern. In the 2:1 with water added sample some of the smaller peaks relate to the hydrate structure. Only the structures from the single crystal experiments seem to be present.

In general 1:1 crystallisations produce 1:1 structures as products and the same is true for the 2:1 crystallisations producing 2:1 structures. In the case of the 3-picoline the powder spectra show both the 1:1 and 2:1 crystallisations produced the expected 1:1 and 2:1 structures respectively as the major component. This was also true for the 1:1 crystallisations of 2-picoline and the 2:1 4-picoline. The 1:1 crystallisation for the 4-picoline produces the 1:1 4-picoline chloranilic acid structure but not as the main fraction of the product which is the 2:1 in this case. The only non-hydrate crystallisation not to produce the equivalent structure in a significant amount was the 2:1 2-picoline crystallisation that did not produce the related 2:1 2-picoline chloranilic acid structure at all. This shows an ability to target the desired form of picoline chloranilic acid co-crystals.

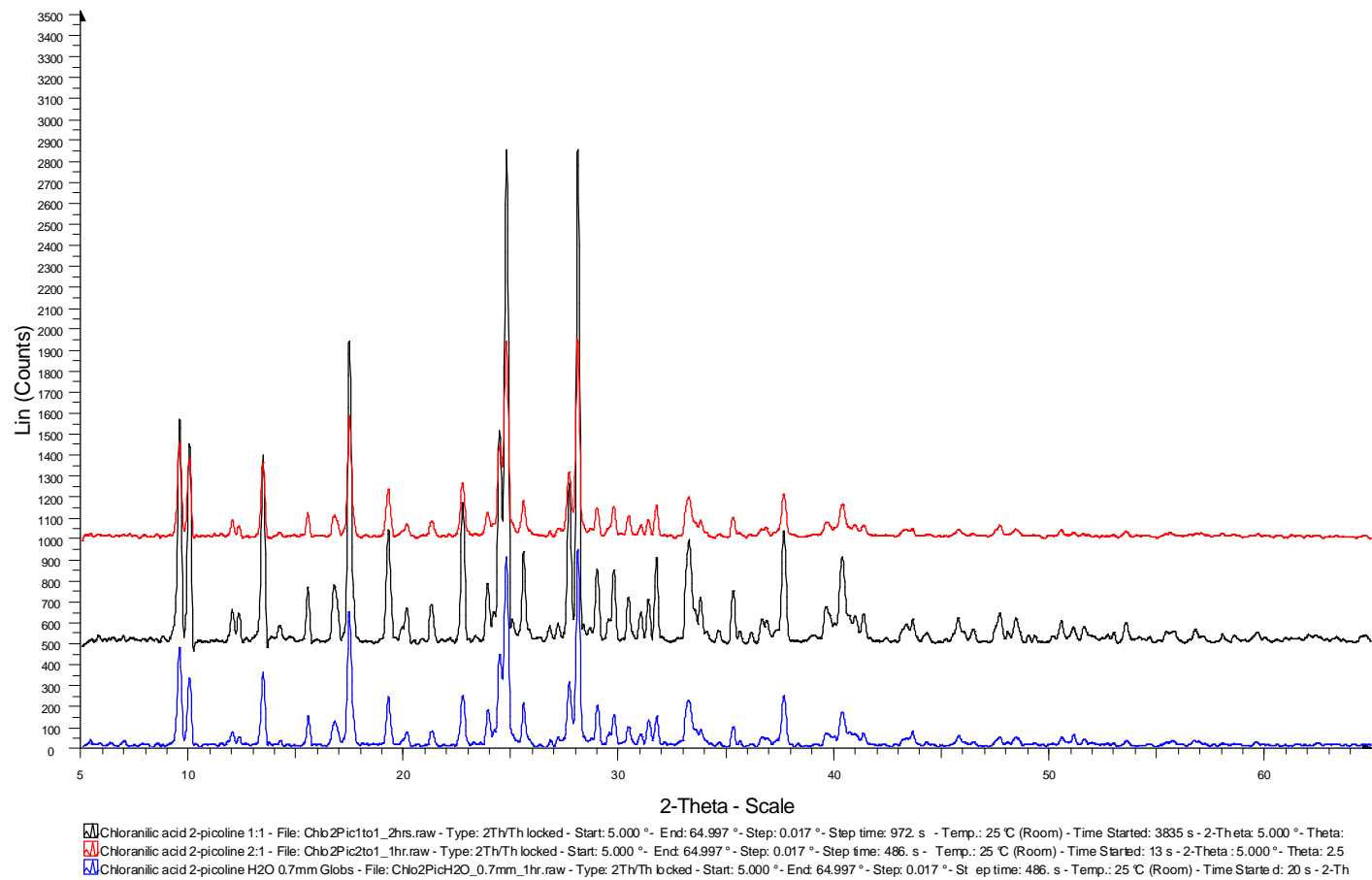


**Figure 8.29** Powder pattern for the crystallisations of 2-picoline and chloranilic acid, *Black-1:1*, *Red-2:1* and *Blue-water*

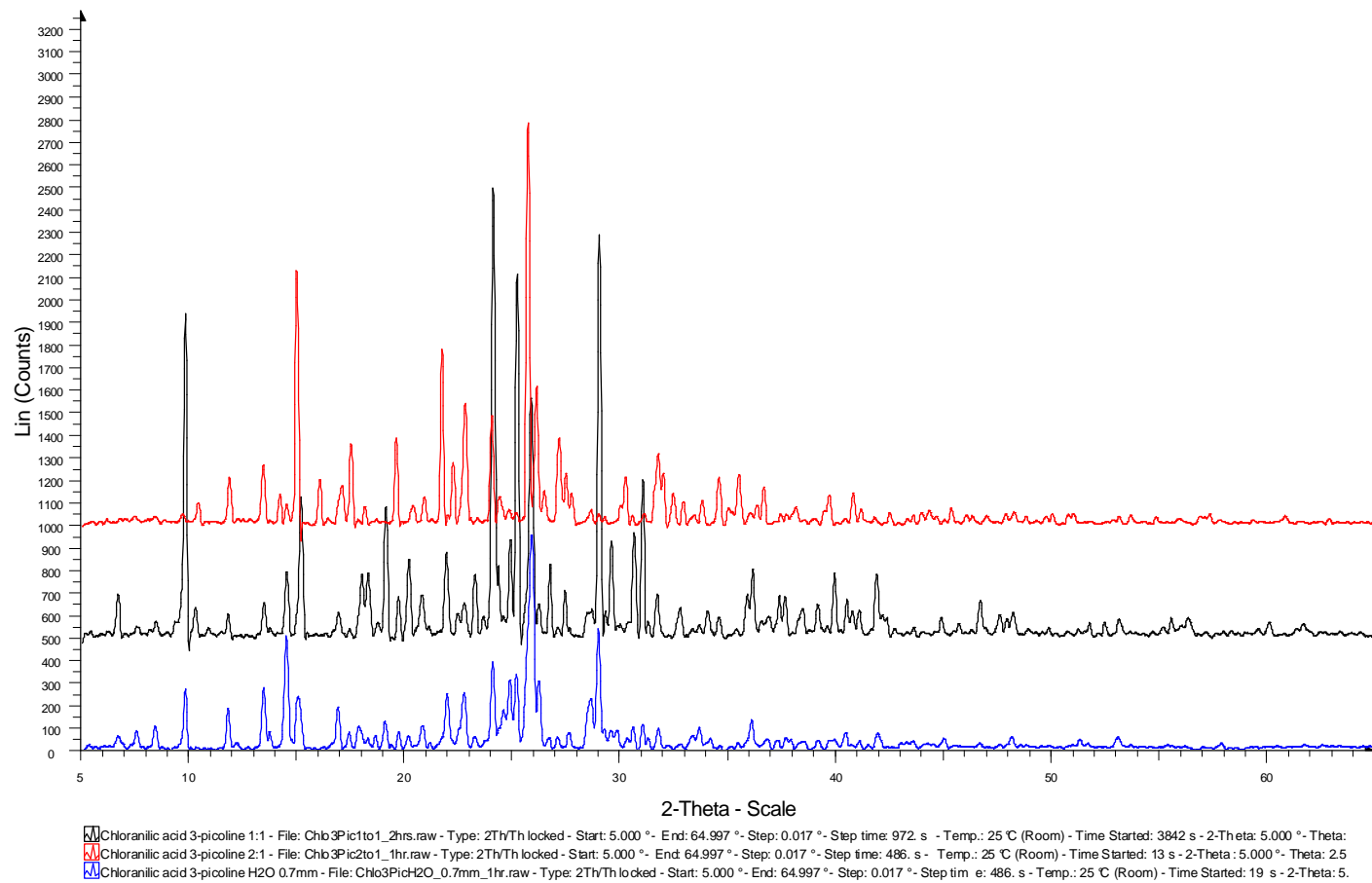


**Figure 8.30** Powder pattern for the crystallisations of 3-picoline and chloranilic acid, Black-1:1, Red-2:1 and Blue-water.

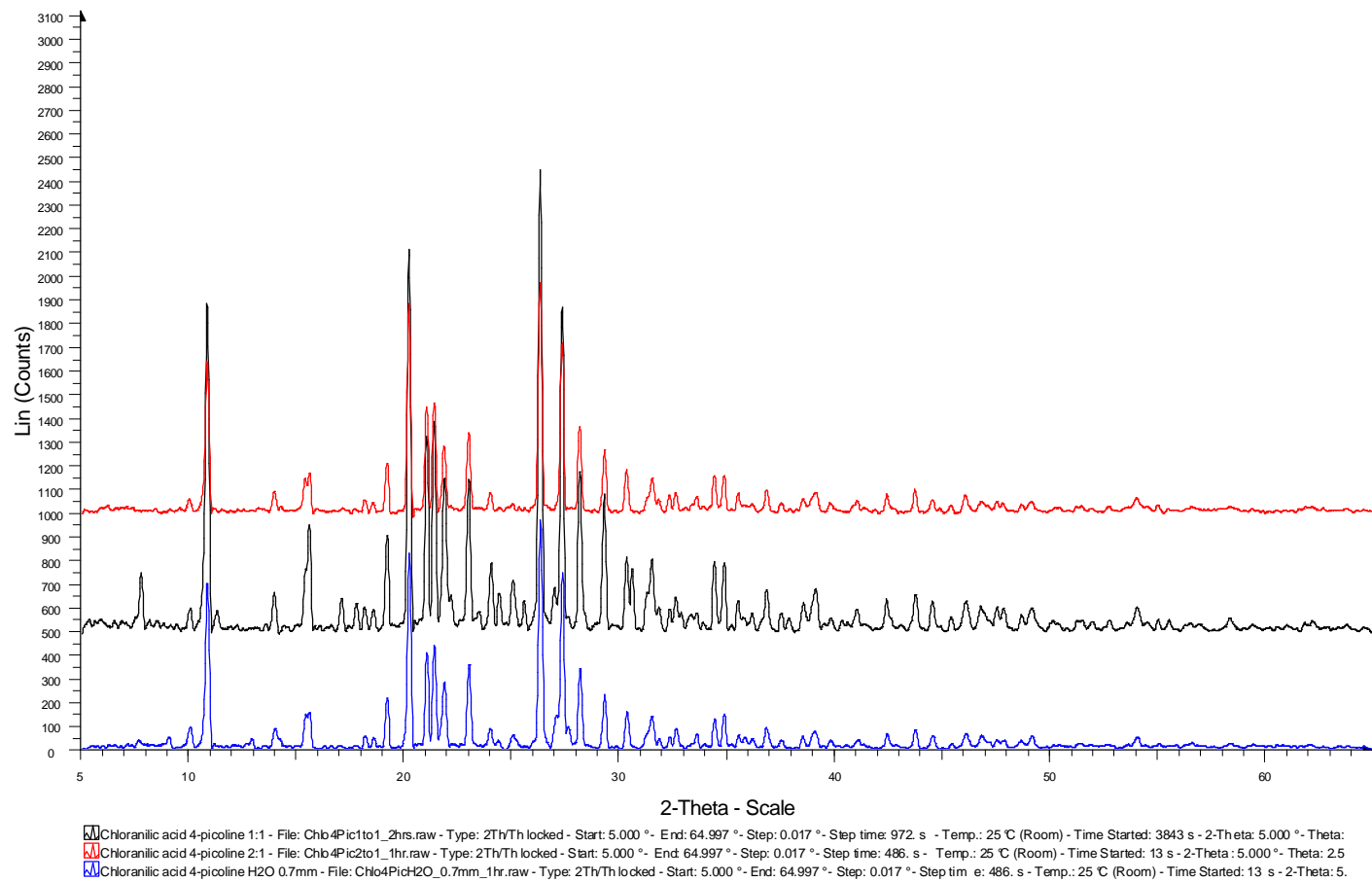


**Figure 8.31** Powder pattern for the crystallisations of 4-picoline and chloranilic acid, *Black-1:1*, *Red-2:1* and *Blue-water*.

## 8.5 Gas phase calculations on the bifurcated hydrogen-bonded 2:1 CA-picoline structures

To complement the experimental results, a set of theoretical computations into the chloranilic acid picoline hydrogen bonded 2:1 synthon present in the co-crystals were carried out. These calculations were performed in the gas phase as the structures lack a three dimensional hydrogen bonded network and therefore calculations in the solid state are likely to be unstable or at least inaccurate. Gas phase calculations can still provide useful insights, however, as they may give an indication of whether the hydrogen-bonded units (synthons) are stable outside the crystal environment and determine the theoretical lowest energy configuration.

The initial structure was taken from the X-ray diffraction experiments, and in the case of 3-picoline where there were two polymorphs, both were used as starting points. The fractional co-ordinates for the atoms were found using Accelrys MS Modeling<sup>127</sup> and an initial low level basis set calculation was run to get approximate positions for a higher level calculation. After the low level calculations, the two forms of the 2:1 3-picoline chloranilic acid converged into the same geometry, so only one was taken on to the higher level. The resulting optimised three structures of the low level basis set were all flat, removing the rotation between the rings of the picoline and the chloranilic acid previously seen in the X-ray structures. The N-H bonds of all the optimised structures are pointed towards one of the oxygens (O1), therefore not showing much bifurcated hydrogen bond characteristic. The effect of the higher-level basis set was to move the hydrogen from the nitrogen back on to the chloranilic acid, returning the molecules to their neutral state.

The calculations were run using the program Gaussian03<sup>75</sup> and took run times varying from a few hours for the quick set up calculations to over a day for the higher level ones. The high level calculation were run at the B3LYP level of theory using the 6-311G\*\* basis set with all the bond lengths, angle and dihedrals free to refine although the symmetry of the HB unit was preserved using the C1 inversion centre in the middle of the chloranilic acid molecule.

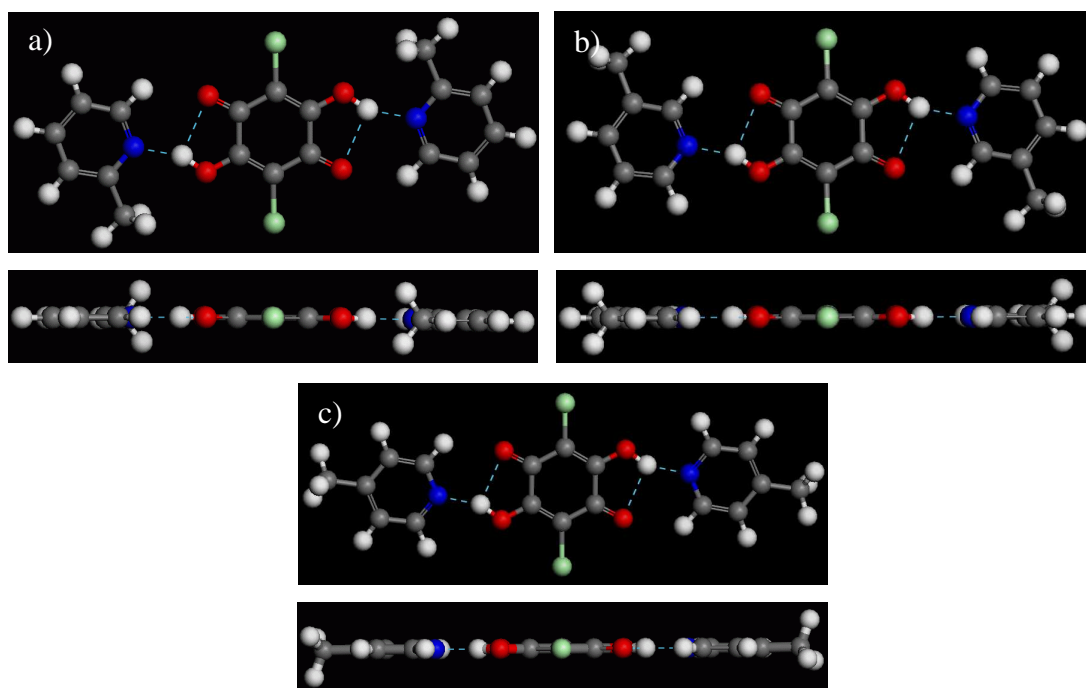


**Figure 8.32** The geometry optimised structures arising from the high level Gaussian03 calculations into the 2:1 HB supramolecular synthons for 2:1 **a)** 2-picoline, **b)** 3-picoline and **c)** 4-picoline, chloranilic acid structures.

The results were very similar for all the three structures **Figure 8.32**. All the 2:1 hydrogen bonded supramolecular synthons become flat, with all the rings of the three molecules lying in the same plane. This could suggest that the lowest energy form for the synthon unit is the flat orientation and that the additional interactions involved in the crystalline environment are responsible for the deviation from the flat form. A second interesting observation is that the hydrogen is located on the chloranilic acid molecule which does not match any of the picoline or lutidine experimental co-crystal structures which all have the hydrogen next to the nitrogen in all the BHB motifs. This suggests that the proton position within the hydrogen bond is heavily affected by being in the lattice.

With the structure geometrically optimised, the next stage was to work out the energies involved in the BHBs. The simplest way to achieve this is to take the total energies of the individual molecules away from the energies of the full HB unit, although the complication is that in the full HB unit the individual molecules use some of the basis sets of the other molecules to reduce their energies. To get round

this the individual molecule energies were calculated with the rest of the structure as ghost molecules; this means they were not included in the final energy but their basis sets were available to be used.

The calculated energies of the three hydrogen bond systems are very similar (2-pic: 12.80 kcal/mol; 3-pic: 13.17 kcal/mol; 4-pic: 13.30 kcal/mol) and fit into what might be described as the medium strength HB range. This would suggest that the position of the methyl group does not greatly affect the nature or strength of the HB.

### 8.6 Additional chloranilic acid co-crystal structures

As well as the two series of lutidines and picolines, a large number of additional crystallisations of co-crystal complexes with chloranilic acid were set up. This included series of different substituted amides and related molecules as well as compounds containing chemical groups known to participate in hydrogen bonding, some of which did not contain any nitrogen or aromatic rings. From the crystallisations carried out in this work a total of 28 new chloranilic acid co-crystals were produced and their structures determined. *Table 8.2* shows the new co-crystal complexes found along with their unit cell dimensions.

Molecule in complex with chloranilic acid	a(Å)	b(Å)	c(Å)	$\alpha(^{\circ})$	$\beta(^{\circ})$	$\gamma(^{\circ})$	Space group
<b>Picolines</b>							
2:1 2-picoline	6.369	8.597	16.628	90	101.451	90	P 2 <sub>1</sub> /c
1:1 2-picoline	7.375	9.147	9.73	101.63	103.92	97.45	P 1
2:1 3-picoline form I	8.642	9.687	10.279	90	102.08	90	P 2 <sub>1</sub> /c
2:1 3-picoline form II	12.049	5.326	13.581	90	96.958	90	P 2 <sub>1</sub> /n
1:1 3-picoline	5.037	9.364	13.35	97.67	98.58	103.66	P 1
3-picoline new hydrate	7.167	12.221	13.381	71.414	86.29	88.917	P 1
2:1 3-picoline dihydrate	9.212	7.349	15.045	90	98.52	90	P 2 <sub>1</sub> /c
2:1 4-picoline	7.952	6.126	17.658	90	96.73	90	P 2 <sub>1</sub> /c
1:1 4-picoline	15.617	4.819	16.3	90	90.27	90	P 2 <sub>1</sub> /n
2:1 4-picoline tetrahydrate	7.268	8.957	16.925	90	98.2	90	P 2 <sub>1</sub> /n
<b>Lutidines</b>							
2:1 2,3-lutidine	7.611	8.292	8.424	65.76	80.55	88.33	P 1
2:1 2,4-lutidine form I	15.699	7.554	16.629	90	90	90	Pbca
2:1 2,4-lutidine form II	9.5	10.05	11.3	68.26	79.15	83.52	P 1
1:1 2,4-lutidine	5.159	11.401	11.639	83.36	88.1	89.9	P 1
2:1 2,5-lutidine	8.074	11.419	10.324	90	100.57	90	P 2 <sub>1</sub> /c
1:1 2,5-lutidine	7.709	11.294	15.572	90	95.54	90	P 2 <sub>1</sub> /c
2:1 2,6-lutidine	7.232	9.256	14.845	90	93.56	90	P 2 <sub>1</sub> /c
1:1 2,6-lutidine	9.111	9.127	9.131	105.21	110.77	93.03	P 1
2:1 3,4-lutidine monohydrate	10.036	7.659	13.948	90	99.62	90	P 2 <sub>1</sub> /c
1:1 3,4-lutidine	10.636	5.19	24.528	90	95.81	90	P 2 <sub>1</sub> /c
2:1 3,5-lutidine trihydrate	10.599	17.72	12.289	90	108.69	90	P 2 <sub>1</sub> /n
<b>Picolinic acids</b>							
2:1 2-picolinic acid	13.949	5.032	14.527	90	118.35	90	P 2 <sub>1</sub> /c
1:1 4-picolinic acid monohydrate	13.024	7.514	13.704	90	94.48	90	P 2 <sub>1</sub> /n
<b>Acetylpyridines</b>							
2:1 2-acetylpyridine	26.836	4.672	18.004	90	119.97	90	C 2/c
1:1 2-acetylpyridine	8.588	13.558	12.1735	90	110.29	90	P 2 <sub>1</sub> /n
2:1 3-acetylpyridine	12.576	5.026	18.38	90	126.51	90	P 2 <sub>1</sub> /c
2:1 4-acetylpyridine	10.844	7.385	12.875	90	111.1	90	P 2 <sub>1</sub> /n
<b>Miscellaneous</b>							
pyridine-3-aldehyde	3.82	19.06	11.387	90	94.153	90	P 2 <sub>1</sub> /n
2:1 ethyl-nicotinate	10.163	14.644	14.888	90	103.983	90	C 2/c
Caffeine	4.7862	8.7615	19.185	89.791	83.581	78.522	P 1
3,5-dimethylpyrazol Hydrate	7.1258	8.9965	8.981	119.471	93.757	99.037	P 1
1:1 Sulfathiazole	9.0519	10.496	10.886	117.64	92.43	111.61	P 1
Pyridinium	3.709	19.5761	9.9005	90	97.033	90	P 2 <sub>1</sub> /c

**Table 8.2** Chloranilic acid complexes determined in this work (with previously determined structures from CSD that fit in series shown in grey), with unit cell dimensions and space group.

It is important to note that although there were several co-molecules not containing amide groups used; none of these have produced complexes with chloranilic acid in this study. These included malonic acid, maleic acid, benzoic acid, 2-, 3- and 4-substituted halobenzoic acids, sucrose, urea, 1,4-benzoquinone, 2,4-dihydroxybenzoic acid, 2,5-dihydroxybenzoic acid, salicylic acid, oxalic acid and fumaric acid. In the CSD<sup>56</sup> a scan of chloranilic acid entries reveals that apart from metal complexes, almost all other complexes formed are with chemicals containing nitrogen in a ring structure. This is important in that it helps illustrate the selectivity and robust nature of the bifurcated ring nitrogen-chloranilic acid oxygen supramolecular synthon.

There are 28 new chloranilic acid co-crystal structures, with some promising signs for the synthesis of further new complexes, made up of nine picoline complexes, seven lutidine complexes, four acetylpyridine complexes, two picolinic acid complexes, as well as co-crystals with caffeine, sulfathiazole, ethyl nicotinate, pyridium, pyridine-3-aldehyde, and a hydrate with 3,5-dimethylpyrazole. The majority contained either the 2:1 or 1:1 hydrogen bonded units similar to those shown for lutidine (*Figure 7.6*). The structures of the 1:1 caffeine chloranilic acid co-crystal, 2:1 sulfathiazole chloranilic acid solvate, and 1:1 3,5-dimethylpyrazol chloranilic acid dihydrate are described below as they are interesting structures and provide additional information relevant to the main study of CA complexes presented here.

#### 8.6.1 Caffeine co-crystals grown from common commercial tea

Initially a light hearted comparison between tea bag brands, a crystallisation experiment of chloranilic acid and the contents of a tea bag also show the selectivity of the molecule. Two crystallisations were set up, in which some of the contents of separate brands of tea bags were put into a sample vial then chloranilic acid dissolved in acetonitrile was added. The vials were covered with parafilm and left for several weeks. Clusters of red needle crystals started to grow at the edge of the container and on top of the tea “leaves”. The structure was determined to be a chloranilic acid caffeine molecular complex (*Figure 8.33*).

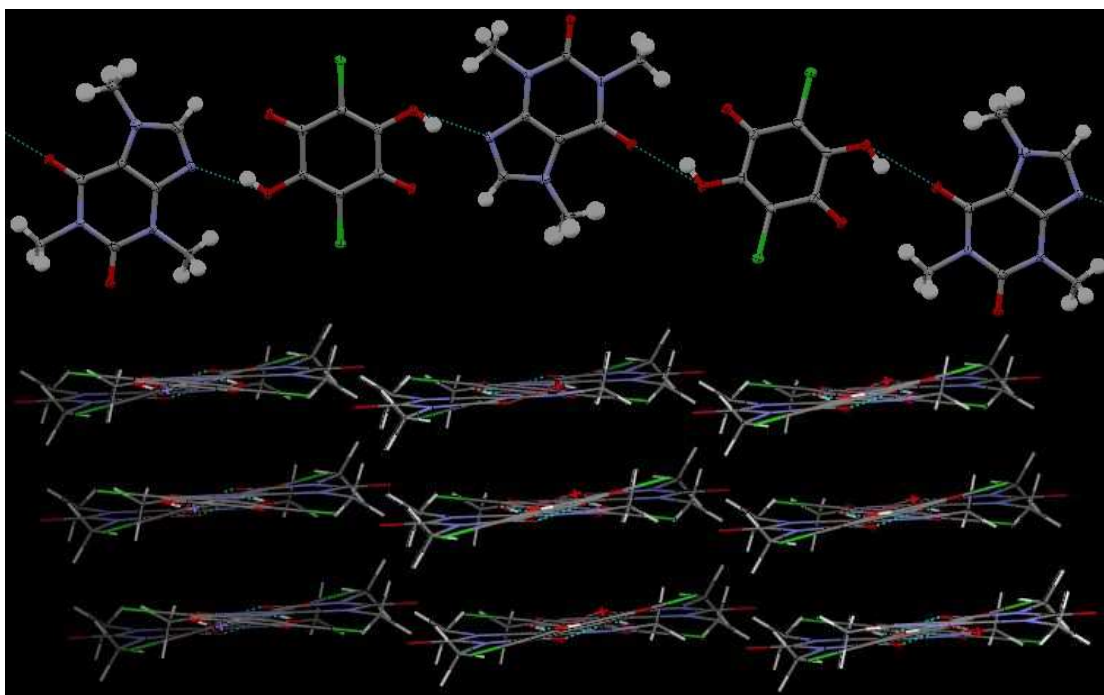


**Figure 8.33** *a)* A hydrogen bonded chain from the structure of 1:1 chloranilic acid caffeine molecular complex grown from tealeaves. *b)* The chains stack flat against each other in a regular pattern.

The caffeine and chloranilic acid molecules form hydrogen bonded chains, alternating between motifs where the chloranilic acid is bonded to the nitrogen in the pyrrole ring, or to a ketone group on the 6-membered ring of the caffeine (**Figure 8.33 a**). These chains then stack flat against each other in a regular array (**Figure 8.33 b**). Unlike in many other complexes studied here, in this case the hydrogen remains on the chloranilic acid and the bonds are mostly non-bifurcated in nature, although there is a slight shift in the hydrogen position towards the second oxygen of the chloranilic acid.

The fact that the chloranilic acid was able to extract exclusively caffeine from the tea highlights two important features, the selectivity of the chloranilic acid towards formation of molecular complexes, as well as the robust nature of the supramolecular synthon.

### 8.6.2 Chloranilic acid with sulfathiazole

Another co-crystal structure of interest is the 2:1 sulfathiazole chloranilic acid solvate complex. Grown from a crystallisation with the sulfathiazole in excess and dissolved in acetonitrile, it forms an interesting netted framework with disordered acetonitrile that forms chains that pass through the channels (*Figure 8.34 a*).

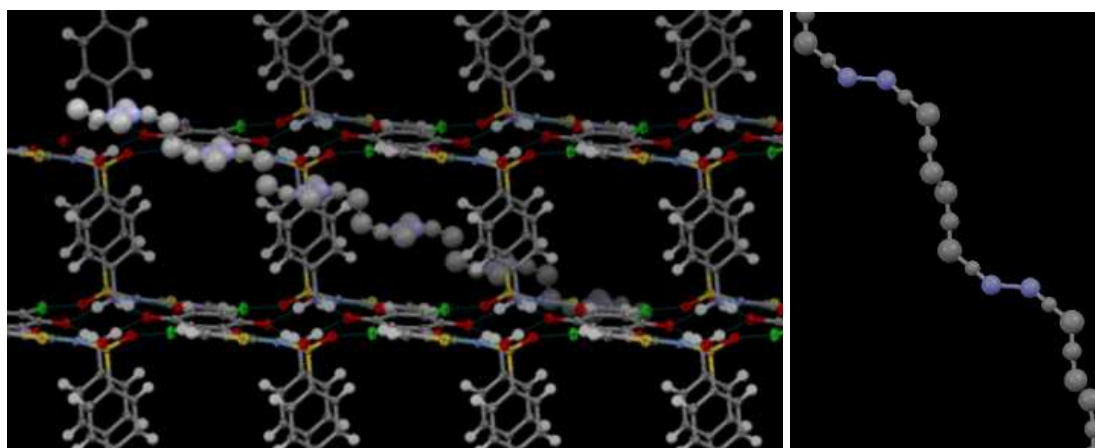


*Figure 8.34 a)* Structure of 2:1 sulfathiazole-chloranilic acid co-crystal complex showing the tubular construction and one of the disordered chains of acetonitrile that passes through the molecular netting frame. *b)* An isolated chain of disordered acetonitrile showing the repeating nature and the approximated molecules.

The solvent molecules form disordered chains which can be clearly identified as groups of three electron density peaks representing the acetonitrile molecules (*Figure 8.34 b*). The assignment of nitrogen and carbon in this chain is only suggestive as the true identities are not entirely clear from the electron density, but they refine reasonably well in the model used.

The rest of the structure other than the disordered solvent refines well and forms a net structure with the large gaps, where the solvent is present. The holes in the structure consist of square formed by the angular/bent-shaped sulfathiazole molecules (*Figure 8.35 b*). The sulfathiazole molecules are held together not only by two N-H...N hydrogen bonds but also by the chloranilic acid through both hydrogen bonding and Cl-O close contacts (*Figure 8.36*). These form zig-zag layers that stack on each other (*Figure 8.35 a*), and the disordered solvent chains weave in and out of the channels that are created. The structure does contain the 2:1 supramolecular synthon

of the chloranilic acid bifurcated to nitrogen on either side but because of the additional acceptor and donor groups present the system is more complex than most of the other examples described elsewhere in this work. Part of the reason for looking at the chloranilic acid co-crystals is in the context of crystal engineering and building in structure components into the co-crystals. A current high profile interest in this area is in forming storage materials especially those that can contain gases, for example hydrogen for fuel cells<sup>128,129</sup>, CO<sub>2</sub> for remediation, etc. Although this material is probably not suitable for such an application, it shows that there is scope for building in significant “holes” just using simple co-crystal combinations.

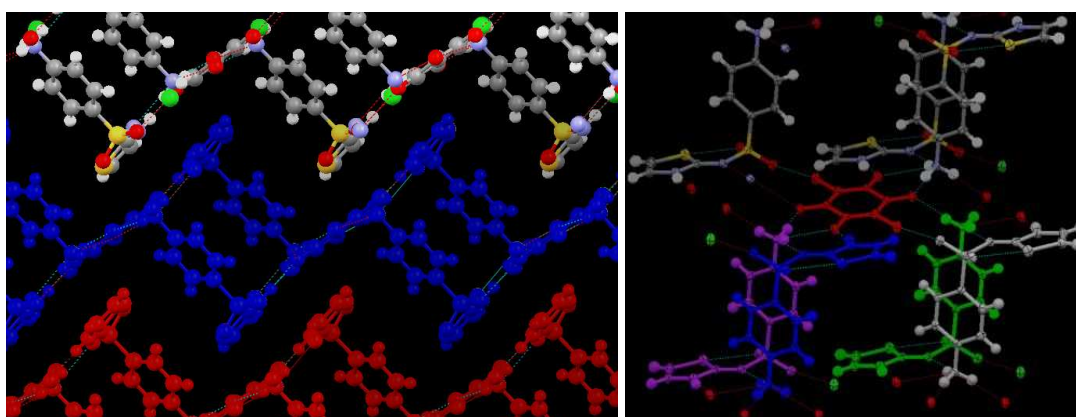


**Figure 8.35** *a) Stacked hydrogen bonded zig-zag layers in the chloranilic acid sulfathiazole complex, b) coloured sulfathiazole molecules forming double rings held together by chloranilic acid (red).*

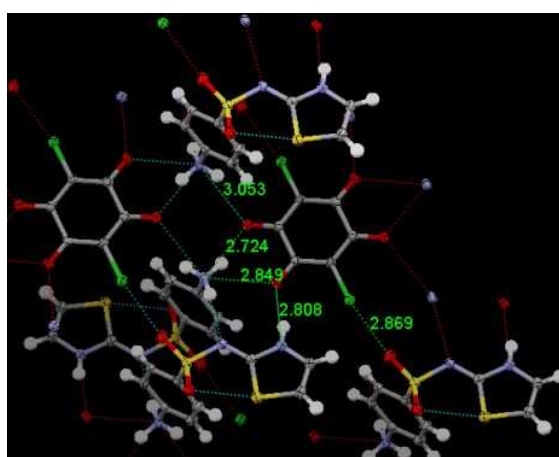


**Figure 8.36** *Bond lengths of HB's and distances of Cl-O close contacts between chloranilic acid and sulfathiazole in the CA:sulfathiazole complex.*

## 8.7 Complexes of bromanilic acid with Picolines

Bromanilic acid is in the same family as chloranilic acid (*Figure 7.1*), allowing it to interact in a similar way. With several uses in analytical chemistry, chloranilic acid is readily available from many suppliers whereas bromanilic acid is harder to acquire and has therefore, despite its similarity to chloranilic acid, been investigated far less frequently and as a consequence far fewer molecular complex structures of bromanilic acid have been published. The few bromanilic acid co-crystal structures that are available in the CSD are mainly from papers looking also at chloranilic acid and the other anilic acids, and used as an example of such. The paper by M.B.Zaman *et al.*<sup>36</sup> covering the crystal engineering aspects of combining bipyridines (4-(2-pyridyl)pyridinium, ethene-1,2-bis(4-pyridinium), 2,2'-dipyridylacetylene, and ethyne-1-(4-pyridyl)-2-(4'-pyridinium)) with bromanilic acid also looks at several other anilic acids including chloranilic acid. The bromanilic acid in these studies formed the same BHB motif that was present in the chloranilic acid co-crystals/complexes. They formed different one-dimensional chain structures that are equivalent to the 2:1 supramolecular synthons formed between the picoline and chloranilic acid although each unit is attached to each other as the amides are of a dipyridyl-type. By growing co-crystals of bromanilic acid with picoline the differences the halogen makes can be explored, as well as examining if the BHB motif and supramolecular synthon are present to the same extent with the change to bromanilic acid.

### 8.7.1 2-picoline 2:1 bromanilic acid

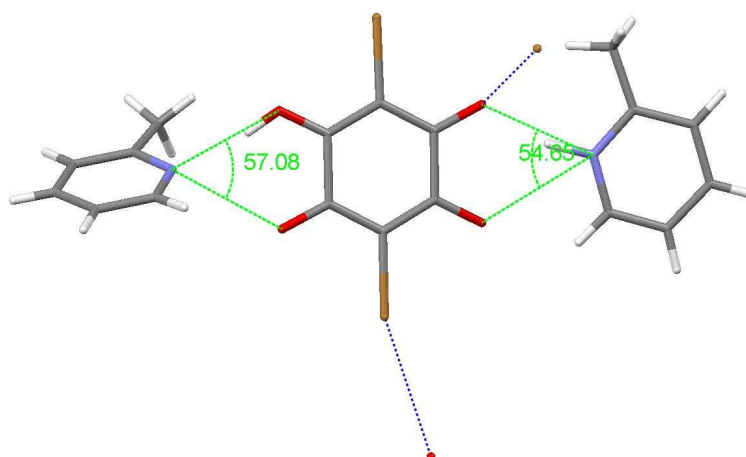


*Figure 8.37* 2-picoline bromanilic acid 2:1 hydrogen bonded unit showing the broken symmetry with the two different angles of the picoline molecule to bromanilic acid.

The 2:1 2-picoline bromanilic acid structure is distinct from other complexes studied here as the symmetry seen in all of the chloranilic acid 2:1 picoline hydrogen bonded unit has been broken, such that the picolines on either side of the bromanilic acid are orientated differently (**Figure 8.37**). Even more importantly only one of the hydrogens has been transferred across the hydrogen bond so that the bromanilic acid is left with one hydrogen. On the side where the hydrogen has been transferred to the nitrogen, the picoline is parallel with the bromanilic acid ring, whereas the non-transferred side has the picoline near perpendicular to the bromanilic acid. In the equivalent 2:1 2-picoline chloranilic acid equivalent co-crystal the picoline was near perpendicular with both protons transferred (**Figure 8.6 a**). There is also a close contact between the Br and O of the bromanilic acid seen in **Figure 8.37** and this forms chains of the HB units that interact in a complex interlocking pattern seen in **Figure 8.38**.

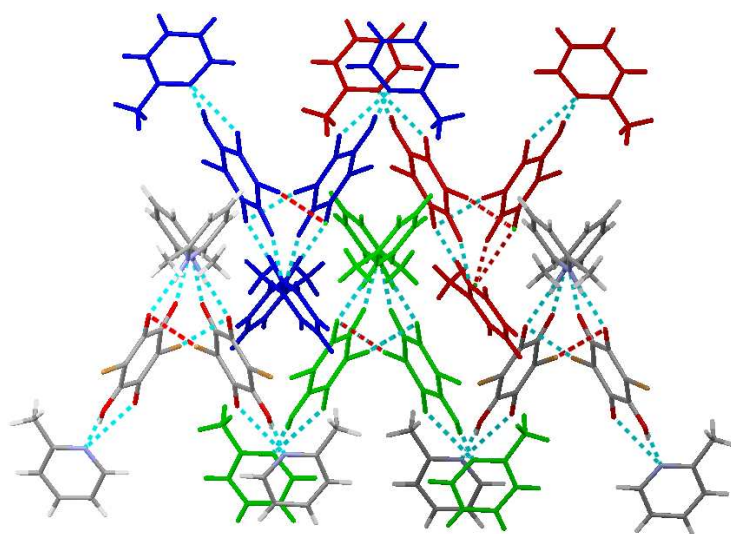


**Figure 8.38** HB units in the 2:1 2-picoline bromanilic acid complex form chains via close contacts between the O and Br. These stack in a complex interlocking style shown here with some of the chains coloured.

### 8.7.2 3-picoline 2:1 bromanilic acid

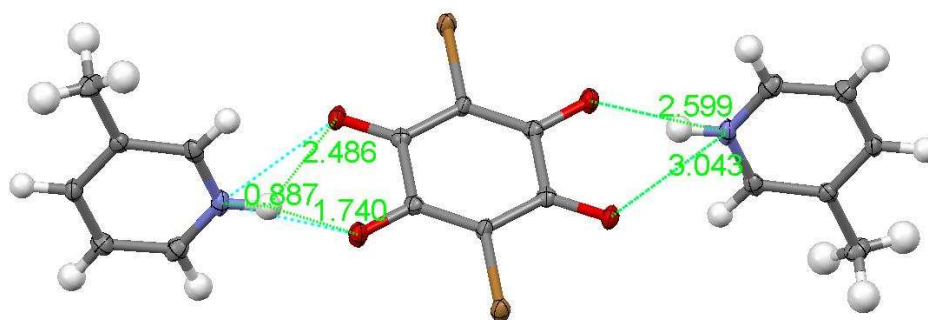


**Figure 8.39** HB unit of 3-picoline bromanilic acid 2:1 co-crystal complex.

The 2:1 3-picoline bromanilic acid structure is almost identical to the form 1 chloranilic acid equivalent and the unit cell differs only slightly.

Bromanilic acid:  $a=8.9567$ ,  $b=9.6191$ ,  $c=10.4275$  Å,  $\alpha=90$ ,  $\beta=103.899$ ,  $\gamma=90^\circ$ ,

Chloranilic acid:  $a=8.642$ ,  $b=9.687$ ,  $c=10.279$  Å,  $\alpha=90$ ,  $\beta=102.08$ ,  $\gamma=90^\circ$ ,

As with the chloranilic acid co-crystal, a 2:1 hydrogen bonded unit is formed in the complex with the picolines at a near perpendicular angle to the bromanilic acid (**Figure 8.39**). The rotated HB unit stacks alternately so that they slot together and allow some  $\pi$ - $\pi$  interactions between the picolines (**Figure 8.40**).

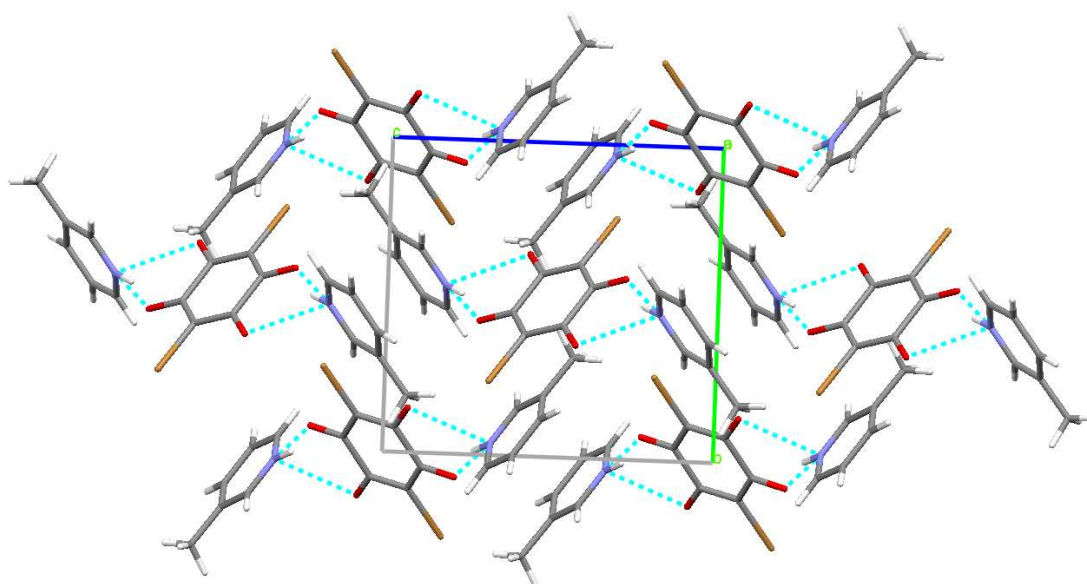


**Figure 8.40** Stacking present in 2:1 3-picoline bromanilic acid co-crystal complex.

### 8.7.3 4-picoline 2:1 bromanilic acid

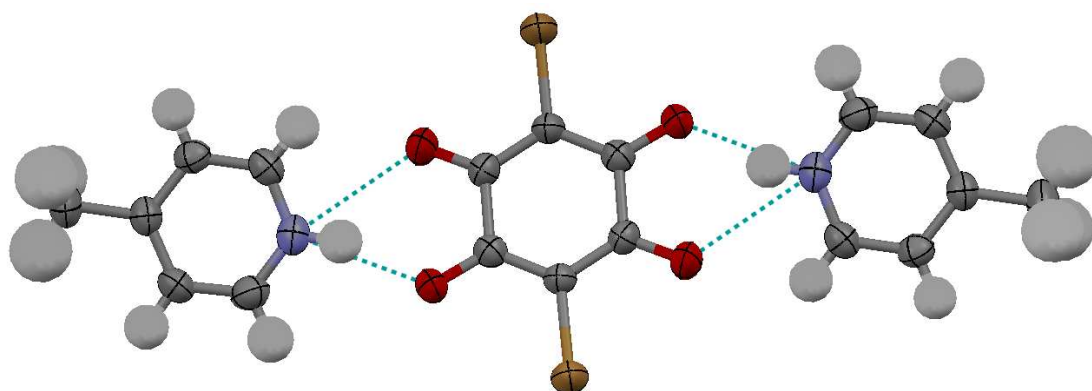


**Figure 8.41** HB unit of 2:1 4-picoline bromanilic acid co-crystal complex.

The 2:1 4-picoline bromanilic acid co-crystal complex has the same hydrogen bonded synthon as seen in the other bromanilic acid structures and has near parallel rings (**Figure 8.41**). The equivalent chloranilic acid co-crystal has a different structure with twisted HB units that stack very differently. The stacking in the 2:1 4-picoline bromanilic acid co-crystal is made from lines of slanted HB units positioned in a face centred pattern (**Figure 8.42**).

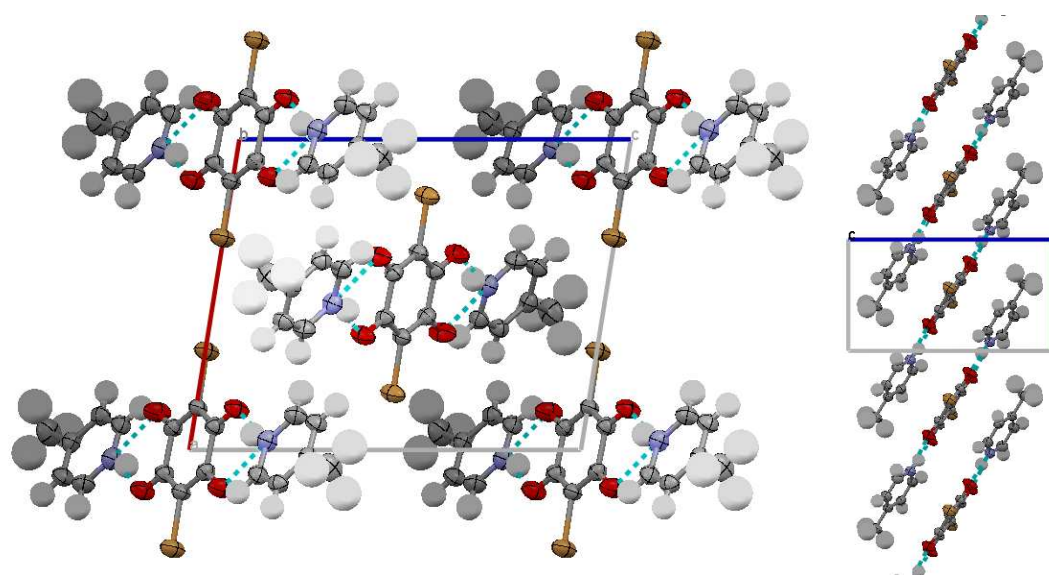


**Figure 8.42 a)** Stacking within the structure of the 2:1 4-picoline bromanilic acid complex, **b)** the diagonal stacking of the HB units viewed along the *a*-axis, showing some  $\pi$ - $\pi$  interactions.

#### 8.7.4 Conclusions on bromanilic acid complexes

The structure of the picoline bromanilic acid co-crystal complexes show the same supramolecular synthon present in the chloranilic acid complexes. In fact the structure of the 2:1 3-picoline bromanilic acid complex is almost exactly like the equivalent 2:1 3-picoline chloranilic acid structure. This shows that the halogen in the anilic acid is not always important, and in the limited studies carried out to date similar trends with the supramolecular synthons can start to be seen with the bromanilic acid that are also established in the chloranilic acid.

Despite the large similarities in the structures it is important to notice that the bromanilic acid 2- and 4- picoline structures are different to the chloranilic acid equivalents. In the 2-picoline case there is only partial deprotonation of the bromanilic acid which is unlike anything seen in the pure chloranilic acid picoline co-crystals and may form part of future investigations into bromanilic acid complexes.

Three structures have been presented here, one 2:1 form for each picoline. It is likely that, similar to the case of the chloranilic acid picoline co-crystals, there are many different varieties of structures, specifically 1:1 and hydrates, that are possible but have not been discovered in the preliminary experiments carried out in this project. All the bromanilic acid crystallisations were done at room temperature and with just a single solvent, reducing the number of sample environments screened in comparison to the case of the chloranilic acid, which is probably the main reason for there being a significantly reduced number of structures found to date. In addition to this, non-crystalline materials were formed in some of the sample vials (specifically some of those where water was present), which may also be bromanilic acid picoline complexes but which cannot be studied with single crystal diffraction techniques.

#### 8.8 Conclusions

A total of 28 new co-crystal complexes of chloranilic acid and three bromanilic acid were produced and their structures solved. There remains the possibility that additional co-crystals were present but not identified especially with the presence of some unassigned powder pattern peaks. In the 31 new structures, and in a large majority of previous structures, a bifurcated hydrogen bonded motif is present. This

motif has been shown to appear in a reliable fashion and is the dominant interaction in the structures of the chloranilic acid co-crystals. In all the picoline and lutidine cases the hydrogen is transferred across from the chloranilic acid to the nitrogen of the co-molecule. Despite this there is an interesting range in position of donor-hydrogen bond between the oxygens of the chloranilic acid. This makes a variety of bifurcated hydrogen bonds (BHB), from symmetrical bonds where both acceptor oxygens are involved equally, to asymmetrical bonds where there is a major N-H...O1 interaction but the accompanying N-H...O2 is a minor part. In some cases this can be put down to additional intermolecular interactions involving the oxygens and in others the crystal environment/packing has a large determining effect.

There were no clear signs of disorder in any of the hydrogen bonds in the structures studied, this includes both the bifurcated hydrogen bonds and the other hydrogen bonds involved in either holding the chloranilic acids together or with solvent waters incorporated in the lattice. Some of the structures did have hydrogen peaks within the hydrogen bonds that were not well defined and circular, this could be a sign of disorder or migration but these were either too weak or not well enough defined to be ruled as anything more than effects of noise or the already diffuse nature of the electrons in a hydrogen bond.

The bifurcated hydrogen bond motif was present as part of two larger supramolecular synthon units in either a 1:1 or 2:1 ratio, shown in *Figure 7.6* for the case of the lutidines. With this work looking at the use of chloranilic acid as a molecule for crystal engineering, these two supramolecular synthons represent valuable building blocks that could be used to build more complex systems and structures, as they turned up in all the picoline and lutidine structures, and the majority of the additional crystallisations, in one of the two alternative forms. Another important feature is the ability of these structures to build themselves around the bifurcated hydrogen bond motif even in crystallisations where other interactions and even hydrogen bonding patterns were possible. The Hirshfeld surface plots were able to show there was a mixture of bifurcation in the BHB and with a trend for the more symmetrical highly bifurcated hydrogen bonds to have stronger additional intermolecular interactions to the chloranilic acid oxygens. The bond lengths and angles of the BHBs in the complexes were in agreement with the observations from the Hirshfeld surfaces about

the level of bifurcation and also revealed a general trend to have smaller angles between the planes of the rings of the molecules for the higher bifurcated BHB. The sum of angles that showed the planarity of the BHB of the picoline chloranilic acid complexes were all close to 360° showing they are nearly flat and suggesting the BHB are relatively strong.

The very selective nature of the chloranilic acid in forming hydrogen-bonded complexes is of benefit in its uses in crystal engineering where it is important to be able to target certain interactions or motifs. Chloranilic acid forms co-crystals with a limited range of molecules, of a particular type; these can be generalised as pyridine-related molecules. There are a few exceptions to this rule, the most notable being water, with the chloranilic acid hydrate forming in many crystallisations if water is present. The selectivity in the formation of chloranilic acid co-crystals can be seen with the results from the crystallisations set up during this project, with only molecules containing nitrogen as part of an aromatic ring forming complexes, this was despite a large collection of molecules not containing this motif being tested. It is also reflected in the published structures in the CSD with the vast majority of the organic compounds involving chloranilic acids being co-crystals with pyridine related molecules. The 2:1 caffeine chloranilic acid co-crystal is a good example where this selectivity is shown. The caffeine was extracted from tea “leaves” by the chloranilic acid, and was the only crystal form to be produced in the crystallisation. This discrimination that chloranilic acid shows makes it ideal for crystal engineering where the reliable interaction can be used to join different small “blocks” or molecules, even in the presence of other hydrogen bonding groups. This is an example of self-assembly with the chloranilic acid only attaching to specific molecules.

As well as the ability to control the resulting structure with the choice of molecule other factors can be used to determine the product. The type of co-crystal(s) formed is sometimes dependent on the starting ratios of the molecules used in the crystallisation attempt. This can be seen simply with the chloranilic acid co-crystals where in the majority of cases the ratio of chloranilic acid to co-molecule affected the ratio of these molecules in the product crystal as well as often determining the type of supramolecular synthon that the product contained. In the case where the picolines and lutidines were in excess the majority of the resultant crystals were 2:1 co-crystals

and these contained the 2:1 hydrogen bonded supramolecular synthon, whereas use of small amounts of the picolines and lutidines often resulted in some 1:1 co-crystals being produced and where this happened most had the 1:1 synthon.

No temperature effects were observed apart from a loose trend of some slightly better crystals from the lower temperature crystallisations where the evaporation process was slowed. The fact the known 2:1 2-picoline chloranilic acid structure was not present in any of the powder patterns could be an effect of temperature as only heated samples of the 2:1, 1:1 and 2:1 with water solutions were tested but this would have to be confirmed with further powder measurements for samples prepared at different temperatures.

The choice of solvate is often another factor in governing the product formed but is limited for chloranilic acid because it is reluctant to dissolve in anything apart from acetonitrile and DMSO. The one significant solvent effect revealed was in the presence of water which often resulted in a hydrate product being produced although not always exclusively. The other solvate to be grown was the case of the 2:1 sulfathiazole chloranilic acid containing a disordered chain of acetonitrile. This interesting, potentially porous, structure shows some of the functionality that could be built in to a product crystal, with solvent channels being created by the sulfathiazole.

Although not a complex theoretical study, the calculations into the chloranilic acid picoline 2:1 HB units in the gaseous state were able to give evidence that suggests that the flat formation of synthon is preferred and importantly the 2:1 HB unit made up of the three molecules is stable out of the crystal environment. This gives additional support for the utility of this synthon in crystal engineering.

Many of the experimental structures contain non-flat synthons in the solid-state, which appears to go against the results of the calculations, but as the calculations are done in the gas phase the diffraction experiments will differ because of the crystal environment. Therefore this shows that the packing and additional interactions present in the solid-state are probably very important in determining the way the picolines orientate in relation to the chloranilic acid.

The three 2:1 picoline bromanilic acid co-crystals also have the 2:1 HB synthon present. In the case of the 3-picoline co-crystal the structure was almost identical to the chloranilic acid equivalent, showing that the halogen of the anilic acid is not always a large driving force in the crystal structure. On the other hand the 2- and 4-picoline bromanilic co-crystal complexes are different to their chloranilic acid equivalents especially in the case of the 2-picoline. In the 2:1 2-picoline bromanilic acid co-crystals the 2:1 synthon is unusual as on either side of the bromanilic acid the BHB are different, compared with all the other complexes of picoline and lutidine where the synthons have a rotational symmetry, with both BHB being crystallographically identical.

## 9. Conclusions and Forward Look

### 9.1 Investigation of possible cooperative hydrogen bond disorder in 2,4-dihydroxybenzoic acid

Alternating tautomers have been well documented in carboxylic acid dimers, where the two hydrogens transfer between the two oxygens producing two different forms in the solid state. The average structure, as seen in a diffraction experiment, has the hydrogens partially occupying both positions, resulting in a disordered HB. 2,4-dihydroxybenzoic acid has the added complexity of the intramolecular HB between the hydroxyl group in the ortho position and the carboxylic acid, which introduces a third possible tautomeric form.

The possibility of cooperative effects in the dihydroxybenzoic acid materials prompted a multi-temperature X-ray diffraction study of the second polymorph of 2,4-dihydroxybenzoic acid, but the results were inconclusive. The presence of hydrogen disorder within the dimer hydrogen bond and cooperative effects between the intra- and inter-molecular hydrogen bonds could not be ruled out. Difference Fourier maps of the intramolecular and dimer HBs did have additional electron density peaks in the area of the HBs but this was not distinct enough to conclusively separate it from the background noise.

A neutron diffraction experiment was undertaken on SXD at ISIS and good refinements were obtained for data at 20 K, 90 K and 150 K. Difference Fourier maps of the three hydrogen bonds showed well localised spherical troughs that represented the nuclear density of the protons. Therefore a decisive conclusion was reached that the protons within the three hydrogen bonds are not disordered.

#### 9.1.1 2,4-dihydroxybenzoic acid calculations

To accompany the neutron experiment a complimentary theoretical study into the energies of the three possible tautomers was carried out. Tautomer II which involved the transfer of the proton across the intramolecular HB was found to be unstable and ruled out. The energy difference between tautomer I and III was found to be 8.64

$\text{kJmol}^{-1}$ , in favour of the dominant crystallographically observed configuration form I, which is considerably larger than the energy differences between configurations in similar carboxylic acid dimers that show unambiguous proton disorder. The deformation electron density map of form I begins to explain why tautomer I is the preferred form, revealing that the two oxygens of the dimer take up different orientations which affect the lone pairs and their abilities to be the acceptor for the intramolecular bond. Therefore overall the calculations agree with the neutron results, showing that form I, the tautomer found in the neutron experiments, has the lowest energy.

The results of the neutron and computational experiments would appear to contradict the initial X-ray diffraction experiment that showed possible secondary density peaks that could have indicated hydrogen disorder in at least two of the hydrogen bonds. However the X-ray results only provided an indication of possible disorder and although insufficient to prove disorder, the result did merit further experiments to clarify the suspected abnormal behaviour. The use of neutron diffraction confirmed that no proton disorder existed and was backed up with the calculations, which also gave some explanation to the observation.

A further possibility, though less likely given the comprehensive set of techniques used in the study of the 2,4-dihydroxybenzoic acid structure, is that although the proton of the hydrogens doesn't show any sign of a second position, the electron density could still show anomalous effects. The electrons are far more mobile than the proton, so it is possible that even if the proton is in a stable state the electron density around it could show anomalous behaviour.

## **9.2 Investigation of possible cooperative hydrogen bond disorder in 2,5-dihydroxybenzoic acid**

The isomeric structure 2,5-dihydroxybenzoic acid also has the potential to display similar hydrogen bonding disorder. The X-ray experiments were less ambiguous than the 2,4-dihydroxybenzoic acid case with only minor effects present if any. A neutron experiment on SXD allowed the refinement of the structure at 20 K, 100 K and 200 K, revealing no disorder to be present in any of the hydrogen bonds of the molecule. The

difference Fourier maps show well defined spherical troughs representing the hydrogen positions. The neutron experiment was able to rule out conclusively any disorder of the protons in any of the hydrogen bonds up to a temperature of 200 K.

### **9.3 Proton migration in isonicotinamidium formate**

Isonicotinamidium formate forms a dimeric hydrogen bonded structure through the amide group, along with two N...O single hydrogen bonds, one of which is short/strong in nature. The X-ray diffraction experiments suggested that secondary electron density peaks may be present in the dimer and the strong single hydrogen bonds. Neutron data at 40 K, 100 K, 150 K and 200 K was collected on SXD and provided reliable refinements. The difference Fourier maps showed no secondary nuclear density in any of the hydrogen bonds and well defined proton positions. However on further examination of the proton positions within the strong HB between the molecules, a different feature of interest and relevance was observed - a small temperature dependent migration of the proton across the bond.

### **9.4 Neutron diffraction studies of 2-iodoanilinium picrate**

There are three forms of 2-iodoanilinium picrate, form I of which shows the optical property of thermochromism, where there is a change of colour caused by a proton transfer over a temperature range. A study of this effect planned to use neutron diffraction, but unfortunately form I, in which the thermochromism is most prominent, did not produce crystals of sufficient size for neutron diffraction. However, large crystals of form II, which is also believed to exhibit proton transfer (but not thermochromism), were obtained. The effect was thought to occur between 330 and 360 K from X-ray studies. Due to the crystal quality degrading because of overheating, only data for 300 K, 310 K and 320 K were obtained. The 300 K and 320 K data produced good refinements and difference Fourier maps of the hydrogen bond had minimal background, with a well defined near spherical trough representing the proton position. The 310 K data refinement was not as good quality with large background noise. The experiment thus showed that no proton transfer was present between 300 K and 320 K but does not rule out the possibility of the transfer above 330 K where it is expected to occur from the X-ray studies.

## 9.5 Neutron diffraction studies of malonic acid

As noted above, carboxylic dimer hydrogen bonds are well known for proton transfer caused by switching between alternate forms. The triclinic structure of malonic acid contains two different dimers and has been shown by a variety of techniques, predominantly NMR, to show proton disorder. An SXD neutron diffraction experiment was carried out to map the transfer rate between the proton positions via site occupancy refinements. The multiple temperature experiment was intended to sample the structure at a large number of temperatures although only three temperatures were able to be refined to reasonable quality, 75 K, 140 K and 200K. The difference Fourier maps for 75 K did not show any evidence of second positions for the protons in the dimer, instead they showed well-defined single position spherical proton density peaks. The 140 K map showed a minor elongation of the proton along the HB, possibly indicating the onset of site disorder. Unfortunately the map for 200 K has a large systematic background because of the reduced quality of the data. The lack of data at higher temperatures makes it impossible to tell if the indicators of disorder of hydrogen H2 at 140 K are a real effect.

A second neutron experiment on VIVALDI at ILL has been carried out on malonic acid with the aim of measuring the higher temperatures. Currently the data from this experiment is still being processed, but the quality of the frame images is high so good refinements are expected.

## 9.6 Molecular complexes of Chloranilic acid

Chloranilic acid has been the main focus of the X-ray diffraction work of this project, with an aim of assessing the suitability of this molecule for applications in crystal engineering and examining bifurcated hydrogen bonds. Chloranilic acid has been shown to readily combine with amide based molecules forming bifurcated hydrogen bonded complexes. Twenty-eight new complexes of chloranilic acid have been formed, nine of which were with picolines and seven with lutidines. The possibility of more new co-crystals having been produced but not discovered was not ruled out especially with some powder pattern peaks not accounted for.

The chloranilic acid complexes with lutidine and picoline all contain one of the two larger supramolecular synthon units in either a 1:1 or 2:1 ratio, shown in *Figure 7.6* for the case of the lutidines. With this work looking at the use of chloranilic acid as a molecule for crystal engineering, these two supramolecular synthons represent reliable building blocks that could be used to build more complex systems and structures. Another important feature is the ability of these structures to build themselves around the bifurcated hydrogen bond motif even in crystallisations where other interactions and even hydrogen bonding patterns were possible.

The two synthons share a common BHB motif formed between two of the O atoms of the chloranilic acid and the N atom from the lutidine. This motif is common to all the new chloranilic acid structures and a large majority of the previously seen structures. This motif has been shown to appear in a reliable fashion and is the dominant interaction in the structures of the chloranilic acid co-crystals.

The hydrogen atom in the BHB is located on the nitrogen in all the lutidine and picoline structures, meaning that it has transferred across from the chloranilic acid. From examining the difference Fourier maps none of the structures show any clear indications of disorder although a few did have small additional secondary peaks, or unusual patterns of electron density but in these cases large background noise could account at least in part for the effects.

The geometry of the BHBs was examined with the use of difference Fourier maps, Hirshfeld surface plots and a comparison of bond lengths and angles. The conclusions drawn from the Hirshfeld surfaces are consistent with the bond parameters and represent a quick and easy way of assessing this type of interaction visually. The geometry of the BHB showed a large variation between the structures, with some near symmetrical, to cases where they could be described as a single HB because of the bond lengths; in the latter, however, since the pyridine ring is positioned between the oxygens it is likely that the second oxygen is participating in the interaction and therefore determining the position of the pyridine ring relative to the chloranilic acid. Several trends could be observed between the level of bifurcation in the interaction and other aspects of the hydrogen bond. Where a complex has a high level of symmetry, generally the oxygens of the chloranilic acid have additional

interactions, especially further HBs, in which they are involved. This could arise due to the additional interactions making the two oxygens more equivalent whereas the standard single and double nature of the bonds naturally leads to asymmetry. The higher bifurcated HB also tended to have small angles between the planes of the rings of the two molecules. As a whole, all the structures showed close to flat BHB which suggests the BHBs are relatively strong. As well as the additional interactions the environment and crystal packing are other factors determining the position of the nitrogen-hydrogen bond relative to the oxygens of the chloranilic acid.

One of the main focuses of studying chloranilic acid is its use in crystal engineering where the aim is to be able to control of the resulting product and therefore its properties and structure. The project showed that a high level of manipulation can be achieved with chloranilic acid through the choice of co-molecule, starting ratio of components and choice of solvents. A level of control over the supramolecular synthon obtained by variation of starting ratios was also shown. The powder data of both the lutidine and the picolines chloranilic acid co-crystals shows that the initial ratio of starting compounds was often reflected in the ratio between components of the predominant resulting crystalline material. Where the lutidine or picoline were in excess the resulting crystalline structures showed at least part and often a majority of the pattern resulting from the 2:1 complexes with the chloranilic acid. The crystallisations where approximate molar equivalents of the two molecules were used, 1:1 structure were generally present in the powder pattern of the resulting crystalline mixture. In addition to this the starting ratios for the crystallisations were shown to have an influence on the supramolecular synthon present in the structures, with only one exception found that did not adopt the supramolecular synthon that related to the stoichiometry of the structure (i.e. with 2:1 or 1:1 crystals containing the 2:1 or 1:1 supramolecular synthon respectively) and in this case the other synthon was present.

Chloranilic acid was also shown to be very selective in the molecules with it forms HB or even co-crystals. The advantage of this in a crystal engineering context is that chloranilic acid would form the target motifs even where other functional groups (carboxylic acid groups, amides, alcohols...) are present. This selective self-assembly can allow small blocks or molecules to be joined together into larger networks but keeping the freedom and flexibility to build the desired functionality into the block.

The results of the multiple crystallisations set up with a large variety of molecules with different functional groups showed that in general only pyridine-related molecules (containing one or more nitrogen as part of an aromatic ring) formed co-crystals with chloranilic acid although there were a few exceptions. A search of the CSD showed that the vast majority of organic compounds in co-crystal structures with chloranilic acid contain a pyridine or related ring. Further highlighting this is the exclusive extraction of caffeine from a tea mixture to form the 2:1 caffeine chloranilic acid co-crystal.

Several hydrates were formed where the water was added to the crystallization although generally these were not the exclusive product and often the already known structure of chloranilic acid dihydrate formed as well. It is suspected that the supply of 3,5-lutidine was contaminated with water as all crystallization attempts resulted in the 3,5-lutidine chloranilic acid hydrate even if they were supposed to be dry. An additional solvate was produced in the form of 2:1 sulfathiazole chloranilic acid containing a disordered chain of acetonitrile. This interesting, potentially porous, structure shows some of the functionality that could be built in to a product crystal, with solvent channels being created by the arrangement of the sulfathiazole.

Although each set of crystallisation environments were examined for new single crystal samples and a large number of new structures were found, unassigned peaks in the powder patterns show that other crystalline material was present. This could arise from powder material, crystals that were too small or poor quality to measure with single crystal techniques or that single crystals were present but were not picked out. It is therefore likely that by further targeting the crystallisation environments that have been highlighted by the powder measurements, additional structures will be found.

A majority of the structures from the experimental work had synthons that had a rotation in them (i.e. not flat). The gas-state theoretical study into the picoline chloranilic acid 2:1 supramolecular synthon, when optimized, produced flat and importantly stable units outwith the crystal environment. This would suggest that the packing and additional interactions present in the solid-state are more important than the force that drive the picoline to orientate in parallel with the chloranilic acid in gas-

state calculations, but that the BHB is strong enough to hold the synthon together even out of the crystal environment.

Chloranilic acid has been shown to reliably form the BHB motif and with this motif to form into larger structural units and even to afford a level of functionality. Work into expanding the co-crystallisations beyond lutidines and picolines has already started with the results so far tabulated in *Table 8.2*. Molecules similar to the lutidines/picolines have been targeted although additional functional groups (for example amide or aldehyde groups) allow for a more complex HB architecture to be built round the synthon units. With a larger pool of structures containing the BHB produced in this way, further conclusions can be drawn from their analysis.

#### 9.6.1 *d*SNAP and the geometry of molecular complexes, a forward look

The co-crystallisations of chloranilic acid have produced a large number of new structures all containing a similar fragment, i.e. the bifurcated hydrogen bond (*Chapter 8 and 9*). Individually they reveal lots of information in regard to this bifurcated hydrogen bond but when it comes to comparing the data from several structures the list of bond lengths and angles can rapidly become too large to analyse simply and efficiently. *DSNAP*<sup>74</sup> is a program designed to cluster structures from the Cambridge Structural Database (CSD)<sup>56</sup> using the total geometry of the defined fragment (all atom to atom bond lengths and bond angles). This can allow the user to quickly see which structures are similar (and which are different) so that important trends can be deciphered.

The principle of a *d*SNAP run uses a technique called cluster analysis to group together fragments that have similar geometries. The results are presented in a visually helpful way, as a so-called dendrogram *Figure 9.1*, allowing the user to view and verify the proposed scheme for classifying fragments into clusters of similar geometry<sup>74</sup>. The clustering can be examined at different levels of similarity, allowing the user to see at a glance possible clusterings of the available fragments into groups that are similar. The task for the structural chemist is then to interpret these, and a series of add-on visualisation and analysis tools are available within *d*SNAP when CSD hits are being analysed, which allows this to be done effectively.

Recently, a new development has been introduced into *dSNAP* that allows user structures as well as structures from the CSD to be clustered together. However, this development has not yet been fully integrated into the important visualisation and comparison tools available in *dSNAP*, that allow the structurally significant differences to be analysed most effectively. Once this has been done, or as part of a more extensive manual analysis of the large amount of data available, further structural comparisons on the chloranilic acid complex geometries can be carried out.

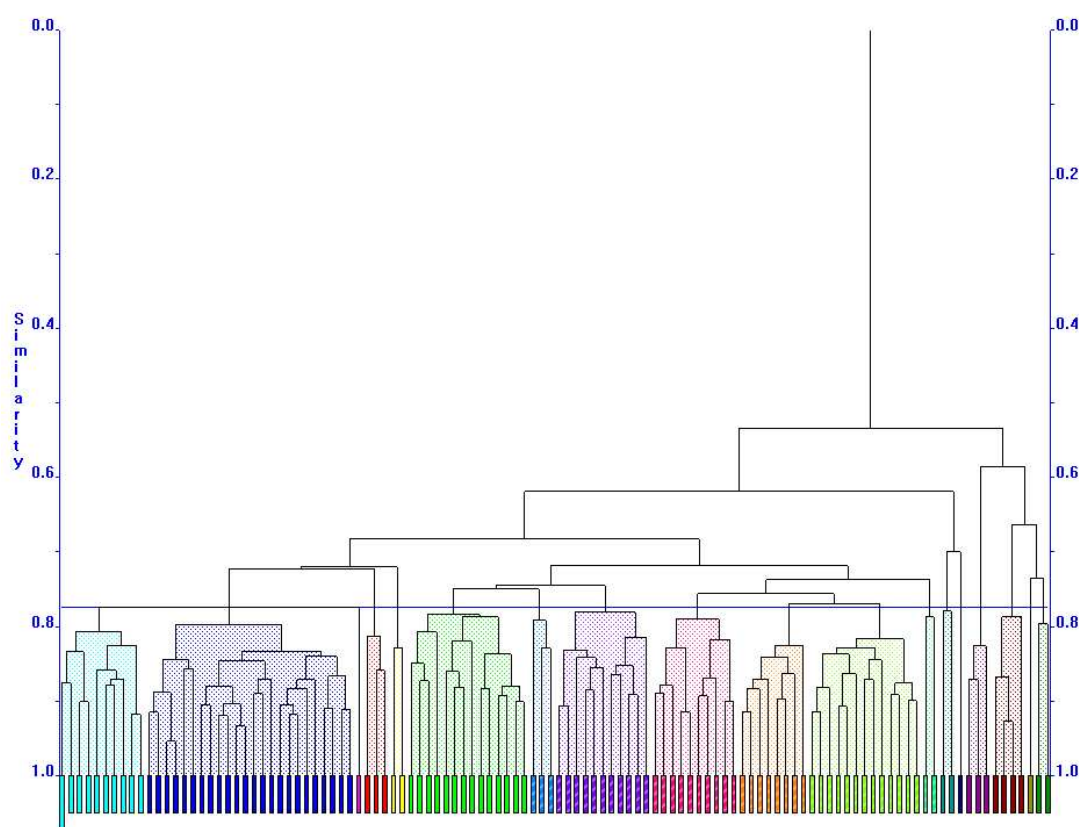


**Figure 9.1** Typical dendrogram from *dSNAP* showing level of similarity between different fragments. Each block at the bottom represents a different fragment coloured to represent the clustering. The lower a fragment is joined to another fragment by a tie-bar the more similar it is. The fragments are separated into the clusters by a cut level which can be moved up and down changing the level of similarity. Further tools are available in *dSNAP* that allow the geometries in each cluster to be analysed effectively; these will soon be fully available for user-input structures such as those determined in this work.

### 9.6.2 VIVALDI data on 2:1 2,4-lutidine chloranilic acid form I

An experiment on VIVALDI at the ILL has provided sufficient data to provide a refinement of the structure of 2:1 2,4-lutidine chloranilic acid form I, although this is not to the same standard seen in the structures from SXD. The results of this experiment showed the proton position in the BHB to be well defined with no disorder present, backing up the X-ray diffraction refinement. The structure from the refinement had a few strange atomic displacement parameters for some of the atoms but otherwise was stable and matched the structure defined by the X-ray experiment.

### 9.7 Molecular complexes of bromanilic acid

Three new 2:1 picoline bromanilic acid co-crystals were also formed, and contained the 2:1 HB synthon present in the chloranilic acid complexes. This brings the total of new structures produced in this work to 31. In the case of the 3-picoline co-crystal the structure was almost identical to the chloranilic acid equivalent, showing that the halogen of the anilic acid is not always a large driving force in the crystal structure. On the other hand the 2- and 4- picoline bromanilic co-crystal complexes are different to their chloranilic acid equivalents especially in the case of the 2-picoline. In the 2:1 2-picoline bromanilic acid co-crystals the 2:1 synthon is unusual as on either side of the bromanilic acid the BHB are different, where-as in all the other complexes of picoline and lutidine the synthons have a rotational symmetry, with both BHB being crystallographically identical.

### 9.8 Additional Future work

The calculations into how the ratio of HF:DFT in different basis sets affects the barrier energy within HBs were able to show several trends in the data. An accurate calculation to calculate the exact energy of the barrier energy in H<sub>2</sub>O<sub>2</sub> would allow the determination of the best ratio of DFT:HF for this type of calculation by extrapolating from the graph for each basis set.

Several experiments in this project have been run on VIVALDI but due to technical problems and difficulties integrating the data only a limited number of these have been fully refined to date. It is expected that these will provide useful results when fully processed in the near future.

**Table 9.1** X-ray refinement data of chloranilic acid (CA) complexes with picoline (P).

	1:1 2-P CA	2:1 2-P CA			1:1 3-P CA			2:1 3-P CA Form 2
T/K	100	100	200	RT 300	100	200	RT 300	100
Diffractionmeter	KappaCCD	Rigaku Rapid	Rigaku Rapid	Rigaku Rapid	Apex II	Apex II	Apex II	KappaCCD
Formula	C <sub>12</sub> H <sub>9</sub> Cl <sub>2</sub> NO <sub>4</sub>	C <sub>9</sub> H <sub>8</sub> ClNO <sub>2</sub>	C <sub>9</sub> H <sub>8</sub> ClNO <sub>2</sub>	C <sub>9</sub> H <sub>8</sub> ClNO <sub>2</sub>	C <sub>12</sub> H <sub>9</sub> Cl <sub>2</sub> NO <sub>4</sub>	C <sub>12</sub> H <sub>9</sub> Cl <sub>2</sub> NO <sub>4</sub>	C <sub>12</sub> H <sub>9</sub> Cl <sub>2</sub> NO <sub>4</sub>	C <sub>9</sub> H <sub>8</sub> ClNO <sub>2</sub>
M / g-mol <sup>-1</sup>	302.11	197.62	197.62	197.62	302.11	302.11	302.11	197.62
space group	P 1	P 2 <sub>1</sub> /c	P 2 <sub>1</sub> /c	P 2 <sub>1</sub> /c	P 1	P 1	P 1	P 2 <sub>1</sub> /n
a / Å	7.3752(15)	6.369(3)	6.398(3)	6.419(3)	5.0366(2)	5.0539(2)	5.0718(2)	12.0490(5)
b / Å	9.1468(18)	8.597(3)	8.657(4)	8.692(4)	9.3637(4)	9.3895(5)	9.4052(5)	5.32600(10)
c / Å	9.7296(19)	16.628(6)	16.684(7)	16.727(7)	13.3491(7)	13.4239(8)	13.5038(8)	13.5813(6)
α / °	101.63(3)				97.669(2)	97.829(2)	98.035(2)	
β / °	103.92(3)	101.451(17)	101.23(2)	101.031(19)	98.579(3)	98.064(3)	97.534(3)	96.958(2)
γ / °	97.45(3)				103.660(2)	103.501(3)	103.372(3)	
V / Å <sup>3</sup>	612.9(3)	892.3(6)	906.4(7)	916.1(7)	595.51(5)	603.77(6)	611.54(6)	865.13(5)
Z	2	4	4	4	2	2	2	4
ρ <sub>calc</sub> / g-cm <sup>3</sup>	1.637	1.471	1.448	1.433	1.685	1.662	1.641	1.517
μ / mm <sup>-1</sup>	0.538	0.390	0.384	0.380	0.554	0.546	0.539	0.403
θ range / °	2.223- 30.015	3.264-30.505	3.246-30.502	3.233-30.488	1.567-35.032	1.556-35.150	1.545-35.077	2.135-30.010
refln (meas./ indep.)	10133/ 2917	11493/2710	11669/2755	11806/2781	13826/5151	14333/5250	14639/7869	11216/2520
R <sub>int</sub>	0.075	0.021	0.018	0.015	0.044	0.051	0.050	0.093
refln (obs. I>2σ(I))	2352	1971	1707	1401	3791	3313	4191	1624
completeness / %	81.4	99.7	99.7	99.6	98.2	97.7	97.3	99.5
data / restr. / param.	2917/0/172	2710/0/142	2755/0/150	2781/0/142	5151/0/172	5250/0/172	4191/0/172	2520/0/150
GooF on F <sup>2</sup>	0.9309	0.9436	0.8756	0.8151	0.9207	0.9600	0.8833	0.9105
R <sub>1</sub> (obs / all)	0.0309/0.0419	0.0398/0.0556	0.0395/0.0646	0.0376/0.0742	0.0368/0.0615	0.0415/0.0848	0.0884/0.1183	0.0425/ 0.0827
wR <sub>2</sub> (obs / all)	0.0703/0.0800	0.0914/0.0955	0.0944/0.1007	0.0968/0.1046	0.0777/0.0941	0.0855/0.1151	0.1224/0.1423	0.0975/ 0.1336
ρ (max / min) / e-Å <sup>-3</sup>	0.44/-0.36	0.42/-0.54	0.39/-0.32	0.33/-0.37	0.79/-0.76	0.80/-0.90	0.57/-0.73	0.92/-0.79
RMS / eÅ <sup>-3</sup>	0.06	0.06	0.05	0.04	0.08	0.07	0.06	0.08

**Table 9.2** X-ray refinement data of chloranilic acid (CA) complexes with picoline (P).

	<b>2:1 3-P CA Form1</b>			<b>3-P CA new hydrate</b>			<b>1:1 4-P CA</b>	<b>2:1 4-P hydrate</b>
T/K	100	200	RT 300	100	200	RT 300	100	RT 293
Diffractionmeter	Rigaku Rapid	Rigaku Rapid	Rigaku Rapid	Rigaku Rapid	Rigaku Rapid	Rigaku Rapid	Rigaku Rapid	Rigaku Rapid
Formula	C <sub>9</sub> H <sub>8</sub> ClNO <sub>2</sub>	C <sub>9</sub> H <sub>8</sub> ClNO <sub>2</sub>	C <sub>9</sub> H <sub>8</sub> ClNO <sub>2</sub>	C <sub>21</sub> H <sub>19</sub> Cl <sub>3</sub> N <sub>2</sub> O <sub>7</sub>	C <sub>21</sub> H <sub>19</sub> Cl <sub>3</sub> N <sub>2</sub> O <sub>7</sub>	C <sub>21</sub> H <sub>19</sub> Cl <sub>3</sub> N <sub>2</sub> O <sub>7</sub>	C <sub>12</sub> H <sub>9</sub> Cl <sub>2</sub> NO <sub>4</sub>	C <sub>9</sub> H <sub>12</sub> ClNO <sub>2</sub>
M / g·mol <sup>-1</sup>	197.62	197.62	197.62	517.75	517.75	517.75	302.11	233.65
space group	P 2 <sub>1</sub> /c	P 2 <sub>1</sub> /c	P 2 <sub>1</sub> /c	P 1	P 1	P 1	P 2 <sub>1</sub> /n	P 2 <sub>1</sub> /n
a / Å	8.642(4)	8.668(4)	8.699(5)	7.167(3)	7.205(2)	7.257(6)	15.617(7)	7.268(9)
b / Å	9.687(4)	9.737(4)	9.795(5)	12.221(6)	12.267(4)	12.299(9)	4.819(2)	8.957(9)
c / Å	10.279(5)	10.376(5)	10.486(5)	13.381(7)	13.453(5)	13.5378(12)	16.300(7)	16.925(18)
α / °				71.414(16)	71.274(13)	71.11(3)		
β / °	102.08(2)	102.55(2)	103.09(2)	86.29(2)	86.638(16)	87.03(4)	90.270(17)	98.20(4)
γ / °				88.917(16)	89.577(13)	90.31(3)		
V / Å <sup>3</sup>	841.5(7)	854.8(7)	870.3(8)	1108.6(9)	1124.1(6)	1141.4(12)	1226.7(9)	1091(2)
Z	4	4	4	2	2	2	4	4
ρ <sub>calc</sub> / g·cm <sup>-3</sup>	1.560	1.535	1.508	1.551	1.530	1.506	1.636	1.423
μ / mm <sup>-1</sup>	0.414	0.408	0.400	0.461	0.454	0.448	0.538	0.344
θ range / °	3.199-30.494	3.190-30.504	3.179-30.487	3.138-27.477	3.119-27.483	3.098-27.498	3.605-27.481	3.237-27.362
refln (meas./ indep.)	8503/2566	8675/2613	8816/2647	13635/5070	14954/5150	14609/5186	15239/2812	5793/2435
R <sub>int</sub>	0.022	0.026	0.031	0.031	0.020	0.038	0.130	0.063
refln (obs. I>2σ(I))	2097	2035	1758	2997	3151	2558	989	920
completeness / %	99.9	99.8	99.8	99.7	99.7	98.5	99.8	98.4
data / restr. / param.	2562/0/142	2609/0/142	2647/0/143	5066/0/298	5150/0/298	5186/0/355	2812/0/172	1625/0/137
GooF on F <sup>2</sup>	0.9433	0.9201	1.0022	0.9462	0.9950	1.0276	1.1669	0.9429
R <sub>1</sub> (obs / all)	0.0394/0.0495	0.0371/0.0483	0.0419/0.0645	0.0371/0.0715	0.0342/0.0631	0.0362/0.0877	0.0365/0.0927	0.0668/0.1171
wR <sub>2</sub> (obs / all)	0.1183/0.1280	0.0962/0.0997	0.1035/0.1095	0.0707/0.1045	0.0513/0.0711	0.0787/0.1309	0.0598/0.1139	0.1401/0.1831
ρ (max / min) / e-Å <sup>-3</sup>	0.63/-0.44	0.32/-0.35	0.35/-0.35	0.64/-0.62	0.54/-0.47	0.61/-0.46	1.07/-0.90	0.85/-0.84
RMS / eÅ <sup>-3</sup>	0.010	0.08	0.06	0.12	0.05	0.05	0.10	0.10

**Table 9.3** X-ray refinement data of chloranilic acid (CA) and bromanilic acid (BA) complexes with picoline (P).

	2:1 4-P CA			2:1 2-P BA	2:1 3-P BA			2:1 4-P BA
T/K	100	200	RT 293	200	100	200	RT 293	RT 293
Diffractometer	Rigaku Rapid	Rigaku Rapid	Rigaku Rapid	Apex II	KappaCCD	KappaCCD	KappaCCD	Rigaku
Formula	C <sub>9</sub> H <sub>8</sub> ClNO <sub>2</sub>	C <sub>9</sub> H <sub>8</sub> ClNO <sub>2</sub>	C <sub>9</sub> H <sub>8</sub> ClNO <sub>2</sub>	C <sub>9</sub> H <sub>8</sub> BrNO <sub>2</sub>				
M / g-mol <sup>-1</sup>	197.62	197.62	197.62	242.07	242.07	242.07	242.07	242.07
space group	P 2 <sub>1</sub> /c	P 2 <sub>1</sub> /c	P 2 <sub>1</sub> /c	P 2 <sub>1</sub> /a	P 2 <sub>1</sub> /c	P 2 <sub>1</sub> /c	P 2 <sub>1</sub> /c	P 2 <sub>1</sub> /n
a / Å	7.952(5)	8.037(5)	8.192(5)	14.4697(3)	8.9567(2)	8.9682(2)	8.9877(2)	10.3629(10)
b / Å	6.126(3)	6.099(3)	6.099(2)	7.7602(2)	9.6191(3)	9.6690(3)	9.7222(3)	6.9785(10)
c / Å	17.658(8)	17.679(8)	17.721(9)	16.3645(5)	10.4275(3)	10.5115(3)	10.6082(3)	12.9325(10)
α / °								
β / °	96.73(3)	96.56(3)	96.259(19)	100.306(2)	103.8990(10)	104.265(2)	104.675(2)	99.162(10)
γ / °								
V / Å <sup>3</sup>	854.2(7)	861.0(7)	880.1(8)	1807.89(8)	872.08(4)	883.38(4)	896.71(4)	923.31(18)
Z	4	4	4	8	4	4	4	4
ρ <sub>calc</sub> / g-cm <sup>-3</sup>	1.537	1.524	1.491	1.779	1.844	1.820	1.793	1.741
μ / mm <sup>-1</sup>	0.408	0.405	0.396	4.510	4.675	4.615	4.547	4.416
θ range / °	3.263-27.460	3.246- 27.464	3.217-27.475	1.265-32.112	2.342-30.022	2.342-30.015	2.342-29.987	3.191-27.479
refln (meas./ indep.)	8250/1869	8586/1916	8757/1954	38236/6283	12194/2540	12638/2573	12674/2609	7597/2099
R <sub>int</sub>	0.064	0.027	0.027	0.112	0.059	0.066	0.064	0.039
refln (obs. I>2σ(I))	880	1012	779	2491	1931	1690	1371	1169
completeness / %	95.9	97.3	97.2	99.1	99.7	100	99.8	99.4
data / restr. / param.	1869/0/142	1916/0/142	1950/0/142	2491/0/235	2540/0/122	2573/0/119	2609/0/119	2099/0/119
GooF on F <sup>2</sup>	1.0420	1.0969	1.0563	0.9241	0.9183	0.9499	0.9799	0.9794
R <sub>1</sub> (obs / all)	0.0439/0.0931	0.0330/0.0750	0.0297/0.0978	0.0495/0.1612	0.0263/0.0428	0.0306/0.0626	0.0347/0.0939	0.0362/0.0732
wR <sub>2</sub> (obs / all)	0.0694/0.1062	0.0330/0.0539	0.0422/0.0844	0.0973/0.1270	0.0519/0.0617	0.0581/0.0771	0.0633/0.0924	0.0677/0.0978
ρ (max / min) / e-Å <sup>-3</sup>	0.68/-0.68	0.51/-0.49	0.56/-0.71	1.07/-0.95	0.85/-0.73	1.02/-0.88	0.97/-1.18	0.88/-0.96
RMS / eÅ <sup>-3</sup>	0.09	0.05	0.04	0.12	0.11	0.10	0.9	0.10

**Table 9.4** X-ray refinement data of chloranilic acid (CA) complexes with lutidine (L).

	2:1 2,3-L CA			2:1 2,4-L CA Form1	2:1 2,4-L CA Form2	2:1 2,5-L CA	2:1 2,6-L CA	2:1 3,4-L CA hydrate
T/K	100	200	300	100	100	100	RT?	100
Diffractionmeter	KappaCCD	KappaCCD	KappaCCD	Apex II	Apex II	KappaCCD	Apex II	Apex II
Formula	C <sub>10</sub> H <sub>10</sub> ClNO <sub>2</sub>	C <sub>10</sub> H <sub>12</sub> ClNO <sub>3</sub>						
M / g·mol <sup>-1</sup>	211.65	211.65	211.65	211.65	211.65	211.65	211.65	229.66
space group	P 1	P 1	P 1	P <i>bca</i>	P 1	P 2 <sub>1</sub> / <i>c</i>	P 2 <sub>1</sub> / <i>c</i>	P 2 <sub>1</sub> / <i>c</i>
a / Å	7.6107(10)	7.6285(9)	7.5912(8)	15.699(2)	9.4975(5)	8.0737(3)	7.2320(5)	10.036(2)
b / Å	8.2915(11)	8.4457(10)	8.5677(9)	7.5535(8)	10.0524(5)	11.4186(5)	9.2551(6)	7.6591(17)
c / Å	8.2915(11)	8.4637(11)	8.7312(9)	16.629(2)	11.2979(6)	10.3238(4)	14.8454(6)	13.948(3)
α / °	65.756(3)	64.525(3)	62.263(2)		68.260(3)			
β / °	80.550(3)	80.685(3)	86.979(3)		79.150(3)	100.566(2)	93.562(3)	99.620(14)
γ / °	88.331(3)	88.002(3)	80.919(3)		83.516(3)			
V / Å <sup>3</sup>	477.72(11)	485.42(10)	496.18(9)	1971.9(4)	982.91(9)	935.62(7)	991.73(10)	1057.0(4)
Z	1	1	1	8	4	4	4	4
ρ <sub>calc</sub> / g·cm <sup>-3</sup>	1.471	1.448	1.417	1.426	1.430	1.502	1.417	1.443
μ / mm <sup>-1</sup>	0.370	0.364	0.356	0.359	0.360	0.378	0.356	0.347
θ range / °	2.689-36.306	2.673-36.178	2.636-36.242	2.450-30.637	1.965-24.542	2.566-29.985	3.523-30.082	2.058-26.475
refln (meas./ indep.)	8128/4385	8278/4455	7444/4370	25213/3033	20376/3256	13445/2716	19299/2811	9752/2162
R <sub>int</sub>	0.014	0.011	0.009	0.041	0.030	0.073	0.086	0.038
refln (obs. I>2σ(I))	3862	3526	1731	1863	2302	1633	1326	1369
completeness / %	94.9	95.7	91.0	99.5	99.2	99.7	96.4	99.2
data / restr. / param.	4385/0/127	4447/0/154	2011/0/157	3033/0/127	3256/0/253	2716/0/128	1326/0/127	2162/0/136
GooF on F <sup>2</sup>	0.8796	0.9602	1.0644	1.0000	0.9521	0.9563	0.9848	1.0358
R <sub>1</sub> (obs / all)	0.0280/0.0327	0.0356/0.0463	0.0327/0.0382	0.0358/0.0587	0.0315/0.0459	0.0361/0.0778	0.0890/0.1942	0.0384/0.0653
wR <sub>2</sub> (obs / all)	0.0695/0.0747	0.0952/0.0989	0.0825/0.0843	0.0788/0.1144	0.0684/0.0866	0.0737/0.1025	0.1187/0.1479	0.0824/0.1175
ρ (max / min) / e-Å <sup>-3</sup>	0.54/-0.26	0.49/-0.32	0.19/-0.19	0.54/-0.45	0.38/-0.30	0.73/-0.70	0.59/-0.67	0.52/-0.55
RMS / eÅ <sup>-3</sup>	0.06	0.05	0.04	0.08	0.05	0.07	0.07	0.06

**Table 9.5** X-ray refinement data of chloranilic acid (CA) complexes with lutidine (L) and other pyridine related molecules.

	<b>2:1 3,5-L CA hydrate</b>	<b>Pyridinium CA</b>	<b>2:1 Caffeine CA</b>	<b>Sulfathiazole CA acetonitrile</b>	<b>3,5-Dimethylpyrazol Hydrate CA</b>	<b>1:1 Isonicotinic acid CA hydrate</b>	<b>2:1 2-picolic acid CA</b>	<b>1:1 2-acetylpyridine CA</b>
T/K	100	100	100	100	100	100	100	100
Diffractionmeter	Apex II	KappaCCD	Apex II	KappaCCD	KappaCCD	Apex II	KappaCCD	Apex II
Formula	C <sub>20</sub> H <sub>26</sub> Cl <sub>2</sub> N <sub>2</sub> O <sub>7</sub>	C <sub>8</sub> H <sub>6</sub> ClNO <sub>2</sub>	C <sub>14</sub> H <sub>12</sub> Cl <sub>2</sub> N <sub>4</sub> O <sub>6</sub>	C <sub>14</sub> H <sub>13</sub> Cl <sub>1</sub> N <sub>4</sub> O <sub>4</sub> S <sub>2</sub>	C <sub>8</sub> H <sub>11</sub> ClN <sub>2</sub> O <sub>3</sub>	C <sub>12</sub> H <sub>9</sub> Cl <sub>2</sub> NO <sub>7</sub>	C <sub>9</sub> H <sub>7</sub> Cl <sub>2</sub> NO <sub>4</sub>	C <sub>13</sub> H <sub>9</sub> Cl <sub>2</sub> NO <sub>5</sub>
M / g-mol <sup>-1</sup>	477.34	183.59	403.18	400.86	218.64	350.11	228.61	330.12
space group	P 2 <sub>1</sub> /n	P 2 <sub>1</sub> /c	P1	P 1	P1	P 2 <sub>1</sub> /n	P 2 <sub>1</sub> /c	P 2 <sub>1</sub> /n
a / Å	10.5990(5)	3.7090(2)	4.7862(10)	9.0519(18)	7.1258(6)	13.0245(9)	13.9493(12)	8.5878(15)
b / Å	17.7196(9)	19.5761(16)	8.7615(19)	10.496(2)	8.9965(7)	7.5136(5)	5.0323(5)	13.558(2)
c / Å	12.2885(6)	9.9005(7)	19.185(5)	10.886(2)	8.9813(5)	13.7042(10)	14.5270(11)	12.1735(19)
α / °			89.791(15)	117.64(3)	119.471(4)			
β / °	108.688(2)	97.033(4)	83.581(15)	92.43(3)	93.757(5)	94.475(3)	118.350(4)	110.293(6)
γ / °			78.522(17)	111.61(3)	99.037(3)			
V / Å <sup>3</sup>	2186.23(19)	713.44(9)	783.3(3)	822.9(3)	488.17(7)	1337.02(16)	897.45(14)	1329.5(4)
Z	4	4	2	2	2	4	4	4
ρ <sub>calc</sub> / g-cm <sup>3</sup>	1.450	1.709	1.709	2.487	0.374	1.739	1.692	1.649
μ / mm <sup>-1</sup>	0.342	0.481	0.459	1.304	1.487	0.523	0.417	0.509
θ range / °	2.093-26.371	2.081- 29.992	1.068-26.491	2.19-27.00	2.627- 29.988	2.078- 28.092	1.659- 35.062	2.332- 25.373
refln (meas./ indep.)	21889/4459	5916/ 2059	14536/3188	16160//3598	3719/3719	13944/ 3134	17556/3908	12620/2436
R <sub>int</sub>	0.025	0.053	0.039	0.120	0.033	0.030	0.053	0.029
refln (obs. I>2σ(I))	2394	1363	1828	2134	2009	2511	2011	1673
completeness / %	99.8	98.8	98.9	99.9	84.7	96.5	98.8	99.5
data / restr. / param.	4459/0/280	2059/0/109	3188/0/235	3598/0/220	2406/0/127	3134/0/199	2011/0/136	2423/0/214
Goof on F <sup>2</sup>	0.9745	0.9334	1.0076	0.958	0.9330	0.8643	0.9130	0.9216
R <sub>1</sub> (obs / all)	0.0348/0.0766	0.0518/ 0.0904	0.0394/0.0809	0.1244/0.0582	0.0506/ 0.0628	0.0282/0.0358	0.0434/0.1093	0.0292/ 0.0482
wR <sub>2</sub> (obs / all)	0.0744/0.1114	0.1125/ 0.1409	0.0890/0.1316	0.1743/0.1379	0.1040/ 0.1087	0.0690/0.0794	0.0961/0.1222	0.0649/ 0.0842
ρ (max / min) / e-Å <sup>-3</sup>	0.66/-0.64	1.04/-0.94	1.21/-0.80	0.458/-0.531	0.62/-0.47	0.45/-0.38	0.49/-0.58	0.50/- 0.51
RMS / eÅ <sup>-3</sup>	0.11	0.10	0.08	0.09	0.07	0.06	0.06	0.07

**Table 9.6** Xray refinement data chloranilic acid (CA) complexes with pyridine related molecules.

	<b>2:1 2-acetylpyridine CA</b>		<b>2:1 3-acetylpyridine CA</b>	<b>2:1 4-acetylpyridine CA</b>			<b>2:1 pyridine-3-aldehyde</b>	
T/K	100	200	100	100	200	RT 293	100	200
Diffractionmeter	Rigaku Rapid	Apex II	Apex II					
Formula	C <sub>10</sub> H <sub>8</sub> ClNO <sub>3</sub>	C <sub>9</sub> H <sub>8</sub> ClNO <sub>3</sub>	C <sub>9</sub> H <sub>8</sub> ClNO <sub>3</sub>					
M / g-mol <sup>-1</sup>	225.63	225.63	225.63	225.63	225.63	225.63	211.60	211.60
space group	C2/c	C2/c	P 2 <sub>1</sub> /c	P 2 <sub>1</sub> /n	P 2 <sub>1</sub> /n	P 2 <sub>1</sub> /n	P 2 <sub>1</sub> /n	P 2 <sub>1</sub> /n
a / Å	26.836(9)	27.055(9)	12.576(3)	10.844(15)	10.867(3)	10.900(2)	3.8206(2)	3.8671(2)
b / Å	4.6718(13)	4.6621(13)	5.0260(10)	7.385(6)	7.3705(18)	7.3808(15)	19.0607(12)	19.0999(11)
c / Å	18.004(7)	18.311(7)	18.380(4)	12.875(14)	12.941(4)	13.018(3)	11.3866(7)	11.3703(6)
α / °								
β / °	119.970(11)	120.430(11)	126.51(3)	111.100(13)	110.632(12)	109.85(3)	94.153(3)	94.247(2)
γ / °								
V / Å <sup>3</sup>	1955.4(11)	1991.5(11)	933.8(5)	961.9(19)	970.1(5)	985.1(4)	827.03(8)	837.52(8)
Z	8	8	4	4	4	4	4	4
ρ <sub>calc</sub> / g-cm <sup>-3</sup>	1.533	1.505	1.605	1.558	1.545	1.521	1.699	1.678
μ / mm <sup>-1</sup>	0.374	0.368	0.392	0.381	0.377	0.372	0.436	0.431
θ range / °	3.156-27.483	3.119-27.481	3.260- 27.419	3.064- 27.443	3.036-27.478	2.993-27.487	2.087-27.509	2.089-27.568
refln (meas./ indep.)	20749/2234	20943/2266	13483/ 2115	44486/2188	21250/2218	21217/2257	8552/1867	8673/1892
R <sub>int</sub>	0.065	0.029	0.085	0.018	0.017	0.034	0.023	0.021
refln (obs. I>2σ(I))	1102	1065	600	1789	1797	1123	1679	1670
completeness / %	99.7	99.6	98.8	99.9	100	99.9	99.3	98.6
data / restr. / param.	2231/0/157	2263/0/136	2115/0/136	2182/0/157	2212/0/160	2250/0/160	1867/0/127	1892/0/127
GooF on F <sup>2</sup>	1.7095	1.7397	1.0321	0.9526	0.9371	0.7591	0.9088	0.8989
R <sub>1</sub> (obs / all)	0.0321/ 0.0704	0.0348/0.0750	0.0574/ 0.1662	0.0241/ 0.0285	0.0255/0.0303	0.0233/0.0445	0.0253/0.0281	0.0264/0.0298
wR <sub>2</sub> (obs / all)	0.0697/ 0.0817	0.0483/0.0941	0.1501/ 0.2791	0.0595/ 0.0602	0.0640/0.0649	0.0577/0.0689	0.0622/0.0653	0.0679/0.0729
ρ (max / min) / e-Å <sup>-3</sup>	0.65/-0.52	0.55/-0.56	0.98/-1.17	0.43/-0.20	0.38/-0.21	0.28/-0.24	0.40/-0.40	0.36/-0.30
RMS / eÅ <sup>-3</sup>	0.08	0.07	0.10	0.05	0.04	0.05	0.07	0.06

**Table 9.7** X-ray refinement data 2,4- and 2,5- dihydroxybenzoic acid.

	2,4-dihydroxybenzoic acid				2,5-dihydroxybenzoic acid			
T/K	90	100	120	150	100	150	200	350
Diffractionmeter	KappaCCD							
Formula	C <sub>7</sub> H <sub>6</sub> O <sub>4</sub>							
M / g·mol <sup>-1</sup>	154.00	154.00	154.00	154.00	154.00	154.00	154.00	154.00
space group	P 2 <sub>1</sub> /n							
a / Å	3.6686(5)	3.6721(5)	3.6742(5)	3.6854(5)	5.5591(2)	5.5751(2)	5.5929(3)	5.6491(3)
b / Å	22.333(3)	22.341(3)	22.341(3)	22.367(3)	4.8698(2)	4.8787(2)	4.8891(2)	4.9306(3)
c / Å	8.0046(11)	8.0070(10)	8.0065(10)	8.0085(11)	23.3593(9)	23.4030(9)	23.4513(9)	23.6191(11)
α / °								
β / °	99.630(3)	99.602(3)	99.567(3)	99.448(3)	93.448(2)	93.223(2)	92.978(2)	92.277(3)
γ / °								
V / Å <sup>3</sup>	646.58(15)	647.68(14)	648.08(15)	651.20(15)	631.23(4)	635.54(4)	640.39(5)	657.35(6)
Z	4	4	4	4	4	4	4	4
ρ <sub>calc</sub> / g·cm <sup>-3</sup>	1.583	1.580	1.580	1.572	1.622	1.611	1.598	1.557
μ / mm <sup>-1</sup>	0.133	0.132	0.132	0.132	0.136	0.135	0.134	0.130
θ range / °	1.824-33.819	1.823-33.036	1.823-33.090	1.821-33.070	1.747-27.565	1.743-30.014	1.739-30.152	1.726-30.083
refln (meas./ indep.)	5720/2022	7808/1964	7722/1963	7557/1933	1463/1463	13345/1850	13366/1864	10330/1839
R <sub>int</sub>	0.047	0.040	0.036	0.036	0.080	0.076	0.078	0.102
refln (obs. I>2σ(I))	1301	1139	1139	1059	847	729	684	597
completeness / %	77.5	79.4	79.4	77.8	99.7	99.7	98.7	95.9
data / restr. / param.	2019/0/107	1963/0/106	1963/0/106	1933/0/106	1463/0/120	1287/0/120	1297/0/124	1336/0/124
GooF on F <sup>2</sup>	0.9636	0.9453	0.9458	1.0324	0.9784	0.0937	1.0558	1.0377
R <sub>1</sub> (obs / all)	0.0541/0.1132	0.0509/0.1047	0.0508/0.1046	0.0540/0.1162	0.0391/0.0739	0.0368/0.0718	0.0398/0.0817	0.0469/0.1109
wR <sub>2</sub> (obs / all)	0.0976/0.1317	0.1046/0.1228	0.1044/0.1226	0.1132/0.1404	0.0994/0.1302	0.0930/0.1302	0.1044/0.1469	0.1253/0.1878
ρ (max / min) / e-Å <sup>-3</sup>	0.71/-0.83	0.81/-0.76	0.82/-0.76	0.77/-0.72	0.52/-0.52	0.51/-0.55	0.43/-0.52	0.46/-0.50
RMS / eÅ <sup>-3</sup>	0.0.8	0.08	0.08	0.07	0.08	0.08	0.07	0.07

**Table 9.8** X-ray refinement data isonicotinamidium formate and neutron refinement data for 2,4-lutidine chloranilic acid from VIVALDI, ILL.

	Isonicotinamidium Formate						2,4-lutidine CA 2:1 F1
T/K	100	150	170	200	300	T/K	40
Diffractionmeter						Diffractionmeter	VIVALDI
Formula	C <sub>7</sub> H <sub>8</sub> N <sub>2</sub> O <sub>3</sub>	C <sub>7</sub> H <sub>8</sub> N <sub>2</sub> O <sub>3</sub>	C <sub>7</sub> H <sub>8</sub> N <sub>2</sub> O <sub>3</sub>	C <sub>7</sub> H <sub>8</sub> N <sub>2</sub> O <sub>3</sub>	C <sub>7</sub> H <sub>8</sub> N <sub>2</sub> O <sub>3</sub>	Formula	C <sub>10</sub> H <sub>10</sub> ClNO <sub>2</sub>
M / g·mol <sup>-1</sup>	168.15	168.15	168.15	168.15	168.15	M / g·mol <sup>-1</sup>	211.65
space group	P 2 <sub>1</sub> /c	space group	P bca				
a / Å	3.7048(2)	3.7262(3)	3.7348(3)	3.7511(3)	3.8147(15)	a / Å	15.699(2)
b / Å	27.3246(17)	27.3394(19)	27.3514(19)	27.368(2)	27.492(10)	b / Å	7.5533(8)
c / Å	7.4741(5)	7.4897(5)	7.4965(5)	7.5084(6)	7.568(3)	c / Å	16.279(2)
α / °						α / °	
β / °	96.704(5)	96.433(5)	96.305(5)	96.091(5)	94.95(3)	β / °	
γ / °						γ / °	
V / Å <sup>3</sup>	751.45(8)	758.19(10)	761.15(10)	766.47(10)	790.7(5)	V / Å <sup>3</sup>	1930.4(4)
Z	4	4	4	4	4	Z	8
ρ <sub>calc</sub> / g·cm <sup>-3</sup>	1.486	1.473	1.467	1.457	1.412	ρ <sub>calc</sub> / g·cm <sup>-3</sup>	1.455
μ / mm <sup>-1</sup>	0.118	0.117	0.117	0.116	0.112	μ / mm <sup>-1</sup>	0.001
θ range / °	2.844-30.544	2.836-30.464	2.833-30.509	1.488-30.502	2.801-30.484	λ range / Å	3.24-27.53
refln (meas./ indep.)	8135/2184	8194/1885	8247/2195	8295/2210	8493/2257	refln (meas./ indep.)	13208/1602
R <sub>int</sub>	0.030	0.028	0.036	0.026	0.030	R <sub>int</sub>	0.2535
refln (obs. I>2σ(I))	1437	1038	1023	985	752	refln (obs. I>2σ(I))	1191
completeness / %	94.3	94.3	94.0	94.0	93.3	completeness / %	72.22
data / restr. / param.	2184/0/109	1548/0/109	1554/0/109	1562/0/109	1611/0/109	data / restr. / param.	1602/0/218
GooF on F <sup>2</sup>	0.9168	0.7809	0.7533	0.9640	0.9423	GooF on F <sup>2</sup>	1.214
R <sub>1</sub> (obs / all)	0.0652/ 0.1072	0.0540/0.0864	0.0539/0.0863	0.0546/0.0937	0.0556/0.1311	R <sub>1</sub> (obs / all)	0.1002/0.1629
wR <sub>2</sub> (obs / all)	0.1463/ 0.1670	0.1311/0.1468	0.1289/0.1437	0.1253/0.1463	0.1343/0.1881	wR <sub>2</sub> (obs / all)	0.2077/0.1887
ρ (max / min) / e·Å <sup>-3</sup>	0.68/ -0.65	0.46/-0.41	0.41/-0.42	0.39/-0.45	0.39/-0.41	ρ (max/min) / fm·Å <sup>-3</sup>	0.099/-0.097
RMS / eÅ <sup>-3</sup>	0.09	0.08	0.08	0.07	0.06	RMS / fmÅ <sup>-3</sup>	0.02

**Table 9.9** Neutron refinement data for 2,4- and 2,5- dihydroxybenzoic acid and Isonicotinamidium formate.

	2,4-dihydroxybenzoic acid			2,5-dihydroxybenzoic acid			Isonicotinamidium formate	
T/K	20	90	150	20	100		40	100
Diffractionmeter	SXD ISIS	SXD ISIS						
Formula	C <sub>7</sub> H <sub>6</sub> O <sub>4</sub>	C <sub>7</sub> H <sub>8</sub> N <sub>2</sub> O <sub>3</sub>	C <sub>7</sub> H <sub>8</sub> N <sub>2</sub> O <sub>3</sub>					
M / g·mol <sup>-1</sup>	154.00	154.00	154.00	154.00	154.00	154.00	168.15	168.15
space group	P 2 <sub>1</sub> /n	P 2 <sub>1</sub> /c	P 2 <sub>1</sub> /c					
a / Å	3.656(2)	3.669(2)	3.686(2)	5.545(3)	5.564(3)	5.597(3)	3.7070(4)	3.669(2)
b / Å	22.329(11)	22.3473(12)	22.368(13)	4.877(3)	4.879(3)	4.897(3)	27.430(4)	22.3473(12)
c / Å	8.009(4)	8.012(4)	8.015(4)	23.3506(11)	23.3903(11)	23.470(13)	7.5060(10)	8.012(4)
α / °								
β / °	99.76(4)	99.63(4)	99.44(4)	93.62(3)	93.43(3)	92.97(4)	96.850(5)	99.63(4)
γ / °								
V / Å <sup>3</sup>	644.4(6)	647.7(5)	651.9(7)	630.1(5)	633.8(5)	642.4(6)	757.78(17)	647.7(5)
Z	4	4	4	4	4	4	4	4
ρ <sub>calc</sub> / g·cm <sup>-3</sup>	0.066	0.053	0.035	0.094	0.061	0.038	1.474	1.579
μ / mm <sup>-1</sup>								
λ range / Å	0.6947-7.5466	0.696-7.4735	0.6984-7.588	0.6956-6.9615	0.6929-6.9613	0.697-6.9583	0.6959-6.9103	0.6992-6.9057
refln (meas./ indep.)	8839/8839	5840/5840	4920/4920	8671/8671	8723/8723	8249/8249	4416/4416	5840/5840
R <sub>int</sub>								
refln (obs. I>2σ(I))	8839	5840	4920	8671	8723	8249	4416	5840
completeness / %								
data / restr. / param.	8839/0/264	5840/0/242	4920/0/242	8671/0/263	8723/0/ 264	8249/0/286	4416/0/269	5840/0/242
Goof on F <sup>2</sup>	1.048	1.013	1.047	1.429	1.058	0.978	1.109	1.013
R <sub>1</sub> (obs / all)	0.0789/0.0789	0.0813/0.0813	0.0744/0.0744	0.0927/0.0927	0.0796/0.0796	0.0815/0.0815	0.0764/0.0764	0.0813/0.0813
wR <sub>2</sub> (obs / all)	0.2129/0.2129	0.2226/0.2226	0.1931/0.1931	0.2903/ 0.2903	0.2251/ 0.2251	0.2300/0.2300	0.2182/0.2182	0.2226/0.2226
ρ (max/min) / fm-Å <sup>-3</sup>	0.496/-0.322	0.333/-0.211	0.187/-0.135	0.708 /-0.468	0.452/ -0.265	0.305/ -0.168	3.092/ -3.011	0.333/-0.211
RMS / fmÅ <sup>-3</sup>	0.07	0.05	0.04	0.08	0.06	0.04	0.66	0.53

**Table 9.10** Neutron refinement data for Isonicotinamidium formate, 2-Iodoanilinium Picrate and Malonic acid.

	Isonicotinamidium formate		2-Iodoanilinium Picrate			Malonic acid		
T/K	150	200	300	310	320	75	140	200
Diffractionmeter	SXD ISIS	SXD ISIS	SXD ISIS	SXD ISIS	SXD ISIS	SXD ISIS	SXD ISIS	SXD ISIS
Formula	C <sub>7</sub> H <sub>8</sub> N <sub>2</sub> O <sub>3</sub>	C <sub>7</sub> H <sub>8</sub> N <sub>2</sub> O <sub>3</sub>	C <sub>12</sub> H <sub>9</sub> IN <sub>4</sub> O <sub>7</sub>	C <sub>12</sub> H <sub>9</sub> IN <sub>4</sub> O <sub>7</sub>	C <sub>12</sub> H <sub>9</sub> IN <sub>4</sub> O <sub>7</sub>	C <sub>3</sub> H <sub>4</sub> O <sub>4</sub>	C <sub>3</sub> H <sub>4</sub> O <sub>4</sub>	C <sub>3</sub> H <sub>4</sub> O <sub>4</sub>
M / g·mol <sup>-1</sup>	168.15	168.15	374.03	374.03	374.03	104.00	104.00	104.00
space group	P 2 <sub>1</sub> /c	P 2 <sub>1</sub> /c				P1	P1	P1
a / Å	3.7330(4)	3.7754(4)	7.345(4)	7.339(5)	7.349(5)	5.3300(10)	5.3360(10)	5.3310(10)
b / Å	27.442(4)	27.479(4)	8.272(3)	8.268(5)	8.323(5)	5.1620(10)	5.1650(10)	5.1650(10)
c / Å	7.5213(10)	7.5499(10)	13.688(8)	13.696(10)	13.707(6)	11.2390(10)	11.2500(10)	11.2600(10)
α / °			75.84(3)	75.73(4)	75.75(4)	103.450(10)	103.260(10)	103.130(10)
β / °	96.605(5)	95.974(5)	74.15(4)	74.06(4)	74.04(4)	136.410(10)	136.150(10)	135.750(10)
γ / °			75.72(3)	75.66(4)	75.69(4)	84.590(10)	84.760(10)	84.770(10)
V / Å <sup>3</sup>	765.38(17)	778.99(17)	761.2(7)	759.9(9)	766.7(8)	206.09(6)	207.80(6)	209.52(6)
Z	4	4	2	2	2	2	2	2
ρ <sub>calc</sub> / g·cm <sup>-3</sup>	1.459	1.434	1.632	1.635	1.620	1.676	1.662	1.649
μ / mm <sup>-1</sup>								
θ range / °	0.7039-6.8457	0.7032-6.9215	0.6981-6.958	0.7007-6.9061	0.698-6.9556	0.6942-6.8114	0.697-6.8265	0.698-6.8376
refln (meas./ indep.)	3074/3074	2823/ 2823	7882/7882	2575/2575	5489/ 5489	3589/3589	1663/1663	2191/ 2191
R <sub>int</sub>								
refln (obs. I>2σ(I))	3074	2823	7882	2575	5489	3589	1663	2191
completeness / %								
data / restr. / param.	3074/0/258	2823/0/247	7882/0/408	2575/0/408	5489/0/408	3589/0/ 211	1663/0/210	2191/0/211
GooF on F <sup>2</sup>	1.047	1.372	1.001	1.133	1.308	1.220	1.466	1.788
R <sub>1</sub> (obs / all)	0.0787/0.0787	0.0796/0.0801	0.0708/0.0708	0.1061/0.1061	0.0930/ 0.0932	0.0697/ 0.0697	0.2280/0.2280	0.1701/ 0.1701
wR <sub>2</sub> (obs / all)	0.2293/0.2293	0.2592/0.2607	0.1919/0.1919	0.2707/0.2707	0.2687/ 0.2696	0.2494/0.2494	0.3003/ 0.3003	0.3749/ 0.3749
ρ (max/min) / fm-Å <sup>-3</sup>	1.897/-2.198	1.672/-1.580	1.034/ -0.808	1.122/-0.811	2.124/ -1.435	0.303/ -0.206	0.175/-0.127	0.348/ -0.243
RMS / fmÅ <sup>-3</sup>	0.51	0.40	0.20	0.21	0.52	0.04	0.03	0.06

## References

- 1 L. Pauling, *J. Am. Chem. Soc.* **1931**, 53, 137-1400.
- 2 W. M. Latimer and W. H. Rodebush, *J. Am. Chem. Soc.* **1920**, 42, 1419-1423.
- 3 M. L. Huggins, *J. Phys. Chem.* **1922**, 26, 601-625.
- 4 G. A. Jeffrey, *An Introduction to Hydrogen Bonding*; Oxford University Press, Oxford, **1997**.
- 5 T. S. G. R. Desiraju, *The Weak Hydrogen Bond in Structural Chemistry and Biology*; Oxford University Press, Oxford, **1999**.
- 6 J. Gaultier and C. Hauw, *Acta Cryst.* **1969**, B25, 546-548.
- 7 S. Eppel, and J. Bernstein, *Acta Cryst.* **2008**, B64, 50-56.
- 8 I. Rozas, I. Alkorta, and J. Elguero, *J. Phys. Chem* **1998**, 102, 9925-9932.
- 9 R. D. Parra, S. Bulusu and X. C. Zeng, *J. Chem. Phys.* **2005**, 122, 184325.
- 10 K. A. Lyssenko, D. V. Lyubetsky, A. B. Sheremetev and M. Yu. Antipin, *Russian Chem. Bull. Int. Ed.* **2005**, 54, 924-932.
- 11 H. Dadon and J. Bernstein, *J. Inorg. Chem.* **1997**, 36, 2898-2900.
- 12 P. A. Giguere, *J. Chem. Phys.* **1987**, 87, 4835-4839.
- 13 J. Sponer, and P. Hobza, *J. Am. Chem. Soc.* **1994**, 116, 709-714.
- 14 M. Meyer, M. Brandl and J. Suhnel, *J. Phys. Chem. A* **2001**, 105, 8223-8225.
- 15 J. Gaultier and Hauw, *Acta Cryst.* **1969**, B25, 546-548.
- 16 R. E. Banks, R. A. DuBoisson, R. G. Pritchard, and A. E. Tipping, *Acta Cryst.* **1995**, C51, 1427-1429.
- 17 J. L. Balderson, M. A. Fernandes, J. P. Michael, and C. B. Perry, *Acta Cryst.* **2007**, C63, o734-o738.
- 18 A. Parkin, M. Adam, R. I. Cooper, D. S. Middlemiss, and C. C. Wilson, *Acta Cryst.* **2007**, B63, 303-308.
- 19 P. Gilli, V. Bertolasi, L. Pretto, V. Ferretti and G. Gilli, *J. Am. Chem. Soc.* **2004**, 126, 3845-3855.
- 20 P. Gilli, V. Bertolasi, L. Pretto, and G. Gilli, *J. Mole. Struct.* **2006**, 790, 40-49.
- 21 T. Steiner, I. Majerz, and C. C. Wilson, *Angew. Chem. Int. Ed.* **2001**, 40, 2651-2654.
- 22 A. Parkin, S. M. Harte, A. E. Goeta, and C. C. Wilson, *New. J. Chem.* **2004**, 28, 718-721.
- 23 C. C. Wilson and A. E. Goeta, *Angew. Chem. Int. Ed.* **2004**, 43, 2095-2099.

- <sup>24</sup> C. C. Wilson, K. Shankland, N. Shankland, *Z. Kristallogr.* **2001**, *216*, 303-306.
- <sup>25</sup> V. Thalladi, B. S. Goud, V. J. Hoy, F. H. Allen, J. A. K. Howard and G. R. Desiraju, *Chem. Commun.* **1996**, 401-402.
- <sup>26</sup> P. Vishweshwar, A. Nangia and V. M. Lynch, *Cryst. Eng. Comm.* **2003**, *5*, 164-168.
- <sup>27</sup> N. Shan, A. D. Bond and W. Jones, *Tetrahed. Lett.* **2002**, *43*, 3101-3104.
- <sup>28</sup> A. C. B. Aakeroy and A. M. Beatty, *Aust. J. Chem.* **2001**, *54*, 409-421.
- <sup>29</sup> H. Li, M. Eddaoudi, M. O'Keeffe and O. M. Yaghi, *Nature* **1999**, *402* 276-279.
- <sup>30</sup> O. M. Yaghi, G. Li, and H. Li, *Nature* **1995**, *378*, 703-706.
- <sup>31</sup> K. Eda and Y. Iriki, *Chemistry Letters* **2005**, *34*, 612-613.
- <sup>32</sup> S. Upreti, and A. Ramanan, *Cryst. Growth Des.* **2006**, *6*, 2066-2071.
- <sup>33</sup> G. M. Day, W. D. S. Motherwell, H. L. Ammon, S. X. M. Boerrigter, R. G. Della Valle, E. Venuti, A. Dzyabchenko, J. D. Dunitz, B. Schweizer, B. P. van Eijck, P. Erk, J. C. Facelli, V. E. Bazterra, M. B. Ferraro, D. W. M. Hofmann, F. J. J. Leusen, C. Liang, C. C. Pantelides, P. G. Karamertzanis, S. L. Price, T. C. Lewis, H. Nowell, A. Torrisi, H. A. Scheraga, Y. A. Arnautova, M. U. Schmidt, and P. Verwer, *Acta Cryst.* **2005**, *B61*, 511-527.
- <sup>34</sup> B. P. van Eijck, *Acta Cryst.* **2005**, *B61*, 528-535.
- <sup>35</sup> C. B. Aakeroy, B. M. T. Scott, and J. Desper, *New. J. Chem.* **2007**, *31*, 2044-2051.
- <sup>36</sup> Md. B. Zaman, M. Tomura, Y. Yamashita, *J. Org. Chem.* **2001**, *66*, 5987-5995.
- <sup>37</sup> H. Ishida, and S. Kashino, *Z. Naturforsch.* **2002**, *57a*, 829-836.
- <sup>38</sup> Md. K. Kabir, H. Tobita, H. Matsuo, K. Nagayoshi, K. Yamada, Keiichi Adachi, Y. Sugiyama, S. Kitagawa and S. Kawata, *Crystal Growth & Design* **2003**, *3*, 791-798.
- <sup>39</sup> Md. B. Zaman, M. Tomura, Y. Yamashita, *Chem. Commun.* **1999**, 999-1000.
- <sup>40</sup> Md. B. Zaman, M. Tomura, Y. Yamashita, *J. Org. Chem.* **2001**, *66*, 5987-5995.
- <sup>41</sup> C. I. Beristain, A. Vazquez, H. S. Garcia, and E. J. Vernon-Carter, *Lebensm.-Wiss. u-Technol.* **1996**, *29*, 645-647.
- <sup>42</sup> A. D. Bond, *Chem. Commun.* **2003**, *2*, 250-251.
- <sup>43</sup> PolySNAP: G. Barr, W. Dong and C. J. Gilmore, *J. Appl. Cryst.* **2004**, *37*, 658-664.
- <sup>44</sup> Clegg, W. *Crystal Structure Determination*; Oxford Science Publications, **1998**; Oxford Science Publications Vol. 60.

- 45 Wilson, C. C. *Single Crystal Neutron Diffraction From Molecular Crystals*;  
World Scientific, **2000**.
- 46 W. C. Röntgen, *Nature* **1896**, 53, 274-276.
- 47 D. Sherwood, *Crystals X-rays and Proteins*; Longman Group Limited, 1976.
- 48 W. H. Bragg and W. L. Bragg, *Proc. Royal Soc. Lon. A* **1913**, 88, 428.
- 49 Wm. Bragg, *Nature* **1923**, 111, iii-x.
- 50 D. Watkin, *J. Appl. Cryst.* **2008**, 41, 491-522.
- 51 H. M. Rietveld, *Acta Cryst.* **1966**, 22, 151-152.
- 52 H. M. Rietveld, *J. Appl. Cryst.* **1969**, 2, 65-71.
- 53 CRYSTAL 2003: V. R. Saunders, R. Dovesi, C. Roetti, R. Orlando, C. M.  
Zicovich-Wilson, N. M. Harrison, K. Doll, B. Civalleri, I. J. Bush, Ph. D'Arco,  
M. Llunell
- 54 CASTEP: S. J. Clark, M. D Segall, C. J. Pickard, P. J. Hasnip, M. J. Probert, K.  
Refson, M. C. Payne *Z. Kristallogr.* **2005**, 220, 567-570.
- 55 W. Koch, and M. C. Holthausen, *A Chemist's Guide to Density Functional  
Theory*; WILEY-VCH, **1999**.
- 56 F. H. Allen, *Acta Cryst.* **2002**, B58, 380-388.
- 57 Bruker AXS: EVA, Powder diffraction evaluation program
- 58 Nonius Kappa-CCD Four circle diffractometer. Nonius BV, Delft, The  
Netherlands. <http://www.nonius.nl/products/sms/kappa/>
- 59 APEX2: Bruker AXS, **2007**.
- 60 CRYSTALCLEAR: Rigaku/MSK 2006.
- 61 SHELXL/SHELXS: G. M. Sheldrick, *Acta Cryst.* **2008**, A64, 112-122.
- 62 WINGX/MAPVIEW: L. J. Farrugia *J. Appl. Cryst.* **1999**, 32, 837-838.
- 63 P. W. Betteridge, J. R. Carruthers, R. I. Cooper, K. Prout, and D. J. Watkin, *J.  
Appl. Cryst.* **2003**, 36, 1487.
- 64 SIR97: A NEW PROGRAM FOR SOLVING AND REFINING CRYSTAL  
STRUCTURES A. Altomare, M. C. B., M. Camalli, G. Cascarano, C.  
Giacovazzo, A. Guagliardi, A. G. G. Moliterni, G. Polidori, R. Spagna.
- 65 <http://www.isis.rl.ac.uk/>.
- 66 <http://www.ill.eu/>.
- 67 D. A. Keen, M. J. Gutmann, C. C. Wilson, *J. Appl. Cryst.* **2006**, 39, 714-722.

- 68 MERCURY: C. F. Macrae, P. R. Edgington, P. McCabe, E. Pidcock, G. P. Shields, R. Taylor, M. Towler, J. van de Streek, *J. Appl. Cryst.* **2006**, *39*, 453-457.
- 69 XP: Bruker AXS **2000**.
- 70 MCE- Marching Cubes ELD Rohlicek J, Husak M, *J. Appl. Cryst.* **2007**, *40*, 600
- 71 CrystalExplorer 1.5.1 S.K. Wolff, D.J. Grimwood, J.J. McKinnon, D. Jayatilaka, M. A. Spackman
- 72 ChemSketch ACD/Labs 8.00 Release. May 2005
- 73 Universal Analysis 2000 TA Instruments
- 74 dSNAP: G. Barr, W. Dong, C. J. Gilmore, A. Parkin and C. C. Wilson, *J. Appl. Cryst.* **2005**, *38*, 838-841.
- 75 M. J. Frisch, G. W. Trucks, H. B. Schlegel, G. E. Scuseria, M. A. Robb, J. R. Cheeseman, J. A. Montgomery, Jr., T. Vreven, K. N. Kudin, J. C. Burant, J. M. Millam, S. S. Iyengar, J. Tomasi, V. Barone, B. Mennucci, M. Cossi, G. Scalmani, N. Rega, G. A. Petersson, H. Nakatsuji, M. Hada, M. Ehara, K. Toyota, R. Fukuda, J. Hasegawa, M. Ishida, T. Nakajima, Y. Honda, O. Kitao, H. Nakai, M. Klene, X. Li, J. E. Knox, H. P. Hratchian, J. B. Cross, V. Bakken, C. Adamo, J. Jaramillo, R. Gomperts, R. E. Stratmann, O. Yazyev, A. J. Austin, R. Cammi, C. Pomelli, J. W. Ochterski, P. Y. Ayala, K. Morokuma, G. A. Voth, P. Salvador, J. J. Dannenberg, V. G. Zakrzewski, S. Dapprich, A. D. Daniels, M. C. Strain, O. Farkas, D. K. Malick, A. D. Rabuck, K. Raghavachari, J. B. Foresman, J. V. Ortiz, Q. Cui, A. G. Baboul, S. Clifford, J. Cioslowski, B. B. Stefanov, G. Liu, A. Liashenko, P. Piskorz, I. Komaromi, R. L. Martin, D. J. Fox, T. Keith, M. A. Al-Laham, C. Y. Peng, A. Nanayakkara, M. Challacombe, P. M. W. Gill, B. Johnson, W. Chen, M. W. Wong, C. Gonzalez, and J. A. Pople, Gaussian 03, Revision C.02; Gaussian, Inc., Wallingford CT, **2004**.
- 76 S. Sadhukhan, D. Munoz, A. Adamo, G. E. Scuseria, *Chem. Phys. Lett.* **1999**, *306*, 83-87.
- 77 M. J. Gutmann *SXD2001 User's Guide*, **2004**.
- 78 M. Plazanet, N. Fukushima, M. R. Johnson, A. J. Horsewill, H. P. Trommsdorff, *J. Chem. Phys.* **2001**, *115*, 3241-3248.
- 79 C. C. Wilson, N. Shankland, A. J. Florence, *Chem. Phys. Lett.* **1996**, *253*, 103-107.
- 80 M. Neumann, D. F. Brougham, C. J. McGloin, M. R. Johnson, A. J. Horsewill, and H. P. Trommsdorff, *J. Chem. Phys.* **1998**, *109*, 7300-7311.

- 81 A. J. Horsewill, C. J. McGloin, H. P. Trommsdorff, and M. R. Johnson, *Chem. Phys. Lett.* **2003**, *291*, 41-52.
- 82 D. F. Brougham, A. J. Horsewill, and R. I. Jenkinson, *Chem. Phys. Lett.* **1997**, *272*, 69-74.
- 83 C. L. Nygren, C. C. Wilson, and J. F. C. Turner, *J. Phys. Chem. A* **2005**, *109*, 2586-2593.
- 84 C. C. Wilson, X. Xu, A. J. Florence and N. Shankland, *New J. Chem.* **2006**, *30*, 979-981.
- 85 C. C. Wilson, N. Shankland and A. J. Florence, *J. Chem. Soc., Faraday Trans.* **1996**, *92*, 5051-5057.
- 86 D. S. Middlemiss, M. Facchini, C. A. Morrison and C. C. Wilson, *Cryst. Eng. Comm.* **2007**, *9*, 777-785.
- 87 A. V. Stepanov and M. P. Tsvirko, *J. Appl. Spec.* **2004**, *71*, 462-468.
- 88 V. Horneffer, K. Deisewerd, H.-C. Ludemann, F. Hillenkamp, M. Lage, and K. Strupat, *International J. Mass Spect.* **1999**, *185/186/187*, 859-870.
- 89 M. Haisa, S. Kashino, S-I. Hanada, K. Tanaka, S. Okazaki and M. Shibagaki, *Acta Cryst.* **1982**, *B38*, 1480-1485.
- 90 A. J. Horsewill, D. F. Brougham, R. I. Jenkinson, C. J. McGloin, H. P. Trommsdorff, and M. R. Johnson, *Ber. Bunsenges. Phys. Chem.* **1998**, *102*, 317-324.
- 91 C. C. Wilson, X. Xu, A. J. Florence, and N. Shankland, *New. J. Chem.* **2006**, *30*, 979-981.
- 92 M. S. Adam, M. J. Gutmann, C. K. Leech, D. S. Middlemiss, A. Parkin, L. H. Thomas and C. C. Wilson, *In preparation* **2008**.
- 93 M. Schmidtman, M. J. Gutmann, D. S. Middlemiss and C. C. Wilson, *Cryst. Eng. Comm.* **2007**, *9*, 743-745.
- 94 M. Schmidtman and C. C. Wilson, *Cryst. Eng. Comm.* **2008**, *10*, 177-183.
- 95 M. Tanaka, H. Matsui, J-i. Mizoguchi, and S. Kashino, *Bull. Chem. Soc. Jpn.* **1994**, *67*, 1572-1579.
- 96 C. Muthamizhchelan, K. Saminathan, J. Fraanje, R. Peschar, and K. Sivakumar, *Analyt. Sci.* **2005**, *21*, 61-62.
- 97 G. Smith, U. D. Wermuth, P. C. Healy, *Acta Cryst.* **2004**, *E60*, o1800-o1803.
- 98 A. Parkin, C. K. Spanswick, C. R. Pulham and C. C. Wilson, *Acta Cryst.* **2005**, *E61*, 1087-1089.

- <sup>99</sup> D. Chopra, V. Thiruvengatam, and T. N. G. Row, *Cryst. Growth Des.* **2006**, *6*, 843-845.
- <sup>100</sup> R. G. Delaplane, W. I. F. David, R. M. Ibberson, and C. C. Wilson, *Chem. Phys. Lett.* **1993**, *201*, 75-78.
- <sup>101</sup> M. Tremayne, B. M. Kariuki, K. D. M. Harris, K. Shankland and K. S. Knight, *J. Appl. Cryst.* **1997**, *30*, 968-974.
- <sup>102</sup> S. Idziak and N. Pislewski, *Chem. Phys.* **1987**, *111*, 439-443.
- <sup>103</sup> R. Colsonet, C. Gardienet, B. Henry and P. Tekely, *Angew. Chem. Int. Ed.* **2002**, *47*, 4743-4745.
- <sup>104</sup> J. de Villepin, M.-H. Limage, A. Novak, N. Toupry, M. Le Postollec, H. Poulet, S. Ganguly and C. N. R. Rao, *J. Raman Spec.* **1984**, *15*, 41-46.
- <sup>105</sup> J. A. Goedkoop, and C. H. MacGillavry, *Acta Cryst.* **1965**, *10*, 125-127.
- <sup>106</sup> N. R. Jagannathan, S. S. R., and E. subramanian, *J. Chem. Cryst.* **1994**, *24*, 75.
- <sup>107</sup> V. R. Thalladi, M. Nusse and R. Boese, *J. Am. Chem. Soc.* **2000**, *122*, 9227-9236.
- <sup>108</sup> R. Srinivasa Gopalan, P. Kumaradhas, G. U. Kulkarni, and C. N. R. Rao, *J. Mol. Struct.* **2000**, *521*, 97-106.
- <sup>109</sup> D. la Tour, *Ann. Phys. (Leipzig)* **1932**, *18*, 234.
- <sup>110</sup> D. Bougeard, J. D. Villepin, A. Novak, *Spectrochimica Acta* **1988**, *44A*, 1281-1286.
- <sup>111</sup> E. Krogh Andersen, *Acta Cryst.* **1967**, *22*, 188-191.
- <sup>112</sup> E. Krogh Andersen, *Acta Cryst.* **1967**, *22*, 191-196.
- <sup>113</sup> S. Horiuchi, R. Kumai, and Y. Tokura, *Chem. Commun.* **2007**, *23*, 2321-2329.
- <sup>114</sup> H. Ishida, *Acta Cryst.* **2004**, *E60*, o1900-o1901.
- <sup>115</sup> H. Ishida, *Acta Cryst.* **2005**, *E60*, o2005-o2006.
- <sup>116</sup> H. Ishida and S. Kashino, *Acta Cryst.* **1999**, *C55*, 1149-1152.
- <sup>117</sup> Md. B. Zaman, M. Tomura, Y. Yamashita, *Org. Lett.* **2000**, *2*, 273-275.
- <sup>118</sup> MD. Akhtaruzzaman, M. Tomura, K. Takahashi, J-I. Nishida and Y. Yamashita, *Supramolecular Chem.* **2003**, *15*, 239-243.
- <sup>119</sup> H. Ishida and S. Kashino, *Acta Cryst.* **2001**, *C57*, 476-479.
- <sup>120</sup> H. Ishida, *Acta Cryst.* **2004**, *E60*, o2506-o2508.
- <sup>121</sup> E. Hoffman, *Fresenius' J. Analyt. Chem.* **1962**, *185*, 372-376.
- <sup>122</sup> K. Basavaiah, and V. S. Charan, *V. S. C. Turk. J. Chem.* **2002**, *26*, 653-661.
- <sup>123</sup> L. B. Carr, O. N. Rambo, and T. V. Feichtmeir, *J. Histochem. Cytochem.* **1969**, *9*, 415-417.

- <sup>124</sup> H. S. R. Barreto, R. C. R. Barreto, and I. P. Pinto, *J. Chromatog* **1961**, 5, 5-8.
- <sup>125</sup> H. Ishida, and S. Kashino *Z. Naturforsch.* **2002**, 57a, 829-836
- <sup>126</sup> Y. M. Issa, *Spectrochimica Acta* **1984**, 40A, 137-140.
- <sup>127</sup> MS Modeling v3.0.0.0 Accelrys Inc, **2003**.
- <sup>128</sup> Byung-Joo Kima, Young-Seak Leeb and Soo-Jin Park. *Int. J. Hyd. Energy*, **2008**, 33, 4112-4115
- <sup>129</sup> M. Avilaa, L. Reguerab, J. Rodríguez-Hernándezc, J. Balmasedad and E. Reguera *J. Solid State Chem*, **2008**, 181, 2899-2907.